INSTRUMENTATION AND EARLY PERFORMANCE OF AN INNOVATIVE PRESTRESSED PRECAST PAVEMENT SYSTEM

A Thesis
presented to
the Faculty of the Graduate School
University of Missouri – Columbia

In Partial Fulfillment
of the Requirements for the Degree

Master of Science

---

by
CODY L. DAILEY, E.I.

Dr. Vellore S. Gopalaratnam, P.E., Thesis Advisor

December 2006

The undersigned, appointed by the Dean of the Graduate School, have examined the thesis entitled

INSTRUMENTATION AND EARLY PERFORMANCE OF AN INNOVATIVE PRESTRESSED PRECAST PAVEMENT SYSTEM

presented by

Cody L. Dailey, E.I.

a candidate for the degree of

Master of Science

and hereby certify that in their opinion it is worthy of acceptance.

_____

Dr. Vellore S. Gopalaratnam, P.E.

_____

Dr. Glenn Washer, P.E.

_____

Dr. Sanjeev K. Khanna

_____

John P. Donahue, P.E.

ACKNOWLEDGEMENTS

I would like to acknowledge funding for the experimental project from the Federal Highway Administration (FHWA) and Missouri Department of Transportation (MoDOT). Sunil Vanikar, Mark Swunland and Sam Tyson of the FHWA and Eric Krapf and Barry Horst of the MoDOT District office were actively involved in the implementation of the project. Funding from MoDOT for the research project (RI03-007) via the Missouri Transportation Institute (MTI, Director Bill Ankner) is also gratefully acknowledged. Engineering support for the project contracted by FHWA with Transtec Group, Inc. (Dave Merritt, Design Engineer) played an important role in design and implementation of the instrumentation/monitoring program. I extend specific thanks to John Donahue, with the MoDOT pavement group, who has played an active role in both the development of this project as well as my own professional development.

I would like to thank Jim Copeland from the MoDOT district office who took time from a very busy schedule to help the team survey the pavement. Finally, from MoDOT, the help of Terry Fields, senior construction inspector, is greatly appreciated.

I would also like to thank professionals from Concrete Products Incorporated (CPI) and Gaines Construction for their support with incorporating the research portions of the project. Andrew Maybee and Jimmy Davis from CPI were very hospitable and accommodated our changing needs without question.

I extend a special thanks to my advisor Dr. V.S. Gopalaratnam. You have provided unmatched mentorship through my undergraduate and graduate development.

Had it not been for the accomplished standard you set for the work you produce, I would not have had this opportunity.

There have been many who have provided peripheral help. I would like to thank Grant Luckenbill for providing reliable dedicated assistance as an undergraduate. I wish you luck with completion of this project. I would like to thank Rich Oberto and Patrick Earney for their seasoned technical advice and help with instrumentation.

I would like to thank God, my family, and my friends. To my parents Bob and Cathy Dailey, thank you for supporting my decisions throughout my education. To my sister Heidi, thank you for showing me what unsurpassed determination and strength can accomplish. To my future wife Jennifer Hall, thank you for your patience and support throughout. You have been my inspiration and motivation. I hope to reciprocate that when you get your masters in architecture!

TABLE OF CONTENTS

ACKNOWLEDGEMENTS ..... **II**

TABLE OF CONTENTS ..... **IV**

LIST OF TABLES ..... **IX**

LIST OF FIGURES ..... **XI**

NOMENCLATURE / LIST OF NOTATIONS ..... **XIX**

ABSTRACT ..... **XXII**

1. INTRODUCTION **1**

1.1. NEED FOR EXPEDITED PAVEMENT CONSTRUCTION 1
1.2. PRECAST ROADWAY PROJECTS IN THE UNITED STATES 2
1.2.1. FHWA Concrete Pavement Technology Program (CPCT) Task 58 2
1.2.2. Missouri Precast Pavement Project 3
1.3. OBJECTIVES OF INSTRUMENTATION 4
1.3.1. Need for Experimental Investigation 4
1.3.2. General Information 4
1.3.3. Curing and Early Age Performance 5
1.3.4. Transfer of Pretensioning Force 6
1.3.5. Transfer of Post-Tensioning Force 6
1.3.6. In-Service Performance 7
1.3.7. Long-Term Performance 7
1.4. ORGANIZATION OF THESIS 8

2. BACKGROUND INFORMATION **9**

2.1. EVOLUTION OF PRECAST ROADWAY PANELS 9
2.1.1. Introduction—Rigid Pavement vs. Flexible Pavement 9
2.1.2. AASHTO Design Procedure 11
2.1.3. Cast in Place Technology 11
2.1.3.1. Jointed Concrete Pavement 11
2.1.3.2. Jointed Reinforced Concrete Pavement 12
2.1.3.3. Continuously Reinforced Concrete Pavement 13
2.1.3.4. Issues with Current Cast-in-Place Construction 14
2.1.4. Use of Prestressed, Precast Concrete Pavements 15
2.2. PRECAST AND PRESTRESSED ROADWAY SYSTEMS IN SERVICE 16
2.2.1. Prestressed Pavement Projects 17
2.2.1.1. Full Scale Prestressed Pavement in Pennsylvania (1973) 17
2.2.1.2. Full Scale Prestressed Pavement in Arizona (1977) 18

2.2.1.3. Prestressed Concrete Overlay at O'Hare Airport (1980) 19
2.2.1.4. CTR Pilot Project in McLennan County, Texas (1985) 20
2.2.2. Precast Pavement Projects 22
2.2.2.1. Full Depth Repair on US 287 Near Fort Collins, Colorado (2000). 22
2.2.2.2. Precast Panels on Tappan Zee Toll Plaza, New York (2001) 23
2.2.2.3. Precast Panels at Washington Dulles Airport (2001/2002) 26
2.2.2.4. Precast Panels on Taxiway D-D at Laguardia Airport (2002) 26
2.2.2.5. Precast Repair Trials on HWY 427 Toronto, ON, Canada (2004) ... 28
2.2.2.6. Precast Panels on TH 62 in Minnesota (2005) 29
2.2.3. Prestressed Precast Concrete Pavement (PPCP) Projects 30
2.2.3.1. PPCP on I-35 in Georgetown, TX (2001) 30
2.2.3.2. PPCP on I-10 in El Monte, California (2004) 33
2.2.3.3. Other Demonstration Projects 35
2.3. SIGNIFICANCE OF MISSOURI'S INSTRUMENTATION PROGRAM 35

3. PROJECT INFORMATION AND CONSTRUCTION 37

3.1. GENERAL INFORMATION 37
3.2. PANEL DESIGN AND FABRICATION 39
3.2.1. General Information and Specifications 39
3.2.2. Fabrication Procedure 40
3.2.3. Base Panels 45
3.2.4. Joint Panels 46
3.2.5. Anchor Panels 49
3.3. BASE PREPARATION 50
3.3.1. Leveling Course 50
3.3.2. Friction Reduction Layer 51
3.4. CONSTRUCTION 52
3.4.1. Joint Sealant 52
3.4.2. Alignment 52
3.4.3. Post-Tensioning 54
3.4.4. Problems During Construction 54
3.5. GROUTING AND FINISH-WORK 59

4. EXPERIMENTAL PROGRAM 60

4.1. FIELD INSTRUMENTATION 60
4.1.1. General Information on Instrumentation 60
4.1.1.1. Test Section Layout 60
4.1.1.2. Instrumentation Labeling 61
4.1.1.3. Instrumentation Plan and As-Built Information 62
4.1.1.3.1. Panel A31 62
4.1.1.3.2. Panels C1, B1, B2, and B3 63
4.1.1.3.3. Panel A32 67
4.1.1.3.4. Panel B4 69
4.1.2. Embedded Instrumentation 70
4.1.2.1. Instrumented Rebar 70

4.1.2.1.1. Rebar Fabrication 71
4.1.2.1.2. Instrumented Rebar Calibration 71
4.1.2.1.3. Advantages of Instrumented Rebar 73
4.1.2.2. Vibrating Wire Strain Gages 73
4.1.2.2.1. Vibrating Wire Gage Specifications and Theory 74
4.1.2.2.2. Vibrating Wire Thermal Compensation and Calibration 74
4.1.2.2.3. Advantages of Vibrating Wire Strain Gages 77
4.1.2.3. Vibrating Wire Strandmeters 77
4.1.2.3.1. Vibrating Wire Strandmeter Specifications 78
4.1.2.3.2. Vibrating Wire Strandmeter Calibration 78
4.1.2.3.3. Advantages of Vibrating Wire Strandmeter 80
4.1.2.4. Thermocouples 80
4.1.2.5. Installation of Devices 82
4.1.3. Data Acquisition System 86
4.1.3.1. General Information 87
4.1.3.2. Terminal Junction Boxes 87
4.1.3.3. Cables and Connectors 92
4.1.3.4. Main Data Acquisition Box 93
4.1.3.4.1. AM416 Multiplexers 93
4.1.3.4.2. Power Supply 95
4.1.3.4.3. CR10X Datalogger 95
4.1.3.4.4. AVW1 Vibrating Wire Interface 97
4.1.3.5. Remote Communication Equipment 98
4.1.4. External Instrumentation 98
4.1.4.1. Total Station Survey Equipment 98
4.2. LABORATORY STUDIES 99
4.2.1. General 99
4.2.2. Compression Tests 101
4.2.3. Creep Tests 102
4.2.4. Shrinkage Tests 102
4.2.5. Rapid Chloride Permeability Tests 104
4.2.6. Freeze Thaw Tests 104
4.2.7. Flexure Tests 108

5. MATERIAL PROPERTIES 109

5.1. CONCRETE PROPERTIES 109
5.1.1. Mix Design 109
5.1.2. Summary of Concrete Performance (Lab Studies) 111
5.2. PRESTRESSING STRANDS 112
5.3. REINFORCING BAR 112

6. HYDRATION AND EARLY AGE RESPONSE 114

6.1. INTRODUCTION 114
6.2. DATA FROM EARLY AGE ANALYSIS 115
6.2.1. Theoretical Calculations 116

6.2.1.1. Theoretical Measured Concrete Strain (Thermal) 116
6.2.1.2. Theoretical Measured Rebar Strain (Thermal) 118
6.2.1.3. Explanation of Instrumented Rebar Readings 118
6.2.2. Measured Curing Temperature 120
6.2.3. Measured Curing Strains 123

7. STRESS TRANSFER 131

7.1. INTRODUCTION 131
7.2. PRETENSIONING STRESS TRANSFER STRAINS 133
7.2.1. Theoretical Strain Calculations 133
7.2.1.1. Theoretical Transverse Strains 133
7.2.2. Theoretical Longitudinal Strains 139
7.2.3. Measured Strains During Transfer 140

8. POST-TENSIONING DURING CONSTRUCTION 146

8.1. INTRODUCTION 146
8.2. POST-TENSIONING DATA AND ANALYSIS 148
8.2.1. Theoretical Strain Calculations 148
8.2.1.1. Theoretical Concrete Strains 149
8.2.1.2. Theoretical Strand Strain 152
8.2.2. Concrete Strains During Transfer 152
8.2.3. Post-Tensioning Strand Strains During and After Transfer 157

9. SERVICE PERFORMANCE 160

9.1. INTRODUCTION 160
9.2. DAY TO DAY SERVICE PERFORMANCE 162
9.2.1. Daily Temperature Variation 162
9.2.2. Theoretical Strain Calculations 163
9.2.2.1. Theoretical Concrete Strain 164
9.2.2.2. Theoretical Rebar Strain 164
9.2.3. Measured Daily In-Service Strains 164
9.2.4. Daily Traffic Variation 171
9.3. LONG-TERM MEASUREMENTS 174
9.3.1. Long-Term Strain Measurement 174
9.3.2. Long-Term Global Movement 174
9.3.3. Visual Surveys 176

10. CONCLUSIONS 178

10.1. SUMMARY OF THE RESULTS FROM THE INSTRUMENTATION 178
10.1.1. Hydration and Early Age Performance 178
10.1.2. Pretensioning Transfer 179
10.1.3. Post-Tensioning 179
10.1.4. In-Service 180
10.2. RECOMMENDATIONS FOR FURTHER WORK 181

REFERENCES **183**

APPENDICES **186**

A. DESIGN DOCUMENTS 186
B. PREPARATION OF INSTRUMENTED REBAR (EATHERTON 1999) 195
C. CALIBRATION OF GAGES 199
D. ADDITIONAL STRESS TRANSFER CALCULATIONS 204
E. ADDITIONAL RESULTS AND GRAPHS 207
E.1. Hydration and Early Age Response 208
E.2. Pretensioning Stress Transfer 211
E.3. Post-Tensioning During Construction 213
E.4. Service Performance 214
F. TIMELINE FOR THE PROJECT 218

LIST OF TABLES

TABLE 1.1 – TOTAL USER DELAY COSTS FOR PRECAST AND CONVENTIONAL PAVEMENT CONSTRUCTION FOR A 5-MILE PAVEMENT WITH AN ADT 105,000 VEHICLES PER DAY (MERRRITT, MCCULLOUGH ET AL. 2000). 2

TABLE 4.1 - AS-BUILT INSTRUMENTATION LOCATIONS FOR PANEL A31 63

TABLE 4.2 - AS-BUILT INSTRUMENTATION LOCATIONS FOR PANEL C1 64

TABLE 4.3 - AS-BUILT INSTRUMENTATION LOCATIONS FOR PANEL B1 65

TABLE 4.4 - AS-BUILT INSTRUMENTATION LOCATIONS FOR PANEL B2 65

TABLE 4.5 - AS-BUILT INSTRUMENTATION LOCATIONS FOR PANEL B3 66

TABLE 4.6 - AS-BUILT INSTRUMENTATION LOCATIONS FOR PANEL A32 68

TABLE 4.7 - AS-BUILT INSTRUMENTATION LOCATIONS FOR PANEL B4 70

TABLE 4.8 – SUMMARY OF EXPERIMENTAL SPECIMENS CAST FOR LABORATORY STUDIES (DAVIS 2006). 100

TABLE 5.1 – MIX DESIGN OF CONCRETE USED IN PPCP SYSTEM. 110

TABLE 5.2 – SUMMARY OF EXPERIMENTAL CONCRETE PROPERTIES OF PPCP (DAVIS 2006) 111

TABLE 7.1 - THEORETICAL STRESS AND STRAIN CALCULATIONS FOR A31 138

TABLE 8.1 - THEORETICAL STRAIN CALCULATIONS FOR REBAR DURING POST-TENSIONING 151

TABLE C.1 - CALIBRATION CONSTANTS FOR INSTRUMENTED REBAR 200

TABLE C.2 - CALIBRATION CONSTANTS FOR VIBRATING WIRE GAGES 202

TABLE C.3 - CALIBRATION CONSTANTS FOR STRANDMETERS 203

TABLE D.1 - PRETENSIONING STRESS TRANSFER CALCULATIONS FOR BASE PANELS B1-4 204

TABLE D.2 - PRETENSIONING STRESS TRANSFER CALCULATIONS FOR ANCHOR PANEL C1 205

TABLE D.3 - PRETENSIONING STRESS TRANSFER CALCULATIONS FOR JOINT PANEL A32 206

LIST OF FIGURES

FIGURE 2.1 – PLAN AND SECTION OF JOINTED CONCRETE PAVEMENT (ACPA 2004) 12

FIGURE 2.2 - PLAN AND SECTION OF JRCP (ACPA 2004) 13

FIGURE 2.3 - PLAN AND SECTION OF CRCP (ACPA 2004) 14

FIGURE 2.4 - LOOPED POST-TENSIONING TENDONS (MERRITT, MCCULLOUGH ET AL. 2000) 22

FIGURE 2.5 - PLACEMENT OF PRECAST PANELS ON US 287 IN COLORADO 23

FIGURE 2.6 - REMOVAL OF OLD CONCRETE AT TAPPAN ZEE TOLL PLAZA (MERRITT 2002) 25

FIGURE 2.7 - INSTALLATION OF NEW PANELS AT TAPPAN ZEE TOLL PLAZA (MERRITT 2002) 25

FIGURE 2.8 - INSTALLATION OF PANELS AT LAGUARDIA AIRPORT (AUTHORITY 1997) .. 27

FIGURE 2.9 - PRECAST PANELS IN SERVICE AT LAGUARDIA AIRPORT (AUTHORITY 1997) 28

FIGURE 2.10 - FULL WIDTH PANEL PLACEMENT ON GEORGETOWN, TX PPCP (MERRITT 2002) 32

FIGURE 2.11 - FULL WIDTH PANEL PLACEMENT ON GEORGETOWN, TX PPCP (MERRITT 2002) 32

FIGURE 2.12 - PLACEMENT OF PANEL ON I-10 EL MONTE, CALIFORNIA 34

FIGURE 2.13 - VIEW OF EXPANDED ROADWAY ON I-10 EL MONTE, CALIFORNIA 34

FIGURE 3.1 – OVERALL PPCP SECTION LAYOUT WITH DRIVING LANES SHOWN (25 PANELS PER SECTION; SECTION 3 IS HEAVILY INSTRUMENTED) 38

FIGURE 3.2 – TYPICAL SECTION OF PPCP PANEL ASSEMBLY AND LAYOUT 38

FIGURE 3.3 – TYPICAL PANEL SECTION LOOKING WITH THE DIRECTION OF TRAFFIC 40

FIGURE 3.4 – OILED PRECAST BED AFTER REMOVING PREVIOUS TWO PANELS 42

FIGURE 3.5 – STRESSING STRANDS IN TWO PANELS 42

FIGURE 3.6 – INSTALLING POST-TENSIONING DUCTWORK THROUGH PRETENSIONED STRANDS 43

FIGURE 3.7 – PLACEMENT AND CONSOLIDATION OF CONCRETE FOR A BASE PANEL 43

FIGURE 3.8 – HAND LEVELING CONCRETE OF ONE PANEL JUST AFTER PLACEMENT 44

FIGURE 3.9 – SCREEDING AND HAND-FINISHING BEFORE FINAL BROOM 44

FIGURE 3.10 – PLAN VIEW OF TYPICAL BASE PANEL 45

FIGURE 3.11 – SECTION OF BASE PANEL LOOKING PERPENDICULAR TO TRAFFIC DIRECTION 46

FIGURE 3.12 – LIFTING ANCHOR (LEFT); CHAIR FOR DRAPING STRANDS (RIGHT) 46

FIGURE 3.13 – PLAN VIEW OF TYPICAL JOINT PANEL 47

FIGURE 3.14 – SECTION OF JOINT PANEL LOOKING PERPENDICULAR TO TRAFFIC DIRECTION 48

FIGURE 3.15 - JOINT PANEL CASTING (LEFT SIDE CURED, RIGHT SIDE READY FOR CASTING) 48

FIGURE 3.16 – PLAN VIEW OF TYPICAL ANCHOR PANEL 49

FIGURE 3.17 – SECTION OF ANCHOR PANEL LOOKING PERPENDICULAR TO TRAFFIC DIRECTION 49

FIGURE 3.18 – ANCHOR PANEL ON POLYPROPYLENE OVER ASPHALT, AND AGGREGATE BASE (MISSOURI PROJECT) 51

FIGURE 3.19 – APPLICATION OF JOINT COMPOUND TO A PPCP PANEL 53

FIGURE 3.20 – UNLOADING PANEL FOR PLACEMENT 53

FIGURE 3.21 – STRESSING THE SECOND SET OF STRANDS IN A TYPICAL MISSOURI PPCP SECTION 55

FIGURE 3.22 – POST-TENSIONING STRAND PUSHER 55

FIGURE 3.23 – KING STRAND WELDED TO FULL STRAND FOR THREADING 56

FIGURE 3.24 – CROOKED PPCP SECTION (BEFORE AND AFTER SHIMMING STARTED) 56

FIGURE 3.25 – SHIM INSTALLED ON THE OUTSIDE SHOULDER OF SEVERAL PANELS 57

FIGURE 3.26 – CLOSED JOINT IN JOINT PANEL AFTER STRESSING OPERATIONS (SAW-CUT ON TOP) 58

FIGURE 3.27 – REPAIRED TRANSVERSE CRACK IN PPCP 58

FIGURE 4.1 - OVERALL VIEW OF TEST-SECTION AND LOCATION OF INSTRUMENTED PANELS 61

FIGURE 4.2 - INSTRUMENTATION PLAN FOR PANEL A31 63

FIGURE 4.3 - INSTRUMENTATION PLAN FOR PANELS C1, B1, AND B2 64

FIGURE 4.4 - INSTRUMENTATION PLAN FOR PANEL B3 66

FIGURE 4.5 - INSTRUMENTATION PLAN FOR PANEL A32 68

FIGURE 4.6 - INSTRUMENTATION PLAN FOR PANEL B4 69

FIGURE 4.7 - SCHEMATIC OF THE STRAIN GAGE CONFIGURATION ON THE STRAIN GAGED BAR 72

FIGURE 4.8 - A FINISHED INSTRUMENTED REBAR ALONG WITH AN INSTRUMENTED BAR YET TO BE WATERPROOFED AND SEALED 72

FIGURE 4.9 - VIBRATING WIRE STRAIN GAGE FROM GEOKON INCORPORATED 76

FIGURE 4.10 - CALIBRATION OF THE VIBRATING WIRE STRAIN GAGES 76

FIGURE 4.11 - BARE STRANDMETER (TOP) AND STRANDMETER SLEEVED WITH PVC TUBE FOR GREASING (BOTTOM) 79

FIGURE 4.12 - STRANDMETER FIXED TO STEEL BAR INSTRUMENTED WITH FOIL GAGES AND AN EXTENSOMETER (THIS PICTURES IS ROTATED 90°) 79

FIGURE 4.13 - THERMOCOUPLES WELDED, BUNDLED, LABELED, AND EPOXY COATED IN LAB 81

FIGURE 4.14 - GAGES BEING LAID OUT FOR TESTING IN LAB 83

FIGURE 4.15 - TRANSVERSE AND LONGITUDINALLY INSTALLED REBAR USING SPACERS AND TIES 83

FIGURE 4.16 - TWO THERMOCOUPLES ZIP-TIED TO FRP FOR THERMAL DEPTH GRADIENT. 84

FIGURE 4.17 - VIBRATING WIRE GAGE ATTACHED TO REBAR WITH SPACERS AND LOOSE TIES 84

FIGURE 4.18 - STRANDMETER INSTALLED IN BLOCK-OUT AROUND POST-TENSIONING STRAND. 85

FIGURE 4.19 - STRANDMETER ENCASED IN PVC TUBE TO ISOLATE IT FROM GROUT. 85

FIGURE 4.20 - JUNCTION BOX BLOCK-OUT IN PANEL WITH WIRES FROM INSTRUMENTATION 88

FIGURE 4.21 - JUNCTION BOX INSIDE PLYWOOD BLOCK-OUT, WITH INSTRUMENTATION AND QUICK CONNECT HOOKED UP (NOTE GREY EPOXY WHERE WIRES ENTER BOX) 88

FIGURE 4.22 - COLD JUNCTION CIRCUIT FOR THERMOCOUPLE COMPENSATION..... 90

FIGURE 4.23 - CIRCUIT FOR STEPPING DOWN INCOMING VOLTAGE TO 4V FOR REBAR EXCITATION 90

FIGURE 4.24 - INSTRUMENTATION HOOKED TO INNER WORKINGS OF JUNCTION BOX FOR MOCK-UP TESTING IN THE LAB 91

FIGURE 4.25 - CONSTRUCTION OF THE SAME PIN-TYPE QUICK CONNECTOR ON A PREVIOUS PROJECT (EATHERTON 1999) 91

FIGURE 4.26 - DIAGRAM OF QUICK CONNECT PIN ASSIGNMENTS FOR INDIVIDUAL PAIRS .. 92

FIGURE 4.27 - SIGNAL CABINET IN SOUTH RIGHT OF WAY OF I-57—HOUSING DATA ACQUISITION SYSTEM; WIRES ENTER FROM BOTTOM 94

FIGURE 4.28 - BARE AM416 MULTIPLEXERS IN BOTTOM OF DATA WHITE DAQ BOX 94

FIGURE 4.29 - 120V TO 12V DC POWER SUPPLY USED TO POWER ENTIRE SYSTEM—FASTENED IN CORNER NEXT TO MULTIPLEXERS..... 96

FIGURE 4.30 - 30AMP POWER DROP (RIGHT), UPS PROTECTION (MIDDLE), DSL MODEM (LEFT) 96

FIGURE 4.31 - NL100 NETWORK LINK (TOP), CR10X DATALOGGER (MIDDLE), AND TWO AVW1 INTERFACES—FASTENED TO LID OF WHITE DAQ BOX..... 97

FIGURE 4.32 – CASTING CREEP, SHRINKAGE, STRENGTH CYLINDERS, AND BEAMS FOR FREEZE-THAW AND FLEXURE (DAVIS 2006)..... 100

FIGURE 4.33 – COMPRESSION TEST SETUP FOR CAPPED 6” DIAMETER CYLINDERS USING 3 LVDTS AND A FORNEY COMPRESSION MACHINE..... 101

FIGURE 4.34 – CREEP LOAD FRAME WITH SEALED AND UNSEALED SPECIMENS (EARNEY 2007-ANTICIPATED). 103

FIGURE 4.35 – SEALED SHRINKAGE SPECIMEN WITH THREE EXTENSOMETERS ATTACHED FOR MEASUREMENT OF SHRINKAGE STRAINS (EARNEY 2007-ANTICIPATED). 103

FIGURE 4.36 – RAPID CHLORIDE PENETRATION TEST SETUP. 105

FIGURE 4.37 – OVERHEAD VIEW OF CABINET USED TO SUBJECT PRISMS TO FREEZE-THAW CYCLES 105

FIGURE 4.38 – SETUP FOR MEASURING FUNDAMENTAL FREQUENCY DURING FREEZE-THAW TESTS. 107

FIGURE 4.39 – PHOTOGRAPH OF THIRD POINT LOADING OF CONCRETE PRISM/BEAM. 107

FIGURE 5.1 – MODULUS OF ELASTICITY FOR INSTRUMENTED REBAR 113

FIGURE 6.1 - COEFFICIENT OF THERMAL EXPANSION FOR CURING CONCRETE (KADA H. 2002) 117

FIGURE 6.2 - RESTRAINT OF INSTRUMENTED REBAR BY SURROUNDING CONCRETE 119

FIGURE 6.3 - SUMMARY OF AVERAGE CURING TEMPERATURES IN EACH PANEL 121

FIGURE 6.4 - EARLY-AGE TEMPERATURES IN THE CROSS-SECTION OF PANEL A32 121

FIGURE 6.5 - EARLY-AGE THERMAL STRAIN HISTORY OF 1ST HALF OF PANEL A32 THROUGH COMPLETION OF 2ND HALF 125

FIGURE 6.6 - EARLY-AGE THERMAL RESPONSE OF PANEL A32 DURING CASTING 2ND HALF 127

FIGURE 6.7 - APPARENT STRAINS AND TEMPERATURE OF PANEL B3 DURING CURING .. 129

FIGURE 7.1 – STRESS TRANSFER OF PRETENSIONED STRANDS AT CPI IN MEMPHIS, TN 132

FIGURE 7.2 – TRANSFER SEQUENCE OF TYPICAL PANELS (TOP) AND JOINT PANELS (BELOW) 132

FIGURE 7.3 - APPLIED PRETENSIONING FORCE AND ECCENTRICITIES FOR CALCULATIONS 135

FIGURE 7.4 - STRESS-BLOCK COMPONENTS OF PRETENSION TRANSFER RELATIVE TO FIGURE 7.3 135

FIGURE 7.5 - ILLUSTRATION OF POISSON'S EFFECT ON A PANEL 140

FIGURE 7.6 – MEASURED TRANSVERSE STRAIN ON PANEL C1 DURING PRETENSION TRANSFER 142

FIGURE 7.7 - MEASURED TRANSVERSE STRAIN ON PANELS B1/B2 DURING PRETENSION TRANSFER 142

FIGURE 7.8 - MEASURED TRANSVERSE STRAIN ON PANELS B3/B4 DURING PRETENSION TRANSFER 144

FIGURE 7.9 - MEASURED LONGITUDINAL STRAIN ON PANEL A32 DURING PRETENSION TRANSFER 144

FIGURE 7.10 - MEASURED LONGITUDINAL STRAIN ON PANEL A32 DURING PRETENSION TRANSFER 145

FIGURE 8.1 - POST-TENSIONING SCHEMATIC OF SECTION 3 147

FIGURE 8.2 - POST-TENSIONING SEQUENCE AND REBAR LOCATIONS AT CROSS-SECTION 147

FIGURE 8.3 - POST-TENSIONING A SECTION OF PAVEMENT 147

FIGURE 8.4 - SCHEMATIC OF FRICTIONAL FORCES ON PANEL/STRAND DURING POST-TENSIONING 148

FIGURE 8.5 – LONGITUDINAL STRAINS AT OUTSIDE SHOULDER (R1) FROM POST-TENSIONING 153

FIGURE 8.6 - LONGITUDINAL STRAINS AT THE OUTSIDE LANE (R2) FROM POST-TENSIONING 153

FIGURE 8.7 - LONGITUDINAL STRAINS AT CROWN (R4) FROM POST-TENSIONING..... 155

FIGURE 8.8 - LONGITUDINAL STRAINS AT THE INSIDE LANE (R5) FROM POST-TENSIONING 155

FIGURE 8.9 - MEASURED FINAL POST-TENSIONING STRAIN THROUGH X-SECTION OF EACH PANEL 156

FIGURE 8.10 - STRAIN DISTRIBUTION IN STRAND AND CONCRETE FROM POST-TENSIONING 156

FIGURE 8.11 - POST-TENSIONING STRAIN LOSS IN CENTER STRAND AFTER JACKING ADJACENT STRANDS 158

FIGURE 8.12 - ENTIRE POST-TENSIONING STRAIN HISTORY OF CENTER STRAND..... 158

FIGURE 9.1 - FINISHED PANEL SYSTEM IN SERVICE 161

FIGURE 9.2 - ANOTHER VIEW OF THE FINISHED PANEL SYSTEM IN SERVICE 161

FIGURE 9.3 - THERMAL RESPONSE OF B3 OVER TWO DAYS IN FEBRUARY (2/12-2/14/06) 166

FIGURE 9.4 - THERMAL RESPONSE OF A32 OVER THREE DAYS IN SEPTEMBER (9/5-9/8/06) 167

FIGURE 9.5 - THERMAL RESPONSE OF B2 OVER SEVEN DAYS IN OCTOBER (10/2-10/9/06) 169

FIGURE 9.6 - THERMAL RESPONSE OF B4 OVER FOURTEEN DAYS IN JULY (7/11-7/25/06) 170

FIGURE 9.7 - TRAFFIC STRAINS IN CONJUNCTION WITH SLIGHT THERMAL CHANGE..... 171

FIGURE 9.8 - TRAFFIC STRAINS SHOWN AT HIGHER MAGNITUDES THAN NOISE 172

FIGURE 9.9 - TRAFFIC DATA WITH MANUAL COUNT OF PASSING TRUCKS 172

FIGURE 9.10 - CLOSE-UP OF STRAIN INDUCED AT R4 BY A SINGLE TRUCK LOAD..... 173

FIGURE 9.11 - SURVEYING JOINT PANEL CORNERS FOR MOVEMENT WITH TOTAL STATION 175

FIGURE 9.12 - GRAPHICAL REPRESENTATION OF GLOBAL MOVEMENT (IN) AT SECTION CORNERS 176

FIGURE 9.13 - LONGITUDINAL CRACK (LEFT) DETERIORATING EXPANSION JOINT (RIGHT) 177

FIGURE 9.14 - GRAPHICAL PLAN OF LONGITUDINAL CRACK (LUCKENBILL 2008-ANTICIPATED)..... 177

FIGURE B.1 - SOLDERING CONNECTIONS ON AN INSTRUMENTED REBAR 196

FIGURE B.2 - APPLYING A COAT OF POLYURETHANE TO INSTRUMENTED REBAR 196

FIGURE B.3 - TEFLON TAPE COVERS THE GAGES AND REDUCES FRICTION WITH OUTER PROTECTIVE LAYERS 197

FIGURE B.4 - APPLICATION OF RUBBER TAPE TO PROTECT THE GAGES FROM FALLING CONCRETE 197

FIGURE B.5 - THE INSTRUMENTED REBAR AFTER SILICON HAS BEEN APPLIED TO THE GAGED AREA 198

FIGURE B.6 - THE FINISHED INSTRUMENTED REBAR NEXT TO AN UN-WATERPROOFED BAR 198

FIGURE C.1 – EXAMPLE GRAPH FROM CALIBRATION OF REBAR 199

FIGURE C.2 – EARLY THERMAL STUDY OF REBAR AND VIBRATING WIRE GAGE IN OVEN .. 201

FIGURE C.3 – GRAPH OF VIBRATING WIRE GAGE CALIBRATION 202

FIGURE C.4 – EXAMPLE GRAPH FROM STRANDMETER CALIBRATION (WITH THERMAL CHANGES) 203

FIGURE E.1 – CURING AND HYDRATION OF PANEL C1 208

FIGURE E.2 – CURING AND HYDRATION OF PANEL B1 209
FIGURE E.3 – CURING AND HYDRATION OF PANEL B4 210
FIGURE E.4 – STRAINS FROM STRESS TRANSFER OF PANEL A31 REBAR 211
FIGURE E.5 – STRAINS FROM STRESS TRANSFER OF PANEL A31 REBAR 211
FIGURE E.6 – STRAINS FROM STRESS TRANSFER OF PANEL A31 LONGITUDINAL REBAR .. 212
FIGURE E.7 – STRAINS FROM STRESS TRANSFER OF PANEL A32 LONGITUDINAL REBAR .. 212
FIGURE E.8 – SUMMARY OF POST-TENSIONING STRAINS IN SECTION 3..... 213
FIGURE E.9 – IN-SERVICE DATA FOR PANEL B3 OVER THREE DAYS IN SEPTEMBER 2006 . 214
FIGURE E.10 – IN-SERVICE DATA FOR PANEL C1 OVER SEVEN DAYS IN OCTOBER 2006 .. 215
FIGURE E.11 – IN-SERVICE DATA FOR PANEL B1 OVER SEVEN DAYS IN OCTOBER 2006 .. 216
FIGURE E.12 – IN-SERVICE DATA FOR PANEL B1 OVER FOURTEEN DAYS IN JULY 2006 ... 217

NOMENCLATURE / LIST OF NOTATIONS

JCP	-JOINTED CONCRETE PAVEMENT
JRCP	-JOINTED REINFORCED CONCRETE PAVEMENT
CRCP	-CONTINUOUSLY REINFORCED CONCRETE PAVEMENT
PPCP	-PRECAST PRESTRESSED CONCRETE PAVEMENT
CPTP	-CONCRETE PAVEMENT TECHNOLOGY PROGRAM
ESAL	-EQUIVALENT SINGLE AXIAL LOAD
k	-MODULUS OF SUBGRADE REACTION
AASHTO	-AMERICAN ASSOCIATION OF STATE HIGHWAY AND TRANSPORTATION OFFICIALS
ADT	-AVERAGE DAILY TRAFFIC
CTR	-CENTER FOR TRANSPORTATION RESEARCH
FHWA	-FEDERAL HIGHWAY ADMINISTRATION
IRI	-INTERNATIONAL ROUGHNESS INDEX
CPI	-CONCRETE PRODUCTS INCORPORATED
PVC	-POLYVINYL CHLORIDE
ASTM	-AMERICAN SOCIETY FOR TESTING AND MATERIALS STANDARD
MODOT	-MISSOURI DEPARTMENT OF TRANSPORTATION
BN	-INSTRUMENTED BASE PANEL LABEL (NUMBER 'N')
CN	-INSTRUMENTED ANCHOR PANEL LABEL (NUMBER 'N')
A3N	-INSTRUMENTED JOINT PANEL LABEL (NUMBER 'N')
RN	-INSTRUMENTED REBAR LABEL (NUMBER 'N')
VN	-VIBRATING WIRE GAGE LABEL (NUMBER 'N')

SN	-STRANDMETER LABEL (NUMBER 'N')
TN	-THERMOCOUPLE LABEL (NUMBER 'N')
VNt	-VIBRATING WIRE GAGE THERMISTOR LABEL (NUMBER 'N')
SNt	-STRANDMETER THERMISTOR LABEL (NUMBER 'N')
KIP	-1,000 POUNDS
HZ	-HERTZ (UNIT FOR FREQUENCY)
MV	-MILLI-VOLTS
μSTR	-MICROSTRAIN
°C	-DEGREES CENTIGRADE
°F	-DEGREES FAHRENHEIT
FRP	-FIBER REINFORCED POLYMER
DC	-DIRECT CURRENT
AC	-ALTERNATING CURRENT
DAQ	-DATA ACQUISITION
RTDM	-REAL TIME DATA MONITORING
LVDT	-LINEAR VARIABLE DISPLACEMENT TRANSDUCERS
RCPT	-RAPID CHLORIDE PERMEABILITY TEST
KN	-KILONEWTON
MPA	-MEGAPASCAL
f_r	-MODULUS OF RUPTURE FOR CONCRETE
G_f	-FRACTURE ENERGY (CONCRETE)
SSD	-SATURATED SURFACE DRY
CTE	-COEFFICIENT OF THERMAL EXPANSION

T	-TEMPERATURE
t	-TIME
ε	-STRAIN
R	-REBAR STRAIN READING
ΔL_{UC}	-UNRESTRAINED CONCRETE EXPANSION (DUE TO ΔT)
ΔL_{US}	-UNRESTRAINED STEEL REBAR EXPANSION (DUE TO ΔT)
ΔL_{R}	-RESTRAINED STEEL REBAR EXPANSION (DUE TO ΔT)
PSI	-POUNDS PER SQUARE INCH
P	-FORCE IN PRESTRESSING STRAND
A	-AREA OF CONCRETE AT A CROSS-SECTION
y	-DISTANCE FROM THE NEUTRAL AXIS TO A SPOT IN THE CROSS-SECTION
I	-MOMENT OF INERTIA
f_{pi}	-INITIAL PRESTRESSING STRESS
f_{pu}	-ULTIMATE PRESTRESSING STRESS
M	-MOMENT
d	-DEPTH OF PANEL
w	-WIDTH OF PANEL
e	-INTERNAL ECCENTRICITY OF STRESSED STRAND
N.A.	-NEUTRAL AXIS
σ	-STRESS
E	-MODULUS OF ELASTICITY
ν	-POISON'S RATIO
n	-NUMBER OF STRANDS STRESSED AT A GIVEN TIME

INSTRUMENTATION AND EARLY PERFORMANCE OF AN INNOVATIVE PRESTRESSED PRECAST PAVEMENT SYSTEM

Cody L. Dailey

Dr. Vellore S. Gopalaratnam, Thesis Advisor

ABSTRACT

Traffic, weather and de-icing salts continually diminish pavement life. Current rehabilitation methods result in traffic congestion and lost work time. The use of prestressed, precast panels for the replacement of damaged roadways and intersections will give designers a significant advantage in improving pavement performance, decreasing construction time, and mitigating user costs.

A pilot project, funded by FHWA, was created for a 1,000 ft (305 m) stretch of pavement on I-57 in southern Missouri. Seven of the 100 precast roadway panels used were instrumented to monitor temperatures, strains, and strand strains during fabrication, construction, and service.

Objectives include examining early hydration temperatures and corresponding strains, comparing transfer strains (both pretensioning and post-tensioning) to analytical predictions, and analyzing service strains related to daily thermal variations, seasonal trends, and traffic. Condition surveys and materials studies complete the year long performance evaluation and are discussed in companion works by Brent Davis and Grant Luckenbill (currently underway).

1. INTRODUCTION

1.1. NEED FOR EXPEDITED PAVEMENT CONSTRUCTION

Pavement technology has and will be an evolutionary process. Increasing traffic volumes, tire pressures, and truck weights combined with extreme temperatures, use of chlorides for deicing, and poor sub-grade performance, continually diminish pavement longevity and challenge designers. Pavements make up the majority of the nations infrastructure. Therefore, repairs exceedingly impede travel (Merritt, McCullough et al. 2000). When high volume areas are decommissioned, user costs climb exponentially with increased volume. Current replacement and rehabilitation methods result in unbearable traffic congestion, causing increased fuel consumption and lost work time. Value engineering can quickly show how user costs are overtaking monetary investments (See Table 1.1). Better methods of repair must be investigated to minimize user costs. As roadways deteriorate beyond repair, realization of timely and efficient construction methods are essential. The use of prestressed, precast panels for the replacement of damaged or un-repairable roadways and urban intersections will give contractors and designers a significant advantage in improving pavement performance, decreasing construction time, and mitigating user costs. However, feasibility and long-term performance for roadway applications must be investigated further before incorporating the new technology for routine use.

Table 1.1 – Total user delay costs for precast and conventional pavement construction for a 5-mile pavement with an ADT 105,000 vehicles per day (Merritt, McCullough et al. 2000).

Construction Method	Placement Rate	Daily User Cost	Total Construction Time	Total User Cost
Conventional Pavement (CRCP, JRCP)	2,000 ft/day	$680,610	20 days	**$13,612,200**
Precast Pavement	500 ft/day	$124,500	53 days	**$6,598,500**

1.2. PRECAST ROADWAY PROJECTS IN THE UNITED STATES

Joint Reinforced Concrete Pavement (JRCP) and Continuously Reinforced Concrete Pavement (CRCP) are both cast-in-place technologies that have continued to evolve. Modern precast pavement technology developed from several projects in the 80's. There have also been cast-in-place post-tensioned projects as well as conventionally reinforced precast projects. The following sections outline the recent research efforts in Precast Prestressed Concrete Pavement (PPCP).

1.2.1. FHWA CONCRETE PAVEMENT TECHNOLOGY PROGRAM (CPCT) TASK 58

The Federal Highway Administration has been proactive in promoting the development of precast pavement technology. FHWA established the Concrete Pavement Technology Program (CPTP) Task 58, "The Use of Precast Concrete Panels to Expedite Highway Pavement Construction." to forward areas in research, development, and technology-delivery activities. The fundamental goal is to foster innovation and

improve the performance and cost-effectiveness of concrete pavements, ultimately reducing user delays (Tyson and Merritt 2005).

Aggressively, FHWA spearheaded funding for two key pilot projects. The first was on a frontage road in Georgetown, TX in 2002. The second project, completed in 2004, was in El Monte, CA. Other states involved in the program include Missouri, Indiana, and Iowa. Each project has unique aspects of design and construction, exploring the full realm of feasibility issues. These projects will be discussed in detail later. The latest pilot project, taking place in Missouri along Interstate 57 near Sikeston, is the focus of this thesis.

1.2.2. MISSOURI PRECAST PAVEMENT PROJECT

Missouri committed to a pilot project in early 2004 by jointly funding a new test section (with FHWA) located on the northbound lanes of I-57 near Charleston, MO. The main objective was to build on technologies from previous projects with variations in design and embedded instrumentation.

During the development stages (Jan 04-Jan 05), parties from FHWA, Transtec Group, Missouri Department of Transportation (MoDOT), the precast industry, and the University of Missouri-Columbia met to discuss logistics. Contractors and project managers were inexperienced with this new technology. Therefore, communication and cooperation became a collective goal for each member. Fabrications issues were discussed by the precasters. Constructability issues were addressed by contractors. The design was drawn up and developed by the Transtec Group from Austin, TX. Finally, a system was developed similar to California's in geometry but different than both previous projects in construction.

1.3. OBJECTIVES OF INSTRUMENTATION

The Missouri pilot project on I-57 near Charleston, MO is the first precast prestressed concrete pavement in the Midwest. It was also the first opportunity for the University of Missouri-Columbia to undertake an instrumentation program on precast concrete pavement. Previous experience with high levels of instrumentation (on an HPC bridge in 1998) proved to be very useful (Eatherton 1999).

1.3.1. NEED FOR EXPERIMENTAL INVESTIGATION

This project is aimed at evaluating the performance of the precast prestressed pavement system subject to more adverse conditions of weather (severe variation in thermal loading in conjunction with use of deicing salts) and traffic (interstate versus frontage road) than the earlier projects. It also includes extensive embedded instrumentation to measure temperatures, strains and strand loads and incorporates automation to allow real-time monitoring during service. As discussed later in the literature review, earlier projects contained minimal amounts of instrumentation and performance evaluation equipment.

Strain and thermal measurements during all stages of construction and in-service will help prove or disprove assumptions made during design and development. These performance statistics will help develop design standards as well as add a level of confidence to future evolutions in PPCP technology.

1.3.2. GENERAL INFORMATION

As stated earlier, the primary goal of the instrumentation program is to develop data that will allow optimization of relevant design parameters and procedures. Specific

goals within this objective include (Gopalaratnam 2004; Gopalaratnam, Donahue et al. 2006):

- Study early age behaviors of prestressed panels. Parameters to investigate include; hydration and shrinkage effects, potential residual stresses, transfer of pre-tensioning, and handling stresses.
- Understand behavior of joint, anchor, and base panels at various stages of construction and service including post-tensioning operations.
- Study prestress losses during post-tensioning and under service conditions.
- Evaluate the overall performance of individual panels and the interaction of the panels within slabs. Specifically curling at joints, chloride ingress, performance under traffic loads, and daily and seasonal thermal effects.

Due to the broad scope of research objectives, conclusions and results are currently summarized in two separate texts. This thesis will focus on the instrumentation, early age performance, and in-service performance of the panels themselves. A companion thesis written by Brent M. Davis titled Evaluation of Prestress Losses an Innovative Prestressed Precast Pavement System will thoroughly cover material studies and theoretical prestress losses. A future thesis, by Grant Luckenbill, will seek to tie theoretical predictions to long-term service performance as well as examine behavior over a wider range of seasonal variations.

1.3.3. CURING AND EARLY AGE PERFORMANCE

One specific objective of the instrumentation program is to measure curing temperatures and corresponding strains. Higher cement contents in conjunction with

steam curing create large internal temperatures during hydration. Rapid hydration means accelerated autogenous and drying shrinkage. After final set, the concrete begins behaving like a typical solid, expanding and contracting with respective increases and decreases in temperature. The geometry of the PPCP panel has a high surface area to volume ratio compared to most precast items and is not conducive for overcoming frictional restraint. This in combination with thermal gradients may cause residual strain in the panels. It is the goal of this program to measure thermal gradients and strains which in turn will allow a better understanding of early-age residual stress levels.

1.3.4. TRANSFER OF PRETENSIONING FORCE

Transfer of pretensioning force is a critical loading stage in the life of the panel. Much of the transfer techniques used today has been learned from experience (Eatherton 1999). It is therefore necessary to monitor the strains produced during transfer to ensure the process does not induce cracking. The panels for the Missouri pilot project were designed with no eccentricities in pretensioning force. The strands were draped to follow the transverse cross-section (see Figure 3.12). Experimentally measured strains will be compared to analytical predictions. Measured strains will show residual eccentricities that may exist throughout the cross-section which in turn may foster future specification refinements.

1.3.5. TRANSFER OF POST-TENSIONING FORCE

The post-tensioning is just as critical as pretension transfer for similar reasons. For the Missouri project, the post-tensioning strands are spaced evenly across the longitudinal cross-section (see Figure 3.3). This even spacing creates an evenly distributed line load across the sloped area. Because the force is equal and the area

decreases toward the edges, the stress and strain is greater at the edges of the pavement. Strain measurements will seek to validate this assumption as well as explore frictional losses in both the ductwork as well as panel/sub-grade interface. Strain measurements and frictional losses in the concrete and the post-tensioning strands themselves will be compared to theoretical values.

1.3.6. IN-SERVICE PERFORMANCE

The influence of ambient temperature fluctuations controls a large portion of the design (Merritt, McCullough et al. 2000). Once each panel is post-tensioned, they become a composite 250' long section. Thermal displacements are compounded and increase exponentially. This is more critical during decreases in temperature because the slab contracts. As the slab contracts frictional forces will cause tensile strains. Conversely, expansion will create compressive strains (not as concerning for concrete). In-service investigation will show thermal and corresponding strain variations. This thesis will discuss strains from traffic and daily/seasonal temperature changes as well as compare measured thermal strains to theoretically calculated magnitudes. Global movement of the sections due to thermal or sub-grade moisture variations and consolidation will be surveyed. The overall objective will be to reinforce design procedures and assumptions as well as provide performance evaluations.

1.3.7. LONG-TERM PERFORMANCE

Long term performance will consist of comparisons between creep and shrinkage prediction models and those losses observed in the field. Seasonal rather than just daily thermal variations will be observed and compared. Early cracking or signs of

deterioration will be noted. As stated earlier, the majority of this information will be compiled in a future thesis by Grant Luckenbill.

1.4. ORGANIZATION OF THESIS

The primary objective of this thesis will be to describe the precast prestressed concrete pavement project, instrumentation, and results from the Missouri pilot project on I-57 near Charleston, MO.

Chapters 1-3 introduce the subject matter. Chapter 1 provides information on how the technology has evolved as well as the overall need for PPCP. It also describes the need for an instrumentation program and the objectives involved. Chapter 2 discusses a review of previous projects and helps provide a background on the technology and known research to date. Chapter 3 discusses specifications explicit to the construction of the Missouri project.

Chapter 4 discusses the experimental program and how it fits in with the procedures and specifications presented in chapter 3.

Chapter 5 briefly outlines the material properties of the precast panels.

Chapters 6-9 present results from the experimental investigation. They are divided in to four important stages in the life of the precast panel: hydration and early age response, stress transfer, post-tensioning, and in-service performance. These chapters present experimental data with explanations and analysis as well as comparisons of theoretical values.

Chapter 10 presents a summary of the results, conclusions, and recommendations for further work.

2. BACKGROUND INFORMATION

2.1. EVOLUTION OF PRECAST ROADWAY PANELS

The main focus of the literature review is to gain an understanding of the innovative topic of precast prestressed pavement panels. Because this is a new field, limited information is available. The review is expanded to include cast-in-place prestressed pavement and conventionally reinforced precast panels. This information can provide valuable insight into concepts that can be used for precast prestressed concrete pavements. The following sections provide background information on the evolution of precast prestressed concrete panels as well as the benefits of rigid pavement versus flexible pavement.

2.1.1. INTRODUCTION—RIGID PAVEMENT VS. FLEXIBLE PAVEMENT

Ridged pavement comprises approximately 7% of our nation's roadway system (Muench 2004). The advantages of rigid pavement compared to flexible asphalt pavement include (Davis 2004):

- 30 plus year expected design life
- The requirement of only two main layers—base and surface course
- The ability to sustain a high number of Equivalent Axle Loads (ESAL's)
- High modulus allows for more efficient load distribution

Corridors with heavy truck and traffic volumes are traditionally constructed with rigid pavement. They comprise the most widely used roadways in the nation, facilitating

interstate commerce at reduced maintenance and user costs (compared to asphalt pavement).

As durable as rigid pavement may be, increases in tire pressures, truck traffic, de-icing salts, and thermal fatigue continually diminish the design life. Major arterial highways connecting suburbs to central business districts and the roads in between are very important to commuters. Current design practices can cause roadways to be shutdown for long periods of time due to construction, causing huge user delays and therefore increased costs (Merritt, McCullough et al. 2000). Although flexible pavements can be constructed quickly, they require more maintenance and in turn more down-time. Decreasing replacement frequency is a major goal in urban areas, and at this time flexible pavement replacement frequency is much higher than rigid pavements (Davis 2004). New and more effective methods of replacement/rehabilitation of rigid pavement are needed to help alleviate delays associated with construction activities.

The use of prestressed, precast panels for the replacement of damaged or un-repairable roadways may be the answer to alleviating user costs. Precast technology has been used in building and bridge construction to help minimize construction time; therefore the use of precast panels on roadways is currently being investigated (Merritt, McCullough et al. 2000). Recognizing the importance of knowledge gained by existing rigid pavement design, this review will focus on current design practices of rigid pavements and discuss the benefits and technology in place for prestressed, precast roadway panels.

2.1.2. AASHTO DESIGN PROCEDURE

The AASHTO Design Guide is a commonly used resource for pavement design. The general design steps outlined within the manual can be summarized as follows:

1. Calculate effective modulus of the subgrade reaction (k). Factors affecting k include: type of base, thickness, loss of support, and depth to bedrock (AASHTO 1993).
2. Determine the required slab thickness. AASHTO provides a nomograph for estimating thickness. Several parameters are required, however: traffic, reliability factor, standard deviation, serviceability loss, elastic modulus of the concrete, modulus of rupture, load transfer coefficient, and drainage coefficient.
3. Design the joints. The spacing of contraction joints will generally be determined by local site conditions. Expansion joints are provided to mitigate buckling due to excessive expansion

2.1.3. CAST IN PLACE TECHNOLOGY

The AASHTO Guide for Design of Pavement Structures demonstrates commonly used design practices for rigid pavements. Three commonly used techniques exist for rigid pavement construction: Jointed Concrete Pavement (JCP), Jointed Reinforced Concrete Pavement (JRCP), and Continuously Reinforced Concrete Pavement (CRCP) (Davis 2004).

2.1.3.1. JOINTED CONCRETE PAVEMENT

Jointed concrete pavement contains no continuous or tensile reinforcing steel. Joints are spaced 15-20 ft (4.6-6.1 m) apart to control natural cracking. Smooth dowels

are embedded at every joint in to transfer load from one slab to the other (Figure 2.1). Pavement thicknesses range from 8-14 in. (20.3-35.6 cm) (ACPA 2004). The base is typically a drainable layer of aggregate or a gap graded asphalt. This type of construction is very popular in throughout the Midwest and Missouri.

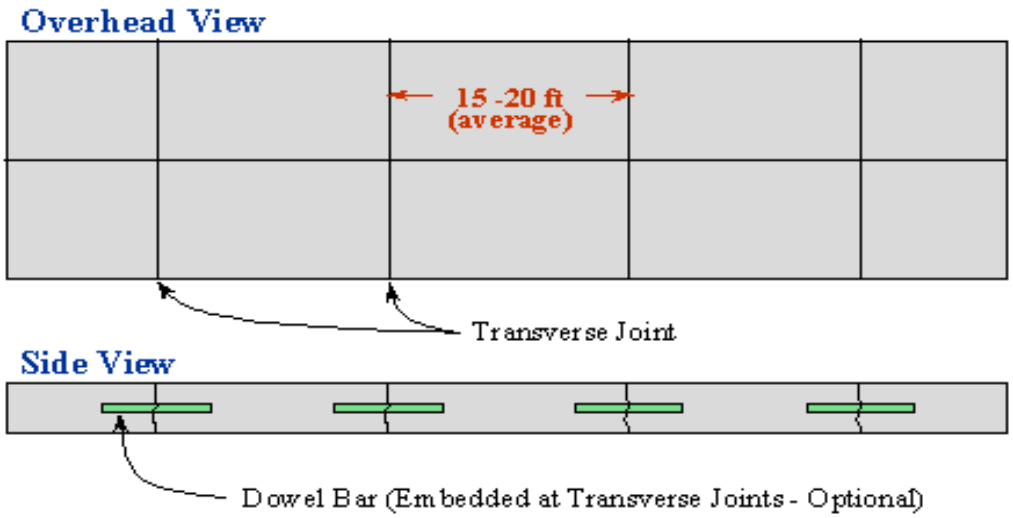

Figure 2.1 – Plan and section of jointed concrete pavement (ACPA 2004)

2.1.3.2. JOINTED REINFORCED CONCRETE PAVEMENT

Jointed reinforced concrete pavement is very similar to JCP. The main difference is that welded wire mesh is placed continuously within the cross-section. The joints are also spaced 30 ft (9.1 m) or farther apart. Cracks form between the joints and are held together by the welded wire mesh. Dowels are also installed at the joint locations (ACPA 2004). Figure 2.2 shows how cracks form between the doweled joints.

AASHTO design of JRCP consists of a nomograph that requires the slab length, steel working stress, and friction factor. It is used in selecting the transverse and longitudinal reinforcement in JRCP (AASHTO 1993).

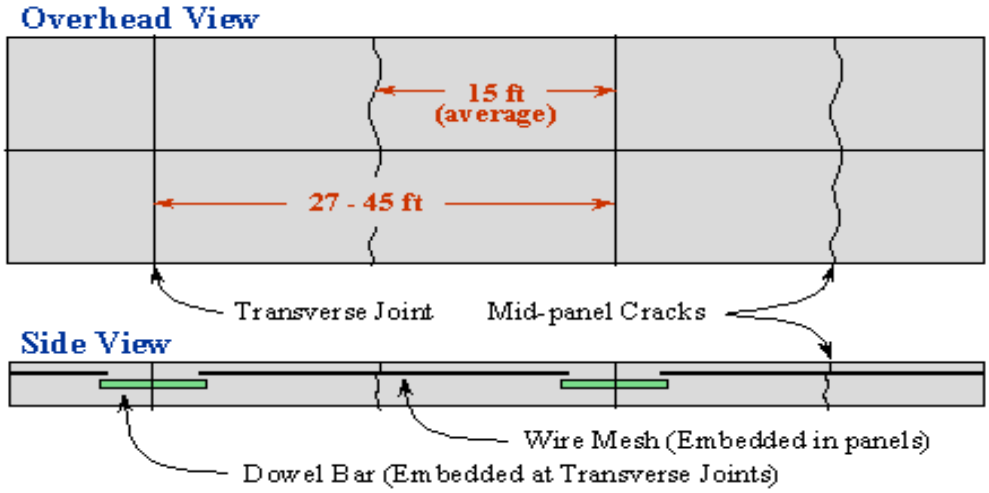

Figure 2.2 - Plan and section of JRCP (ACPA 2004)

2.1.3.3. CONTINUOUSLY REINFORCED CONCRETE PAVEMENT

Continuously reinforced concrete pavement requires no transverse joints. Cracks are expected and generally occur at 2-5 ft (0.6-1.5 m) increments (Figure 2.3). Generally, the crack spacing is predicted during design. Continuous reinforcing steel holds the crack widths together. This consists of continuous rebar, not welded wire mesh. Therefore, the cost of CRCP is much higher than JCP and JRCP. This is often justified by it long-term durability and performance (ACPA 2004).

Longitudinal reinforcement for CRCP requires different design inputs than JRCP. They include: direct tensile strength of the concrete, shrinkage of the concrete at 28 days, thermal coefficient, bar diameters, steel thermal coefficient, and design temperature drop. The additional input is required because the nature of the design requires a target crack spacing along the length of the roadway (AASHTO 1993).

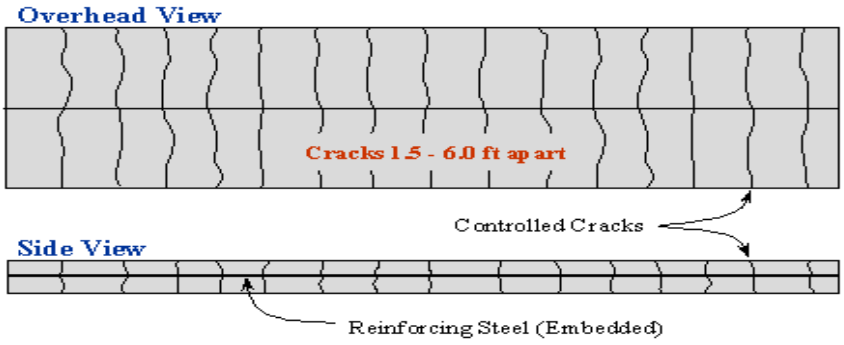

Figure 2.3 - Plan and section of CRCP (ACPA 2004)

2.1.3.4. ISSUES WITH CURRENT CAST-IN-PLACE CONSTRUCTION

Although rigid pavements remain the most suitable roadway for our nation's most traveled corridors, there are issues that can be improved.

Optimizing the use of materials is an important part in improving rigid pavements (Davis 2004). Rigid pavements currently require high volumes of concrete to achieve required design thickness (between 8-14 inches). Currently, pavements need to be this thick in order to reduce the amount of steel (tensile reinforcement) in the cross-section. The addition of a confining or compression force to the pavement in both directions would help reduce thickness requirements. An 8 inch (20.3 cm) slab that's as strong and durable as 14 inch (35.6 cm) thick pavement would greatly reduce material costs (Davis 2004), (Merritt, McCullough et al. 2000).

The on-site curing process is of some concern as well. Weather conditions can change without warning. Sudden cold/hot weather, rain, or other inclement threats may

compromise the integrity of the concrete. Protection from these elements would reduce risk and increase longevity.

Concrete cast directly against the base takes the shape of the base. This causes the underside of cast-in-place panels to be rough, increasing the coefficient of friction between the concrete and sub-grade. When the concrete cures it shrinks (Earney, Gopalaratnam et al. 2006). This in conjunction with thermal expansion and contraction can cause residual stresses to build up in the matrix, leading to accelerated deterioration (Davis 2004).

Cast in place concrete pavement takes several days of curing before it can be opened to traffic. This creates lane drops on major roadways and intersections. Because several days are required for curing, these lanes are down during peak traffic periods. Development of more efficient technology is essential to help mitigate resulting user costs.

2.1.4. USE OF PRESTRESSED, PRECAST CONCRETE PAVEMENTS

In light of the problems with current cast-in-place technology discussed in the previous section, precast prestressed concrete pavements may provide a practical alternative. This evolving technology may mitigate most all of the previously discussed issues.

Precast prestressed pavement will maximize the use of materials. Although there will be voids under precast pavement, the residual prestressing forces will provide enough strength to span these inconsistencies in the subgrade. Increasing the prestressing force helps the panel act like a thicker pavement, therefore, decreasing the amount of concrete required (Merritt, McCullough et al. 2000).

Casting and curing can be done in a controlled environment. Panels can be cast under ideal conditions. Casting can be monitored to help reduce the affects of shrinkage and development of residual stresses (Davis 2004). Curing can be accelerated with steam. Design strength can be achieved in only a couple of days. Casting can also take place during anytime of the year, well ahead of the mandated construction schedule.

High volume intersections and roadways can be fully repaired during off-peak hours. Panels constructed offsite can be placed and post-tensioned at night and then opened to traffic the next morning thus reducing user costs. Table 1.1 in the previous chapter shows the economic advantages of precast pavement. They are advantageous only in areas with high traffic volumes where user costs can overtake the difference in construction costs.

Precast panels have the ability to transfer load more efficiently than conventional cast-in-place sections. When cracks become larger than 0.03-0.04 inches (0.76-1.02 mm), the pavement must rely on aggregate interlock to transfer load to either side of the crack opening (Merritt, McCullough et al. 2000). The ability to transfer load decreases as the crack width increases. The prestressing force helps control crack widths by providing confinement. Load is transferred more efficiently due to the added shear friction at the crack interface (Merritt, McCullough et al. 2000).

2.2. PRECAST AND PRESTRESSED ROADWAY SYSTEMS IN SERVICE

These sections outline specific projects that have contributed to the research and development of precast prestressed concrete pavements. Only projects with published literature are presented. Others may exist that have not been topics of published works. Three types of projects are presented and discussed: prestressed (post-tensioned)

pavements, precast pavements, and prestressed precast pavements. Prestressed precast pavements comprise current research, development, and implementation efforts.

2.2.1. PRESTRESSED PAVEMENT PROJECTS

The initial application of prestressed concrete pavement began in the 1940s in Europe and soon spread to Japan (Chavez, McCullough et al. 2003). Domestic projects involving pretensioning cast-in-place concrete roadways began in the mid 1970s. Stressing operations took place on-site and the concrete was cast over the anchored strands. This required much of the equipment commonly found in precast yards for strand anchorage to be designed for on-site use. The following sections summarize several domestic projects of this nature. Although they may exist, more recent published case studies have not been found on cast-in-place, prestressed pavements.

2.2.1.1. FULL SCALE PRESTRESSED PAVEMENT IN PENNSYLVANIA (1973)

In 1973, the Pennsylvania Department of Transportation (PennDOT) cast the first full-scale prestressed concrete pavement in Pennsylvania. The purpose of the project was to employ prestressing techniques on a production basis (Brunner 1975).

The Pennsylvania project consisted of 23 post-tensioned slabs, each 600 ft (183 m) long. A total of 13,232 ft (4033 m) was paved using a slip-form paver. Each panel was 24 ft (7.3 m) wide and 6 in (15.24 cm) thick. Twelve 7 wire prestressing strands were used in each panel. The concrete was cast on a 6 inch bituminous base. Two layers of polyethylene sheeting were used to reduce friction. Prior to laying the polyethylene sheet, sand was swept on the base to further mitigate friction between the panels and sub-grade (Brunner 1975).

PennDOT used an innovative joint detail (Stover 2004). Three feet was left open between the slabs (the 24' side) for a jacking space. The strands were stressed and the space was filled with concrete. The slab ends were put together with interlocking beams to prevent faulting. After two years, the ride quality of the concrete pavement was excellent. The joints also functioned well, absorbing the expansion and contraction of the slabs (Brunner 1975). After 26 years, although it is reported to have performed reasonably well, cracking, spalling, and joint deterioration have been noted. The pavement is now becoming a maintenance issue and will be rehabilitated soon (Chavez, McCullough et al. 2003).

2.2.1.2. FULL SCALE PRESTRESSED PAVEMENT IN ARIZONA (1977)

In 1977, a project in Arizona became one of four full-scale experiments on prestressed pavement. The others were constructed in Virginia, Pennsylvania, and Mississippi (Powers and Zaniewski 1987).

The Arizona project consisted of a 1.2 mile (1.93 km) section of prestressed pavement on Superstition Freeway in Tempe, Arizona. Thirty prestressed slabs, each 31.5 ft (9.6 m) by 6 in (15.24 cm) thick, were cast on a lean concrete base. Two 12 ft (3.7 m) lanes and one 7.5 ft (2.3 m) shoulders made up the cross section of the pavement. Prestressing reinforcement consisted of sixteen 1/2 in. diameter prestressing strands that were post-tensioned.

Conventionally reinforced concrete joint slabs were placed between the prestressed slabs to facilitate prestress jacking operations (Powers and Zaniewski 1987). Hot Arizona climates meant that joint design was critical. Though a movement of about 1.5 in (3.81 cm) was expected, joints were designed with an additional 0.5 in. gap to

allow for extra expansion. The joints were sealed with a neoprene seal and steel dowel bars were used for load transfer. In order to reduce friction, the base was topped with a sand leveling course and polyethylene sheet similar to the Pennsylvania project. The area was paved using a slip-form paver (Powers and Zaniewski 1987).

Long-term evaluation showed several problems with the design. From the beginning, the ride quality was worse than the ride quality for conventionally reinforced concrete (Powers and Zaniewski 1987). Also, considerable problems were found with the joints namely considerable spalling. This distress was attributed to poor consolidation of concrete around the joint hardware in conjunction with high stresses caused by truck loading. Truck traffic was higher than originally estimated. Design traffic was 26,000 ADT with 1% trucks, but after nine years actual traffic was 98,000 ADT with approximately 3-4% trucks. Additional spalling was noted at mid-span transverse cracks. Also, the concrete developed longitudinal cracks, corner breaks, transverse cracks and other visual signs of distress (Powers and Zaniewski 1987).

2.2.1.3. PRESTRESSED CONCRETE OVERLAY AT O'HARE AIRPORT (1980)

In 1980 a prestressed concrete overlay was placed on Runway 8R-27L at Chicago's O'Hare International Airport. The pavement was designed withstand loading from large 747 aircraft (Stover 2004).

The main surface was constructed over a 12 in (30.5 cm) thick reinforced concrete base pavement and 18 in (45.7 cm) of crushed limestone (bottom). Around 5% of the base pavement was removed. A 1.5 in (38.1 cm) bituminous leveling course was added over the bottom concrete slab. Two layers of polyethylene sheeting were laid atop the leveling course. The overlay was 800 ft (244 m) by 150 ft (46 m) and varied from 8-9 in

(20.3-22.9 cm) thick (east to west for drainage). The varying thickness was accounted for with a 1 in. sleeper slab on the west side. The pavement was placed in 400 ft (122 m) sections with six 25 ft (7.6) paving lanes. (Two sections of 400 ft and six sections of 25 ft make 800 by 150 ft.) Each of the 400 ft. lengths had no transverse joints (Rice 1981).

The slabs were post-tensioned in both the longitudinal and transverse directions. The prestress design dictated 400 psi (2760 kPa) and 225 psi (1550 kPa) for a 20 year design life in the longitudinal and transverse directions respectively. Grout was pumped into the ducts to fill the voids after the stressing operations. The joints were designed to allow for 1.5-2 in (3.8-5.1 cm) of movement. This was accomplished using specially designed joints composed of structural steel members at the edges. The joints were then sealed with a flexible fabric clamped to the steel (Rice 1981).

The project was deemed successful by the Federal Aviation Administration. It was completed within a 60 day time limit, even with heavy rains. After a year of use, the section remained in good condition (Rice 1981). During the last report in 2000, the pavement was found to be still performing well with no significant signs of distress or maintenance concerns (Chavez, McCullough et al. 2003).

2.2.1.4. CTR PILOT PROJECT IN MCLENNAN COUNTY, TEXAS (1985)

In 1983, the University of Texas Austin's Center for Transportation Research (CTR) conducted research studies on design and construction of prestressed concrete for pavement applications (Cable, McCullough et al. 1986). Their report outlines ideas to migrate from cast-in-place prestressed concrete to construction of precast prestressed (post-tensioned and pretensioned) concrete panels. Many of the concepts presented in the report, such as central stressing, transverse pretensioning, and precast joint panels were

very innovative (Stover 2004). They helped give birth to modern advancements in precast prestressed pavements.

In 1985, the University of Texas Austin's Center for Transportation Research (CTR) began a pilot project in McLennan County, Texas. The objective of the prestressed, cast-in-place pavement design was to test some of the concepts presented in the report, as well as other ideas for improving prestressed concrete pavement (Cable, McCullough et al. 1986).

The first concept tested was central stressing. The concept of a central stressing location is an elegant yet simple concept. Prestressing strands from two adjacent sections are jacked against each other in one central location. This process eliminates the need for gap slabs, making the pavement continuous. CTR also tested a new expansion joint detail that had steel support in the form of Nelson bars, a neoprene seal, and dowels for load transfer. A similar joint was used on future precast projects. A single polyethylene sheet was used beneath the slab because of constructability, effectiveness, and economics (Merritt, McCullough et al. 2000).

Another technique they tested was looping post-tensioning strands, as shown in Figure 2.4. This helped provide transverse prestressing to prevent longitudinal cracking. The post tensioned strands also allowed for placement of separate longitudinal slabs by serving as a means to tie the slabs together longitudinally (Merritt, McCullough et al. 2000). This pilot project paved the way for additional testing and migration to precast prestressed panels.

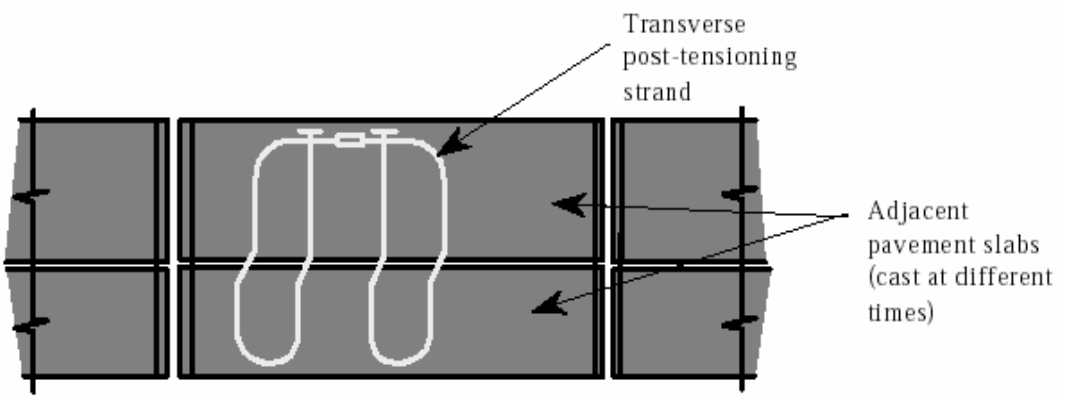

Figure 2.4 - Looped post-tensioning tendons (Merritt, McCullough et al. 2000)

2.2.2. PRECAST PAVEMENT PROJECTS

Unlike prestressed cast-in-place pavements, precast pavements (whether pretensioned or conventionally reinforced) have not been around as long. Precast technology is beginning to gain popularity because the road can quickly be reopened to traffic. Most of the work with precast panels has been accomplished by private firms or state Departments of Transportation (Stover 2004). Considering this, little information has been published. The projects discussed in the next sections are all unique and provide a background for the many uses of precast technology.

2.2.2.1. FULL DEPTH REPAIR ON US 287 NEAR FORT COLLINS, COLORADO (2000)

In December of 2000, the Colorado Department of Transportation (CDOT) used full depth conventionally reinforced precast panels to restore a section of US 287, near Fort Collins, CO. Precast panels were used because of the high traffic volumes and need for expedited construction. Three cracked panels measuring 15 ft x 12 ft x 10 in (4.6 m x 3.7 m x 25.4 cm) were replaced in the restoration project. Expanding foam called Uretek

was used to raise and level the panels to the existing level. Fiberglass panels (also made by Uretek) were then used to "stitch" the sides of the existing and new panels together. The $50,000 pilot project took only three days. Each replaced section was reopened to traffic the same day. CDOT and others in the pavement industry were impressed with the speed of the pavement restoration (Proctor 2000). A picture of the placement is shown in Figure 2.5. No information on the service performance of the restoration is available in published literature.

Figure 2.5 - Placement of precast panels on US 287 in Colorado

2.2.2.2. PRECAST PANELS ON TAPPAN ZEE TOLL PLAZA, NEW YORK (2001)

In 2001 precast panels were used on the Tappan Zee Toll Plaza in Tarrytown, NY. The toll plaza is made up of 13 toll lanes and serves as many as 165,000 vehicles per day. Due to the high traffic volumes, road construction causes large delays and lost user time.

In order to avoid this, the Yonkers Contracting Corp. decided to use conventionally reinforced precast panels.

Roughly 1,064 panels were cast under a demanding time schedule. Work could begin at 10:00 p.m., and the road had to be reopened to traffic by 6:00 a.m. the following day in order to avoid monetary penalties. The panels were cut one night and then replaced the following night.

Yonkers used the Fort Miller Company's Super-Slab panel replacement system (FHWA 2003). According to the Fort Miller Company, Super-Slab is a modular precast concrete slab-on-grade pavement alternative that is fully interlocking and can be installed overnight (Company 2001).

A laser-guided screed was used to level the sub-grade to within a 0.1 inch (2.5 mm), thus helping mitigate the potential for voids under the slab. Grout was also pumped under the slab to fill any voids between the slab and the subgrade. The typical slab length for the toll plaza project was 18 ft (5.5 m). Widths varied from 7-12 ft (2.1-3.7 m). The panels had longitudinal ties on one side (to make the male end) and matching slots on the others (to create the female end). The joints were then sealed with silicone (FHWA 2003). Although it may exist, no information on the current condition of these panels was found. Figure 2.6 and Figure 2.7 show pictures of the construction at the Tappan Zee Bridge Toll Plaza in Tarrytown, New York.

Figure 2.6 - Removal of old concrete at Tappan Zee Toll Plaza (Merritt 2002)

Figure 2.7 - Installation of new panels at Tappan Zee Toll Plaza (Merritt 2002)

2.2.2.3. PRECAST PANELS AT WASHINGTON DULLES AIRPORT (2001/2002)

In June 2001, several panels were replaced at Washington Dulles International Airport. Panels ranged in size from 12.5 ft x 12.5 ft (3.8 m x 3.8 m) to 13 ft x 20 ft (4 m x 6 m) and were all 14 in. (36 cm) thick. Panels were designed with 'stitches' for dowel at the joints. These saw-cut slots or 'stitches' were 36 in. (91 cm) long and 8 in (20 cm) deep. Dowels were installed in the stitches and then filled with a non-expanding polymer to bond the inserts to the slots. The largest advancement came with the use of an expanding high density polyurethane polymer mixture between the panels and the existing base. This was used to level the panels to match adjacent panel and existing pavement elevations. This technique proved to accurately lift the panels as well as provide a stable bearing surface (Farrington, Rovesti et al. 2003).

In October 2002 a similar project was tested at Washing Dulles Airport. Six panels four 25 ft x 25 ft (7.6 m x 7.6 m) and two 25 ft x 40 ft (7.6 m x 12.2 m). Each was 15 in. (38 cm) thick. The base was graded to slope (to drain water) instead of the panel cross-section. This project used conventional base material with grouted dowels and subgrade similar to many other projects (Switzer, Fischer et al. 2003).

2.2.2.4. PRECAST PANELS ON TAXIWAY D-D AT LAGUARDIA AIRPORT (2002)

September of 2002 the New York/New Jersey Port Authority decided to use precast panels on Taxiway D-D at New York's Laguardia International Airport. Two different panel designs were installed over an existing asphalt base. The first design consisted of 16 in (40.6) thick conventional reinforced precast concrete. The second design was 12 in (30.5 cm) thick and was prestressed. Both test areas were 100 ft. x 50 ft (30.5 m x 15.2 m) with individual panels 12 ft x 25 ft (3.7 m x 7.6 m). Similar to

previous projects, grout was pumped under the panels to fill voids. Setting bolts were also installed in each panel. This allowed the panel to be adjusted flush with adjacent panels. It also provided a void to fill during pressure grouting.

Male and female doweled ends were created similar to the Tappan Zee project. These ends were then filled with a quick setting concrete (Chen, Murrell et al. 2003).

Each design took 36 hours for construction (Figure 2.8). The prestressed design was better only in that it was lighter and easier to handle. Both designs have been visually monitored and are performing well with little signs of deterioration (Chen, Murrell et al. 2003).

Figure 2.8 - Installation of panels at Laguardia Airport (Authority 1997)

Figure 2.9 - Precast panels in service at Laguardia Airport (Authority 1997)

2.2.2.5. PRECAST REPAIR TRIALS ON HWY 427 TORONTO, ON, CANADA (2004)

In November of 2004, the Ministry of Transportation Ontario decided to carry out three precast pavement repair trials on an express lane of Highway 427 running through Toronto, ON, Canada. Three methods tested were: the Michigan method, Intermittent Super-Slab® method, and Continuous Super-Slab® method. The latter two methods compose a proprietary design by the Fort Miller Co., Inc., Schuylerville, NY. Each method differed in base preparation and installation (Lane and Kazmierowski 2006).

Three full depth precast concrete slabs 6.6 ft x 12 ft (2 m x 3.65 m) in plan and 9 in. thick were used for both the Michigan Method and the Intermittent Method. The Michigan method used three dowels at each wheel path cast into the precast slab at 12 in. on center. Following removal of the existing concrete, slots were cut into the existing pavement to accommodate the dowels in the precast panel. A cementitious grout was

placed on the existing base prior to setting the precast slab. The slab was set and the exposed dowels were grouted into the precast slots to connect old and new pavements (Lane and Kazmierowski 2006).

For the Intermittent Method, blockouts were cast into the precast slab to accommodate the dowels. Four dowels were installed into the existing pavement (at the wheel paths) at 12 in. on center. The existing base was leveled with precision graded crusher screenings and then compacted. The slab was set and dowels were grouted through ports in the precast slab. Bedding grout was then pumped into the base, through similar ports, to remove voids (Lane and Kazmierowski 2006).

An 82 ft. (25 m) long section of the Continuous Method was constructed. Dowels and blockouts (male and female) were cast alternately into several precast slabs in order to form modular puzzle pieces. The base was prepared with crusher screenings and bedding grout similar to the Intermittent Method. Dowels were drilled and epoxied into the existing pavement at each end (Lane and Kazmierowski 2006).

Overall pavement and construction trials went well. No cracking, spalling, or rocking was documented. The work was also carried out within fast-track time frames. Some surface tolerances were not met but could have been mitigated with diamond grinding (Lane and Kazmierowski 2006)

2.2.2.6. PRECAST PANELS ON TH 62 IN MINNESOTA (2005)

Another application of the Fort Miller Company's Super-Slab ® system is in-service in Minnesota. The repair segment consists of a 218 ft (66 m) stretch of pavement 12 ft (3.7 m) wide. Each of the eighteen precast units was 12 ft x 12 ft (3.7 m x 3.7 m) and 9.5 in. (24 cm) thick. The panels were tied together using dowels embedded into

male and female ends at each side of the precast panels. The panels were allowed to float and were not doweled into the existing pavement longitudinally. Stone dust was used over the existing base to help level the precast panels. Grout was pumped both around the dowels and under the slab to help reduce voids. Panel placement averaged 14 minutes per panel (Mn/DOT 2005).

2.2.3. PRESTRESSED PRECAST CONCRETE PAVEMENT (PPCP) PROJECTS

The combination of precast and prestressed (post-tensioned and pretensioned) technology for roadway panels has come to fruition only in the past seven years. The first attempt at this occurred in the 1960s in South Dakota, and was unsuccessful (Merritt, McCullough et al. 2001). The University of Texas Austin's Center for Transportation Research came up with the basic concepts of a Prestressed Precast Concrete Pavement (PPCP) (Stover 2004). Recent initiatives from the Federal Highway Administration have helped implement those concepts on several pilot projects including the Missouri project.

2.2.3.1. PPCP ON I-35 IN GEORGETOWN, TX (2001)

The Texas pilot project was implemented on a frontage road along I-35 in Georgetown, Texas. CTR partnered with the Texas Department of Transportation (TxDOT) and Granite Construction.

The project consisted of 2300 ft (701 m) of PPCP designed to withstand interstate type loading. Although each panel was 8 inches thick, it behaved like a 14 inch pavement due to the prestressing forces. Full width panels (36 ft or 11 m) and partial width panels (16 ft. and 20 ft. or 4.9 m and 6.1 m) were placed on both sides of a bridge. A total of 339 (123 full and 216 partial width) panels were used. This project is unique in

that a single cross slope of 2% was used instead of a crown in the center of the panel (Merritt, McCullough et al. 2002).

The precaster was able to construct 10 panels every other day. The panels could be placed on-site at a rate of 25 panels every 6 hours (Figure 2.10 and Figure 2.11). Three types of panels were used for construction: expansion joint panels, base panels, and central stressing panels. The central stressing panel was located at the center of a section. Base panels filled the spaces between the central stressing panel and the joint panels at the ends. Strands were anchored at the joint panels and fed through each side before being jacked at the central stressing panel (Merritt, McCullough et al. 2002).

The panels were placed atop a 2 in (5.1 cm) asphalt leveling course and a single layer polyethylene sheet to reduce friction. Each panel was pretensioned in the transverse direction and post-tensioned in the long direction. The partial width panels were also post tensioned transversely to tie the panels together. The block-outs for post-tensioning were filled with a quick setting concrete. Grout was applied to the tendons, through grout vents cast into the joint panels, central stressing panels and every fourth base panel (Merritt, McCullough et al. 2002).

Visual inspections since construction have documented several cracks. The full width panels cracked longitudinally. This may be attributed to a slight crown in the asphalt leveling course. Two panels also experienced minor shrinkage cracks. Cracks due to stress concentrations were documented around the central stressing pockets, access pockets, and the lifting anchor recesses. Some spalling at the joints was also recorded.

Figure 2.10 - Full width panel placement on Georgetown, TX PPCP (Merritt 2002)

Figure 2.11 - Full width panel placement on Georgetown, TX PPCP (Merritt 2002)

The International Roughness Index (IRI) values for the pavement were higher than normally allowed by TxDOT, however it was decided that diamond grinding did not need to take place (Merritt, McCullough et al. 2002).

This project produced significant advancement in knowledge associated with many aspects of the design from the keyways to the grouting and placement costs (Merritt, McCullough et al. 2002). The success of this pilot project proved that prestressed precast pavement works and has opened the door to future research and implementation (Tyson and Merritt 2005).

2.2.3.2. PPCP ON I-10 IN EL MONTE, CALIFORNIA (2004)

An additional pilot project on I-10 in El Monte, California was created to further develop ideas learned during the Georgetown, Texas project. Unlike the Georgetown project, this section was constructed on interstate pavement (Tyson and Merritt 2005).

The panels are 37 ft (11.3 m) long and 8 ft (2.4 m) wide. The length consists of 27 ft (8.2 m) of driving lane and a 10 ft (3 m) shoulder. The total project length was 248 ft (75.6 m) with 31 total panels placed in two post-tensioned sections. As with the Texas project, the panels were pretensioned transversely and post-tensioned longitudinally. Longitudinal post-tensioning strands were epoxy-coated (fine grit impregnated) strands. Unlike the previous project, however, a 1.5% sloping crown that changed to a 5% slope at the shoulder was cast directly into the pavement cross-section. Figure 2.12 and Figure 2.13 show the construction of the roadway expansion on I-10 in El Monte, California (Tyson and Merritt 2005).

Figure 2.12 - Placement of panel on I-10 El Monte, California

Figure 2.13 - View of expanded roadway on I-10 El Monte, California

2.2.3.3. OTHER DEMONSTRATION PROJECTS

The success of the previous Texas and California projects opened the doors for several other demonstrations projects. Several weigh-in-motion sites in Texas, bridge underpasses in Indiana, an approach slab in Iowa, and the Missouri project headline the proliferation of precast pavement projects in the United States.

Texas Department of Transportation plans to construct several Weigh-in-Motion sites around the state. The first is a 500 ft (152 m) section on U.S. 175 near Dallas, TX. The panel thickness is 10 in. (25 cm) and will have blockouts cast into the slab for installation of weigh-in-motion scales (Tyson and Merritt 2005).

Indiana Department of Transportation will use the precast technology to decrease the pavement thickness under bridge over-passes. Several bridges have been hit by trucks that exceed the maximum clearance height. Prestressed pavement will allow a thinner cross-section and decrease risks involved with cast-in-place overlays (Tyson and Merritt 2005).

2.3. SIGNIFICANCE OF MISSOURI'S INSTRUMENTATION PROGRAM

The Missouri project was slated just after the California project. This project is unique in several ways:

- Panels are stressed from the joints instead of a central stressing panel
- The center of each section is anchored with an anchor panel that consists of dowels embedded into the subgrade
- The panels are full width (38 ft or 11.6 m) and have the crown of the road cast between the driving lanes

- They are subjected to adverse conditions of Midwest weather and de-icing salts in conjunction with heavy interstate truck traffic
- The project is competitively bid. This will help provide more realistic estimates of construction costs.
- High levels of instrumentation are embedded in seven cast panels

Relative to the latest projects, the instrumentation program is the most significant contribution to the evolution of precast panels thus far. Although several projects have included visual performance surveys, no extensive monitoring of stressing operations, thermal variations, or traffic strains have been published on PPCP technology. The current instrumentation program not only monitors daily and seasonal thermal and strain variations, it provides valuable data relative to material performance, visual inspections, and long-term durability surveys.

3. PROJECT INFORMATION AND CONSTRUCTION

Much preparation and detailed specifications are required to develop a PPCP system. The following sections outline project information including design, fabrication, construction and finish work.

3.1. GENERAL INFORMATION

The Precast Prestressed Concrete Pavement (PPCP) test section in Missouri replaced a dilapidated 45 year old section of cast in place concrete just west of Charleston, MO on north bound I-57. (I-57 actually runs east to west at the PPCP section.) . Three specific types of panels make up the PPCP system: base panels, joint panels, and anchor panels.

Each panel is 10'-0" x 38'-0" (3 m x 11.6 m). The 38' dimension is perpendicular to traffic. There is a 4'-0" (1.22 m) inside shoulder, two 12'-0" (3.7 m) driving lanes and a 10'-0" (3 m) outside shoulder. The crown starts between the driving lanes and slopes toward the shoulders at 2% to ensure drainage.

A total of 101 ten foot panels replaced 1000 ft (304.8 m) of conventional cast-in-place pavement. A typical pavement section consists of an anchor panel in the center with 11 or 12 base panels on each side. Joint panels are at the very ends. Each of the four sections is roughly 250 ft (76.2 m) long. Figure 3.1 shows the layout of the four sections of pavement (the highlighted section is heavily instrumented and will be discussed later in detail). Figure 3.2 shows the layout of panels within each individual section.

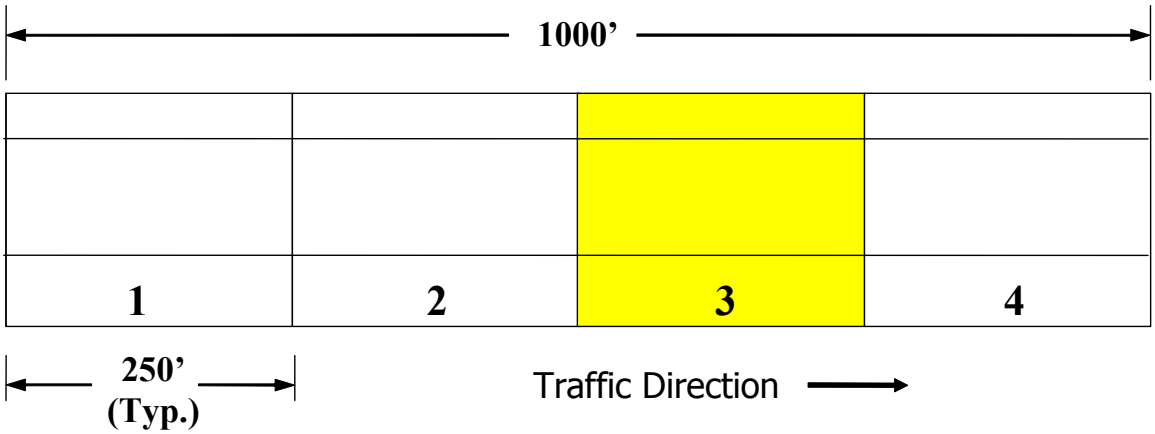

Figure 3.1 – Overall PPCP section layout with driving lanes shown (25 panels per section; Section 3 is heavily instrumented)

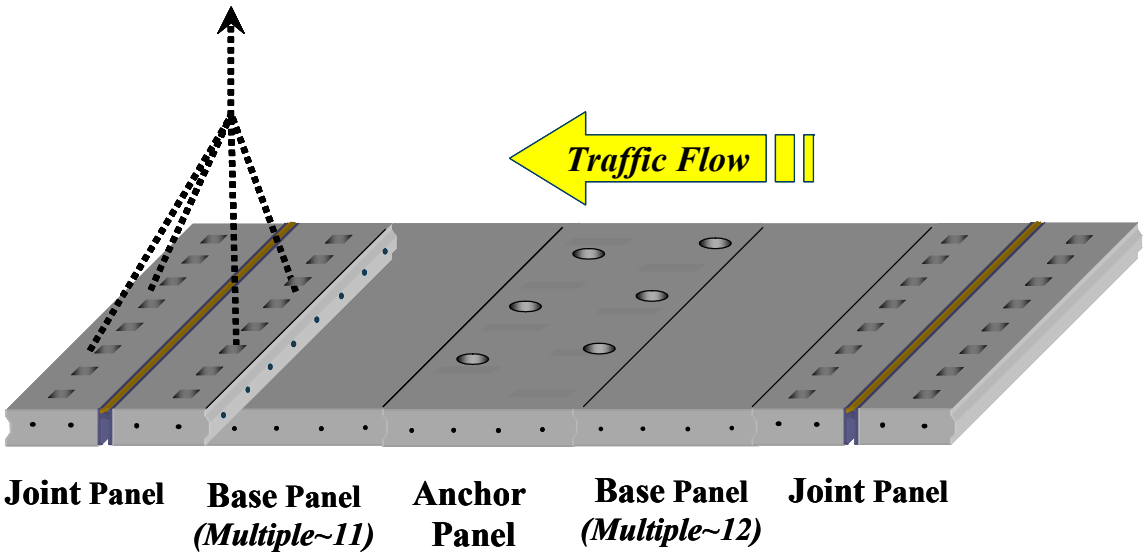

Figure 3.2 – Typical section of PPCP panel assembly and layout

3.2. PANEL DESIGN AND FABRICATION

The Transtec Group from Austin, TX designed the PPCP system consisting of base, anchor, and joint panels. Transtec design drawings can be found in Appendix A. Panel design was funded by FHWA. Like most precast products, full depth PPCP is a detailed operation requiring a great deal of overhead. The following sections discuss specifications and design details relevant to fabrication.

3.2.1. GENERAL INFORMATION AND SPECIFICATIONS

All 101 panels were cast by Concrete Products Incorporated (CPI) in Memphis, TN between mid-October and late December 2005. Each panel is pretensioned in the transverse direction (perpendicular to traffic). Post-tensioning ducts were installed at 2' on center in the longitudinal direction (parallel to traffic) in order to create continuous sections during assembly. The pretensioning and post-tensioning forces will create a compressive 'confining effect' on the matrix of the slab that will reduce tensile stresses, prohibit crack growth, and allow for a thinner section compared to conventional pavement (Tyson and Merritt 2005).

Male and female shear keys were cast into opposite sides of each panel, regardless of type (see Figure 3.3). This provides for vertical load transfer between panels during in-service as well as lines them up during assembly. Match casting the shear keys and producing panels that are interchangeable requires intricate formwork and careful quality control. The following specifications applied to the fabrication of each panel.

- Visual inspection and measurement of formwork was performed by a certified MoDOT inspector before each casting.
- Formwork tolerances were generally 1/8 in (3.2 mm)

- Strength at 28 days was at least 5,000 psi (34.5 MPa)
- Strength before pretension transfer was at least 3,500 psi (24.1 MPa)
- Pretensioning strands were 7-wire 0.5" (1.27 cm) diameter with 270 ksi (1860 MPa) ultimate strength (ASTM A416)
- Initial jacking forces were 75% or ultimate (0.75 x 270 psi = 202.5 psi; 202 psi x 0.153" = 31 kips (138 kN)
- Post-tensioning duct-work could not be out of line (horizontal or vertical) by more than ¼ in (6.4 mm) with individual ends held to 1/8 in (3.2 mm) tolerance.

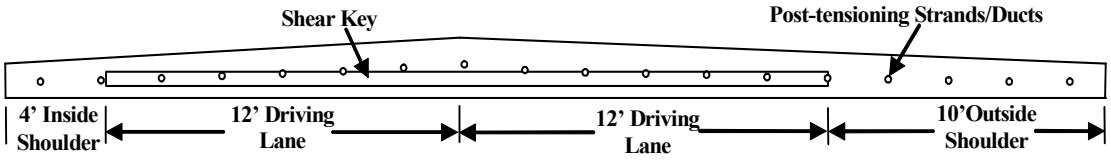

Figure 3.3 – Typical panel section looking with the direction of traffic

3.2.2. FABRICATION PROCEDURE

Panels were cast two at a time on an elevated steel bed. The precast bed used is considered 'self-stressing' in that the initial stress from the strands is transferred into the bed itself (along the entire length) and not resisted by large bulk-heads (see Figure 3.4). Typical day to day operations were as follows:

1. **5:00 am – 8:00 am**: Test strength, steam is shut off, tarp removed, formwork loosened, pretensioning strands cut, panel removed from bed and stacked

2. **8:00 am – 1:00 pm**: Formwork tightened, bed oiled, strands run, strands stressed, ductwork placed, outside rebar placed
3. **1:00 pm – 5:00 pm**: Test air and slump, pour panels, vibrate and consolidate, hand screed, vibratory screed, hand trowel, broom finish, cover, let concrete sit, begin fabricating ductwork for following day, turn steam on before leaving

Figure 3.4 shows the bed after removing the two panels from the night before. If strength was sufficient, panels were typically removed by 8:00 am and the re-tooling process started shortly thereafter. Figure 3.5 shows stressing operations being monitored by Terry Fields (right) senior MoDOT inspector. Terry measured the formwork each morning and monitored stressing, placement, and quality control. Figure 3.6 shows a CPI worker installing post-tensioning ductwork. A slender steel bar was temporarily placed in each piece to provide rigidity and prevent sag. Figure 3.7 shows placement and consolidation of concrete in a typical base panel. The white PVC shown running along the short dimension is the post-tensioning ducts. Although steel bar was temporarily placed inside the PVC, the wooden spacers shown were notched to fit over the ductwork and hold it in place during consolidation. Standard pencil type electric vibrators were used for consolidation. Figure 3.8 and Figure 3.9 show screeding and finish work. Although a broom finish was used, quality control on the finished surface was not as strict as past projects. The entire PPCP section was diamond ground for smoothness.

Figure 3.4 – Oiled precast bed after removing previous two panels

Figure 3.5 – Stressing strands in two panels

Figure 3.6 – Installing post-tensioning ductwork through pretensioned strands

Figure 3.7 – Placement and consolidation of concrete for a base panel

Figure 3.8 – Hand leveling concrete of one panel just after placement

Figure 3.9 – Screeding and hand-finishing before final broom

3.2.3. BASE PANELS

The base panels make up the majority of the pavement, placed between the joint panels and central anchor panel. Ninety two base panels were cast. CPI cast the majority of the base panels first in order to become acclimated and well practiced before attempting joint panels. Figure 3.10 shows a plan view of a typical base panel. Regular 60 ksi (414 MPa) epoxy coated rebar bordered the edges of each panel and is not shown on the schematics. It reinforced the edges and corners where stress concentrations may develop and cause cracking. Each base panel contains eight pretensioning strands as shown in Figure 3.10 and Figure 3.11. The strands on the top are draped to follow the slope of the crown. This ensured there were no out of plane eccentricities developed from the pretensioning force. Draping was done by placing chairs under the top strands at certain places. This raised the strand within the cross section creating equal stress distribution from top to bottom (see Figure 3.12).

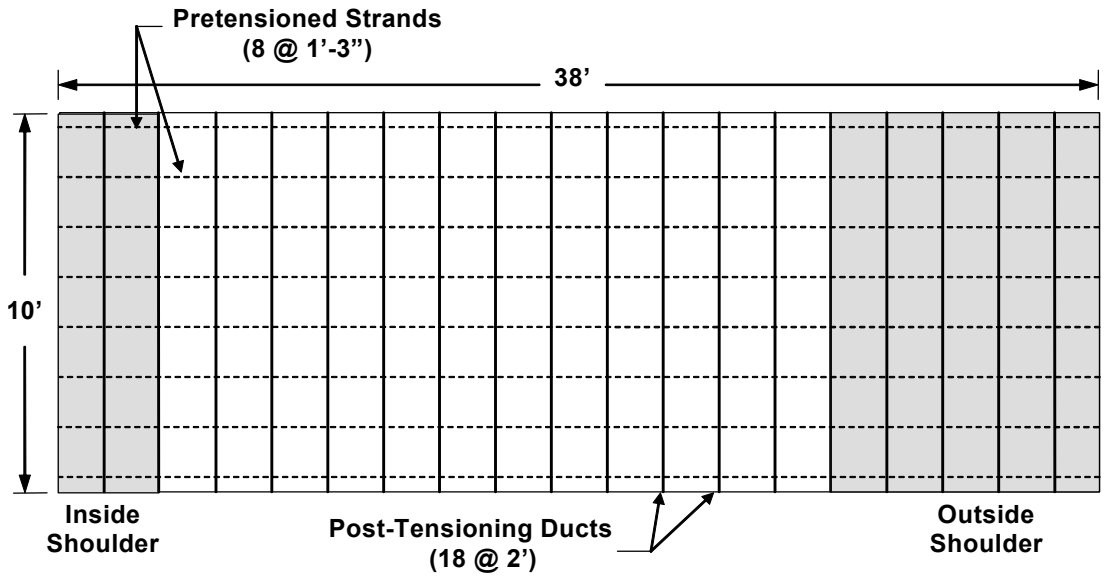

Figure 3.10 – Plan view of typical base panel

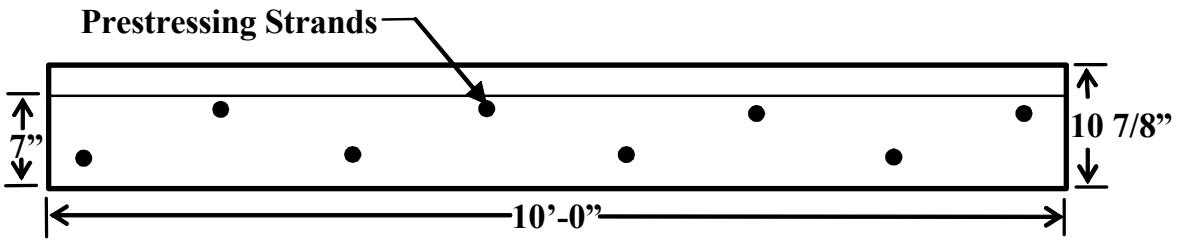

Figure 3.11 – Section of base panel looking perpendicular to traffic direction

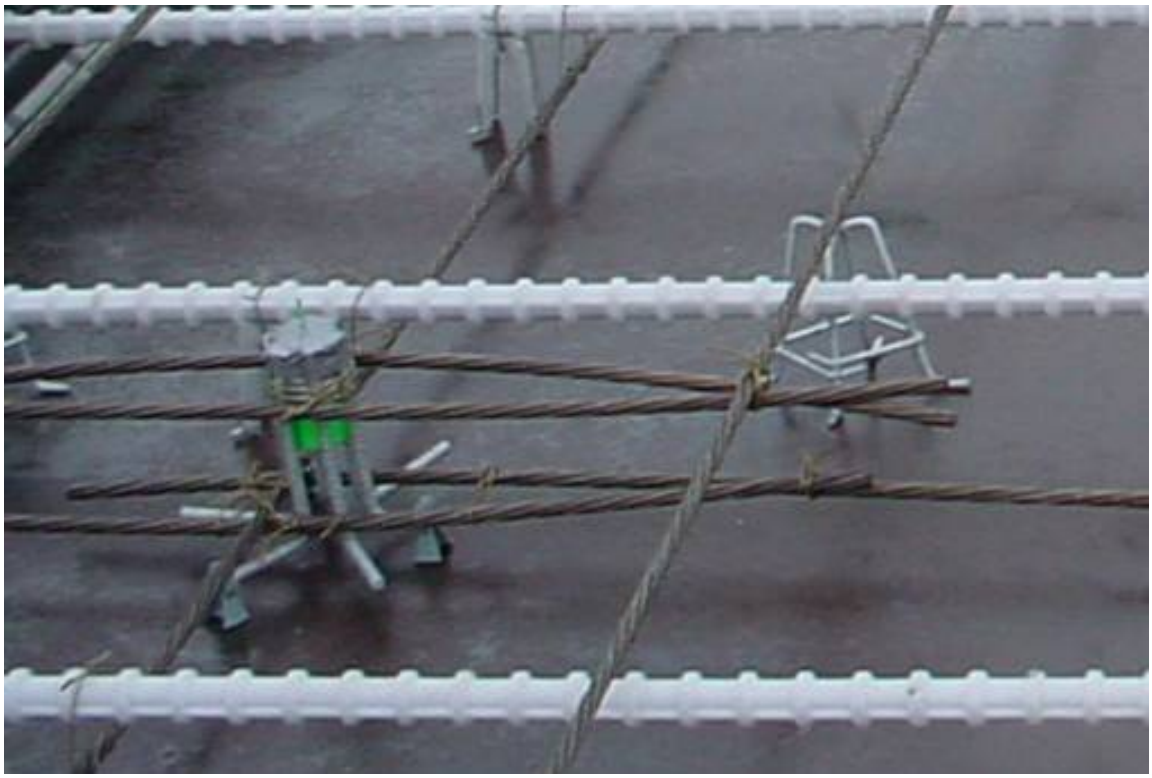

Figure 3.12 – Lifting anchor (left); Chair for draping strands (right)

3.2.4. JOINT PANELS

Joint panel fabrication began mid-December. Due to the complexities of retooling, amount of reinforcement, and nature of the panel itself, each joint panel had to be cast in two separate halves. Figure 3.13 shows a plan view of a typical joint panel.

Block-outs toward the center of the panel allow access to the post-tensioning ducts. These were filled during the final stages of construction. Joint panels have 12 pretensioned strands instead of 8 (see Figure 3.14). The top strands are draped with the slope of the crown (see Figure 3.12). Each half is connected by smooth dowels that provide load transfer between sections (not shown in schematic). These dowels had to be held in place during casting. There also had to be some type of bond-breaker or cold-joint between sections to allow the joint panel to open up during post-tensioning operations. Therefore, a bulkhead was placed in the middle of the bed in order to cast each half separately. Figure 3.15 shows two halves of a joint panel, one side is cured, the other is ready for casting. Five total joint panels were fabricated. Two of the five are located on the ends of the PPCP section and were not cast with post-tensioning block-outs on one side (this side was simply dowelled into conventional cast in place concrete). Two joint panels were fabricated every two days.

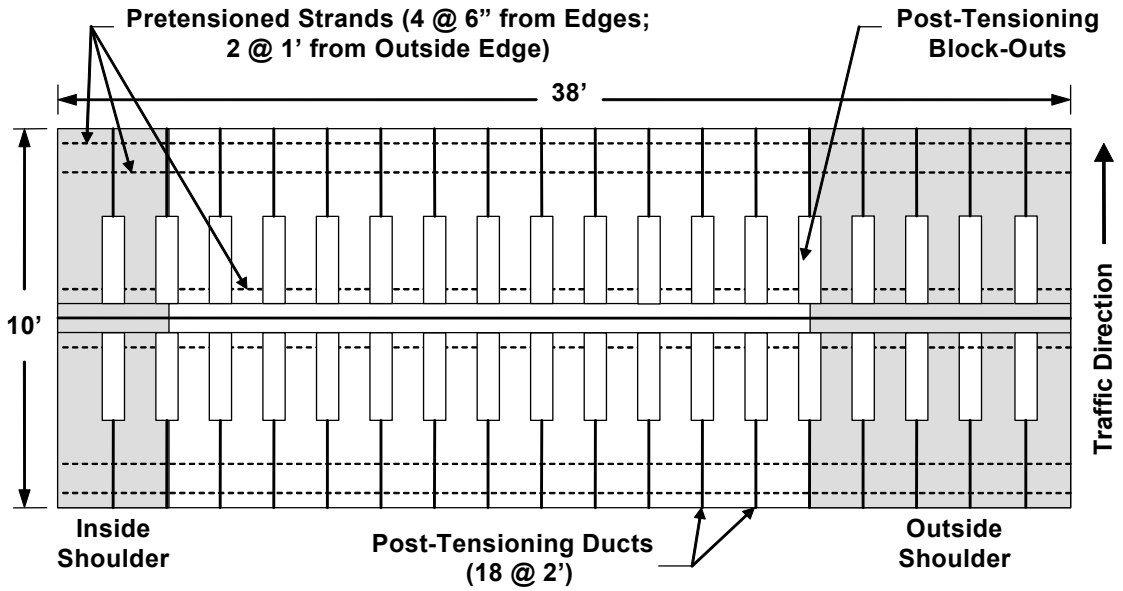

Figure 3.13 – Plan view of typical joint panel

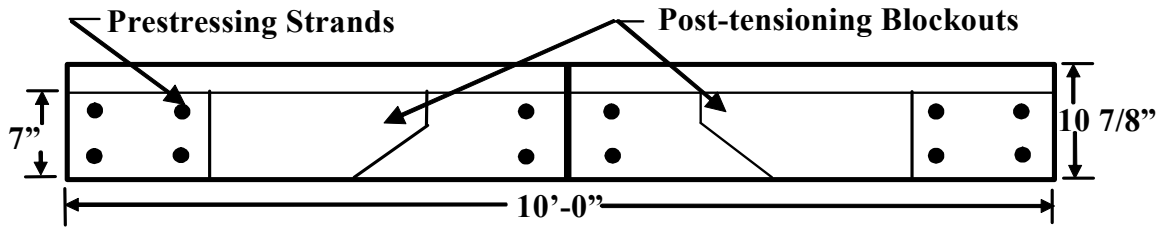

Figure 3.14 – Section of joint panel looking perpendicular to traffic direction

Figure 3.15 - Joint panel casting (left side cured, right side ready for casting)

3.2.5. ANCHOR PANELS

Anchor panels are essentially base panels with full depth holes near the center. These panels are located in the center of each PPCP section and anchor the entire section globally providing for equal expansion and contraction at adjacent joint panels. Dowels were driven into the sub grade through the 4 in (10.2 cm) blocked-out anchor sleeves (see Figure 3.17). They were then grouted, anchoring the entire section. Figure 3.16 shows a plan view of a typical anchor panel. These panels required very little extra labor; therefore, they were cast intermittently with base panels.

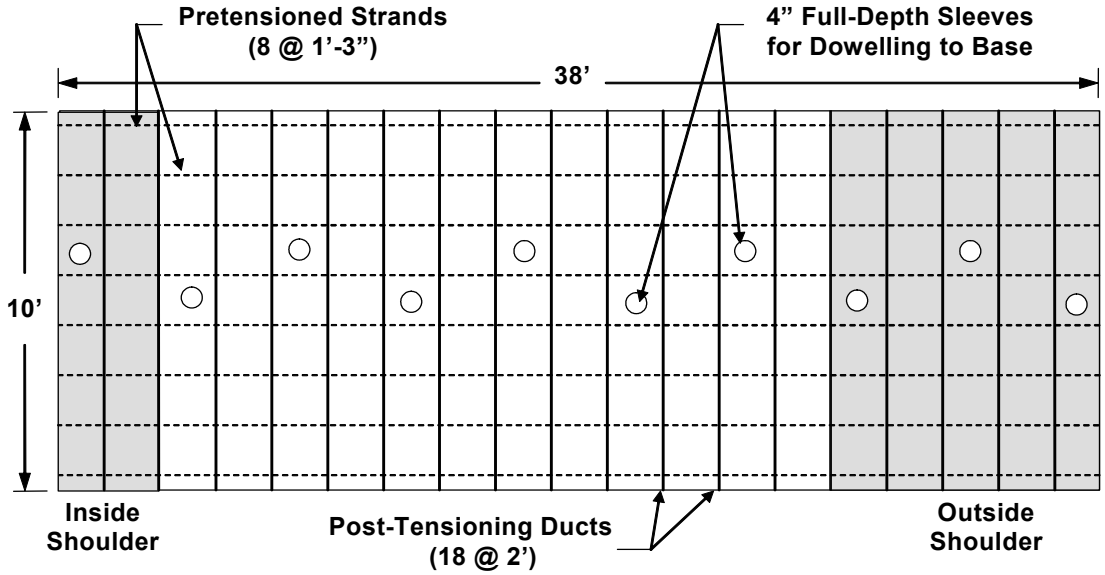

Figure 3.16 – Plan view of typical anchor panel

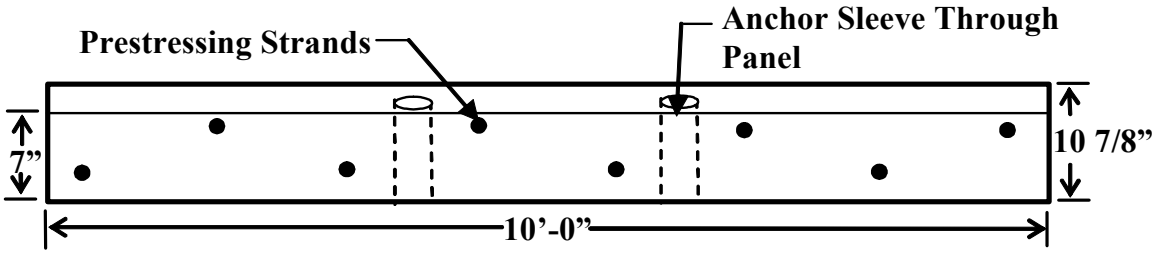

Figure 3.17 – Section of anchor panel looking perpendicular to traffic direction

3.3. BASE PREPARATION

Base preparation is one of the most important steps in construction of PPCP systems. Voids beneath the panels can cause improper alignment or added stress on shear keys. Friction between the panel and the base itself must also be mitigated. Frictional restraint can cause residual tensile stresses and reduce the life of the pavement (Merritt, McCullough et al. 2002).

3.3.1. LEVELING COURSE

Soil-structure interaction with PPCP is inferior to cast-in-place pavement. Slip form pavers use wet concrete, filling uneven voids in the base and creating a smooth driving surface. PPCP is ridged during placement. It must bridge the voids in the base in order to have a smooth riding surface. Therefore, it is desirable to get a consistently level base before placement of PPCP.

For the Missouri project, the contractor chose a gap-graded asphalt base over rock fill. A gap-graded base has a very low percentage of fine aggregates. It allows water to drain freely through the asphalt and into the rock fill below. Recent feasibility studies show that asphalt leveling courses can be placed both quickly and economically and still retain strict tolerances such that voids beneath the precast will be minimal (Merritt, McCullough et al. 2002). It should be noted, however, that mobilization of asphalt paving equipment to place a short section of leveling course is cost prohibitive (Merritt, McCullough et al. 2002). The Missouri project was long enough to justify the asphalt leveling course. Figure 3.18 shows an anchor panel over asphalt base on I-57 near Charleston, MO.

3.3.2. FRICTION REDUCTION LAYER

Long sections of PPCP will expand and contract with daily and seasonal temperature variations. Frictional restraint can cause tensile stresses and allow cracks to propagate, reducing design life. As stated earlier, this is more critical during decreases in temperature because the slab contracts. As the slab contracts frictional forces will cause tensile strains. Conversely, expansion will create compressive strains (not as concerning for concrete).

One of the most effective solutions for mitigating friction has been a single layer of polyethylene sheeting. On previous projects in Texas, it has been proven to be an effective bond breaker, economical, and easy to use during construction (Merritt, McCullough et al. 2002). Figure 3.18 shows an anchor panel over polypropylene sheeting on I-57 near Charleston, MO.

Figure 3.18 – Anchor panel on polypropylene over asphalt, and aggregate base (Missouri project)

3.4. CONSTRUCTION

Gaines Construction from Wentzville, MO was hired to construct the PPCP section. Construction speed was limited by available delivery trucks. Panel placement rates varied between 8 and 25 panels/day. The following sections describe the final construction of the PPCP system on I-57 near Charleston, MO.

3.4.1. JOINT SEALANT

A slow curing two part epoxy type joint compound was used on all of the panel joints during placement. This sealed the joints to prevent water migration and pumping. It also provided lubrication between panels, making alignment much easier. Joint compound was typically applied while the panel was on the truck or just after unloading. Figure 3.19 shows application of joint compound on the female end of a joint panel.

3.4.2. ALIGNMENT

Alignment quickly became an important process. Panels were taken directly from trucks and placed with the adjoined section (Figure 3.20). Each was set, aligned, and two 0.6 in (1.5 cm) diameter post-tensioning strands were fed through. These strands were stressed (at low stress levels) to recover slack and gaps in the section. Not only did the individual panel alignment matter, but global alignment relative to the end of the section was very critical. The following actions outline the steps taken to ensure alignment:

1. The centerline of the PPCP section was surveyed and nails were driven into the asphalt leveling course several feet apart down the centerline.
2. Local panel-to-panel alignment was done with a standard contractor's laser. This laser was surveyed and aligned with the centerline (the nails).

Figure 3.19 – Application of joint compound to a PPCP panel

Figure 3.20 – Unloading panel for placement

3. The centerline of the panel was marked with a PVC pipe stuck into the center post-tensioning duct. When the laser hit the PVC squarely, the center of the panel was in the center of the road.

Global alignment took precedent over panel-panel alignment. Therefore, post-tensioning strands became difficult to thread.

3.4.3. POST-TENSIONING

Once the laborious task of threading eighteen 250 ft long strands through each of the four sections was complete, stressing operations commenced. Each post-tensioning strand is 0.6 in diameter with 270 ksi ultimate strength. They were stressed to 80% of ultimate (about 44 kips or 196 kN each). See Figure 3.3 for a distribution of post-tensioning strands. Gaines stressed two strands at a time working from the inside out (see Chapter 8 for specific order) to eliminate eccentricities. Figure 3.21 shows Gaines Construction stressing two post-tensioning strands. The jacking force was re-applied at the opposite end to ensure uniform stress distribution.

3.4.4. PROBLEMS DURING CONSTRUCTION

The problem that was most taxing on completion time was threading the post-tensioning strands. Each section had at least two strands run one panel at a time. The other sixteen were threaded the full 250 ft. Poor alignment, sagging ducts, and ice were all suspected impediments. Gaines used several techniques to thread the strands. The first was a strand pusher (see Figure 3.22). This mechanical pusher proved moderately effective. The most innovative method was removal of the king wire from a 250 ft seven wire strand. This king strand was welded onto the end of a full strand and pulled through with a back-hoe (see Figure 3.23).

Figure 3.21 – Stressing the second set of strands in a typical Missouri PPCP section

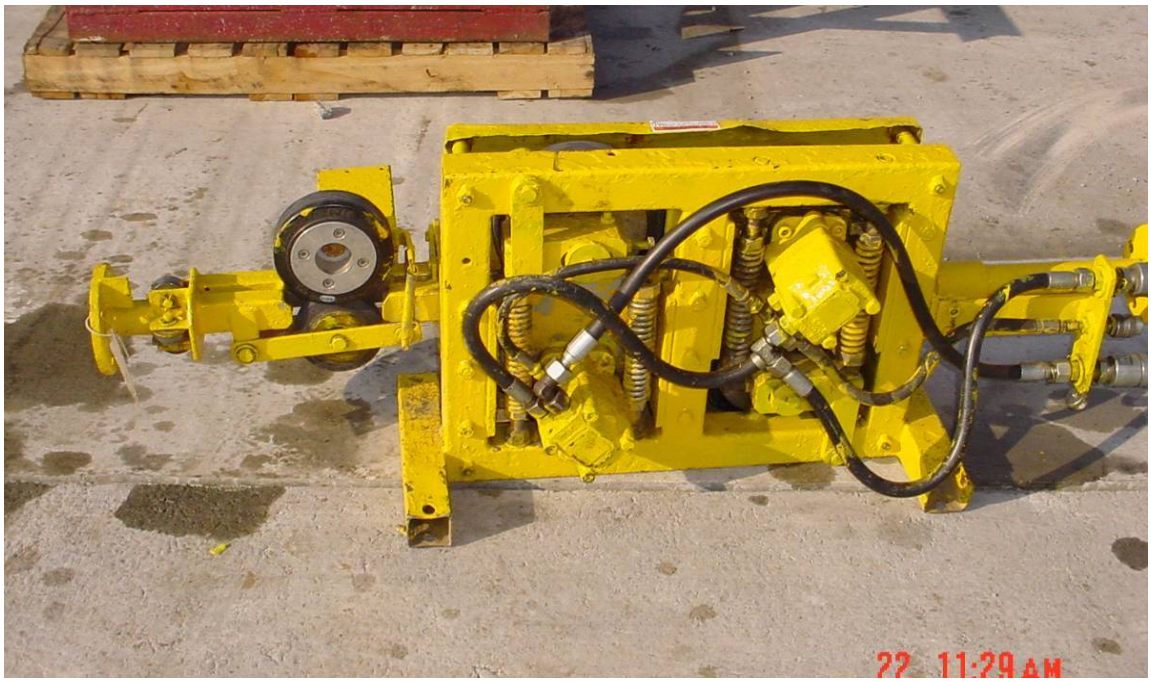

Figure 3.22 – Post-tensioning strand pusher

Figure 3.23 – King strand welded to full strand for threading

Figure 3.24 – Crooked PPCP section (before and after shimming started)

Although the panels seemed to stagger to the north, the centerline crept south. To solve this problem, Gaines installed wooden shims on the south side of several panels (see Figure 3.25).

The joint panels did not open up after stressing. Ideally the joints would have opened during stressing, allowing the installation of expansion material. The tops of the joints were saw-cut in order to create stress concentrations (see Figure 3.26). The joints were pulled apart and expansion material was finally installed as required.

Some panels showed transverse and longitudinal cracking. These cracks became evident in both the casting yard and construction site. Cracks were filled with an epoxy type sealant to prevent freeze-thaw and chloride ingress (see Figure 3.27).

Figure 3.25 – Shim installed on the outside shoulder of several panels

Figure 3.26 – Closed joint in joint panel after stressing operations (saw-cut on top)

Figure 3.27 – Repaired transverse crack in PPCP

3.5. GROUTING AND FINISH-WORK

The last step in the Missouri PPCP construction process is to grout the tendons and fill the block-outs. Grouting provides an extra layer of corrosion protection for the post-tensioning tendons. The PVC duct is not continuous across the joints, therefore, water and chlorides may come in contact with post-tensioning strands (the joint sealer prevents this). Fully bonded tendons will also allow a section to be cut out and replaced toward the end of the design life.

Grout was pumped into vents located at several panels. Figure 3.27 shows two small grout vents just above the repaired crack.

Once grouting was finished the entire driving surface was diamond ground. This specification was a result of poor roughness indices on previous projects.

4. EXPERIMENTAL PROGRAM

The following chapter discusses the experimental program implemented by the University of Missouri-Columbia. The overall experimental program can be broken into two main areas—field instrumentation and laboratory studies.

4.1. FIELD INSTRUMENTATION

Discussion of field instrumentation includes instrumentation layouts in the panel, internal instrumentation, data acquisition systems, and external instrumentation. Field instrumentation is more the focus of this thesis. Laboratory instrumentation is discussed extensively in the companion thesis by Brent Davis (Davis 2006).

4.1.1. GENERAL INFORMATION ON INSTRUMENTATION

The following sections discuss the test section layout, instrumentation plans, labeling, and as-built locations. These sections serve as a reference to the discussion of results and provide critical information with respect to location and nomenclature that helps assemble logical explanations.

4.1.1.1. TEST SECTION LAYOUT

The entire PPCP system was made up of four 250 ft (76.2 m) sections (see Figure 3.1). The third section contains the majority of instrumented panels. In order to study the performance of the entire system, redundant samples from each panel type needed to be studied. Sections 1 and 3 do not have full joint panels with precast sections on each side. Adjacent transitions may affect part of the ‘control’. Section 3 was and is closer to

AC power than Section 2. Therefore, panels were instrumented throughout PPCP Section 3.

Four base panels, two joint panels, and one anchor panel were instrumented. Figure 4.1 shows the location of the instrumented panels within the section. For consistency, instrumented panels were marked similar to the nomenclature used during fabrication. Joint panels were labeled A1, A2, or A3 depending on the type (whether it was a full panel—A3 or an end panel—A1 and A2). The University of Missouri-Columbia instrumented two full joint panels (A3s). Each was labeled A31 and A32 with the direction of traffic. Base panels were labeled 'B' in the casting yard. Four instrumented panels were defined as Panel B1-B4, respectively ordered with the direction of traffic. One anchor panel was instrumented in the center of Section 3 (Panel C1). Panels B1 and B2 were placed to the right of Panel C1, in Figure 4.1, to minimize the amount of instrumentation wire needed. Panel B4 was instrumented in Section 4 to provide redundant measurements on both sides of a joint panel (see Figure 4.1).

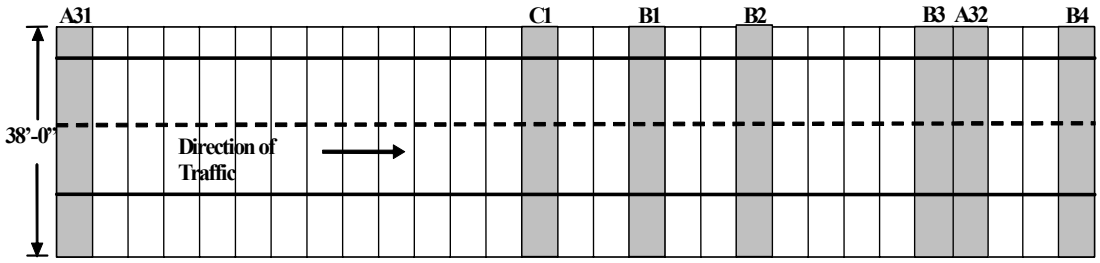

Figure 4.1 - Overall view of test-section and location of instrumented panels.

4.1.1.2. INSTRUMENTATION LABELING

The seven instrumented panels incorporated four types of devices to measure temperature and strain of the concrete and post-tensioning strands. Concrete strain is and

was measured using instrumented rebar and vibrating wire gages. Strain in the post-tensioning strands is/was measured by vibrating wire strandmeters. Thermocouples and thermistors embedded in the vibrating wire gages both measure temperatures in the concrete at various stages. These devices will be discussed extensively in later sections.

Each gage was labeled according to panel and type of gage. Vibrating wire gages are denoted with a 'V', rebar with an 'R', thermocouples with 'T', and strandmeters with 'S'. The panel ID preceded the gage ID. For example the instruments in Panel B1 were labeled B1_R1, B1_V1, B1_T1, and B1_S. For the most part, gage numbers (at the end) were assigned with respect to location. In other words, the R1's in each panel were placed in similar locations.

4.1.1.3. INSTRUMENTATION PLAN AND AS-BUILT INFORMATION

The following sections describe the locations and instrumentation within each panel. The locations chosen are discussed and a plan view of each instrumented panel is presented. As-built information is presented in detail. This will be referenced later in the results chapters to show theories for differences in gage output in different panels. The as-built information is in inches and has been measured from the datum noted on the figures. The 'z' direction is through the depth of the each panel.

4.1.1.3.1. Panel A31

Panel A31 is the farthest panel away from the data acquisition system. In order to minimize power and signal losses, it was instrumented the least. Data acquisition channels were also limited; therefore, there are no thermal devices in Panel A31. This makes conclusions concerning thermal effects nearly impossible. However, despite the quantity of instrumentation, Panel A31 was designed to obtain conclusive pretension

transfer data. Figure 4.2 shows the six rebar placed in Panel A32 and their orientation. Four out of six are in the transverse direction and, compared to other panels, allow for several redundant stress transfer measurements. See Table 4.1 for as-built locations.

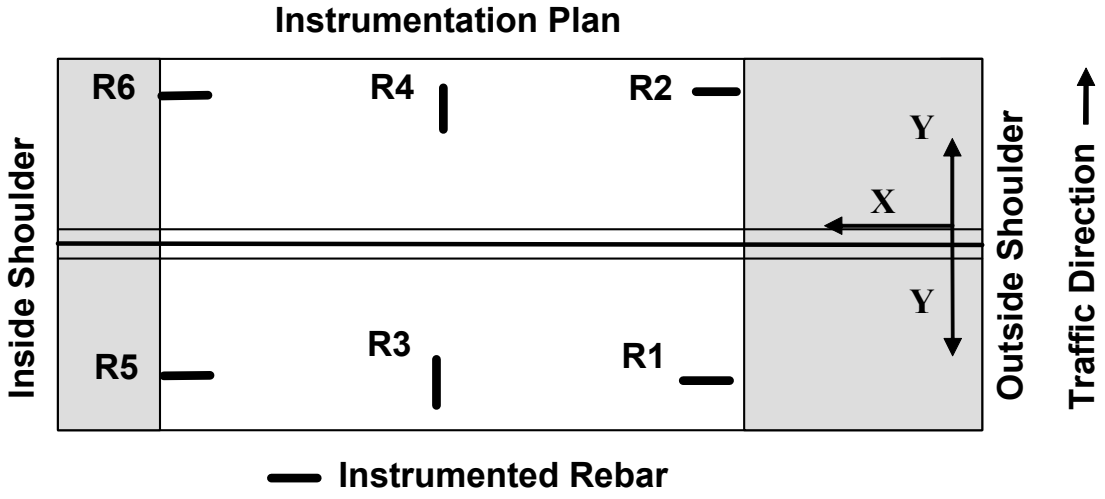

Figure 4.2 - Instrumentation plan for Panel A31

Table 4.1 - As-built instrumentation locations for Panel A31

Gage ID	X (in)	Y (in)	Z (in)
A31-R1	126	56	4
A31-R2	145	48	2.5
A31-R3	267	48	5
A31-R4	236	41	4.5
A31-R5	346	46	4.5
A31-R6	350	44	4.5

4.1.1.3.2. Panels C1, B1, B2, and B3

These three panels provide comprehensive redundancies to the instrumentation program. Each gage is in nearly the same location in all three panels. As shown in Figure 4.3, the instrumented rebar and vibrating wire strain gages were placed together in

every gage location. As-built information can be compared for these panels in Table 4.2 thru Table 4.5.

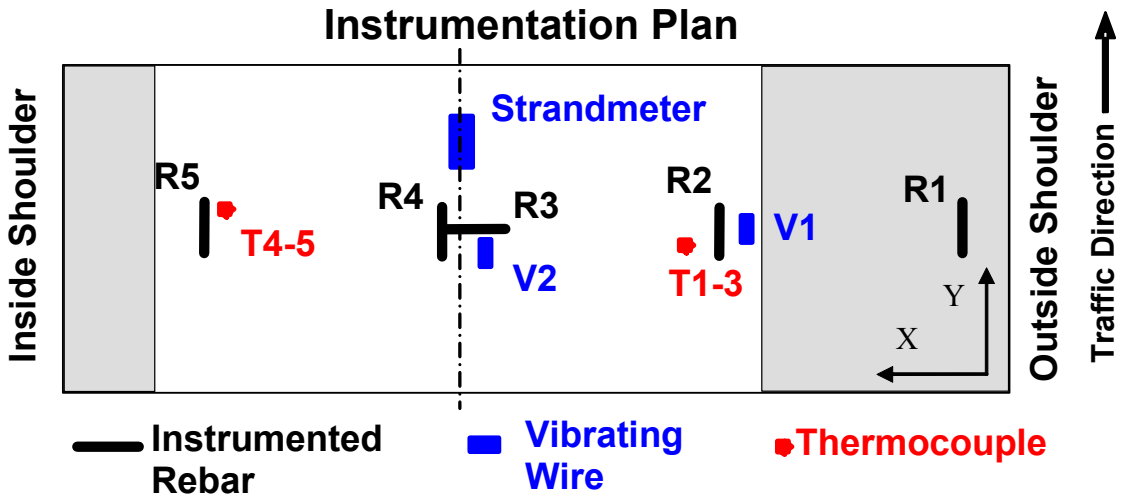

Figure 4.3 - Instrumentation plan for Panels C1, B1, and B2

Table 4.2 - As-built instrumentation locations for Panel C1

Gage ID	X (in)	Y (in)	Z (in)
C1-R1	31	43	3
C1-R2	142	48	4
C1-R3	257	52	2
C1-R4	264	44	4
C1-R5	372	62	4
C1-V1	142	48	4
C1-V2	264	44	4
C1-S	@ Crown in Field	@ Crown in Field	@ Crown in Field
C1-T1	126	75	7
C1-T2	126	75	4
C1-T3	126	75	2
C1-T4	354	68	7
C1-T5	354	68	2

Table 4.3 - As-built instrumentation locations for Panel B1

Gage ID	X (in)	Y (in)	Z (in)
B1-R1	29	60	2.5
B1-R2	137	62	4
B1-R3	252	55	4
B1-R4	256	60	4
B1-R5	378	62	4
B1-V1	137	62	4
B1-V2	256	60	4
B1-S	@ Crown in Field	@ Crown in Field	@ Crown in Field
B1-T1	121	54	6
B1-T2	121	54	3
B1-T3	121	54	1
B1-T4	366	68	7
B1-T5	366	68	3

Table 4.4 - As-built instrumentation locations for Panel B2

Gage ID	X (in)	Y (in)	Z (in)
B2-R1	27	60	4
B2-R2	142	60	4
B2-R3	254	56	4
B2-R4	260	62	4
B2-R5	392	47	4
B2-V1	142	60	4
B2-V2	260	62	4
B2-S	@ Crown in Field	@ Crown in Field	@ Crown in Field
B2-T1	142	67	7
B2-T2	142	67	3
B2-T3	142	67	1
B2-T4	364	52	6
B2-T5	364	52	1

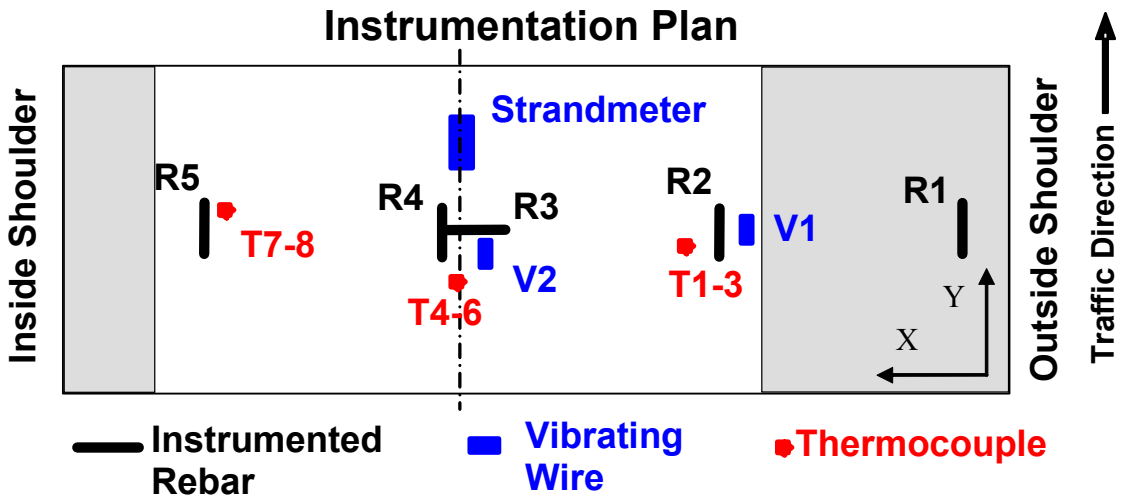

Figure 4.4 - Instrumentation plan for Panel B3

Table 4.5 - As-built instrumentation locations for Panel B3

Gage ID	X (in)	Y (in)	Z (in)
B3-R1	20	46	3
B3-R2	138	62	4
B3-R3	251	54	2
B3-R4	262	59	4
B3-R5	379	60	4
B3-V1	138	62	4
B3-V2	262	59	4
B3-S	@ Crown in Field	@ Crown in Field	@ Crown in Field
B3-T1	145	57	6
B3-T2	145	57	4
B3-T3	145	57	2
B3-T4	289	58	8
B3-T5	289	58	6
B3-T6	289	58	3
B3-T7	361	67	6
B3-T8	361	67	2

The redundancy of the gages serves several purposes. As described in the following sections the instrumented rebar is suitable for short-term incremental and dynamic strain measurements. The vibrating wire strain gage is suitable for long-term measurements. However, due to the settling time of the vibrating wire gage, it is less suited for short-term dynamic strain events like transfer of pretensioning, post-tensioning, transportation strains, or dynamic load tests. Results from the two systems can be compared for quasi static strain events. This redundancy also provides an important check by measuring strain with two different types of transducers at the same location (Eatherton 1999).

The temperature sensors were arranged top to bottom through the depth of the cross-section to investigate thermal gradients. Exterior rebar also measure warping, curling and the differences in thermal effects with respect to slab thickness. The strandmeter shown at the crown was attached to the post-tensioning strand during construction of the PPCP system and will be discussed in detail later.

Panel B3 is identical to Panels C1, B1 and B2 other than that it contains three more thermocouples at the crown (see Figure 4.4 and Table 4.5). This panel is also unique in that it adjoins Joint Panel A32 and could prove critical in obtaining slab strains near the end of the section.

4.1.1.3.3. Panel A32

Panel A32 is the most heavily instrumented panel. It contains eight rebar, eight thermocouples, and four vibrating wire gages. Instrumentation is split nearly equally between Sections 3 and 4. As with most panels, the majority of the instrumentation is oriented in the longitudinal direction (with the direction of traffic).

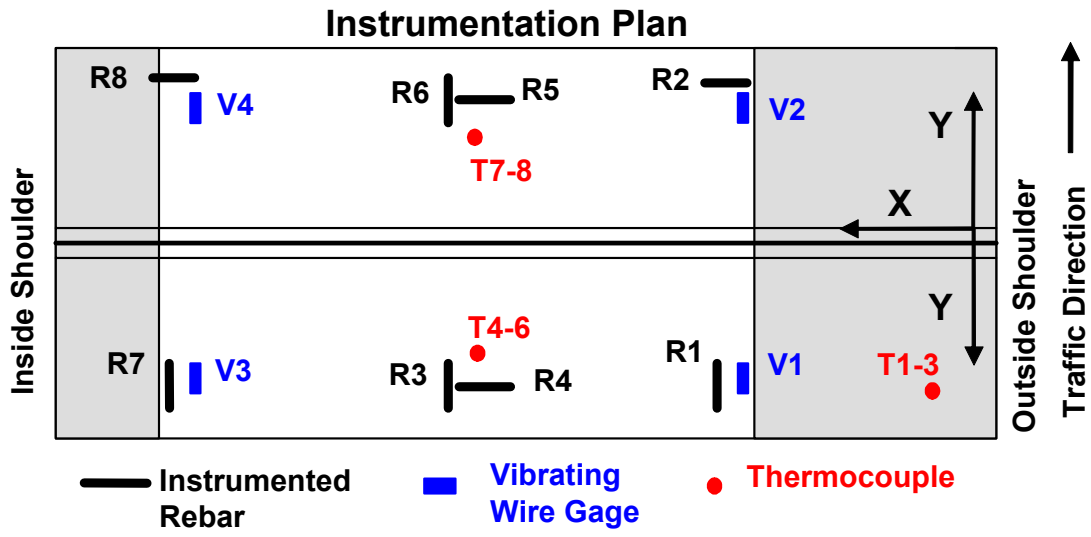

Figure 4.5 - Instrumentation plan for Panel A32

Table 4.6 - As-built instrumentation locations for Panel A32

Gage ID	X (in)	Y (in)	Z (in)
A32-R1	126	56	4
A32-R2	145	48	2.5
A32-R3	254	36	5.5
A32-R4	267	48	5
A32-R5	236	41	4.5
A32-R6	239	48	2
A32-R7	346	46	4.5
A32-R8	363	48	4.5
A32-V1	126	56	4
A32-V2	140	38	5
A32-V3	336	53.5	3.5
A32-V4	349	37	5.5
A32-T1	108	44.5	1.5
A32-T2	108	44.5	3.5
A32-T3	108	44.5	5.5
A32-T4	229	45	1
A32-T5	229	45	4
A32-T6	229	45	7
A32-T7	232	45	1
A32-T8	232	45	6

This was done to measure losses in post-tensioning as well as frictional restraint and joint performance. The magnitude of frictional restraint is much greater in the longitudinal direction. There is 250 ft of concrete expanding and contracting in contact with the base compared to 38 ft in the transverse direction. Rebar 2, 4, 5 and 8 are transverse and proved to be useful in measuring pretensioning transfer.

4.1.1.3.4. Panel B4

Panel B4 is the only panel in Section 4. It is instrumented similar to other base panels but with thermocouples in slightly different locations (see Figure 4.6). Thermocouple seven is near the far corner and helps fill in gaps in the thermographic survey. As stated before, this panel will prove or disprove any anomalies associated with Section 3. Table 4.7 provides as-built information for Panel B4.

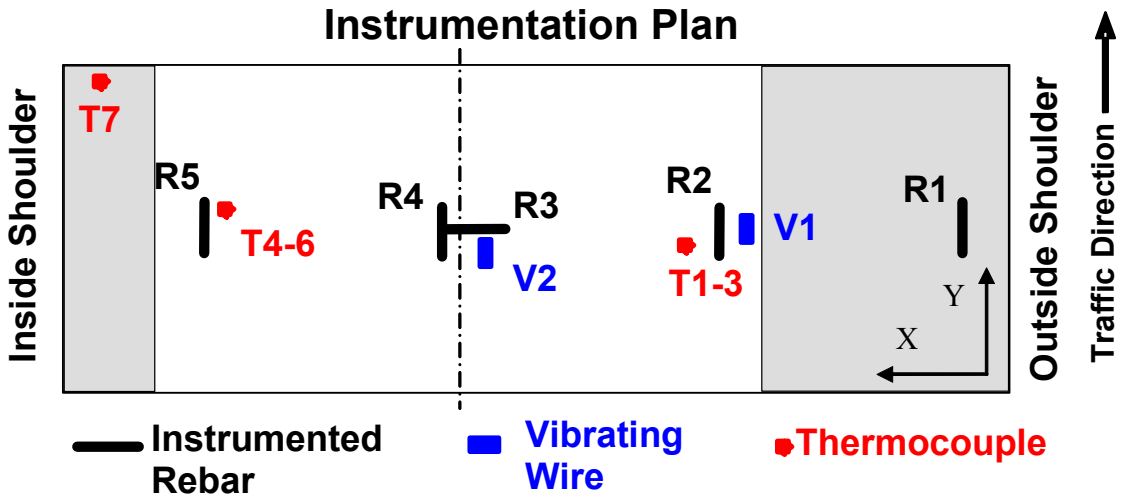

Figure 4.6 - Instrumentation plan for Panel B4

Table 4.7 - As-built instrumentation locations for Panel B4

Gage ID	X (in)	Y (in)	Z (in)
B4-R1	31	61	3
B4-R2	140	63	4
B4-R3	255	54	2.5
B4-R4	264	61	4
B4-R5	375	62	4
B4-V1	140	63	4
B4-V2	264	61	4
B4-T1	145	54	7
B4-T2	145	54	4
B4-T3	145	54	1
B4-T4	355	54	7
B4-T5	355	54	4
B4-T6	355	54	2
B4-T7	423	96	4

4.1.2. EMBEDDED INSTRUMENTATION

The following sections describe the instrumented rebar, vibrating wire strain gages, vibrating wire strandmeters, and thermocouples. They present the specifications, benefits, and utilities of each instrument. Calibration and installation procedures are also discussed.

4.1.2.1. INSTRUMENTED REBAR

The instrumented rebar were fabricated and calibrated at the University of Missouri – Columbia. They consist of a short length of #4 (nominal diameter = 0.5") reinforcing steel bar with a full bridge of strain gages attached to a machined section in the middle of the bar.

4.1.2.1.1. Rebar Fabrication

The steel rebar used was Grade 60 and is common in concrete reinforcement. Ahrens Steel in Columbia, MO delivered twenty foot stock to the MU engineering labs. The bars were then cut to 2 ft (0.6 m) lengths. Each end was milled smooth to roughly 3/8 in (9.5 mm) and then threaded to accommodate calibration. A two inch section in the center was milled to 3/8" for installing full bridge foil strain gages.

After initial machine work, preparations of the instrumented rebar included, strain gage application, waterproofing, and calibration. The preparation of the instrumented rebar is described in detail in Appendix B. The two-inch machined section was degreased, sanded smooth, and cleansed before gluing gages to the steel. Two gages were installed transverse and two were installed longitudinal to the length of the rebar. The ribs on either side of the rebar were used to line up the gages (see Figure 4.7). Power and signal wires were then soldered to the terminal strips.

Waterproofing consisted of several layers of protective materials to guard against corrosion as well as protect the gage during casting. Each was wrapped in Teflon tape (to reduce friction), thick electrical tape to provide padding, then covered in silicone, and wrapped in shrink fit tubing. Figure 4.8 shows an instrumented rebar before and after waterproofing.

4.1.2.1.2. Instrumented Rebar Calibration

The instrumented bars were calibrated using a 110 kip (490 kN) capacity MTS machine. The setup consisted of a 20 kip (89 kN) capacity load cell, a universal joint, a coupling apparatus, and a National Instruments DAQ card. The universal joint minimizes bending during loading.

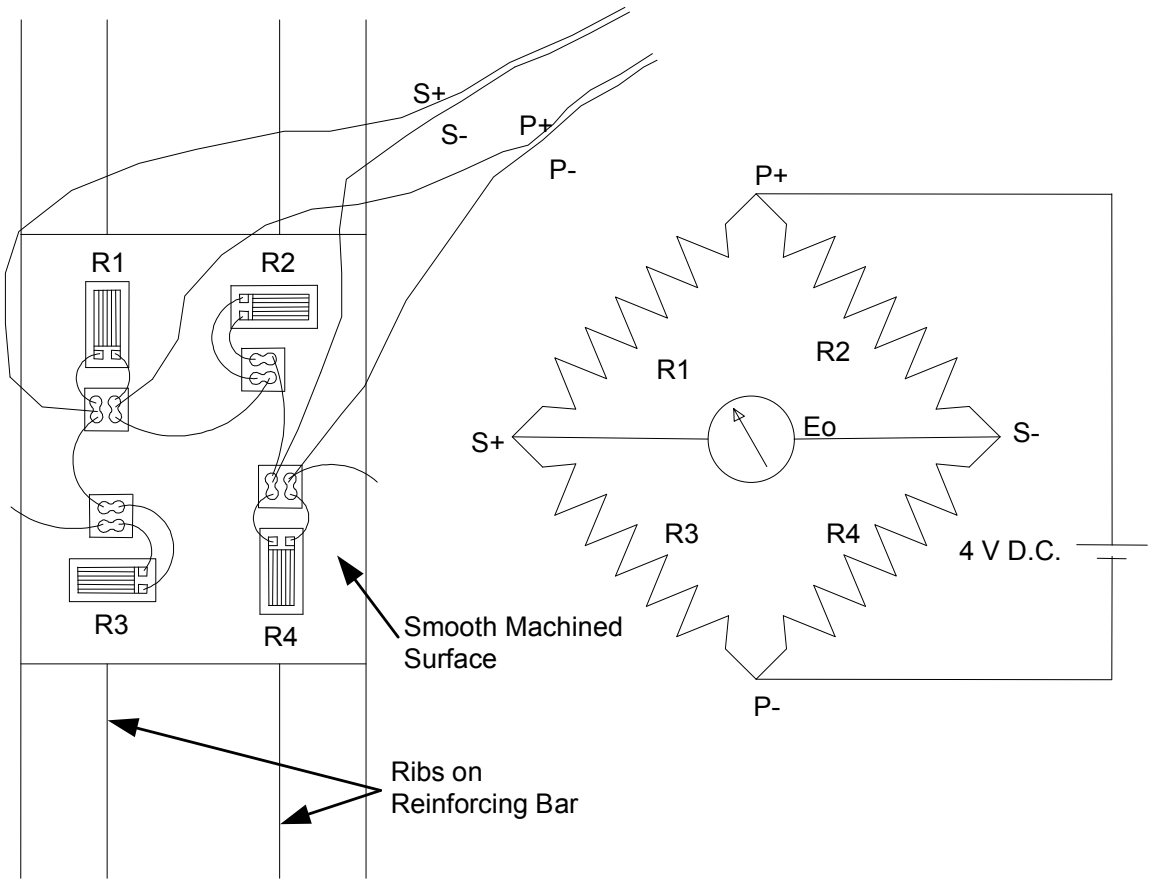

Figure 4.7 - Schematic of the strain gage configuration on the strain gaged bar

Figure 4.8 - A finished instrumented rebar along with an instrumented bar yet to be waterproofed and sealed

The coupling facilitates easy setup and also serves as a safety measure that prevents unanticipated compressive loading. Three cycles of a 0.01 Hz saw-tooth ram displacement-controlled loading was applied during calibration. Calibration constants were obtained in (lbs/mV). An example and results from calibration can be found in Appendix C

Ideally, by using a full bridge of active strain gages thermal effects are cancelled out by opposite legs of the bridge. Thermal tests were performed on instrumented rebar in an oven, water, and concrete. Thermal compensation was adequate. Partial results can be found in Appendix C. Further work on thermal effects is ongoing and will be compiled in the future thesis by Grant Luckenbill.

4.1.2.1.3. Advantages of Instrumented Rebar

Previous projects at the University of Missouri-Columbia have shown good success with instrumented rebar. As stated previously, they easily compensate for thermal effects. They also have a major advantage over vibrating wire gages in that they are dynamically responsive. The strain output due to a change in resistance from foil-type strain gages responds almost instantaneously. It responds as fast as the electricity can travel from the signal tap on the full bridge to the data acquisition system. Vibrating wire gages, however, require settling time.

4.1.2.2. VIBRATING WIRE STRAIN GAGES

The vibrating wire strain gages used for this project were purchased from Geokon Incorporated. A photograph of the 6 in gage length model VCE-4200 embedment type vibrating wire strain gage is shown in Figure 4.9.

4.1.2.2.1. Vibrating Wire Gage Specifications and Theory

The vibrating wire strain gage consists of an encased steel wire between two flanges. Displacement of one flange relative to the other causes the tension in the wire to change much like the tuning of a guitar string. The change in wire tension produces a change in the resonant frequency of the wire (Geokon 1996). Electromagnetic coils, which are housed in a plastic block, are positioned around the center part of the gage. By sending an alternating current through the coils at a range of frequencies the wire becomes excited (Eatherton 1999). After sweeping the range of frequencies the wire continues to vibrate at its resonant frequency. The electromagnetic coils then pick up the signal as an alternating current induced by the wire vibrations (Eatherton 1999). This device is similar to an electric guitar pick-up. The strain in the gage is directly proportional to the square of the resonant frequency (Geokon 1996). The frequency of the alternating current is measured and correlated to strain (Geokon 1996).

The plastic block that contains the coils and the thermistor is attached to the vibrating wire gage by means of a hose clamp (see Figure 4.9). In a previous project, it was found that the strain reading became erratic if the plastic block was jarred away from the sealed wire housing. Toothpicks were included under the hose clamp to help hold the plastic block in place (see Figure 4.9).

4.1.2.2.2. Vibrating Wire Thermal Compensation and Calibration

The length of the wire inside the gage changes with temperature and as a result the tension, natural frequency, and strain measurement are dependent on temperature (Eatherton 1999). Each vibrating wire strain gage includes a thermistor which measures thermal changes related to changes in resistance. The thermistors are included with the

electromagnetic coils in the plastic block so that the strain reading can be corrected using the exact local temperature.

A thermal correction for this effect is provided by the manufacturer, which uses the coefficient of linear thermal expansion of steel (wire material). After some discussions with Geokon, the application of the temperature correction was further clarified. The coefficient provided is 12 μstrain/°C (Geokon 1996). This value only includes the wire within the housing. The coefficient for the entire gage itself is unknown. It includes the housing, springs, and other mechanical parts. Geokon maintains the stance that plastic concrete is stiff enough to restrain all other expanding mechanisms and that the only thing that will be affected by temperature is the encased wire. Thermal effects were investigated with a gage in an oven, in water, and in curing concrete at varying temperatures. Partial results are presented in Appendix C.

Geokon calibrates a sample of a batch of 100 vibrating wire gages. According to conversations with Geokon personnel, they use a setup with three LVDTs similar to what is shown in Figure 4.10. The calibration constants from the sample of gages are averaged and related to the theoretical calibration constant by a simple ratio. A 'batch factor' is produced. This batch factor is provided with each set of gages purchased in that lot and is multiplied by the output to obtain an adjusted strain.

The MU research team duplicated the setup to check the calibration of some of the gages. The gages were all calibrated individually on a 110 kip (489 kN) capacity MTS machine. A three LVDT setup was used as shown in Figure 4.10. By using three LVDTs, potential bending present during calibration was averaged out.

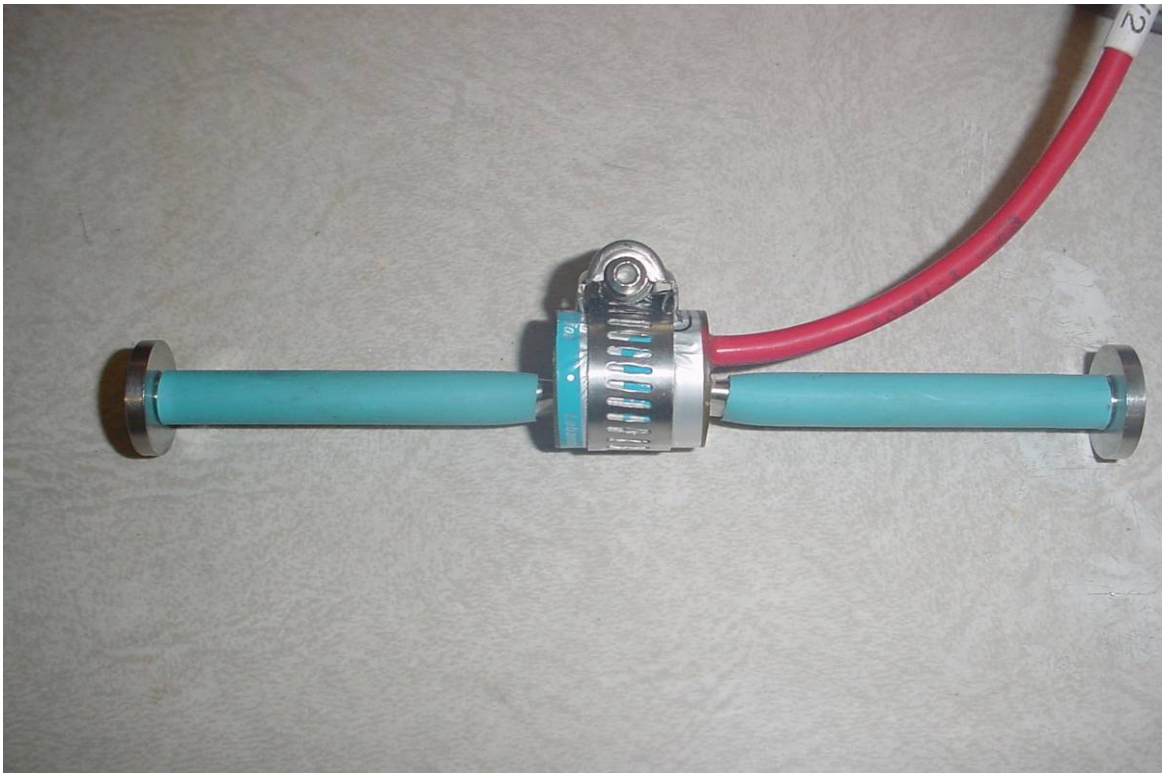

Figure 4.9 - Vibrating wire strain gage from Geokon Incorporated

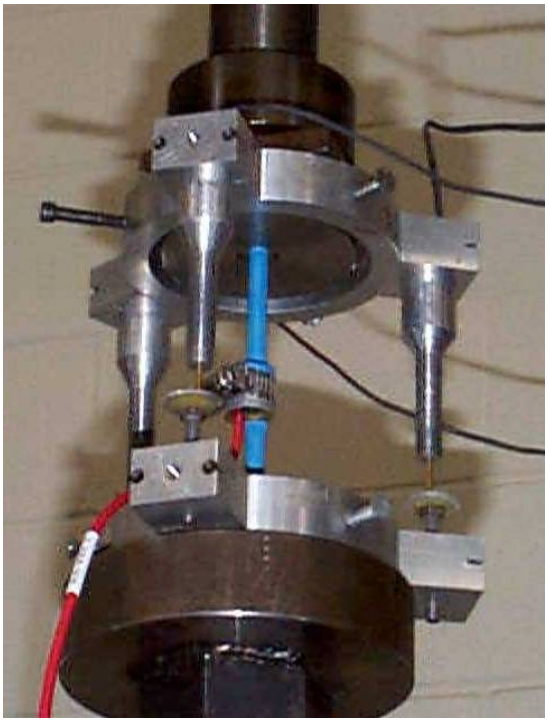

Figure 4.10 - Calibration of the vibrating wire strain gages

Special load plates were used to hold the gage in place. Three cycles of 0.01 Hz sinusoidal ram displacement-controlled loading was applied. A correlation was then obtained between strain and the square of the natural frequency of the vibrating wire gage. Calibration constants were close to those provided by Geokon. The test was only done on a few gages to prevent any possible damage done due to inconsistent preloading. The results of the calibration are given in Appendix C.

4.1.2.2.3. Advantages of Vibrating Wire Strain Gages

Since the vibrating wire strain gage is based on the natural frequency of a wire, instead of a resistance like the strain-gaged bar, the vibrating wire strain gage can be used to measure long-term strain events. Resistance base gages such as the instrumented rebar, require an excitation voltage in order to produce output. If the excitation voltage changes over time (due to thermal effects or readjustment) the output will contain an offset relative to the change in excitation. The vibrating wire strain is based solely on the length and thermal expansion of the wire. If the vibrating wire output is properly corrected (thermally) zero readings can be taken early and then referenced years later to determine long-term strain variations. The only disadvantage is that plucking and reading the wire between the flanges requires settling time. Therefore, it is hard to obtain rapid dynamic strains.

4.1.2.3. VIBRATING WIRE STRANDMETERS

Model 4410 Vibrating Wire strandmeters were also purchased from Geokon Incorporated. The gage operates on the same principles as the model 4200 discussed above. However, clamps at either end allow the gage to be fixed to a pretensioned strand. For the MU research team, this is the first experience with these types of gages.

4.1.2.3.1. Vibrating Wire Strandmeter Specifications

The Geokon vibrating wire strandmeter operates on the exact same frequency based principles described earlier. The only differences are that the gage length is 8 in (20.3 cm) instead of 6 in (15.2 cm), it requires a different frequency range, and it can be fixed to a prestressing strand. The excitation and pickup are also located at the end of the instrument. It is designed to be low profile and isolated from external stress. This is accomplished by sheathing the gage length in PVC and filling the tube with grease. Uncured roofing tape was also supplied with each gage. This was wrapped around the clamps at the ends, thus reducing and cushioning any bearing from external sources (concrete). Figure 4.11 shows a strandmeter with and without the PVC grease tube. Ultimately, the gage is able to measure displacements between the two strand clamps.

4.1.2.3.2. Vibrating Wire Strandmeter Calibration

Although individual calibration information was supplied by Geokon, each gage was calibrated at the University of Missouri-Columbia. Calibration was done on a 110 kip (489 kN) MTS machine similar to that of the rebar calibration. Each gage was clamped to a smooth steel bar. This steel bar was instrumented with full bridge foil gages similar to that of the instrumented rebar. An extensometer was also clipped to the smooth bar to provide a redundant reading. Figure 4.12 shows a rotated view of the test setup including instrumented bar, clip gage, and strandmeter. Three cycles of 0.01 Hz sinusoidal ram displacement-controlled loading was applied through the full range of each gage. A correlation was then obtained between strain and the square of the natural frequency of the vibrating wire gage. Calibration constants were close to those provided by Geokon. See Appendix C for calibration information.

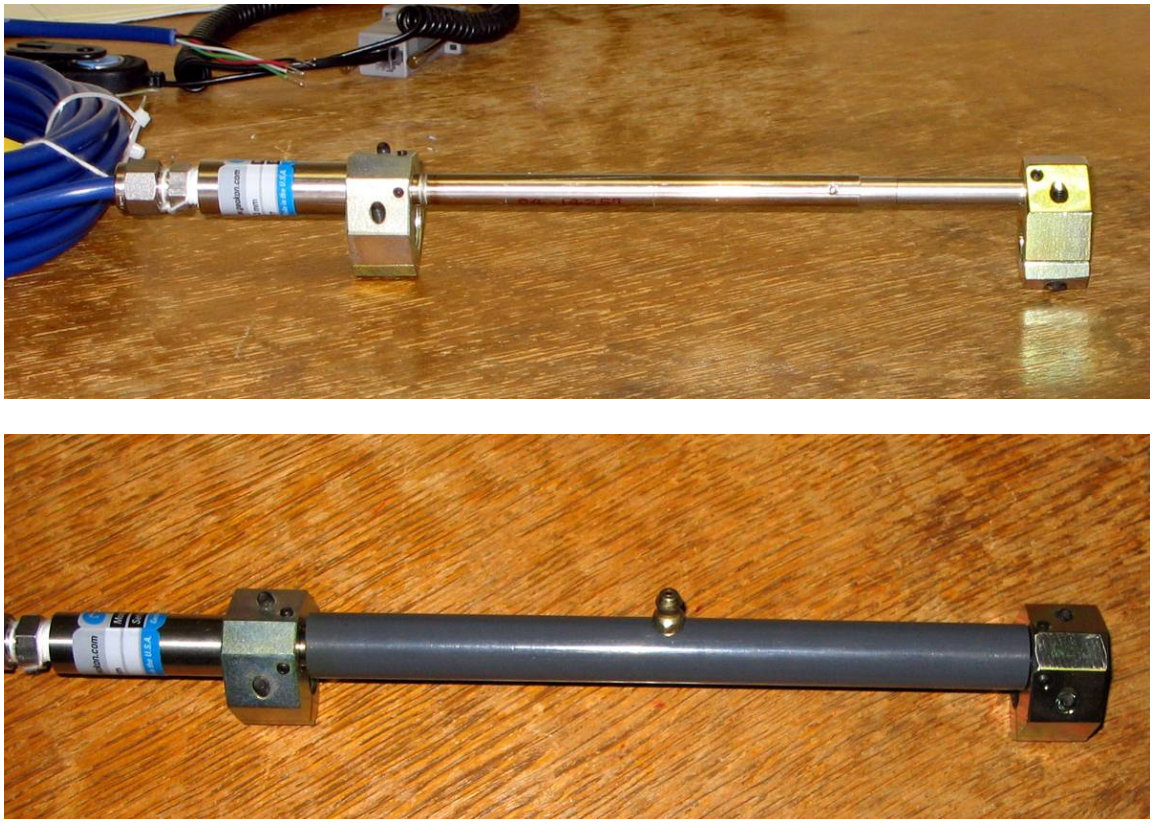

Figure 4.11 - Bare strandmeter (top) and strandmeter sleeved with PVC tube for greasing (bottom)

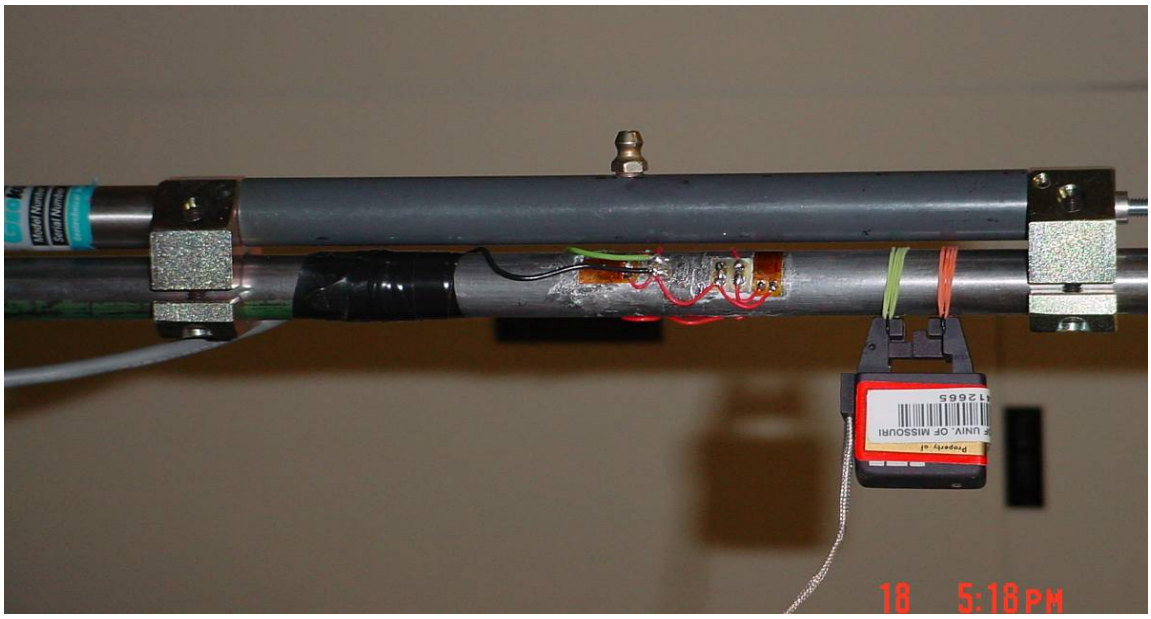

Figure 4.12 - Strandmeter fixed to steel bar instrumented with foil gages and an extensometer (this pictures is rotated 90°)

Unlike the embedded vibrating wire gages, these gages have a very low coefficient of thermal expansion. Thermal expansion only begins to affect the gage where deviations in temperature are greater than 50°C (Geokon 1996). The gages were heated during calibration (by building a box around the setup). Thermal effects were negligible (Appendix C).

4.1.2.3.3. Advantages of Vibrating Wire Strandmeter

Many ideas were discussed on how to measure post-tensioning stress losses during the Missouri PPCP project. The MU research team discussed fabricating load cells for the bearing ends. This would have been taken elaborate machining and fabrication. Vibrating wire strandmeters proved to be an elegant and simple solution for obtaining long-term stress losses in the post-tensioning strands. These gages allow for permanent isolated strain measurements and are robust enough to take data for several years.

4.1.2.4. THERMOCOUPLES

The thermocouples used are Type T, which utilize a copper-constantan junction. The wires are 24 gauge Teflon coated thermocouple wire. The type T thermocouple is rated for a temperature range of –328° to 662° F (-200° to 900° C) (Eatherton 1999).

The wires were cut to the estimated length from the gage location to the terminal box. They were then welded together at the University of Missouri – Columbia using proper thermocouple welding equipment. The wires were labeled using heat shrink label. The welded thermocouple end was then dipped in epoxy and set out to dry. The epoxy protected the thermocouples during installation and helped to insulate against any contact

with the steel in the panel. Figure 4.13 shows a photograph of the thermocouples set out to dry after epoxy was applied to the thermocouple junctions.

The thermocouple works by creating a voltage difference between the two wires that is proportional to the temperature at the junction. To use a thermocouple, the temperature of the connection between the thermocouple wire and terminals must be known. This is known as the cold junction temperature and must be measured at the first place a different metal is introduced in to the signal connections. For this project, the temperature was measured at the junction boxes in each panel. More details of the reference temperature measurement are included in the section on terminal boxes.

Figure 4.13 - Thermocouples welded, bundled, labeled, and epoxy coated in lab

4.1.2.5. INSTALLATION OF DEVICES

All gages were fully tested at the University of Missouri before being installed in the precast panels. The gages were sorted according to the specific panels. A mock panel was drawn on the floor of the lab to cut lead wires and position each gage accurately. Instrumentation programs were then run for each panel in the lab before casting. The lead wires were cut to specific lengths, labeled accordingly, and bundled to streamline gage installation. Figure 4.14 shows the gages laid out in the lab.

Rebar was installed using wooden spacers, wire, and plastic zip-ties. On occasion, plastic chairs were used to hold one end parallel to the panel surface. The gages were installed according to the original instrumentation drawings. Excess lead wire was doubled, bundled, and cast into the concrete. Figure 4.15 shows a transverse and longitudinal gage installed with plastic chairs under the ends. Each gage is tied to adjacent pretensioned strands to prevent movement during consolidation.

To get a profile of temperatures, thermocouples were located at the top, middle, and bottom of the cross-section. Thermocouples were attached to a small vertical piece of FRP bar to obtain this gradient. The FRP is non-ferrous and would not interfere with thermocouple signals during contact. Figure 4.16 shows two thermocouples tied to a short piece of FRP bar.

The vibrating wire gages were attached or "piggy-backed" on the instrumented rebar. Wooden spacers were used to ensure the flanges of the vibrating wire gage did not touch the rebar. The zip ties holding the vibrating wire gages in place were purposely left loose to ensure the gages were not restrained or damaged. Figure 4.17 shows a vibrating wire gage mounted to a rebar with wooden spacers and plastic zip-ties.

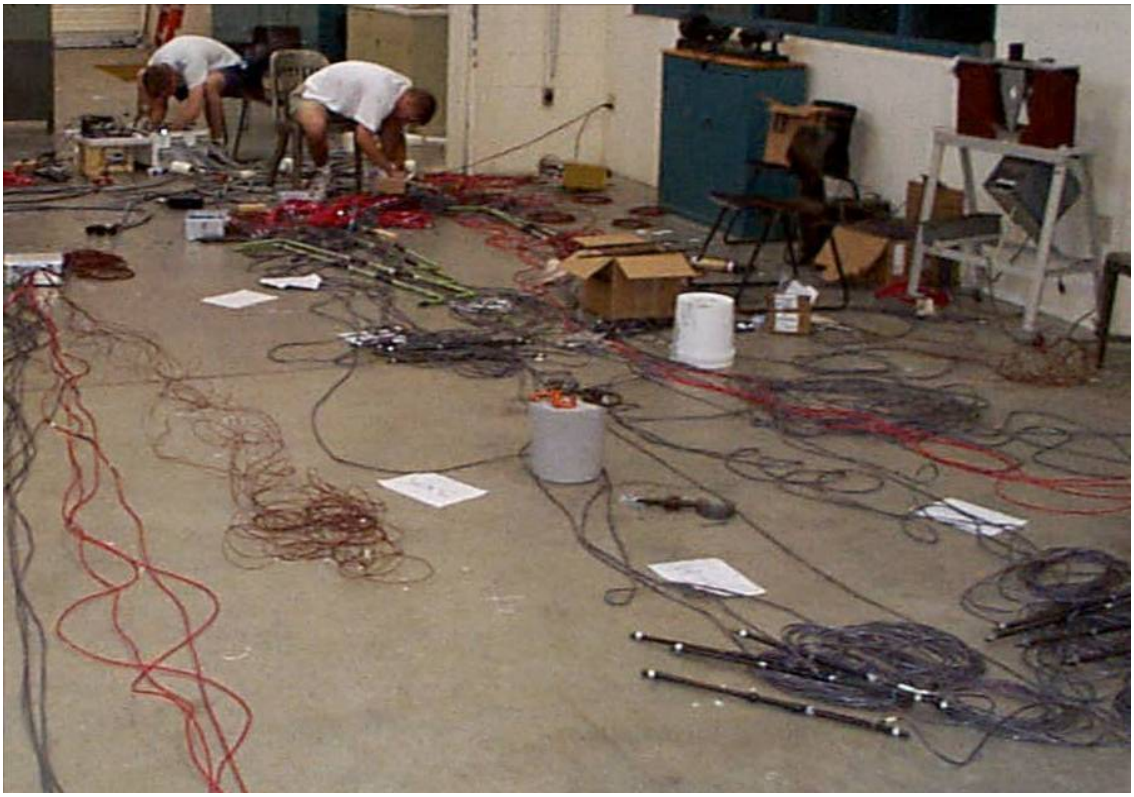

Figure 4.14 - Gages being laid out for testing in lab

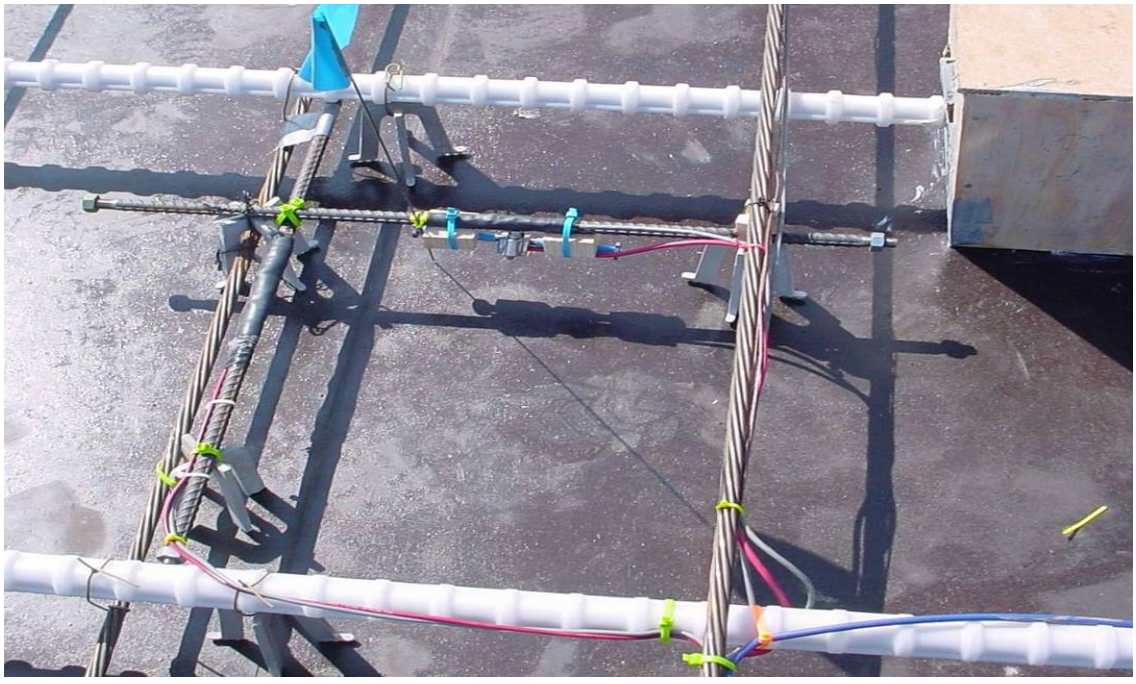

Figure 4.15 - Transverse and longitudinally installed rebar using spacers and ties

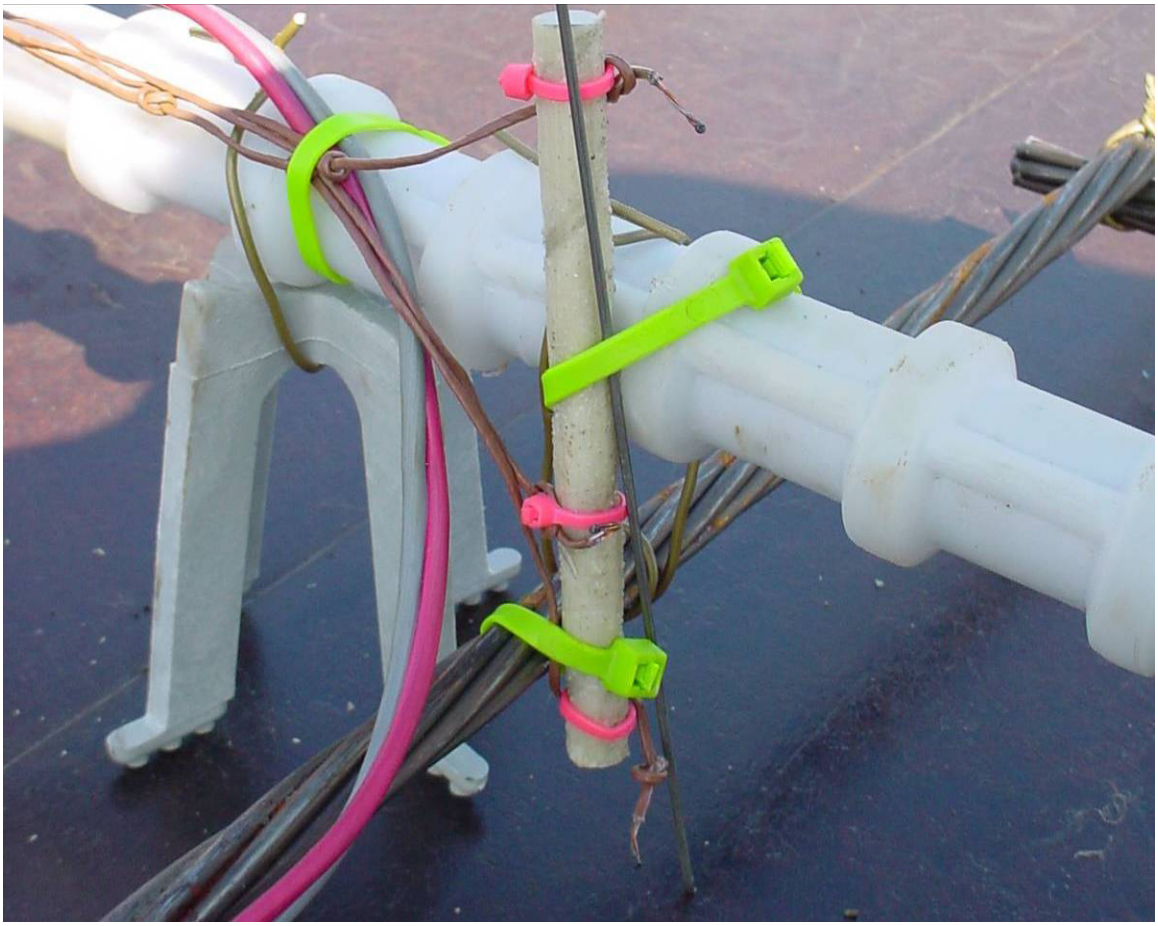

Figure 4.16 - Two thermocouples zip-tied to FRP for thermal depth gradient

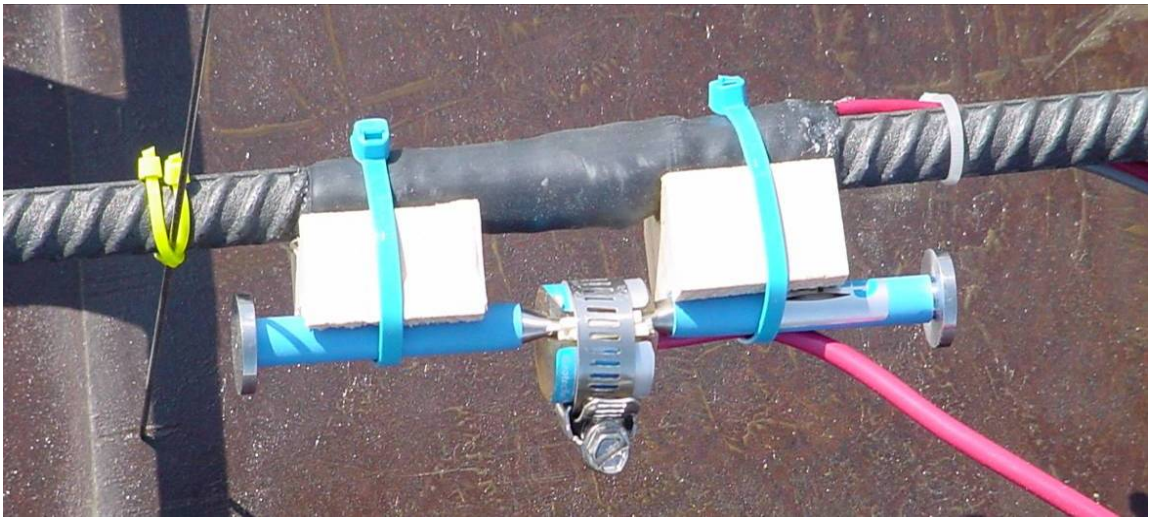

Figure 4.17 - Vibrating wire gage attached to rebar with spacers and loose ties

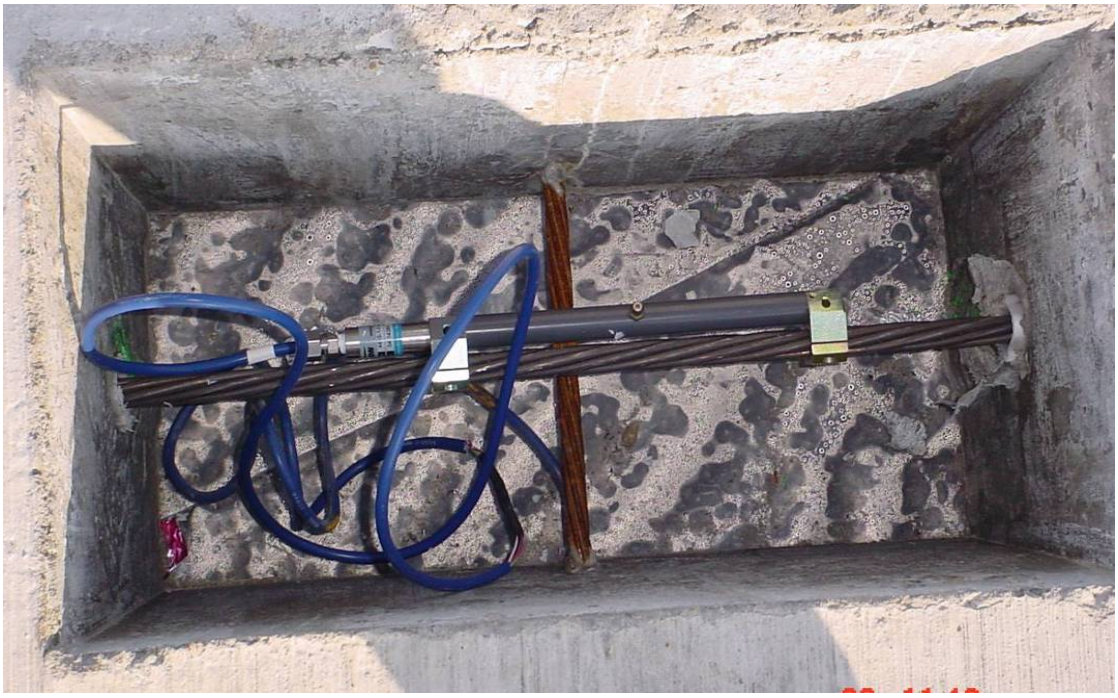

Figure 4.18 - Strandmeter installed in block-out around post-tensioning strand.

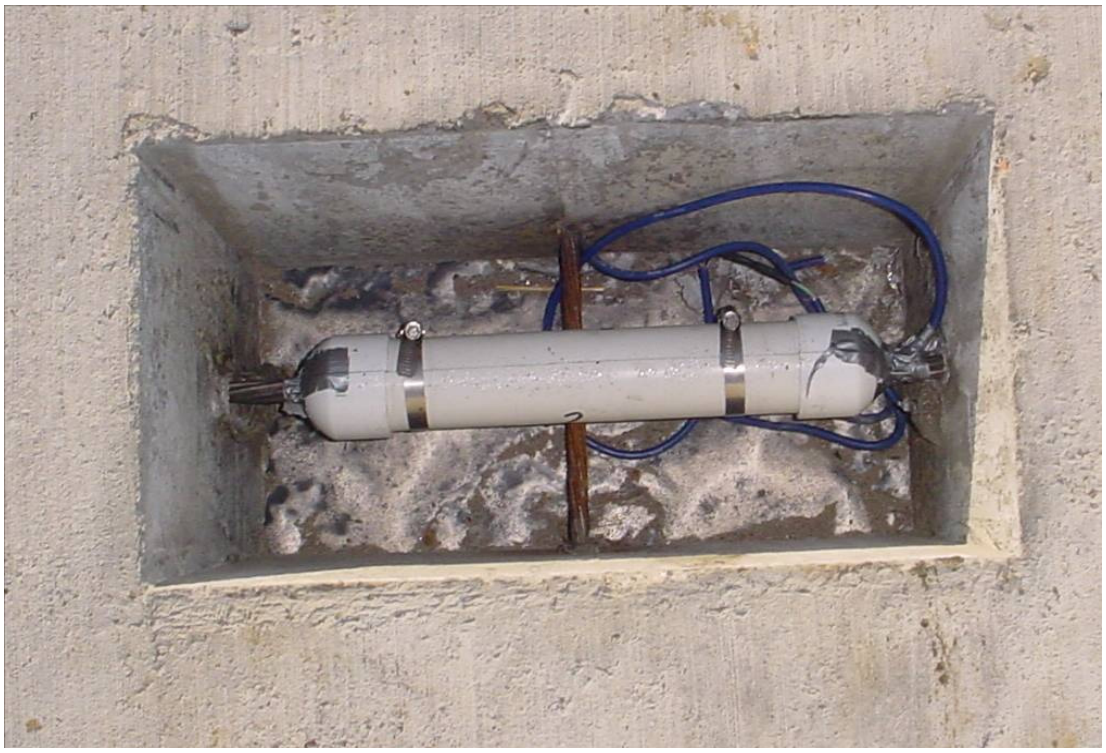

Figure 4.19 - Strandmeter encased in PVC tube to isolate it from grout.

Strandmeters were installed on the post-tensioning strands in the field. In order to send and receive signal, wires were run to a block-out (around the center post-tensioning duct) and terminated during fabrication. Figure 4.15 shows a greased plywood strandmeter block-out in the upper right hand corner. The block-out was removed and the instruments were installed in the field by splicing into existing wires and clamping the gage on the post-tensioning strand. The output of the gage was adjusted and set (by adjusting a set screw) and the grey PVC tube was filled with grease (see Figure 4.18). The clamps were covered in roofing tape and a final PVC jacket was hose-clamped over the entire device to further isolate it from expanding and contracting grout (see Figure 4.19).

4.1.3. DATA ACQUISITION SYSTEM

Nearly one hundred gages were installed in the seven instrumented panels. To efficiently and economically take a large number of measurements was a challenge. The instrumented panels were cast two at a time. Recording temperature gradients and temperature extremes during casting and curing operations was a priority. During pretensioning transfer and post-tensioning transfer, it was necessary to take only strain readings. In-service measurements must combine the most and best strain and thermal measurements possible. There was a need, therefore, for flexibility in the data acquisition system to allow for changes in the parameters being monitored at specific stages in the life of the panels. During casting and curing it was also necessary to be able to move the data acquisition system and switch between panels easily. It was with these goals that the data acquisition system was developed. The following sections describe the hardware for

the data acquisition system used on the Missouri pilot project by the University of Missouri-Columbia.

4.1.3.1. GENERAL INFORMATION

Each gage had to send a signal to and receive power from the main data acquisition system. The lead wires from the gages were routed into terminal boxes cast into each panel (by using a block-out). One terminal box was dedicated to each panel. Cables with detachable connectors were used to connect the terminal boxes to the main data acquisition box. This allowed quick disconnect during fabrication. A datalogger and multiplexers housed in the main data acquisition box were used to excite and read the gages. A network link interface was installed to be able to remotely access the system.

4.1.3.2. TERMINAL JUNCTION BOXES

The terminal boxes served several purposes. First it was necessary to route all of the instrumentation leads efficiently into quick connect cables to go to the main data acquisition box. The terminal box dimensions are 8 in x 12 in x 4 in (20.3 cm x 30.5 cm x 10.2 cm). The leads from the instrumentation were first fed through a hole in the plywood block-out (see Figure 4.20) and then into an opening in the long dimension of the terminal box (see Figure 4.21). A printed circuit board was fabricated at the University of Missouri – Columbia that had screw terminal posts for connecting the leads from the embedded gages to a female pin connection that would send the signal to the main datalogger. This board can be seen on the left side of Figure 4.21. The different gage types were separated on the junction board to allow systematic connection. Short wires, soldered to the bottom of the board, connect to the female pin connection (this is the black object in the upper middle part of Figure 4.21).

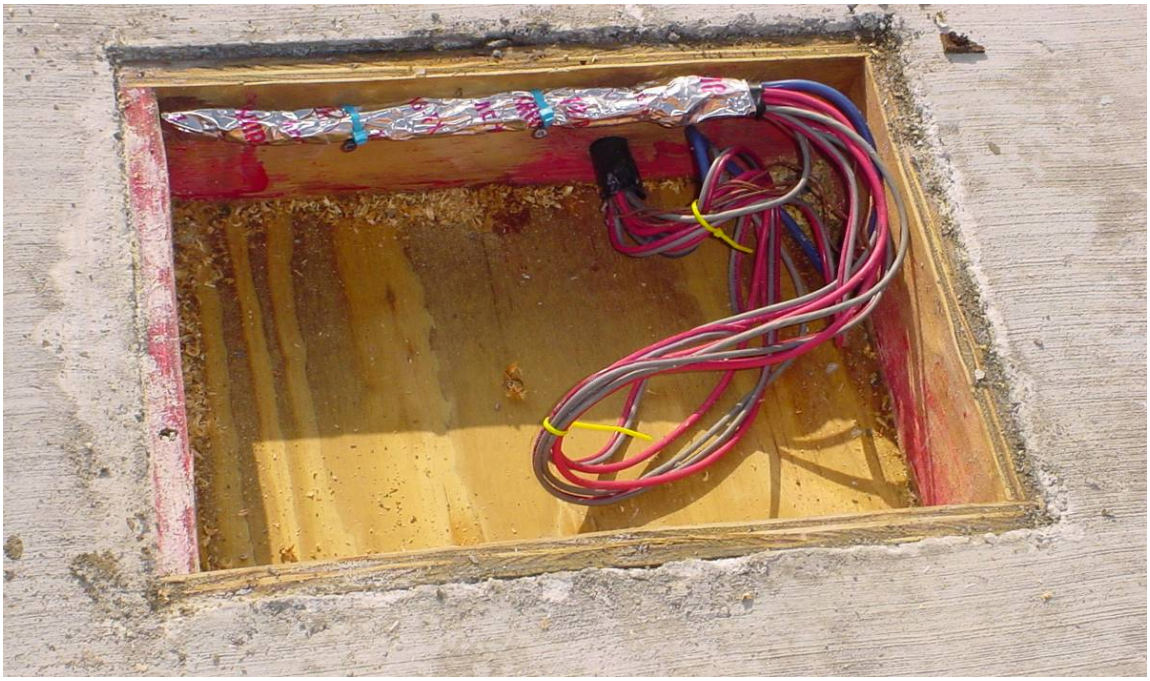

Figure 4.20 - Junction box block-out in panel with wires from instrumentation

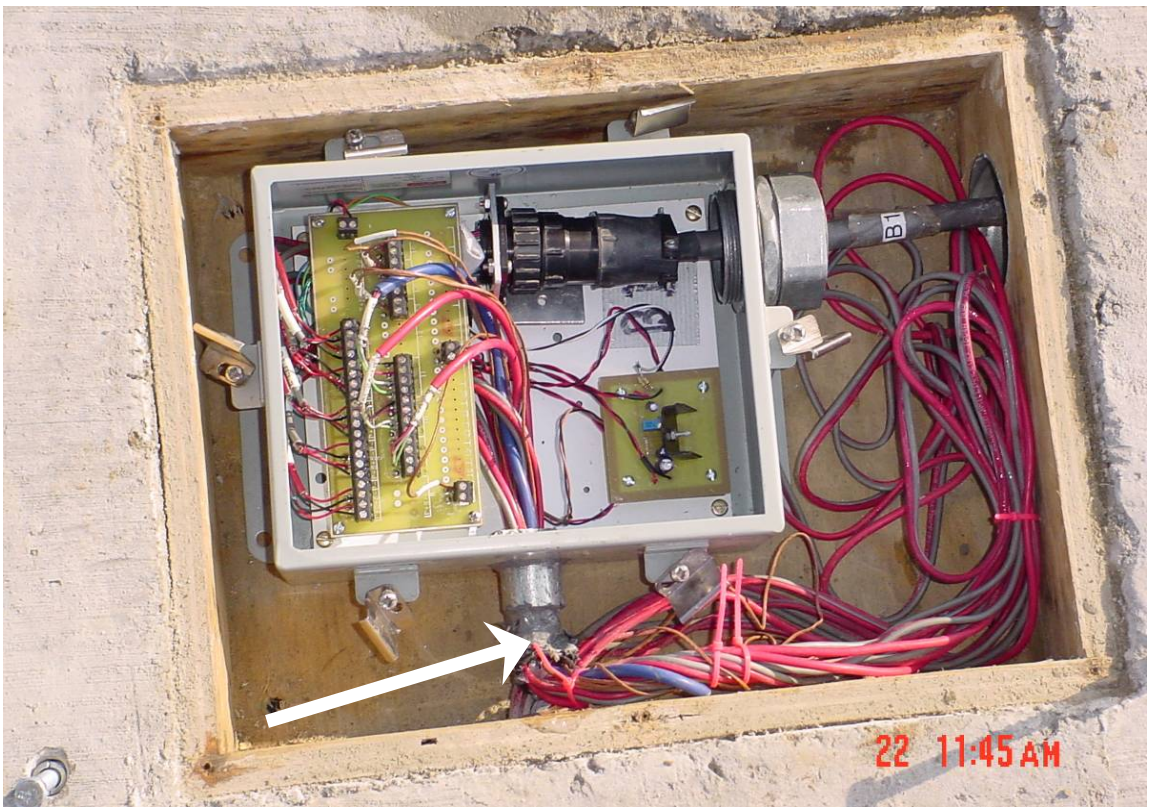

Figure 4.21 - Junction box inside plywood block-out, with instrumentation and quick connect hooked up (note grey epoxy where wires enter box)

The terminal boxes also served as the cold junction reference for the thermocouple readings. As explained in Section 4.1.2.4, it is necessary to know the temperature of the thermocouple terminal junction for the thermocouple temperature measurement to be properly compensated. A temperature sensor obtained from Digi-Key Corporation was used to determine the temperature in each terminal box. The circuit complimenting this sensor can be seen in Figure 4.22. This circuit was placed under the voltage regulator in the junction box in order to save space.

The final function of the junction box was to step down incoming power voltage. A voltage regulator was needed to reduce the 6-8 Volts from the power supply to the 4 Volt excitation used for the instrumented rebar. This was accomplished with the circuit shown in Figure 4.23. A heat-sink was installed on each circuit to dissipate energy efficiently.

There are many advantages to this type of junction box/ block-out. Several weeks passed between casting and panel placement. The instrumentation was unhooked after casting and the junction boxes were removed from the panel. The plywood block-outs allowed the team to remove the box for dry storage and cleaning before construction. Once installed at the job-site, the wires entering the box were sealed with a 3-M two part epoxy. This can be seen on the wires in Figure 4.21.

Another advantage of the junction box was that the mounting plate inside the box was removable. This allowed the research team to remove the inner workings for easier handling and to address maintenance issues. Figure 4.24 shows the mounting plate and circuitry hooked up during mock testing in the MU materials testing lab.

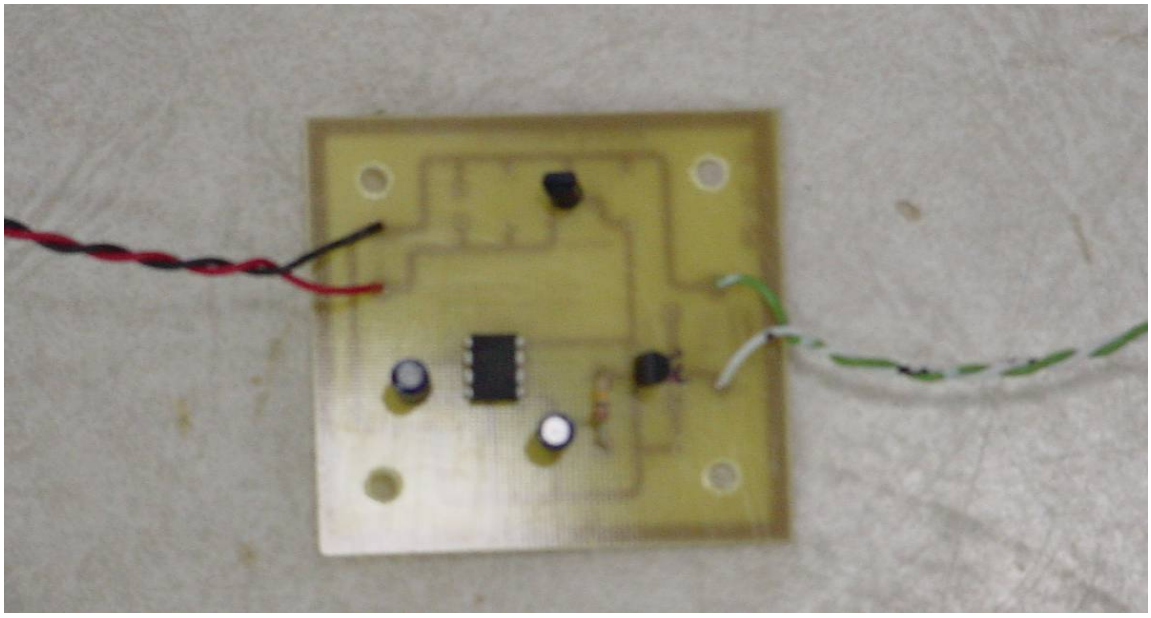

Figure 4.22 - Cold junction circuit for thermocouple compensation

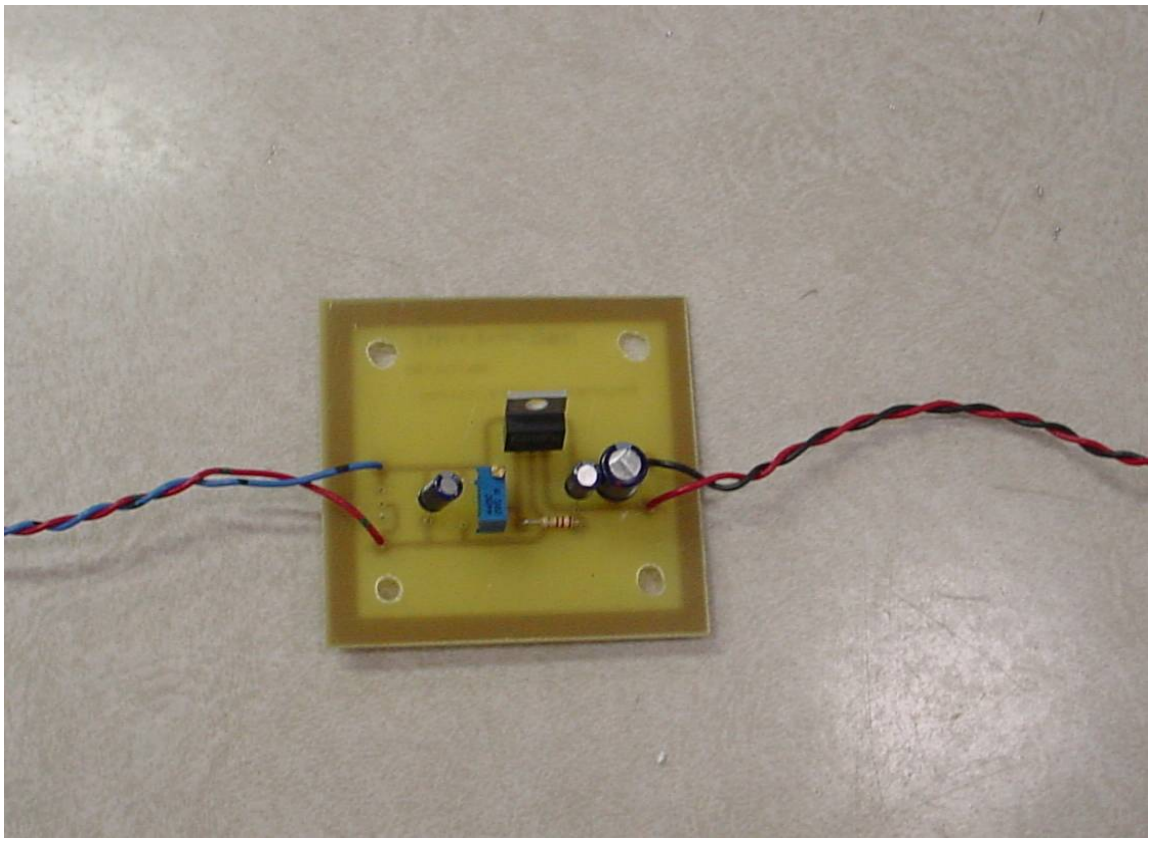

Figure 4.23 - Circuit for stepping down incoming voltage to 4V for rebar excitation

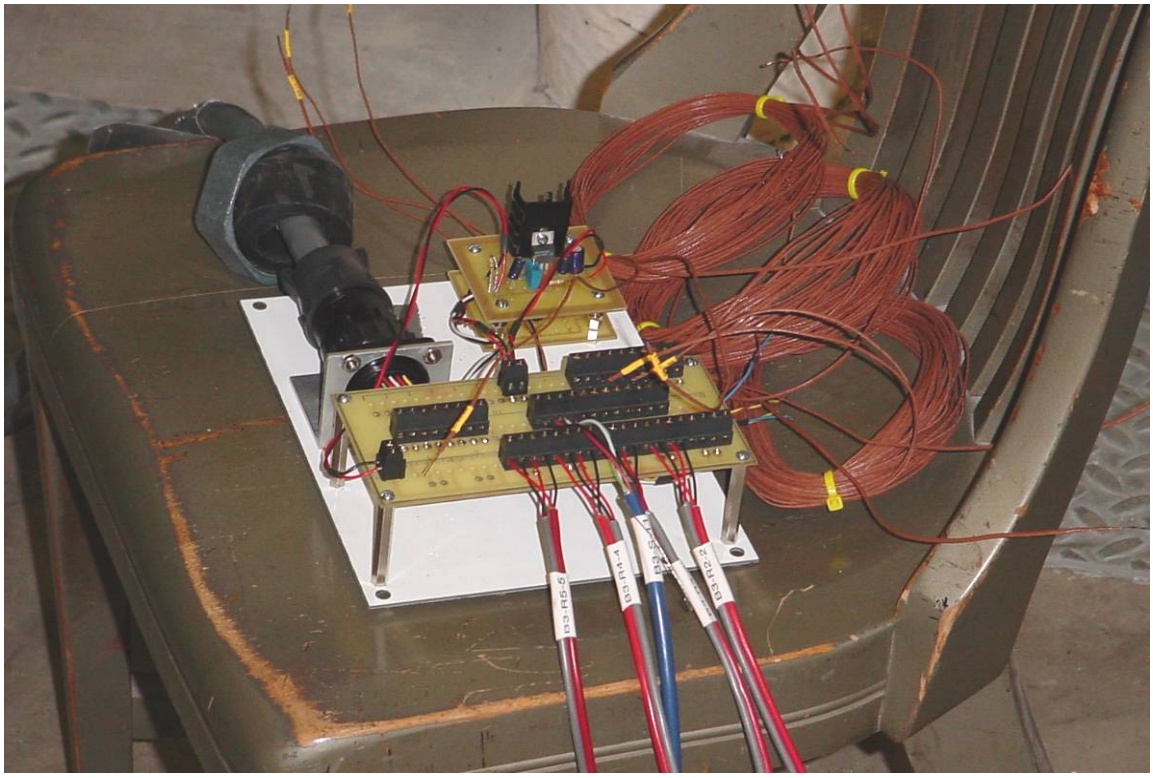

Figure 4.24 - Instrumentation hooked to inner workings of junction box for mock-up testing in the lab

Figure 4.25 - Construction of the same pin-type quick connector on a previous project (Eatherton 1999)

4.1.3.3. CABLES AND CONNECTORS

Seven cables (one for each terminal box) carried the signal wires to the main data acquisition box. The cables are 11, 19, and 27 pair, individually shielded cable obtained from Belden. The connectors are 57 pin circular plastic connectors with gold plated pins and sockets. The pins and sockets were individually soldered onto cable wires and pressed into place in the connector. Part of this tedious process is shown in Figure 4.25 (Eatherton 1999). Each group of pins was assigned an instrument type (see Figure 4.26). Each number on the pin connector was connected to corresponding numbers on the terminal board. This allowed for modular construction as well as the ability to use any cord with any panel (the instrument labels on wires would only be different).

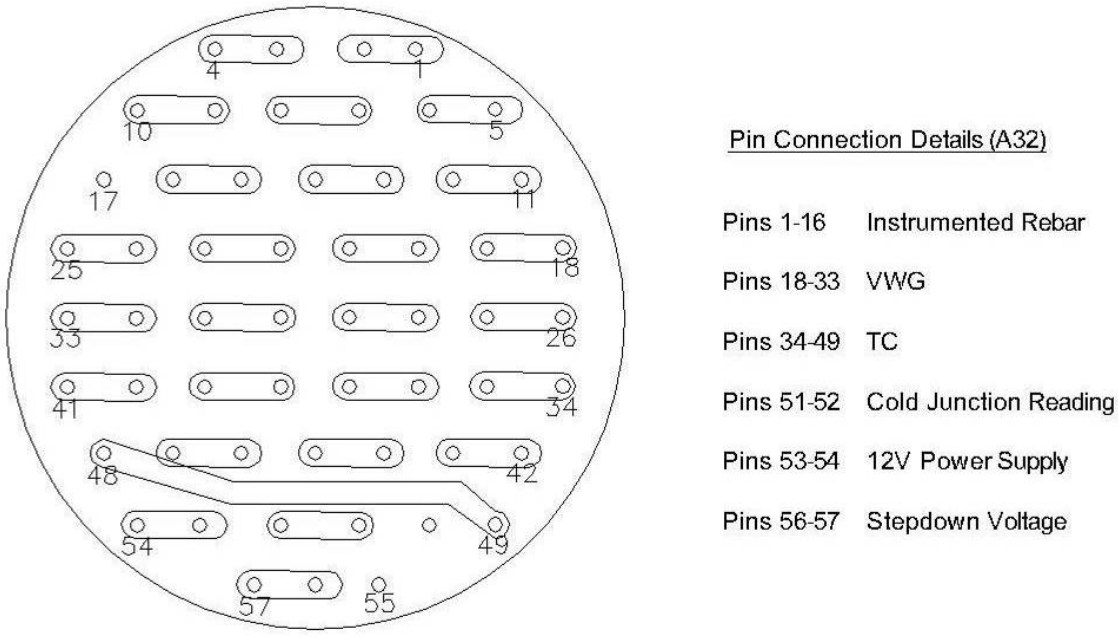

Figure 4.26 - Diagram of quick connect pin assignments for individual pairs

4.1.3.4. MAIN DATA ACQUISITION BOX

The cables from the junction boxes in each panel travel underground and enter a signal cabinet through 6 in (15.2 cm) PVC. The wires then ran into the white data acquisition box pictured in Figure 4.27. One inch thick aluminum clamps were tightened onto the cables to provide strain relief and moisture / bug protection. The cables inside the main box were split up into their individual wire pairs. The wire pairs were stripped, tinned and labeled. The individual wire pairs were connected into the multiplexer terminals in different arrangements depending on which gages needed to be monitored.

4.1.3.4.1. AM416 Multiplexers

The enclosure, multiplexers, datalogger, NL100, and vibrating wire interfaces were obtained from Campbell Scientific, Inc. Three model AM416 relay multiplexers were mounted in the bottom of the main data acquisition box (see Figure 4.28). Each multiplexer is capable of multiplexing 32 differential signals into 2 differential outputs. The total number of instruments that can be read at one time is therefore 96. This would include nearly every instrument; however, certain limitations limit this number to 66. Each vibrating wire gage requires two channels—one for the signal and one for the thermistor. Also the cold junction temperature and step-down voltage was read at each panel. These values are good to have for trouble shooting instrumentation.

It was decided that it would not be economical to purchase more multiplexers and another datalogger to take measurements from all pieces of instrumentation at once. Interstate 57 is also a long way from Columbia, MO. With the proper planning, specific gages critical to in-service conditions were chosen. Data acquisition on any other gages would require a new program and physically switching wires.

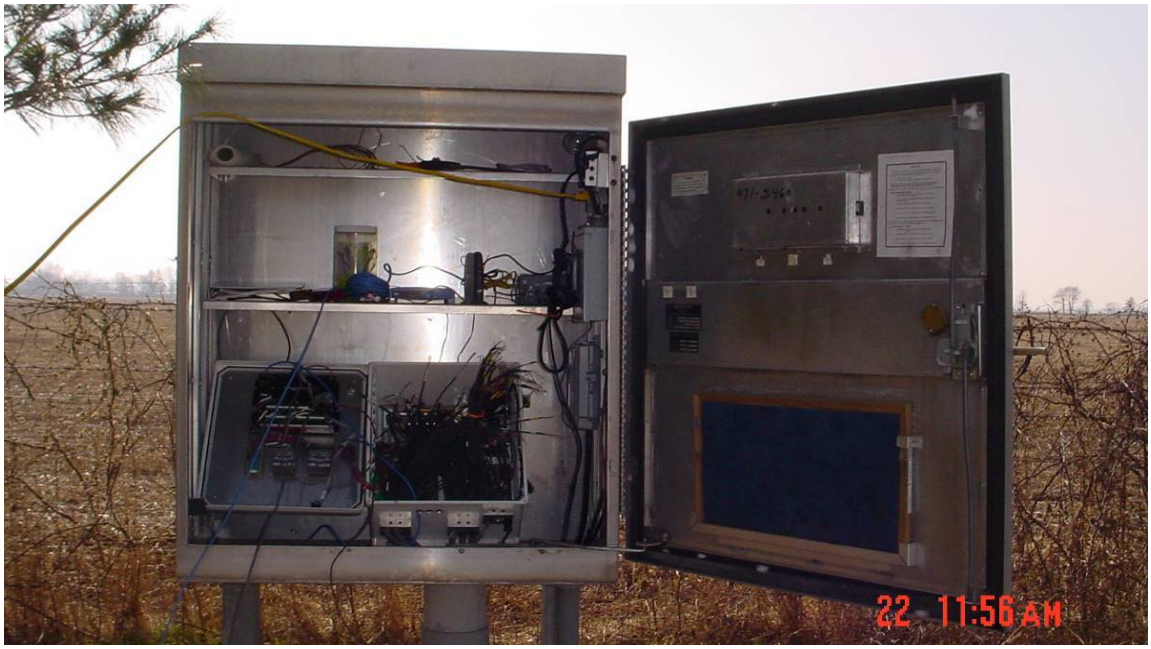

Figure 4.27 - Signal cabinet in south right of way of I-57—housing data acquisition system; wires enter from bottom

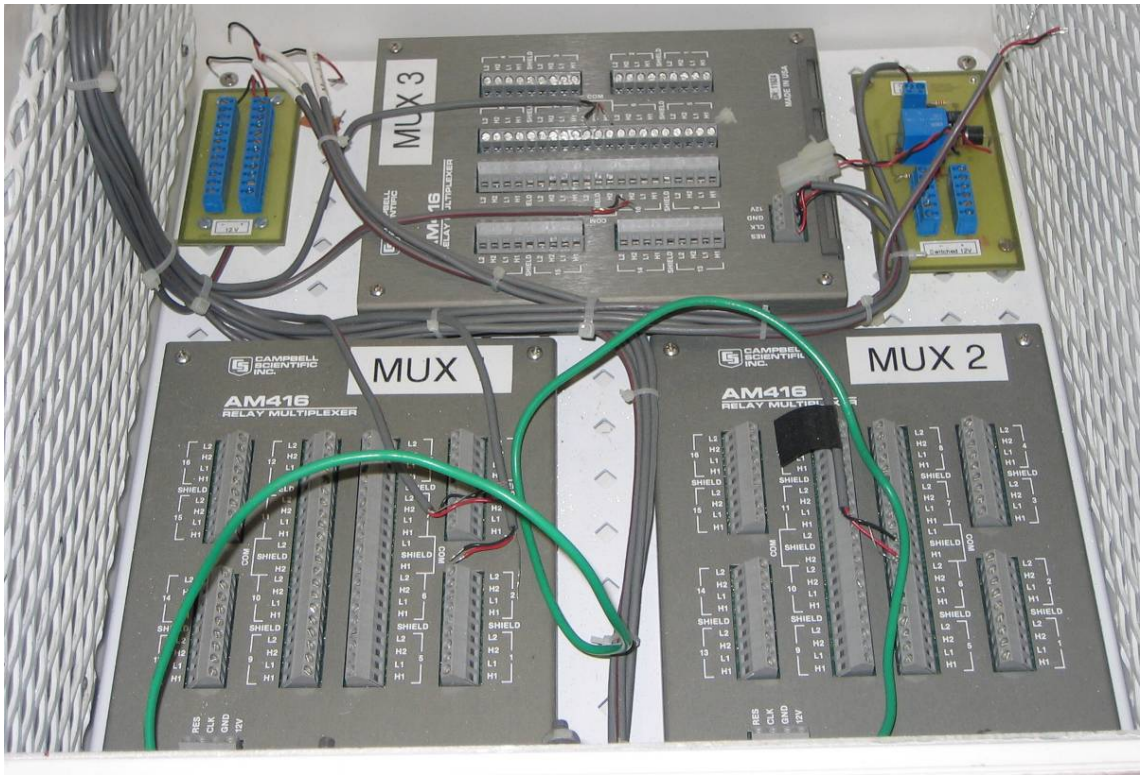

Figure 4.28 - Bare AM416 multiplexers in bottom of data white DAQ box

4.1.3.4.2. Power Supply

Power and phone cable were run underground from a nearby line to the signal cabinet. Two 30 amp feeds power the entire cabinet (see Figure 4.30). A separate linear step down power supply was purchased to run the datalogger, multiplexers, interfaces, and gages (see Figure 4.29). This power supply steps down 120V AC to 12V DC and is protected by a 2 amp fast acting fuse. Twelve volts was run to the datalogger and a separate fabricated circuit board attached to the housing. This circuit stepped the 12 volts down further using three parallel circuits similar to the one located in the junction boxes at each panel. This was done to send varying amounts of power to each panel, thus optimizing energy dissipation and current demand. As described in the section on terminal boxes this voltage is then reduced to 4 volts at each panel.

Steel grating was installed on the sides of the main data acquisition box to allow easy organization of the unused wires. Extra leads from the cables were bundled and tied neatly to the side grating. An aluminum plate with short stand-offs was attached to the lid of the white DAQ box. The NL100, datalogger, and vibrating wire interfaces were attached to the lid (see Figure 4.31).

4.1.3.4.3. CR10X Datalogger

The datalogger is the CR10X model and is shown right under the NL100 in Figure 4.31. It has 6 differential analog inputs, 8 digital I/O ports, 2 excitation ports, and 3 pulse ports. The CR10X accepts a program from a PC over an RS232 port and then runs independently. Data can be downloaded to a PC or laptop. The datalogger is capable of recording up to 62,000 measurements before it begins to overwrite data.

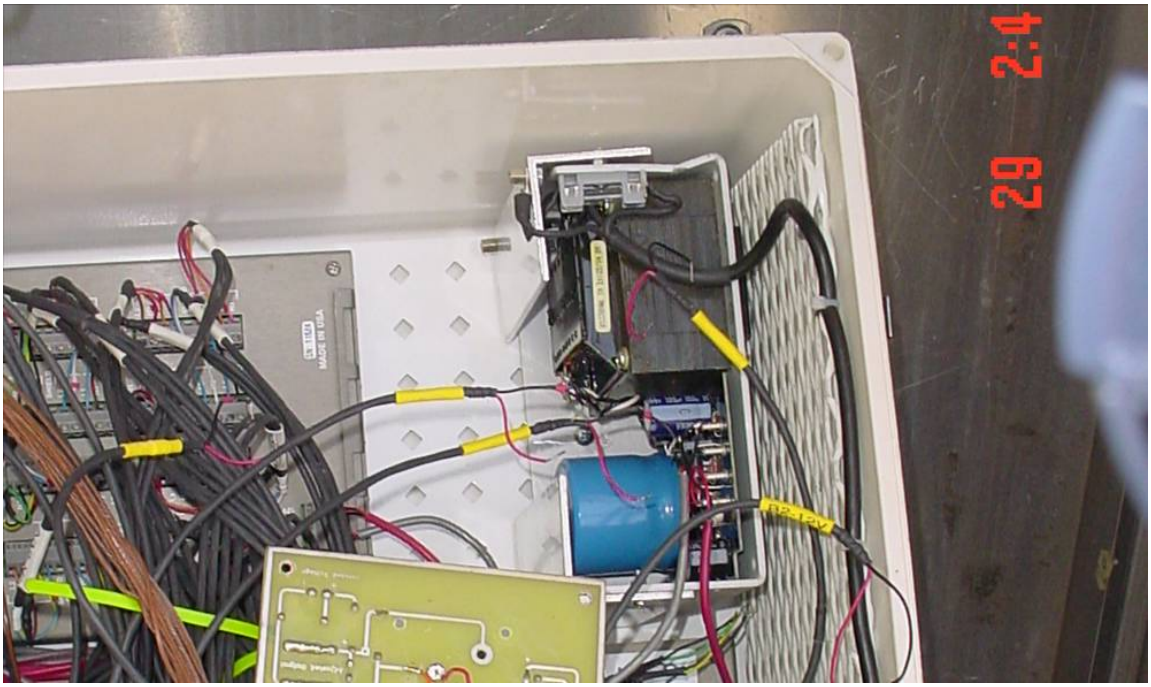

Figure 4.29 - 120V to 12V DC power supply used to power entire system—fastened in corner next to multiplexers

Figure 4.30 - 30amp power drop (right), UPS protection (middle), DSL modem (left)

The Loggernet software provided by Campbell Scientific was used to program as well as download data. The CR10X is programmed to control and switch the multiplexers, compensate thermocouples, reduce vibrating wire data, and store data in array format with individual timestamps

4.1.3.4.4. AVW1 Vibrating Wire Interface

The vibrating wire interfaces (AVW1) are attached below the datalogger in Figure 4.31. These devices provide completion bridges for the thermistors and excitation and signal conditioning for the vibrating wire strain gages. These are required to read the signal from the vibrating wire gages; therefore, the gages are all hooked up to the same multiplexer. That multiplexer is switched by the data logger and the signal is sent to the AVW1 for conditioning. The conditioned signal is then sent to the datalogger for reduction and storage.

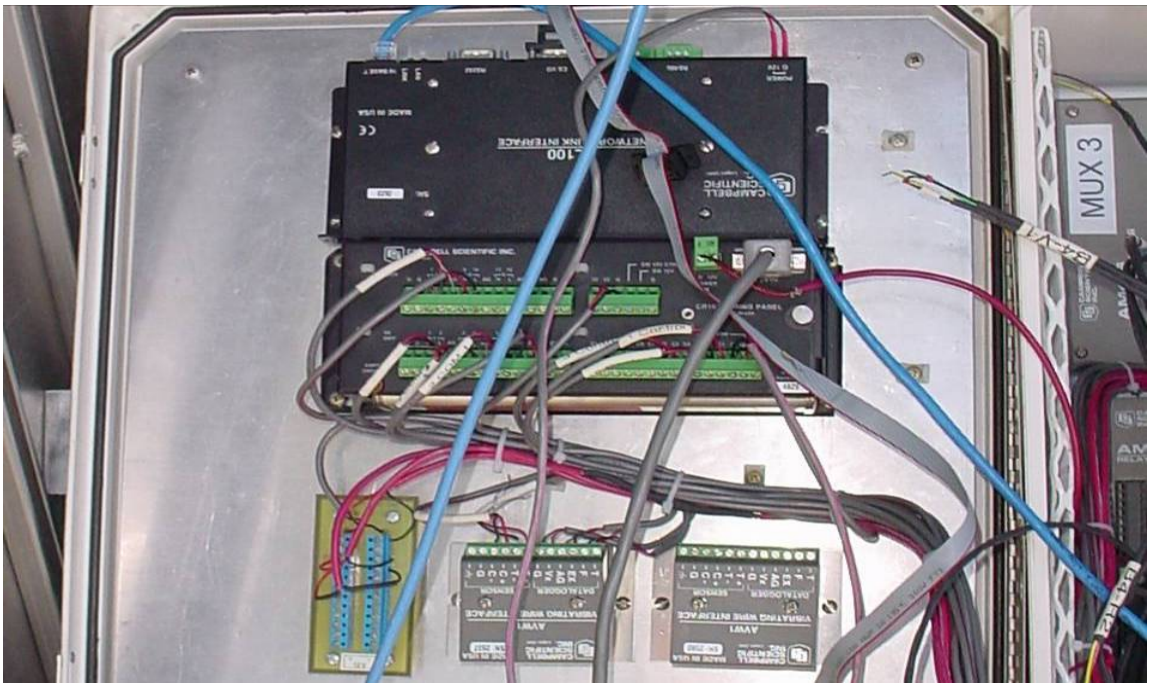

Figure 4.31 - NL100 network link (top), CR10x datalogger (middle), and two AVW1 interfaces—fastened to lid of white DAQ box

4.1.3.5. REMOTE COMMUNICATION EQUIPMENT

Although the datalogger has a sizable amount of storage, it is not practical for the University of Missouri research team to frequently make the four hour trip to Sikeston, MO to download data or change instrumentation programs. For this reason, a network link was installed to remotely access the datalogger. The NL100 (pictured in Figure 4.31) was purchased through Campbell Scientific. Through the Loggernet software provided with the datalogger, the research team is able to connect to the NL100 through a DSL connection installed in the signal cabinet (see Figure 4.30). New programs can then be uploaded, data files can be downloaded and real-time strains and temperatures can even be observed. In the months to come, a website will be constructed using the Real Time Data Monitoring (RTDM) feature of Loggernet to display real time data over the web. This will allow others involved to view samples of in-service data over the World Wide Web.

4.1.4. EXTERNAL INSTRUMENTATION

It is important to monitor internal stresses and strains during in-service conditions, but global movement is also a vital performance based criteria. To measure global movement, drop-in anchors were installed in each corner of the two instrumented joint panels (A31, and A32). A tiny pilot hole was drilled on the head of each anchor to accommodate survey equipment.

4.1.4.1. TOTAL STATION SURVEY EQUIPMENT

A Tapcon total station survey system was and will be used to locate the hole on each bolt. A land marker was installed near the signal cabinet and zero readings were taken by a MoDOT survey crew in early January 2006 before the road was open to

traffic. Since the zero reading, surveys have and will continue to be conducted to obtain global x, y, z movements of pavement Sections 2-4.

Each survey requires three people. A prism is set up on a back-sight installed in the median 300 yards (274 m) west of the test section. The Tapcon gun is centered over the concrete marker near the signal cabinet. The line from that marker to the back-sight is the azimuth or line of reference. Another prism is then held on each marker (in the piloted hole). Distance readings relative to the azimuth are recorded

4.2. LABORATORY STUDIES

As stated earlier this thesis focuses on the early age behavior during curing, stress transfer, and in-service performance. A companion thesis written by Brent M. Davis titled Evaluation of Prestress Losses in an Innovative Prestressed Precast Pavement System will thoroughly cover laboratory studies and theoretical prestress losses. The following sections briefly touch on the setup and general objectives of each laboratory study.

4.2.1. GENERAL

Laboratory studies were conducted to determine important properties regarding the concrete mix design used in fabricating panels. All studies were performed at the University of Missouri-Columbia according to ASTM standards. Specimens were made during the casting of instrumented panel sets. Figure 4.32 shows the research team constructing specimens at CPI's casting yard in Memphis, TN. Table 4.8 shows the date experimental specimens were cast along with the quantity and specimen dimensions/type (Davis 2006).

Table 4.8 – Summary of experimental specimens cast for laboratory studies (Davis 2006).

	Date Cast	6"X12" Cylinders	4"X8" Cylinders	3"X4"X16" Prisms	Creep Specimens	Shrinkage Specimens
Specimen Set 1	10/11/2005	6	0	0	0	0
Specimen Set 2	10/12/2005	6	0	6	5	5
Specimen Set 3	10/13/2005	6	0	0	0	0
Specimen Set 4	12/9/2005	6	4	0	5	0

Figure 4.32 – Casting creep, shrinkage, strength cylinders, and beams for freeze-thaw and flexure (Davis 2006)

4.2.2. COMPRESSION TESTS

The compressive strength of each specimen set was determined at 7, 28, and 56 days of moist curing. The tests were performed in accordance with ASTM C-39, "The Standard Test Method for Compressive Strength of Cylindrical Concrete Specimens" (ASTM 2005). The 6 in x 12 in (12.2 cm x 30.5 cm) cylindrical specimens were first capped to ensure parallel and adequate stress distribution. A 600 kip (2700 kN) Forney concrete compression testing machine pictured in Figure 4.33 was used for the compression tests. Specimens were loaded at a rate of 45-50 psi/s (Davis 2006). Three LVDTs evenly distributed around the specimen with an 8" gage length measured strain for modulus calculations.

Figure 4.33 – Compression test setup for capped 6" diameter cylinders using 3 LVDTs and a Forney Compression Machine.

4.2.3. CREEP TESTS

Creep frames apply a constant load to concrete cylinders and measure the resulting creep strain of concrete over time. This test used spring loaded creep frames designed and implemented on a previous research project at the University of Missouri – Columbia (Earney 2007-Anticipated). At 28 days, four 12 in (30.5 cm) cylinders were loaded into the creep frame shown in Figure 4.34. Each cylinder was sulfur capped and two of the cylinders were sealed with foil tape to block moisture migration. A hydraulic jack was then placed between two steel plates at the top of the frame to apply compressive load to the railroad springs at the bottom. The entire frame shown in Figure 4.34 is located in a walk in freezer that has been converted into an environmental chamber (controlled temperature and humidity). Between each cylinder is a pair of Teflon sheets to reduce friction between capped cylinders. Three 10" extensometers were fastened to brass inserts spaced at 120° around each cylinder. They were averaged to determine the creep strain in each cylinder over time.

4.2.4. SHRINKAGE TESTS

Specimens for creep and shrinkage were prepared and instrumented in the exact same manner. However, shrinkage testing began after one day and the specimens were not loaded. Two sealed and two unsealed specimens were monitored. After preparation, the cylinders were placed in the same hermetically sealed chamber used for creep testing. Figure 4.35 shows a sealed specimen on the shelf in the chamber instrumented with three extensometers for measuring strain. The specimens were monitored for 83 days. Observations between sealed (100% humidity) and unsealed (50% humidity) specimens were recorded and can be found in the companion thesis (Davis 2006)

Figure 4.34 – Creep load frame with sealed and unsealed specimens (Earney 2007-Anticipated).

Figure 4.35 – Sealed shrinkage specimen with three extensometers attached for measurement of shrinkage strains (Earney 2007-Anticipated).

4.2.5. RAPID CHLORIDE PERMEABILITY TESTS

The test setup shown in Figure 4.36 was constructed at the University of Missouri – Columbia for a previous project. The following outline the general procedure and steps for the Rapid Chloride Permeability Test (RCPT) (conducted according to (ASTM 2005).

Two days prior to the 6-hour chloride ion penetration test, 4 in (10.2 cm) diameter cylinders were removed from the moist curing room, de-molded, and coated with a two-part epoxy to seal the sides. The epoxy cured and three specimens (pucks) were cut from each cylinder. The specimens were placed in sealed water filled chamber and vacuum desiccated for three hours in to fully saturate and de-air each puck. Each was removed, towel dried, and placed in the cells shown in Figure 4.36. Two rubber gaskets were placed on each end of the specimen before bolting the cells together. A 60 V potential was induced between each side. The positive terminal was filled with 0.3N NaOH, and the negative side was filled with 3.0% NaCl solution. The data acquisition system (on the right side of Figure 4.36) collected measured current between the two poles for six hours. The area under this current vs. time plot provides a basis for determining the ion penetrability of concrete specimens (Davis 2006).

4.2.6. FREEZE THAW TESTS

The freeze-thaw tests were conducted according to Procedure A of ASTM C-666, (ASTM 2003). ASTM C-215, was used to determine the dynamic modulus of the concrete specimens (ASTM 2002). The following paragraphs describe the procedures followed on four of the six cast prism specimens.

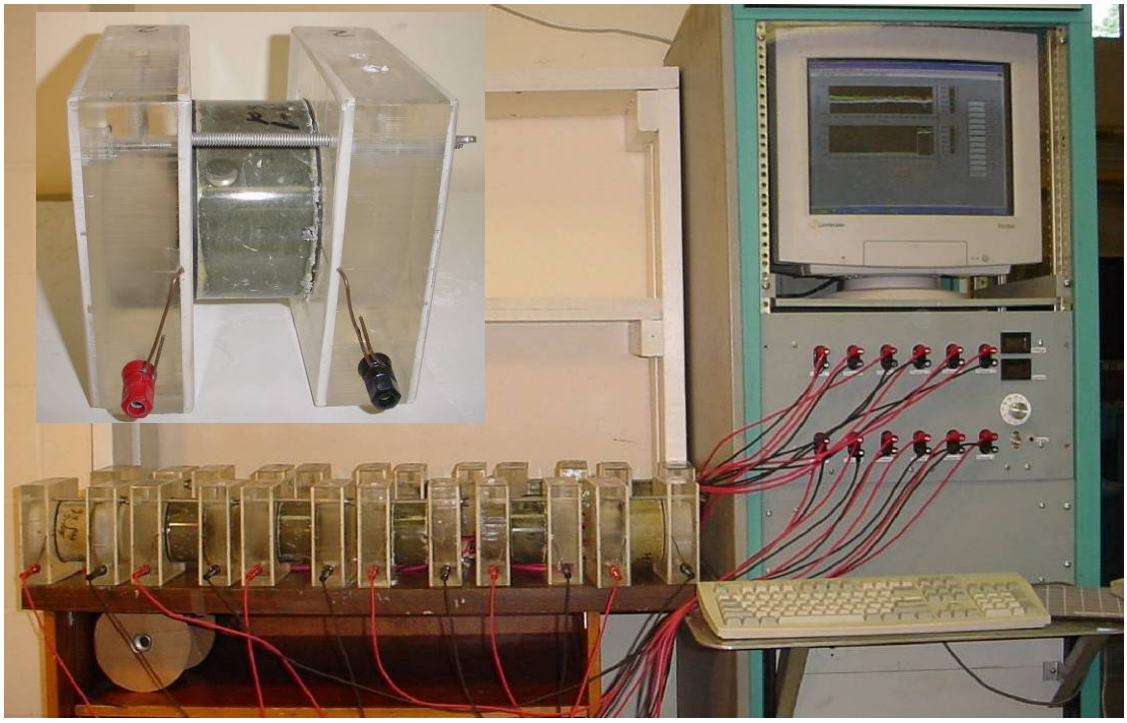

Figure 4.36 – Rapid chloride penetration test setup.

Figure 4.37 – Overhead view of cabinet used to subject prisms to freeze-thaw cycles

The freeze-thaw chamber at the University of Missouri – Columbia is capable of subjecting 18 prisms to approximately 10 freeze-thaw cycles every 24 hours. A single cooling unit freezes the specimens and strip heaters between the specimens thaw the concrete. The chamber is controlled by a concrete prism with two embedded thermocouples. One is connected to a chart recorder to monitor the number of cycles, and the other is connected to a control circuit in order to toggle heating and cooling. Figure 4.37 shows the freeze thaw chamber. Each stainless steel container is filled with water in order to fully submerge the specimens.

The specimens were placed in the freeze-thaw chamber and brought to a temperature of 40°F. Initial readings of weight and fundamental transverse frequency were then taken in order to establish a base-line reading. The specimens were then subjected to approximately 300 freeze-thaw cycles. Measurements of weight and fundamental transverse frequency were taken every 30 cycles.

The test-setup shown in Figure 4.38 was utilized to obtain transverse frequency values. An electromechanical driving unit oscillates the specimen on one end while a light-weight pickup measures the frequency on the other end.

A relative dynamic modulus (each with respect to original reading) is calculated for each measurement and plotted against time. Degradations in stiffness due to freeze thaw cycles can be seen. A durability factor is then calculated based on overall performance.

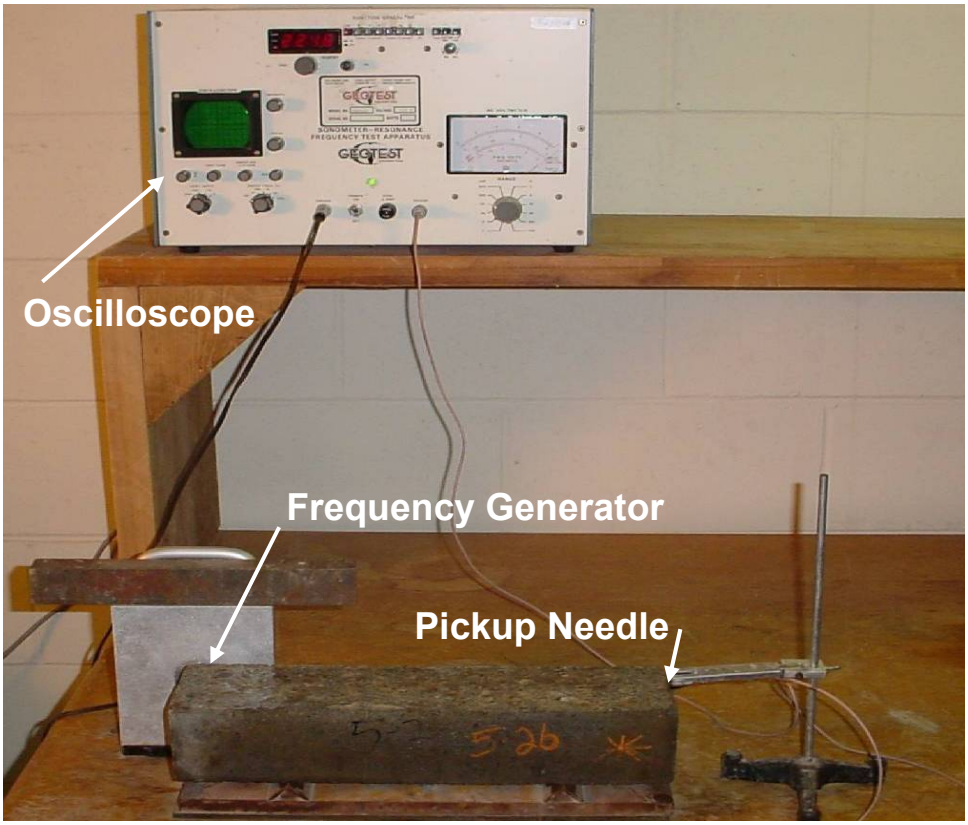

Figure 4.38 – Setup for measuring fundamental frequency during freeze-thaw tests.

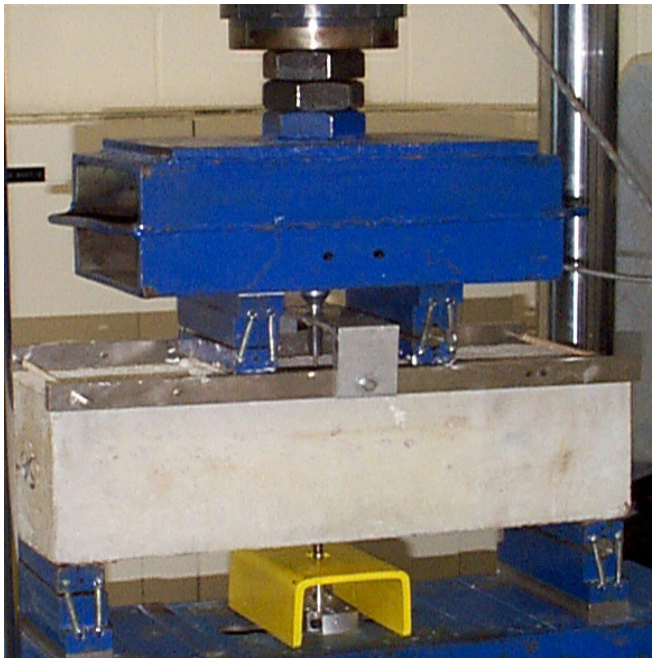

Figure 4.39 – Photograph of third point loading of concrete prism/beam.

4.2.7. FLEXURE TESTS

Flexure tests were performed according to ASTM C 78, "Standard Test Method for Flexural Strength of Concrete" (Using Simple Beam with Third-Point Loading)" (ASTM 2002).

The test setup used at the University of Missouri – Columbia is shown in Figure 4.39. A 110 kip (489 kN) capacity MTS machine with closed loop control was used to deflect two concrete prisms under third point loading (see Figure 4.39). Gross and net deflections of the beam were measured with two LVDTs. The LVDT on the bottom of the specimen measures the gross deflection. This value takes into account beam deflection, local crushing of the concrete, and elastic and inelastic settling at the supports. The second LVDT is fastened to bars riding on top of the specimen. This LVDT measures the deflection of the beam only (net deflection).

The beam specimens used are the same size as freeze thaw (14 in x 4 in x 3 in) or (35.6 cm x 10.2 cm x 7.6 cm). Each specimen was loaded until failure. Load and deflections (net and gross) were recorded. Values calculated at the conclusion of the experiment include; the modulus of rupture (f_r), the Young's modulus (E_c), the total energy absorbed, and the fracture energy (G_f) (Davis 2006).

5. MATERIAL PROPERTIES

The following sections describe the material properties and performance characteristics of materials used in construction and instrumentation of the PPCP system near Sikeston, MO. As stated earlier, detailed discussions on material property results and performance can be found in the companion thesis by Brent M. Davis titled Evaluation of Prestress Losses in an Innovative Prestressed Precast Pavement System (Davis 2006)

5.1. CONCRETE PROPERTIES

The following sections describe the mix design and performance of concrete used for fabricating the PPCP system. A summary of results from lab studies is presented as well.

5.1.1. MIX DESIGN

CPI Inc. designed the mix used for constructing the PPCP system and tailored it to meet MoDOT specifications. Details of the mix design are summarized in Table 5.1. The water content reported is the total water content including moisture present in the aggregates. The coarse and fine aggregate weights are for aggregates in a saturated surface dry (SSD) moisture state. The mix was designed for a release strength of 3,500 psi (24 MPa) (with steam curing over-night) and 28 day strength of 5,500 psi (38 MPa) (500 psi higher than specified by MoDOT). The minimum specified air-entrainment was 5%, and the maximum specified slump was 6 in. Internal concrete temperatures had to be at least 16 °C (60 °F) in order to cast.

The Type I Portland cement was purchased from Buzzi Unicem in Festus Missouri. The fine aggregate was Crowley's Ridge Sand from Razor Rock in Harrisburg, AR, and the coarse aggregate was MoDOT #7 Salem Limestone from Vulcan Materials – Reed Quarry in Grand Rivers, KY. Admixtures used were manufactured by Degussa Admixtures, Inc. The admixtures include MB-AE 90, an air-entraining agent, Glenium 3000 NS, a full-range water-reducer, and Pozzolith 200 N, a water-reducer (Degussa 2006). The water used was Memphis municipal potable water. It was heated on very cold days to keep the concrete warm enough for casting.

Table 5.1 – Mix design of concrete used in PPCP system.

Constituent	Precast Pavement Mix
Cement	722 lb/yd^3
Fine Aggregate	1162 lb/yd^3
Coarse Aggregate	1766 lb/yd^3
Water	28.25 gal
Water - Cement Ratio	0.326
Air Entrainment Admixture	MB AE 90 1 -3 oz / yd^3
Full-Range Water-Reducer	Glenium 3000NS 4 - 8 oz / 100 lb Cement
Water Reducing Admixture	Pozzolith 200N 2 -5 oz / 100 lb Cement

5.1.2. SUMMARY OF CONCRETE PERFORMANCE (LAB STUDIES)

Table 5.2 shows a summary of experimental laboratory results of the concrete used in the Sikeston, MO PPCP system. Strength values were nearly 50% above the 5,000 psi specified by MoDOT. Nearly all performance parameters are 'on par' with a well designed concrete mix except the chloride permeability. Several specimens tested showed poor resistance to chloride ingress. Please refer to the companion thesis for an in-depth analysis of experimental results as well as comparisons with theoretical predictions.

Table 5.2 – Summary of experimental concrete properties of PPCP (Davis 2006)

Tests Performed	Parameter	Experimental Result
Results from Compressive Strength Laboratory Studies (ASTM C 39)	28 Day Strength, f'_c psi (MPa)	7,190 (49.6)
	28 Day Ultimate Strain, ε_{ult} in/in	0.00154
	28 Day Modulus of Elasticity, E_c psi (MPa)	5.69×10^6 (3.92×10^4)
	56 Day Strength, f'_c psi (MPa)	8,830 (60.9)
	56 Day Ultimate Strain, ε_{ult} in/in	0.00159
	56 Day Modulus of Elasticity, E_c psi (MPa)	6.26×10^6 (4.31×10^4)
Results from Flexural Laboratory Studies (ASTM C 78)	Modulus of Rupture, f_r psi (MPa)	872 (6.01)
	Fracture Toughness, G_f lb-in/in^2 (N-m/m^2)	0.237 (41.2)
Results from Freeze-Thaw Laboratory Studies (ASTM C 666 Procedure A)	Durability Factor, DF	97%
Results from Chloride Permeability Laboratory Studies (ASTM C 1202)	28 Day Charge Passed, Q_s Coulombs	3,999
	112 Day Charge Passed, Q_s Coulombs	3,151

5.2. PRESTRESSING STRANDS

The prestressing strands are uncoated, seven-wire, low-relaxation, ½ in (1.3 cm) diameter, Grade 270 strands conforming to AASHTO 203. Theoretical values for area and modulus of elasticity are 0.153 in^2 (1 cm^2) and 28,500 ksi (197 MPa) respectively (PCI 1999). The post-tensioning strands are only different in that the diameter is 0.6 in (1.5 cm) and the area is 0.217 in^2 (1.4 cm^2) (PCI 1999). They can sustain more force. Each spool must meet rigorous ASTM and PCI specifications; therefore, specific values and deviations from theoretical were not investigated. They were also not expressly vital for relative comparisons and calculations. Figure 3.23 shows a picture of a 0.6 in. post-tensioning strand.

5.3. REINFORCING BAR

Tension tests were performed on the reinforcing steel that was used to fabricate the instrumented rebar. The ½ in. diameter (#4) grade 60 reinforcing steel bars were supplied by Ahrens Steel of Columbia, Missouri. They are the largest part of the instrumentation program. Due to the calibration method (cal factor in lb/mV) the modulus must be determined in order to calculate strain.

A two foot long specimen was tested in tension. The ends of the specimen were threaded with ½ in.-13 threads for approximately one inch. The center of the specimen was lathed down to a diameter of 3/8 in. (9.5 mm) for approximately two inches of the specimen. An extensometer with a 0.5 in. (12.7 mm) gage length was attached to this section of reduced area.

Tension loading was applied within the elastic region of the steel. The extensometer measured strain over ½ in. (1.3 cm) of the milled section. Figure 5.1 shows

a graph of the results of the modulus test. The bar was not yielded. Experimental yield strength is immaterial to results comparisons. The modulus of elasticity of the steel used for the strain-gaged bars was determined to be 27,400,000 psi (1.9 x 10^5 MPa).

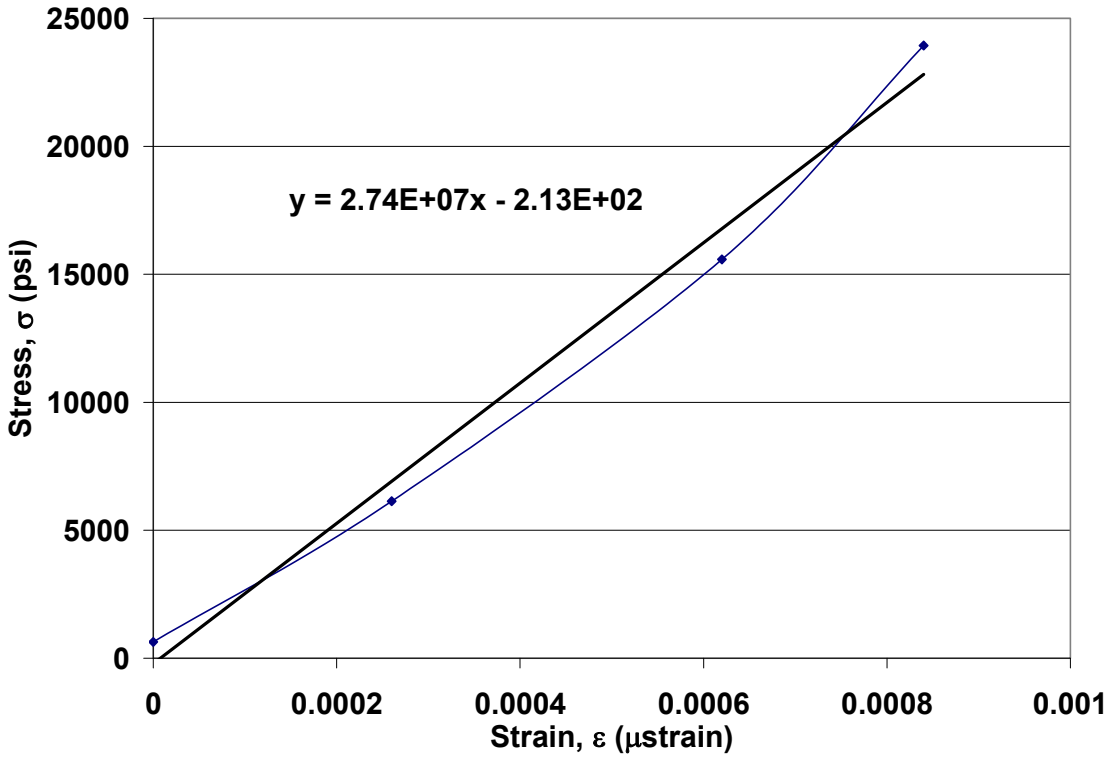

Figure 5.1 – Modulus of elasticity for instrumented rebar

6. HYDRATION AND EARLY AGE RESPONSE

6.1. INTRODUCTION

The prestressed concrete panels used for the rehabilitation of I-57 near Sikeston, MO were cast during October-December, 2005 by Concrete Products Incorporate (CPI) in Memphis TN. The MU Research Team made two separate trips to instrument the seven designated panels. The first trip took place during the week of October 10, 2005. Four designated base panels (Panels B1-4) and anchor Panel (C1) were instrumented. During the second trip, the week of December 4, 2005, the two remaining joint panels were instrumented.

The MU research team spent several hours organizing and getting ready for installation each day. Pretensioning took place around 8:00 AM each day. The forms were then put back together and prepared for concrete placement. To minimize interference with CPI employees the research team waited until the panels were almost ready for casting before beginning installation. Instrumentation was installed and tested prior to concrete placement to ensure all systems were working properly. The instrument locations were then flagged to ensure they were not damaged by CPI personnel during panel fabrication. Readings were taken before and during placement to obtain baseline references for each gage. Casting began around 2:00 PM every day. Steam was turned on around 6:00 PM. Curing readings were taken all night until pre-stress transfer the next morning.

6.2. DATA FROM EARLY AGE ANALYSIS

Analysis of hydration and early age response of reinforced concrete can be a difficult task. Prediction of thermal mechanical behavior becomes complex due in part to the following phenomena:

- Steel expands and contracts at a consistent linear thermal coefficient that happens to be roughly twice that of hardened concrete (~12 μstr/°C steel compared to ~6 μstr/°C limestone concrete) (Shackelford and Alexander 2001).
- Concrete changes thermal properties (namely expansive) as it transitions from plastic to solid (Kada H. 2002; Earney, Gopalaratnam et al. 2006).
- Hydration is an exothermic reaction which adds heat to whole system (Eatherton 1999).
- As concrete hydrates it shrinks (Earney, Gopalaratnam et al. 2006). This is counterintuitive to the fact that the system heats during hydration.
- While the concrete shrinks the steel will continue to expand with added heat (Shackelford and Alexander 2001).
- Small amounts of friction from external steel formwork resist thermal movements as well as apply stresses to the outer surface during differential expansion.
- Thermal gradients develop through the depth of the cross-section causing corresponding internal strain gradients
- Differences exist between instantaneous and steady-state thermal response of the rebar and surrounding concrete. The concrete (with a very large

surface area) heats and responds to thermal changes at a different rate than that of the embed rebar.

The experimental program is further complicated by strain measuring devices such as vibrating wire strain gages that have their own coefficient of thermal expansion. This gage expansion may or may not be restrained by plastic concrete. The following sections discuss the theoretical predictions (based on idealized analysis of thermal changes), thermal data, and strain data in conjunction with hydration and external conditions such as steam curing and ambient temperature changes.

6.2.1. THEORETICAL CALCULATIONS

The following sections outline theoretical prediction models used during early age hydration. The difference between measured rebar strain and concrete strain is also discussed at great length. These discussions will be referenced in later chapters dealing with thermal strains (namely in-service results).

6.2.1.1. THEORETICAL MEASURED CONCRETE STRAIN (THERMAL)

Theoretical estimates shown on the figures in this chapter are based strictly on thermal predictions developed from a tri-linear model of the Coefficient of Thermal Expansion (CTE) of curing concrete. As stated earlier, the thermo-mechanical complexities of this composite system at early ages are a challenge to analyze. The theoretical curves have, as a result, been idealized to show predictions based on the thermal expansion and contraction of the concrete and rebar. They allow for an approximate comparison between the magnitudes of strains measured and those expected under ideal conditions. The following equation was used to calculate the expected thermal strain of hydrating concrete:

$$\Delta \varepsilon_{Thermal\ /\ Concrete} = CTE_{Concrete} \times (T_1 - T_0) \qquad \textbf{6.1}$$

'T' represents temperature at two distinct times (t_1 and t_0). The 'CTE' is the Coefficient of Thermal Expansion based on the tri-linear model from Kada (see Figure 6.1). Early age thermal gradients were small; therefore, an average temperature was used to simplify the analysis. The tri-linear CTE model shows that concrete behaves much like a fluid in its plastic state. After estimated initial set it begins transitioning to solid state (estimated final set) where it retains these thermal properties for the life of the composite (Kada H. 2002; Earney, Gopalaratnam et al. 2006). Kada's model was slightly modified for the Missouri research project. It originally assumed a final CTE of 8 μstr/°C resulting from studies on high performance concrete. Based on known thermal data for Missouri limestone aggregate, the team assumed a final CTE of 6 μstr/°C.

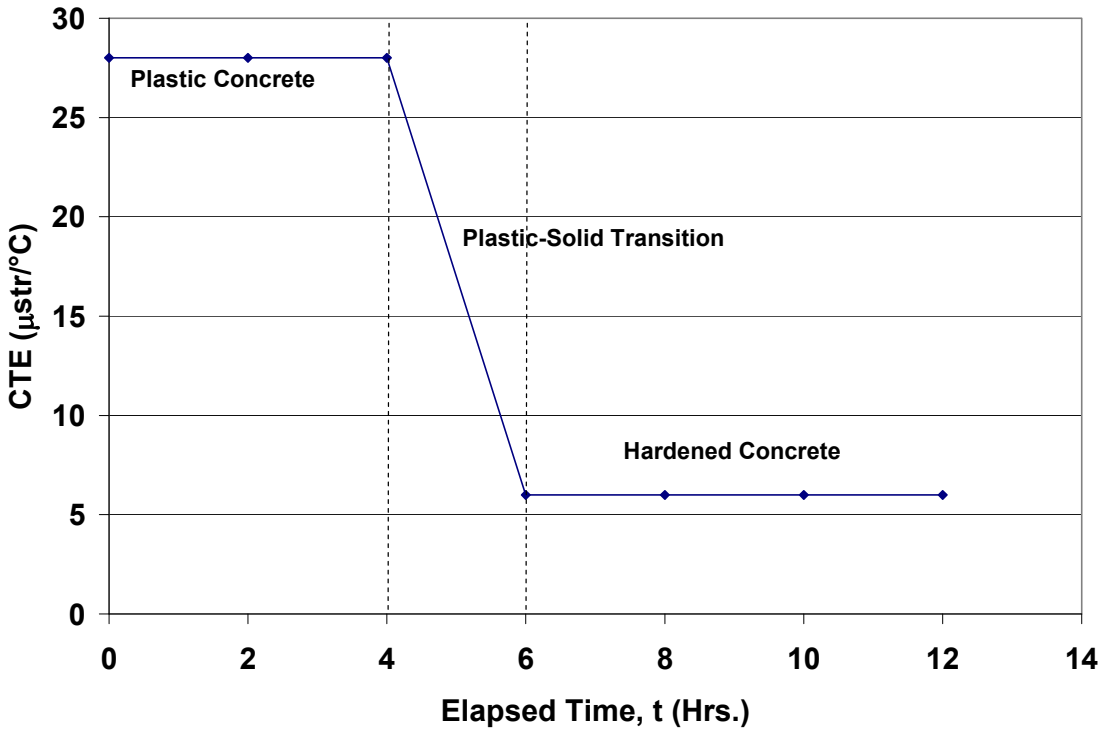

Figure 6.1 - Coefficient of thermal expansion for curing concrete (Kada H. 2002)

6.2.1.2. THEORETICAL MEASURED REBAR STRAIN (THERMAL)

Theoretical measured rebar strain is calculated similar to concrete. The following equation is used to calculate the expected thermal rebar strain shown in all of the thermal related figures:

$$\Delta\varepsilon_{Thermal\ /\ Steel} = \left(CTE_{Concrete} - CTE_{Steel}\right) \times \left(T_1 - T_0\right) \qquad \textbf{6.2}$$

The CTE for steel is assumed constant for the observed range of temperatures. The CTE for concrete changes based on the tri-linear model from Kada and corresponds to the respective time 't' during data acquisition. The concrete CTE is 6 μstr/°C and steel is 12 μstr/°C.

6.2.1.3. EXPLANATION OF INSTRUMENTED REBAR READINGS

It is important to note that the two theoretical curves represent expected concrete and rebar strain. Rebar readings are measured rebar strain. To convert measured rebar strain into estimated thermal concrete strain the following equation would be used:

$$\Delta\varepsilon_{Concrete} = \left(\frac{CTE_{concrete}}{CTE_{concrete} - CTE_{rebar}}\right) \times \left(R_1 - R_0\right) \qquad \textbf{6.3}$$

The 'R' values are reported rebar strain. The CTE for steel rebar is higher than that of concrete (Shackelford and Alexander 2001). The first part of this equation creates a negative scalar value that is multiplied with measured rebar strain (R1-R0). With increased temperature the rebar show compression because the gages on the steel rebar are thermally self compensating. To explain further, consider Figure 6.2 with these actions and results.

1. Assume the initial strain reading is zero. An unrestrained (no concrete) instrumented rebar of length L is heated and allowed to expand to a length of $L+\Delta L_{us}$.
2. The final strain reading will remain zero. The gages on the rebar compensate for the thermal strain.
3. Due to the lower CTE, embedding the rebar in concrete (Figure 6.2) provides restraint on this free expansion and the concrete pushes the rebar into compression (a distance of: $\Delta L_{us}-\Delta L_r$).
4. Therefore, although the total displacement (ΔL_r) of the instrumented rebar is positive (extension), it outputs this compressive strain: $(\Delta L_{us}-\Delta L_r)/L$.

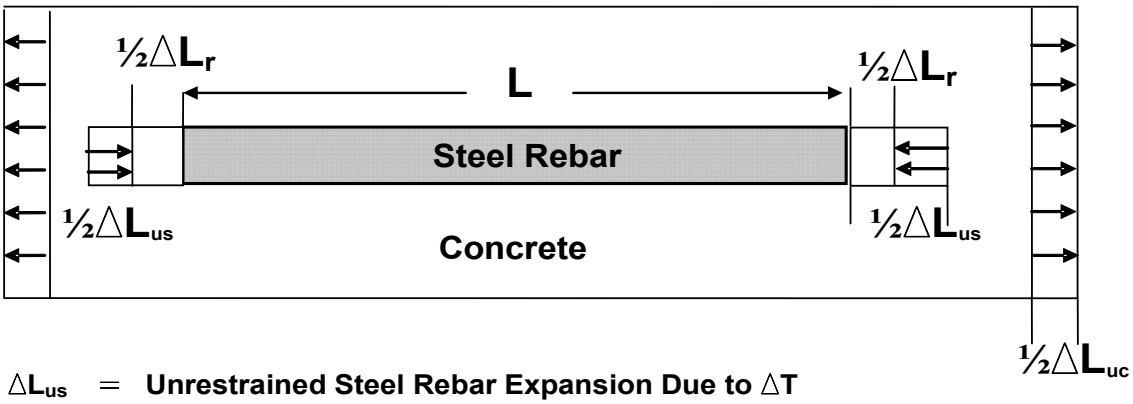

ΔL_{us} = **Unrestrained Steel Rebar Expansion Due to ΔT**

ΔL_r = **Restrained Steel Rebar Expansion Due to ΔT**

ΔL_{uc} = **Unrestrained Concrete Expansion Due to ΔT**

Figure 6.2 - Restraint of instrumented rebar by surrounding concrete

At this time, not enough information is known about the actual CTE of the concrete mix. Therefore, rather than including the same assumption in both the

theoretical curve and measured rebar strain curves, the rebar results have been left in their purest form—rebar strain. Comparisons can be drawn by examining the shape and magnitudes of the different curves. A future thesis by Grant Luckenbill will include results from an in-depth study on the thermal interaction between the instrumented rebar and concrete.

6.2.2. MEASURED CURING TEMPERATURE

Figure 6.3 summarizes the average curing temperatures for each panel. Panels B1 and B2 curing temperatures are lower (on average) than the rest. This may be attributed to the fact that steam environment temperatures averaged 34°C (93°F) in Panels B1 and B2 and 54°C (129°F) in the rest of the panels. The curve shown for Panel A32 is shaped differently because it started at a lower ambient temperature and increased rapidly when the steam curing started. Average ambient temperatures for Panels B1, B2, B3, B4, and C1 were around 20°C (68°F). Panel A32 was cast in December and had an average ambient temperature of 8°C (46°F). Based on the relative steam curing environment temperatures, it can be inferred that Panel A32 was insulated much better than Panels B1 and B2. CPI used a double tarp during joint panel casting in mid December, 2005.

Maximum measured curing temperatures were 5-10°C (9-18°F) greater than the external steam curing environment temperatures (see Figure 6.6 and Figure 6.7). This higher temperature, beyond external heat sources (steam), can be attributed to exothermic hydration in the concrete (Eatherton 1999). This trend was typical in nearly all panels.

Figure 6.4 shows the curing temperatures in joint Panel A32 as measured by thermocouples and vibrating wire thermistors. The temperatures shown are a snap-shot summary of near peak temperatures during curing of the second half of Panel A32.

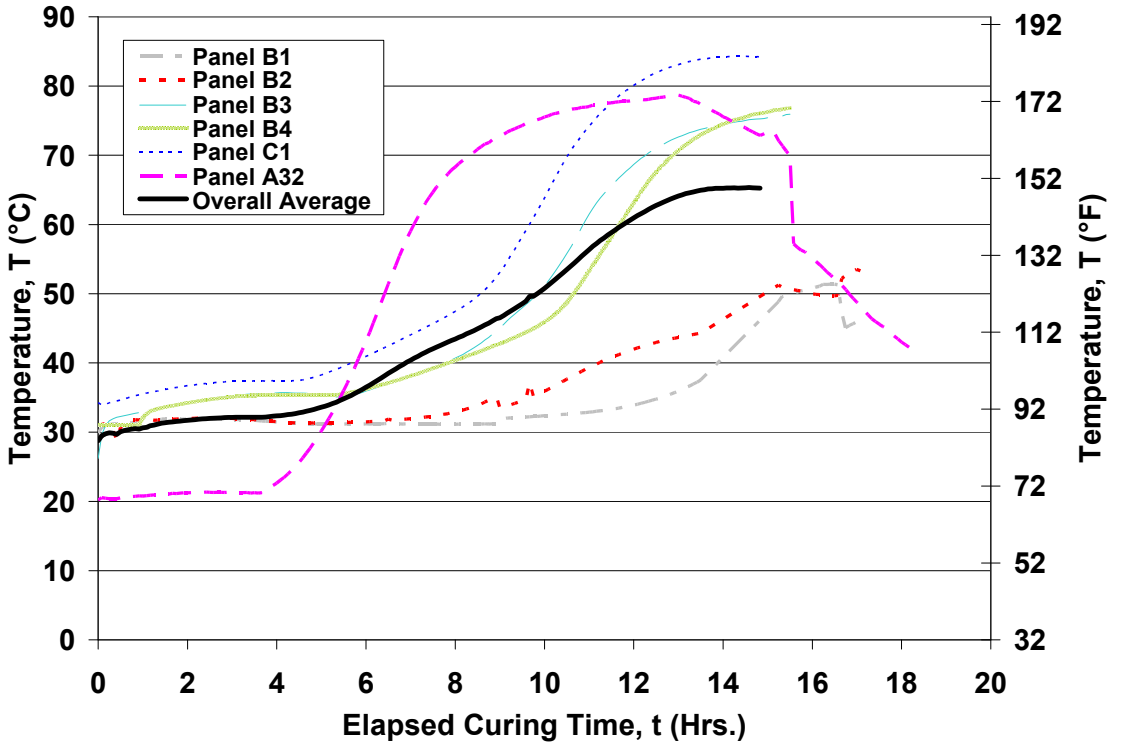

Figure 6.3 - Summary of average curing temperatures in each panel

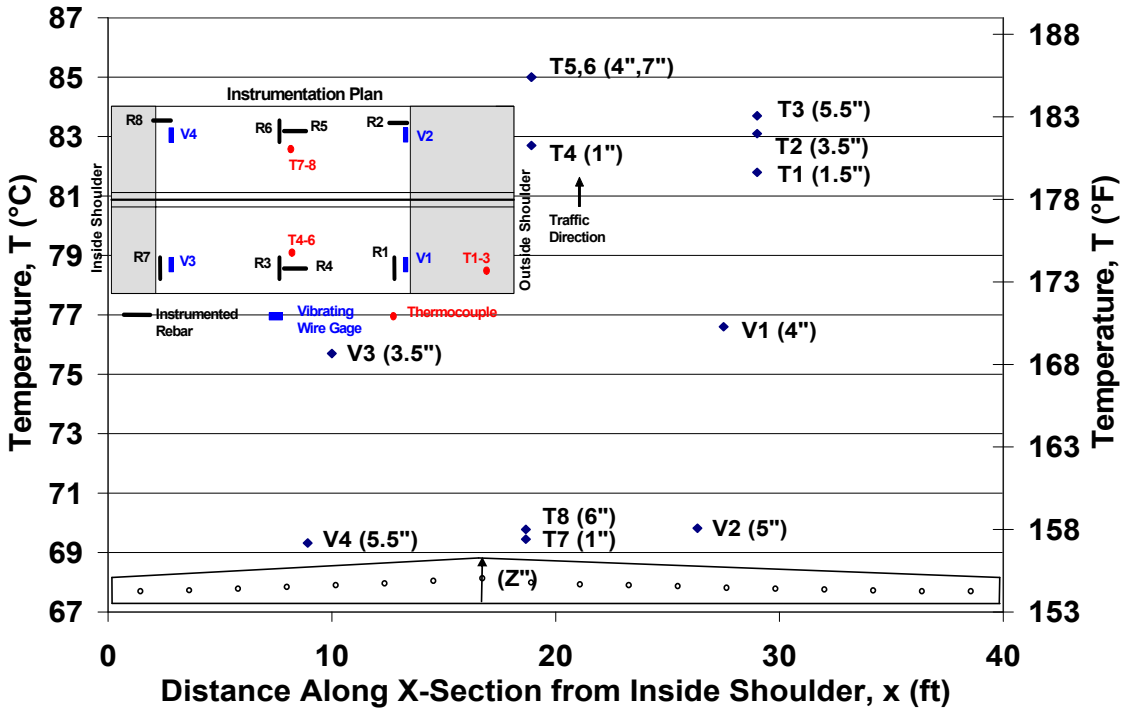

Figure 6.4 - Early-age temperatures in the cross-section of Panel A32

There was very little noticeable difference in Thermocouples T1-6. These are located within the uncured plastic half of Panel A32. Thermocouples T5 and T6 have slightly higher temperature readings than adjacent measurements from Thermocouples T1-3. They are toward the center, within a larger cross-section and thermal mass.

The vibrating wire gage thermistors are encapsulated in a hardened resin that insulates the sensor and makes it less sensitive to dynamic changes in temperature. Therefore, they lag the thermocouple measurements.

The average temperature of these six thermocouples is 83.4 °C (182°F) with a standard deviation of 1.5 °C (2.7°F). If it is assumed that the concrete has a CTE ranging between 6-8 μstr/°C, then these small differences in temperature create a strain gradient less than 15 μstr. This is very small compared to the overall strains during curing (less than 3%). These residual strain gradients, if large enough, can be responsible for premature cracking (Emborg and Bernander 1994).

The temperature sensors in the cured 1st half report lower temperatures than the uncured 2nd half. The external temperature is the same for both the cured and uncured halves. Hydration is an exothermic reaction (Eatherton 1999). The temperature difference reported by T1-6, V1, and V3 due to heat of hydration is roughly 13°C (23°F). Figure 6.6 shows the differences between the internal temperature of the cured and uncured sections.

Collectively, temperature sensors performed well, displaying accurate consistent trends. Note that ambient and steam curing environment temperature histories were recorded during each casting.

6.2.3. MEASURED CURING STRAINS

Readings from the strain-gaged bar and vibrating wire strain gage were recorded during curing. Before hardening the concrete is plastic, and is able to flow like a liquid. After hardening the concrete is solid with time-dependent strength and stiffness development. Strains are at best defined in a nebulous manner when concrete is in this early age transition (Eatherton 1999). Strains recorded during these early ages are hence termed "apparent strains" to highlight this fact. However, it is interesting to study relative strain development compared to measured curing temperature at these early ages when hydration and liquid to solid transition takes place. Even if strain magnitudes during these early ages are not relevant, *relative* magnitudes, transitions, and trends offer valuable information on potential distributions of residual stresses. The apparent strain in the instrumented rebar and vibrating wire strain gages show what types of strains are induced in these gages by movement in the concrete and therefore *relative* magnitudes and peaks (in conjunction with curing temperatures) become meaningful. In all graphs for strains, compressive strain is represented as a negative strain value and tension as a positive strain value (this convention is valid for all plots in this thesis).

For all six panels instrumented (with both thermal and strain measuring devices), the trends in apparent strain and temperature are related. Panel A32 is unique in that it was monitored over several days. The first half was cast on Friday, December 9, 2005. The panel was monitored all weekend and the second half was cast the following Monday, December 12, 2005. Figure 6.5 shows the entire curing strain history of Panel A32 from casting of the first half to stress transfer. The instrumented rebar go into compression during curing of the first half. This is an expected result of shrinkage and

thermal expansion of the rebar in the concrete. At roughly 10 hrs, the concrete begins to lose heat. This is marked by a gain in tensile strain due to thermal contraction (the rebar contracts more than the concrete will allow—showing tensile strain).

During casting of the first half, maximum compressive rebar strains occur at the highest curing temperatures (which happen to be higher than steam curing environment temperatures). Theoretical strains are most likely lower magnitude because, unlike the measured strains, they do not account for added compressive strain due to shrinkage. The difference between theoretical thermal rebar strain and measured strain is 200-300 μstr (Figure 6.5). As stated earlier, the theoretical curve is based solely on the coefficient of thermal expansion. It proves to be useful as it shows the same shape and trend as the measured apparent strains, implying that a majority of the recorded response is due to thermal effects. Up until curing of the second half, each action causing thermal change (steam off, tarp removed) can be seen with subsequent changes in temperature and related strain.

The shape of the theoretical rebar strain curve matches measured rebar trends—especially Rebar 6 (Figure 6.5 and Figure 6.6). Rebar 6 is the only transverse rebar in the first half of Panel A32. It shows a different trend during curing of the second half (hour 53—Figure 6.5 and hour 5—Figure 6.6) than longitudinal rebar (Rebar 2, 5, and 8 in Figure 6.5 and Figure 6.6). The sharp jump in tensile strain seen in the longitudinal rebar is not visible in strain readings from Rebar 6. This may be due to a difference in external restraint in the long direction from the formwork. This formwork may restrain the concrete from straining instantaneously when the steam curing starts.

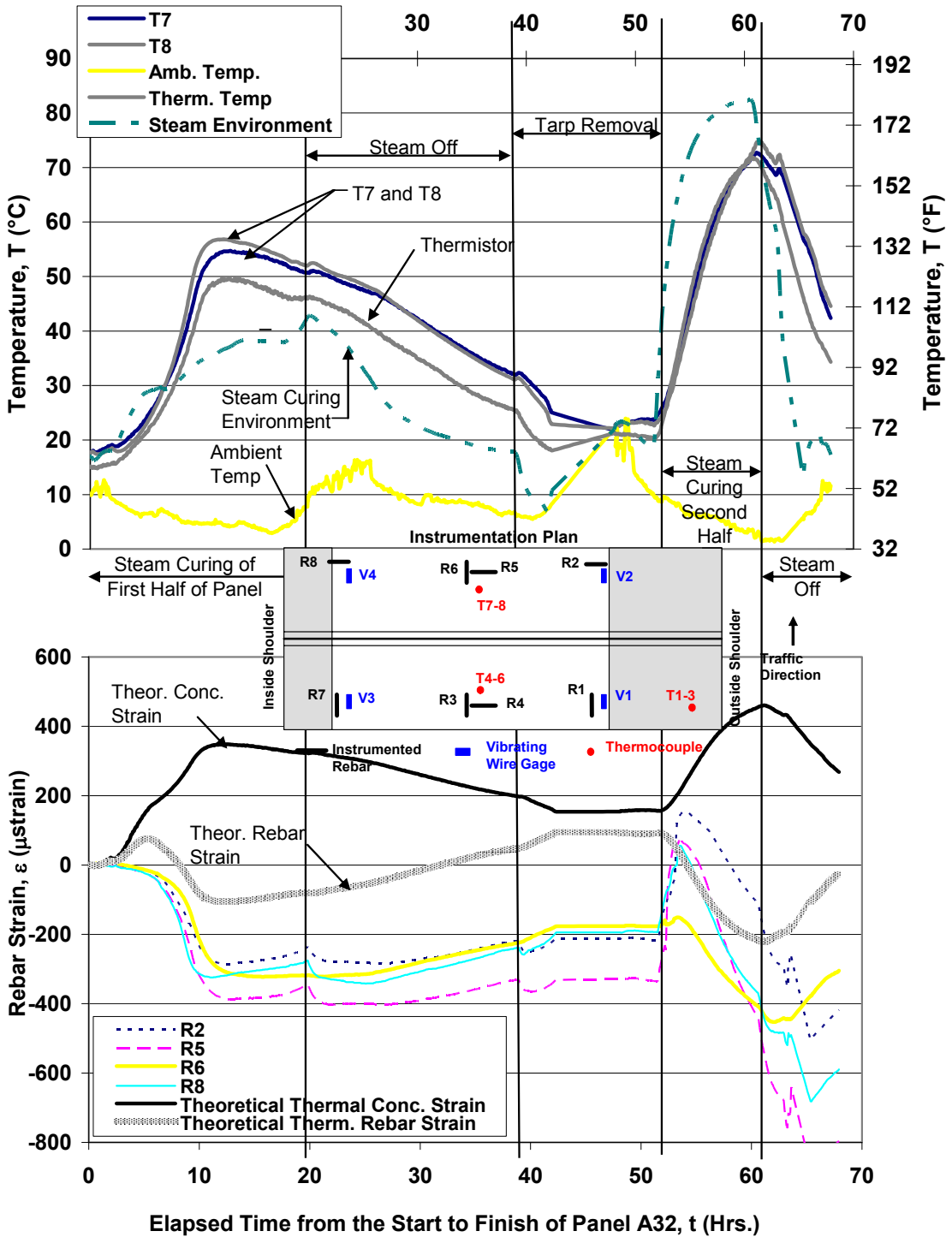

Figure 6.5 - Early-age thermal strain history of 1st half of Panel A32 through completion of 2nd half

To explain this sharp jump further, Figure 6.6 shows all of the rebar in Panel A32 and their comparative response during curing of the second half. (This graph includes part of response shown in the last half of Figure 6.5 for Rebar 2, 5, 6, and 8 in conjunction with response from rebar in the curing 2nd half). The rebar in the solid first half show signs of expansion as soon as steam curing starts. The differences between rebar subjected to curing strains and those under solid-state thermal response are highlighted. When steam curing begins (4hrs) the rebar in the plastic second half of Panel A32 begin to compress. The rebar in the solid first half expand and then fall into compression as noted earlier. Based on the thermal discussion earlier, the rebar should go into compression because the steel expands more than the concrete will allow. The exception shown in Figure 6.5 and Figure 6.6 (with hardened concrete) can most likely be attributed to the difference in thermal mass as well as delays in steady state and instantaneous thermal effects between the rebar and concrete.

When the steam is turned on, the concrete is instantaneously 'shocked' with a high-heat external source. The concrete mass around the rebar quickly begins to heat and expand before the temperature of the steel bar can 'catch up' and reach a similar steady-state condition. Therefore, due to this delayed response, the concrete pulls the rebar into tension. After time, the rebar heats and compresses as expected. The fact that theoretical values are close for both halves also supports this theory.

It can be inferred that this effect can be seen in the hardened concrete because plastic concrete does not have the bond strength to fully restrain the rebar. It is also possible that the formwork is providing more restraint in the long direction, mitigating this effect on Rebar 6.

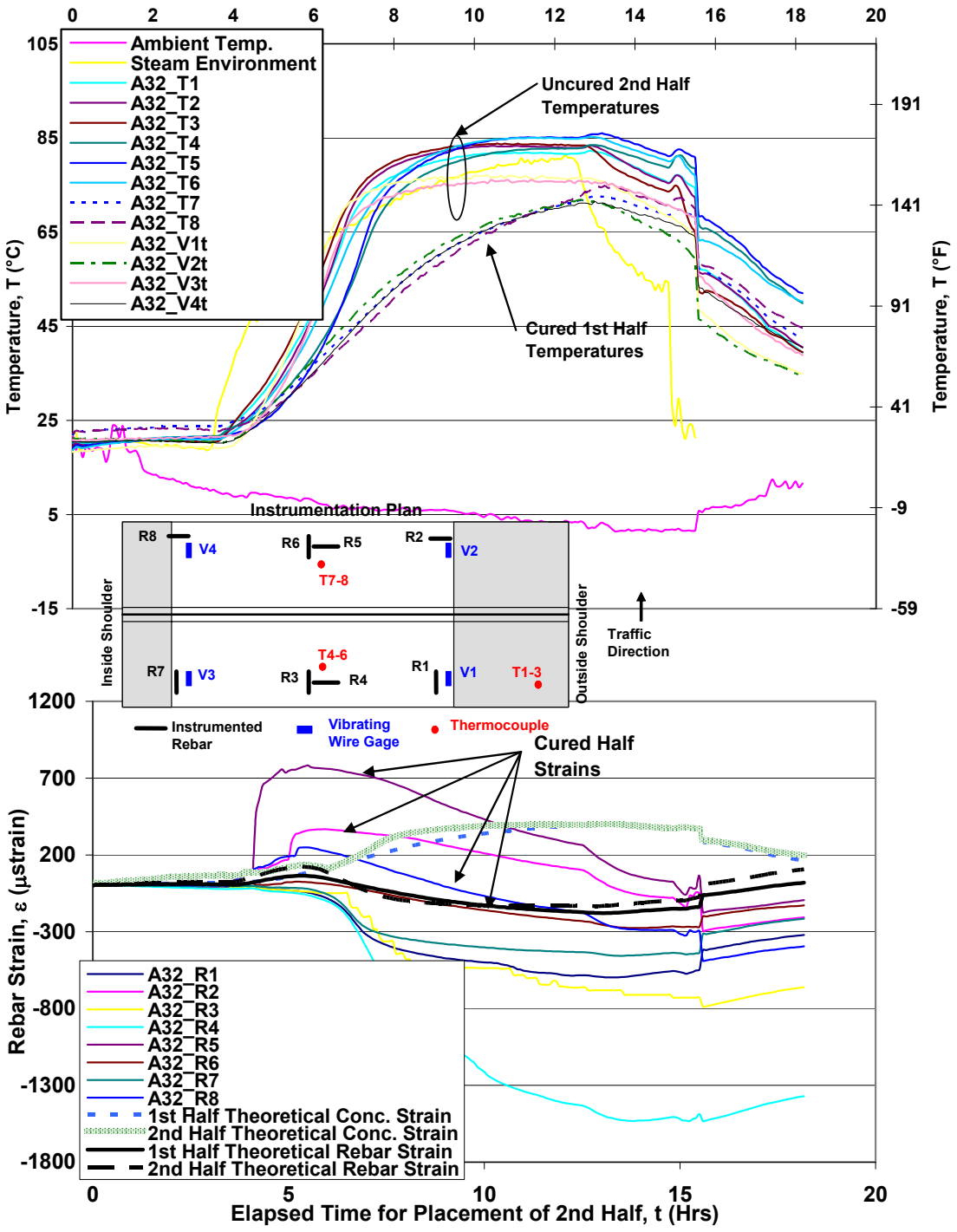

Figure 6.6 - Early-age thermal response of Panel A32 during casting 2nd half

Another important comparison can be drawn between the temperature measurements of the plastic and cured concrete subjected to the same external heat source (steam). The curing half is roughly 15-20°C (27-36°F) higher. This can again be attributed to the additional heat generated by hydrating cement.

Figure 6.7 provides a representative example of curing strains and temperatures measured in the five typical panels (Panels C1, B1-4). Note that measured rebar strains are again higher than theoretical rebar strains by 100-220 μstr. Rebar 1 shows higher response early on because it is located in the thinnest part of the cross-section. The heat from the steam takes less time to achieve steady-state conditions in the thinner section compared to the thicker section.

Vibrating wire gages and instrumented rebar show different trends. The vibrating wire strain gage operates on the principle that the natural frequency of a wire is dependent on its length and is proportional to strain. But, since the length of that wire changes with temperature, the vibrating wire strain gage output is temperature dependent. A correction for this effect is given by the manufacturer. The correction is based on the fact that the wire is made of steel and the coefficient of linear thermal expansion of steel is 12.2 μstr/°C. The correction provided by the manufacturer is to add a tensile strain of 12.2 μstr/°C to the uncorrected reading (Geokon 1996). Because the CTE of the gage is known, the equation used to reduce the vibrating wire output produces a measured total concrete strain.

$$\Delta\varepsilon_{VW-Concrete} = \left(V_1 - V_0\right) + 12.2 \times \left(T_1 - T_0\right) \qquad \textbf{6.4}$$

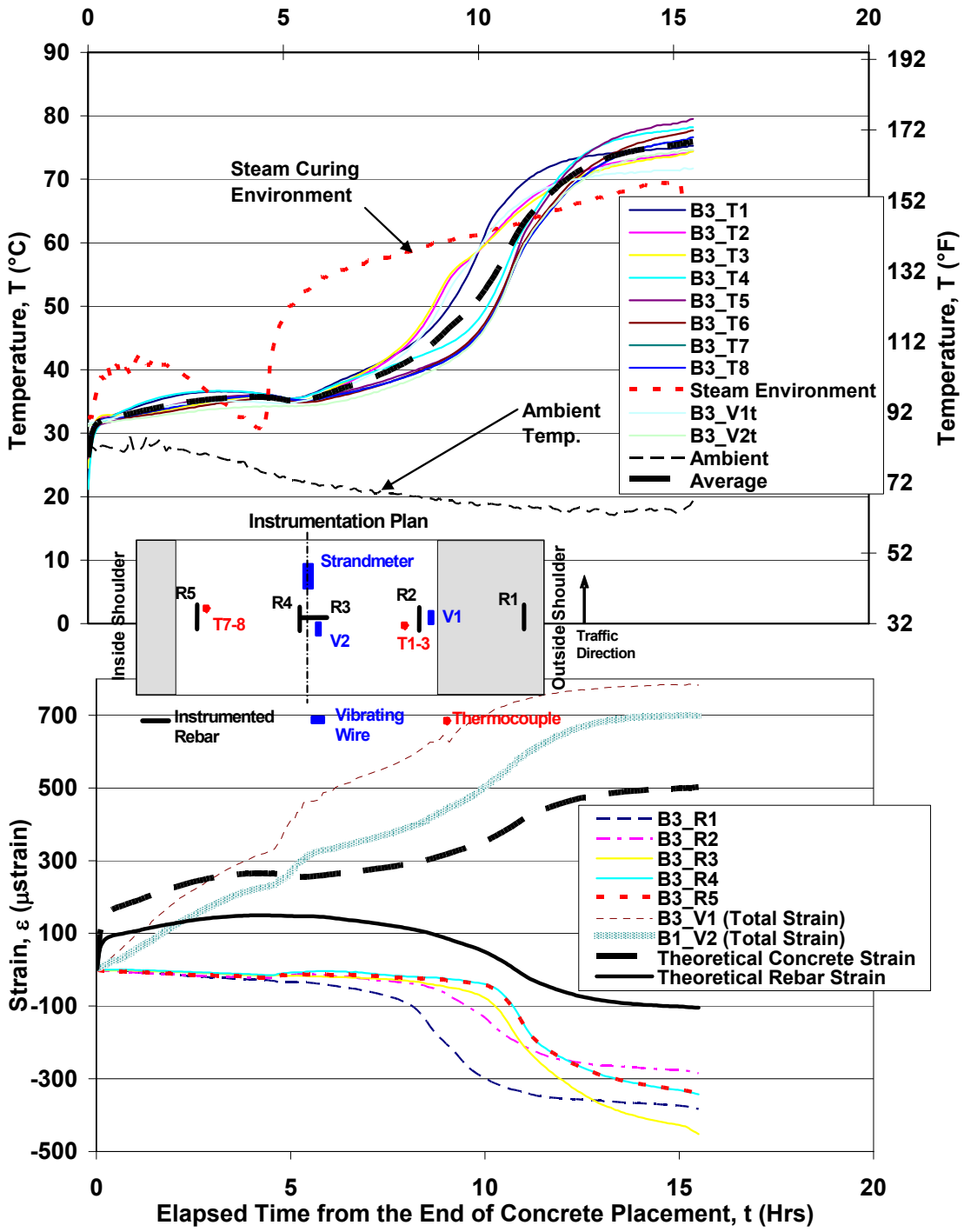

Figure 6.7 - Apparent strains and temperature of Panel B3 during curing

Figure 6.7 shows vibrating wire strain readings corrected for temperature. A sudden slope change in both the vibrating wire and rebar output occurs around 5 hrs and is most likely initial/final set transition of the concrete. The vibrating wire gage shows significant response early on compared to the rebar. This is due to the difference in magnitudes of forces required to induce the same strain in each device. The vibrating wire gage can be strained through its full range simply by squeezing the device in one hand. It is equipped with flanges than help engage even plastic concrete. According to Geokon, fresh concrete bears on the flanges and can provide enough force to strain the gage (Geokon 1996).

Although the rebar can be equally responsive, it requires a fully bonded section to develop the potential to measure the full effect of external strains. It takes a great deal of force to strain the rebar through its full range (can not be done without a machine). Plastic concrete does not have enough bond strength with the rebar to induce early curing strains. Therefore, the rebar showed little response before final set (up to about 6 hrs.). The vibrating wire gages show tension early and continue to show signs of thermal expansion. It is evident that shrinkage strains are not greater than thermal strains because the slope of the output does not exhibit signs of compression.

7. STRESS TRANSFER

7.1. INTRODUCTION

Stress transfer is one of the most critical steps in the life of a prestressed member. Proper stress transfer extends the life of a prestressed member by controlling cracks and providing a confining compression that increases toughness and design strength (Merritt, McCullough et al. 2000). Improper eccentricities or insufficient strength during transfer can easily cause buckling failures and stress cracks (Naaman 2004).

Each morning, the MU research team stopped the curing data acquisition program and switched to a program that measured only rebar strain. Transfer strains were monitored at a high data acquisition rate during stress transfer. Thermal effects during stress transfer are insignificant and vibrating wire gages are inherently incapable of dynamic strain measurements. As long as the strength of the concrete was at least 3,500 psi (24 MPa), panels were de-molded and the transverse pretensioning strands were cut (Figure 7.1). Each strand was cut in two places simultaneously on opposite ends of the bed. The order of transfer was staggered from one side to the other as to minimize build-up of eccentricities on the cross-section. Figure 7.2 illustrates the strand cutting sequences for both joint panels and regular base panels. Note how strands were cut using an alternating pattern. The entire process took only a matter of minutes

The following sections outline the theoretical calculations for both longitudinal and transverse strain expected during stress transfer. Several graphs of data are presented and discussed along with theoretical comparisons.

Figure 7.1 – Stress transfer of pretensioned strands at CPI in Memphis, TN

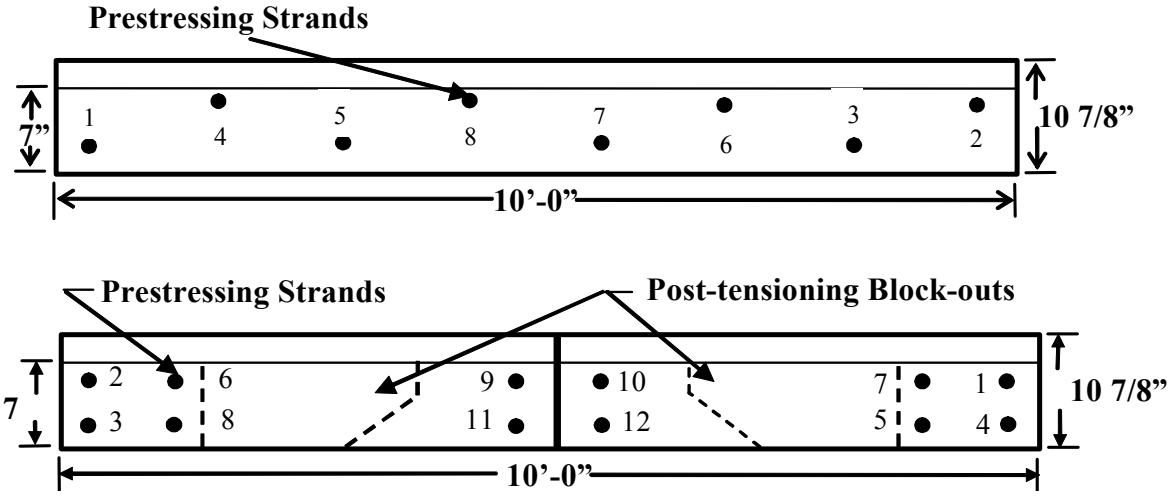

Figure 7.2 – Transfer sequence of typical panels (top) and joint panels (below)

7.2. PRETENSIONING STRESS TRANSFER STRAINS

Measured pretensioning strains can readily be compared to calculated theoretical strains. During stress transfer, the concrete in the panel undergoes strain in both the longitudinal and transverse directions. The following sections outline the mechanics involved in predicting pretensioning strains. Later sections will point out the relationships between measured, theoretical, transverse, and longitudinal strains.

7.2.1. THEORETICAL STRAIN CALCULATIONS

Theoretical calculations comprise two categories: longitudinal and transverse. Both use similar mechanics of materials approaches to predict uniaxial strains within the cross-section.

For both calculations, it is assumed that the chairs placed under the top strands during fabrication were located to sufficiently remove any out of plane eccentricities during stress transfer.

7.2.1.1. THEORETICAL TRANSVERSE STRAINS

To calculate the predicted strain at individual rebar, one must first find the stress at that location. Theoretical transverse strains (perpendicular to traffic) are calculated based on the following basic stress equation (Naaman 2004):

$$\sigma = \frac{P}{A} + \frac{My}{I} \qquad \textbf{7.1}$$

Where ‘P’ is the force in the prestressing strand, ‘A’ is the area of the cross-section of interest (perpendicular to the force), ‘M’ is the moment from a particular strand created by the eccentricity ‘e’ of the force from the neutral axis, ‘y’ is the distance from the neutral axis where the stress value is desired, and ‘I’ is the calculated moment inertia

of the cross-section perpendicular to the applied force. The first term represents the pure compressive force that the released strand applies to the cross-section. This creates a uniform stress distribution along the cross-section. The second term represents the internal bending caused by the eccentricity of the applied force from the strand. This force in the pretensioning strand 'P' is calculated using the area of the pretensioning tendon 'A_{strand}' (in this case it is 0.153 in^2 (1 cm^2) for ½" diameter strands) and the initial pretensioning stress 'f_{pi}':

$$P = A_{Strand} \times f_{pi} \qquad \textbf{7.2}$$

The f_{pi} term is dictated by the designer to be 75% of the ultimate strength f_{pu} (270 ksi or 1860 MPa). The f_{pi} and strand size is the same for each panel at every location, therefore, the applied force 'P' used for calculations is a constant—31 kip (138 kN).

Figure 7.3 shows the eccentricity of the pretensioned force 'P'. This force and eccentricity make up the 'M' term in the equation. The eccentricity is different depending on the strand location. Therefore the 'M' term becomes 31e.

The area term 'A' in the denominator of the first term (compressive force) is the area of the cross-section at the rebar of interest. The area is calculated by multiplying the depth 'd' of the panel at the rebar of interest and the width 'w'. The width is the 10'-0" (3.05 m) longitudinal (with traffic) dimension.

The inertia 'I' in the denominator of the second stress term is the inertia of the cross-section in bending about the strong axis. This is based on bending that is in the plane of the panel (English units):

$$I = \frac{1}{12} \times d \times (wx12)^3 = 1440d \qquad \textbf{7.3}$$

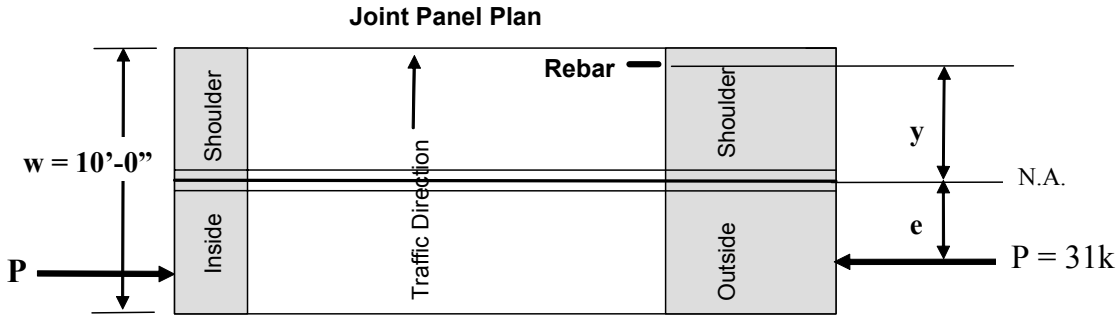

Figure 7.3 - Applied pretensioning force and eccentricities for calculations

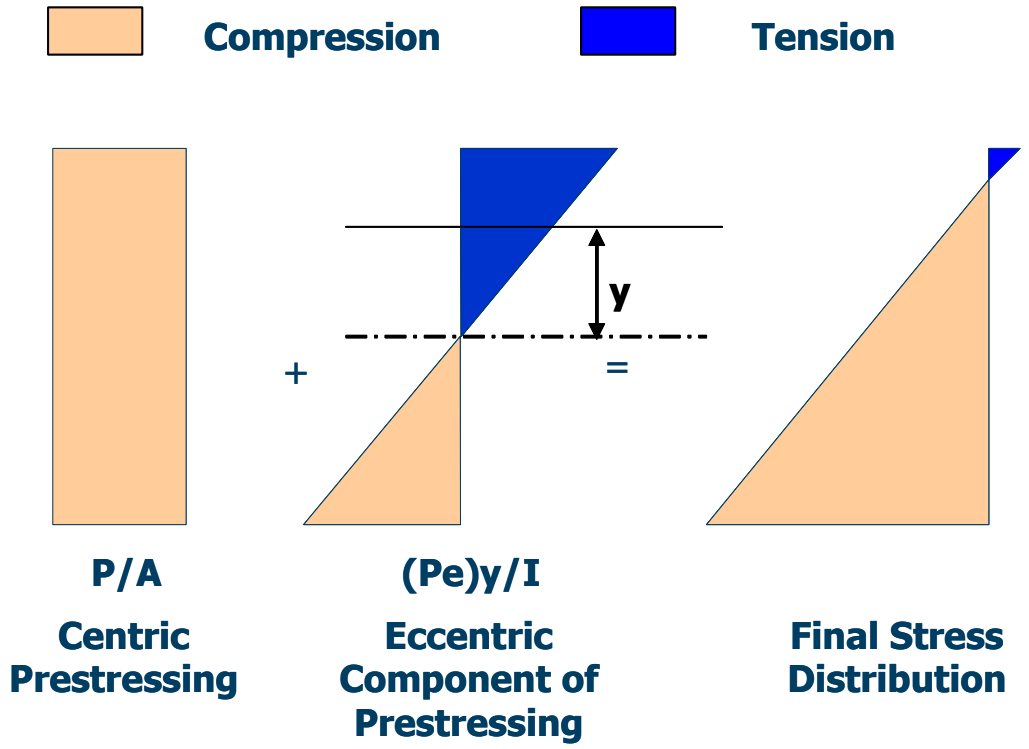

Figure 7.4 - Stress-block components of pretension transfer relative to Figure 7.3

The distance ‘y’ is merely the distance from the neutral axis to the rebar. Do not confuse this with the commonly used ‘c’ term. Typically ‘c’ is used to calculate the extreme fiber stresses. Because none of the rebar lie on the outside fiber of the panel, the ‘y’ term designates a distance between the neutral axis and the extreme fiber. Figure 7.3 and Figure 7.4 illustrate the terms and stresses discussed.

After substitution, the stress equation (Equation 7.1) at a single rebar after one particular strand is cut can be simplified to the following (English units):

$$\sigma = \frac{31}{120}\left(\frac{1}{d} + \frac{e \times y}{12}\right) \qquad \textbf{7.4}$$

The depth, eccentricity, and distance ‘y’ differ based on the location of the individual rebar and prestressing strand. The stresses were calculated at each rebar using the principles outlined above and these steps:

1. The ‘e’, ‘y’ and ‘d’ values were tabulated for each rebar and every respective strand. The eccentricities are based on the designed pretensioning strand spacing and the ‘y’ and ‘d’ values on as-built information. The ‘y’ and ‘d’ values are constant for each individual rebar. Only the eccentricity of each pretensioned strand changes.
2. A positive or negative sign was assigned to the ‘e’ or ‘y’ to create the proper tensile or compressive stress relative to the internal bending moment. For example: if the strand being cut was on the same side of the neutral axis as the rebar measuring the strain, the stress value from bending (My/I) would be a positive compressive stress at the rebar. Rebar on the other side of the neutral axis would measure a negative tensile strain.

3. For each rebar, the stress induced by each pretensioned strand was tabulated in a column in Excel (see Table 7.1). The stress from strand 2 is additive to the previous stress from strand 1, therefore, a running sum was used to calculate the total stress after each strand was cut.
4. Each stress value (running sum value) was then converted to strain (Table 7.1) and graphed against measured values.

Once uniaxial stresses were calculated converting them to uniaxial strain values was effortless with Hooke's Law:

$$\varepsilon = \frac{\sigma}{E} \qquad \textbf{7.5}$$

The modulus of elasticity 'E' for normal weight concrete is then calculated based on the expected 3,500 psi concrete strength (f'_c) at stress transfer (Nawy 2003):

$$E = 57{,}000 \times \sqrt{f'_c} = 3{,}372 ksi; \left(23{,}250 MPa\right) \qquad \textbf{7.6}$$

Field observations showed that the concrete strength was very close to the estimated 3,500 psi (24 MPa). In fact, some panels required curing an extra couple of hours until the strength reached 3,500 psi (24 MPa). Experimental data also proved this strength assumption to be fairly accurate. Additional calculations are located in the appendix.

A31

Material Properties

Steel		Concrete	
Yield Strength (ksi)	270	Inertia (in^4)	1224000
Modulus (ksi)	28500	Poisson's Ratio	0
Strand Diameter (in)	1	28d Strength (psi)	7187
Strand Area (in^2)	0	Time @ Stress (day)	1
Percentage of Stress	1	f'c (psi)	3500
Stress in Strand (ksi)	203	Modulus (psi)	3372165
Force in Strand (lbs)	30983		

Rebar 2, 6	Depth 'd' (in)	9	Area (in^2)	1020		Rebar 3 and 4 Strain
Joint Panel Strand	Stress P/A (psi)	Moment Arm 'e' of Force (in)	Rebar from N.A. 'y' (in)	Stress My/I (psi)	Strain (µstr)	
1	-30	54	-48	-66	-28	5
2	-61	-54	-48	0	-18	3
3	-91	-54	-48	66	-8	1
4	-122	54	-48	0	-36	6
5	-152	48	-48	-58	-62	10
6	-182	-48	-48	0	-54	9
7	-213	48	-48	-58	-80	13
8	-243	-48	-48	0	-72	12
9	-273	-6	-48	7	-79	13
10	-304	6	-48	0	-90	14
11	-334	-6	-48	7	-97	16
12	-365	6	-48	0	-108	17

Rebar 3,4	Depth 'd' (in)	11	Area (in^2)	1272		
Based on Poisson's effect						
Rebar 1,5	**Depth 'd' (in)**	**9**	**Area (in^2)**	**1020**		
Joint Panel Strand	Stress P/A	Moment Arm 'e' of Force (in)	Rebar from N.A. 'y' (in)	Stress My/I (psi)	Strain (µstr)	
1	-30	54	48	66	10	
2	-61	-54	48	0	-18	
3	-91	-54	48	-66	-46	
4	-122	54	48	0	-36	
5	-152	48	48	58	-28	
6	-182	-48	48	0	-54	
7	-213	48	48	58	-46	
8	-243	-48	48	0	-72	
9	-273	-6	48	-7	-83	
10	-304	6	48	0	-90	
11	-334	-6	48	-7	-101	
12	-365	6	48	0	-108	

Table 7.1 - Theoretical stress and strain calculations for A31

7.2.2. THEORETICAL LONGITUDINAL STRAINS

Although the largest strain during pretension transfer is perpendicular to the applied force, Poisson's effect dictates that if there is not lateral confinement there will be a volumetric strain perpendicular to the applied force and opposite in sign (see Figure 7.5) (Boresi and Schmidt 2003).

$$\upsilon = -\frac{\varepsilon_{Longitudinal}}{\varepsilon_{Transverse}} \qquad \textbf{7.7}$$

The transverse strain in the denominator is the compressive strain applied by the pretensioning force (and previously calculated). The longitudinal strain is measure by embedded rebar perpendicular to the applied transverse pretensioning force (such as Rebar 3 and 4 in Table 7.1). This strain is easily obtained using the above equation and the known Poisson's ratio for concrete of 0.2 (Naaman 2004).

The only thing required to solve for the longitudinal strain is a reference strain from another adjacent transverse rebar. The problem with using these values is that all of the rebar are at different cross-sections (as far as overall depth) and the stress at each location will be different. This is because the same force is applied throughout but the cross-sectional area changes with panel width. Therefore, it should be noted that because these calculations were done using the known transverse strain from other rebar this equation was adjusted to reflect the stress/strain at the cross-section where the longitudinal rebar was placed. It was scaled using a ratio of cross-sectional areas at the referenced rebar location and the longitudinal rebar location as follows:

$$\varepsilon_{Longitudinal} = -0.2 \times \varepsilon_{Transverse} \times \left(\frac{A_{@\,\mathrm{Ref\,Rebar}}}{A_{@\,Longit.}} \right) \qquad \textbf{7.8}$$

Values for longitudinal rebar strain due to Poisson's effect were tabulated in Excel and graphed against measured values. Table 7.1 shows calculated values for longitudinal Rebar 3 and 4. These values followed measured trends. Additional calculations are located in Appendix D.

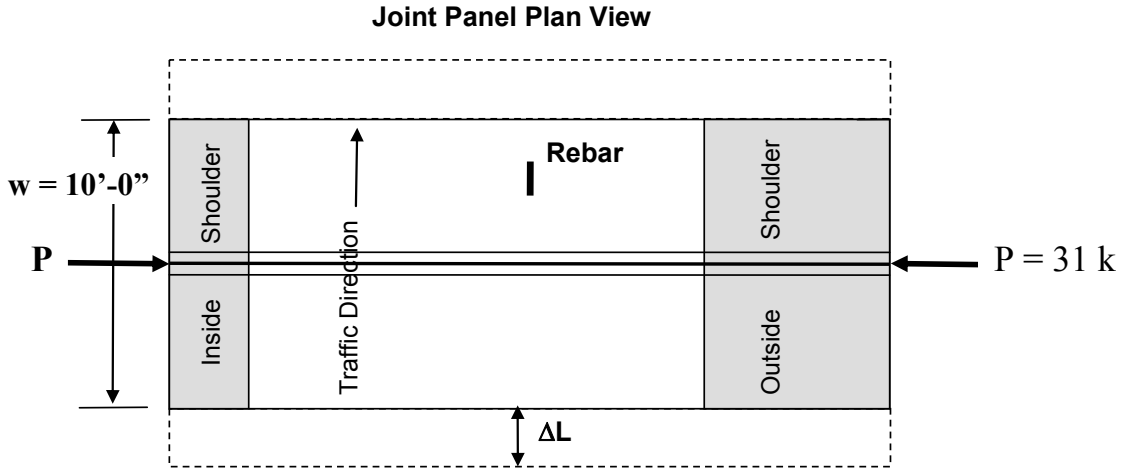

Figure 7.5 - Illustration of Poisson's effect on a panel

7.2.3. MEASURED STRAINS DURING TRANSFER

Measured strains during transfer were very well defined and consistent. It was desired to take data at a high acquisition rate during stress transfer. This meant that the vibrating wire gages, which require settling time, and thermal measuring devices needed to be removed from the curing program as they were not appropriate to the nature of required measurements. Data acquisition during stress transfer required physically switching wires on the multiplexers from the curing program locations. Unwanted instruments were removed and those that were needed were moved to the top of the 'click' order on the multiplexers. This had to be done in a timely fashion in order to not hold up CPI before stress transfer. Therefore, only transverse rebar were measured in the

typical base panels. The joint panel complexities allowed for more setup time. Every rebar was measured during pretension transfer.

Figure 7.6 shows the measured transverse strain of Rebar 3 in Panel C1. Note that after each strand was cut there was a subsequent added compressive strain. The cutting of Strands 1-8 can be easily seen by counting the 'stair' steps. Rebar 3 is in the middle of the slab toward the neutral axis, therefore, there are no eccentric strains shown during stress transfer. These eccentric strains would be marked by a sudden gain in tensile strain. The measured strains in Figure 7.6 are 9% less than theoretical. This can be attributed largely to frictional restraints. Rebar 3 is also in the middle of the slab. The panel strains from each side toward the center, therefore, frictional loss is most likely greatest in the center of the panel. Additional data points may have shown the overall strain growing closer to theoretical values. This would have caused unwanted delays in the construction yard. Adjacent uncut strands also restrain the surrounding matrix. Both of these factors were not accounted for in the idealized theoretical calculations due to the complexities in accurately modeling these influences.

Rebar 3 is in the same x and y location for Panels B1-B4 (refer to the previous as-built tables). Rebar 3 in Panel C is 3" closer to the center-line and slightly closer to the crown of the panel than the other base panels. It is in a deeper cross-section, hence, the lower overall strain. Figure 7.7 and Figure 7.8 show the measured strains relative to essentially the same theoretical curves (on each graph) for B1-B4.

It is evident that Panels B1/B2 and B3/B4 were cast at the same time with the same mix. The strains between the rebar (on the same graph) are nearly identical.

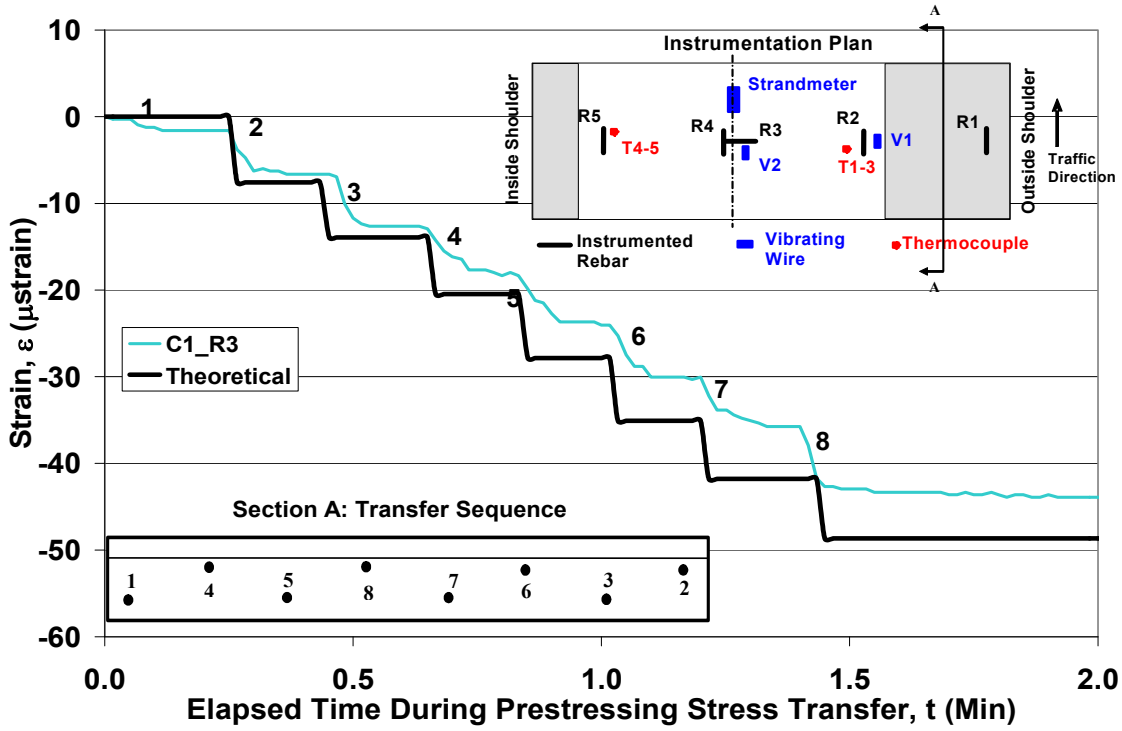

Figure 7.6 – Measured transverse strain on Panel C1 during pretension transfer

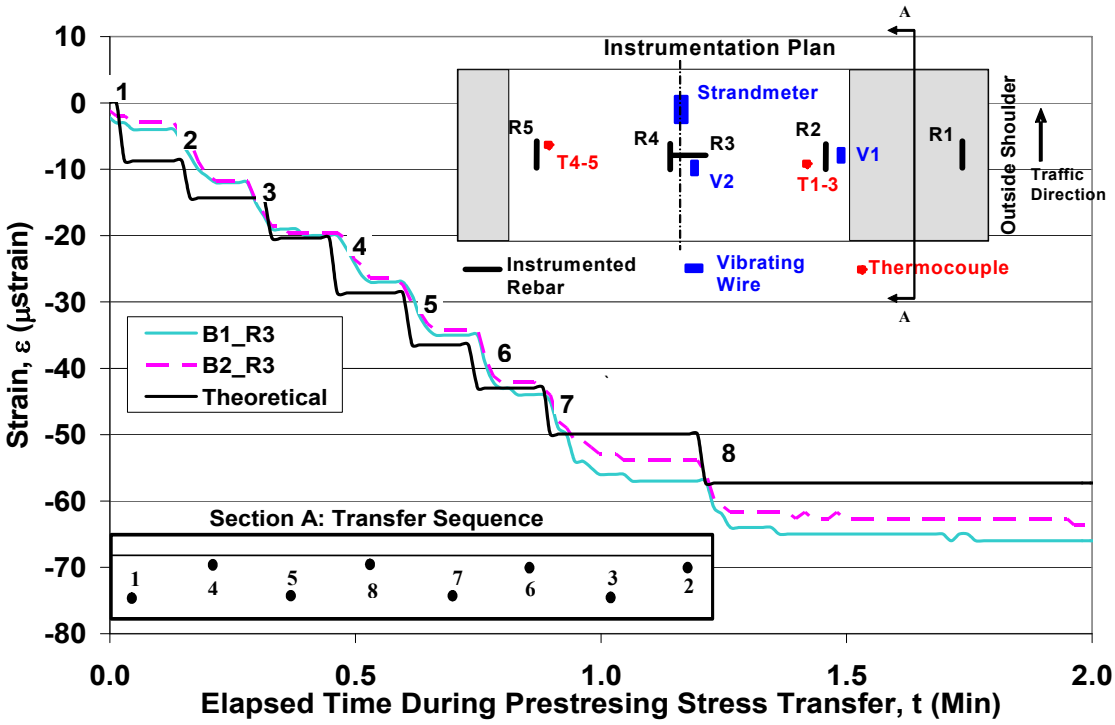

Figure 7.7 - Measured transverse strain on Panels B1/B2 during pretension transfer

Considerably higher strains were measured for Panels B1 and B2 than Panels C1, B3, and B4. Panels B1 and B2 may have had a lower strength and modulus at the time of transfer. This would create the higher strain readings (for the same stresses) as shown in Figure 7.7. Also, Rebar 3 in Panels C1, B3, and B4 are 2" from the bottom of the cross-section. Rebar 3 in Panels B1 and B2 are 4" from the bottom. Compared to Panel C1, the compressive strains appear to be lower toward the bottom fiber (Figure 7.6 and Figure 7.8). This could be an indication of inconsistent draping of the top strands. Chairs were place under Strands 4, 8, 6, and 2. These chairs may have been too close to the edges allowing the strands to run close to the top fiber of the panel. This would create eccentricities that would cause a 'reverse camber'. For example if the chairs were placed such that a strand was 0.5" on either side of the center of the cross-section, it would create a 3-4 μstr gradient at the top or bottom fiber. If several strands were eccentric, out-of-plane bending will begin to escalate.

The converse may be true for Panels B1 and B2. The strands may be too close to the bottom causing excess compressive strain greater than what is predicted under theoretical assumptions.

The longitudinal rebar for Panel A32 are presented in Figure 7.9 and Figure 7.10. These graphs show how the eccentricities during stress transfer will even affect the perpendicular Poisson's strain. Rebar 1, 6, and 7 show both tension and compression as stress is transferred on each side and eccentricities develop.

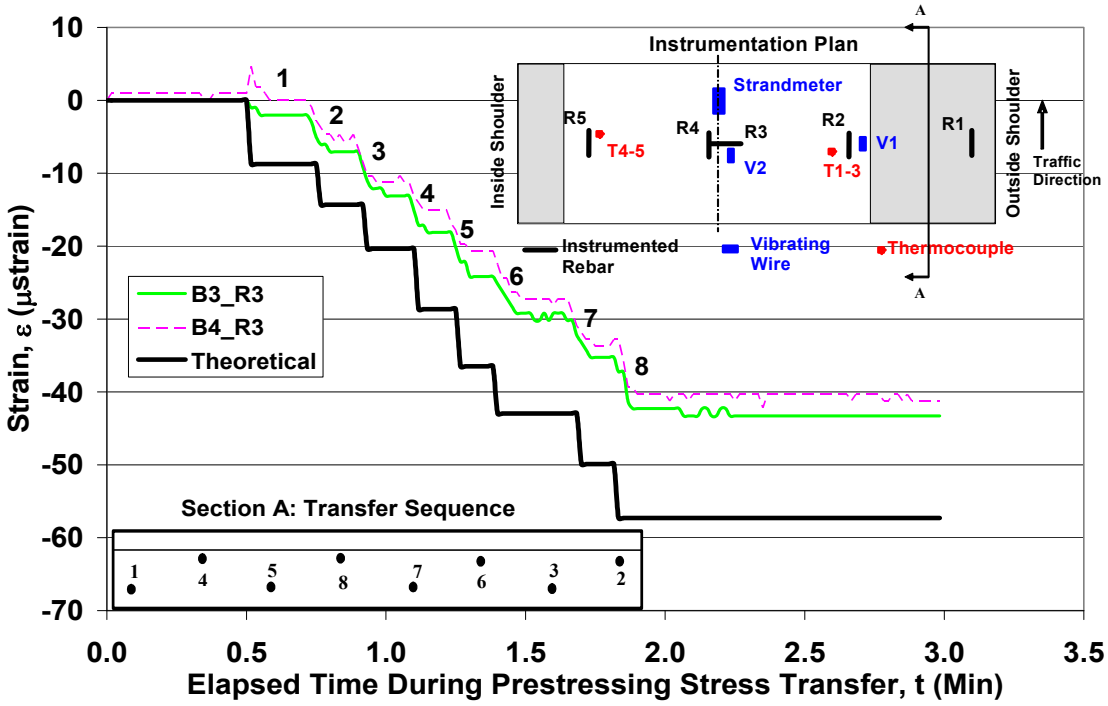

Figure 7.8 - Measured transverse strain on Panels B3/B4 during pretension transfer

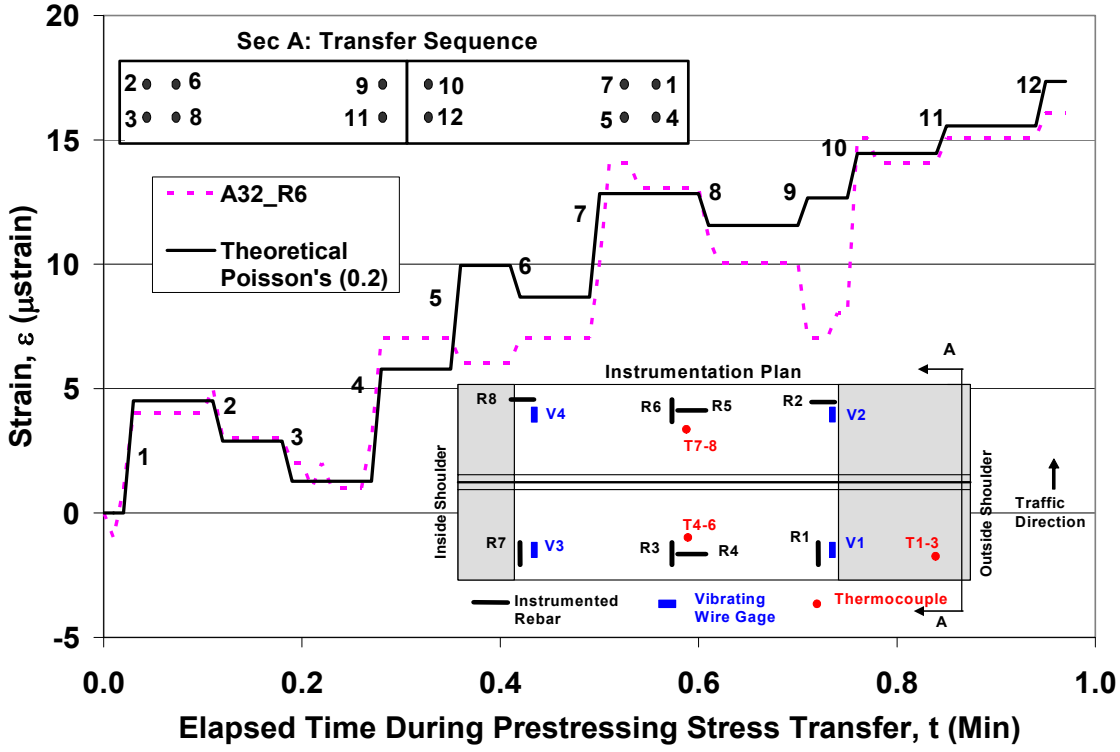

Figure 7.9 - Measured longitudinal strain on Panel A32 during pretension transfer

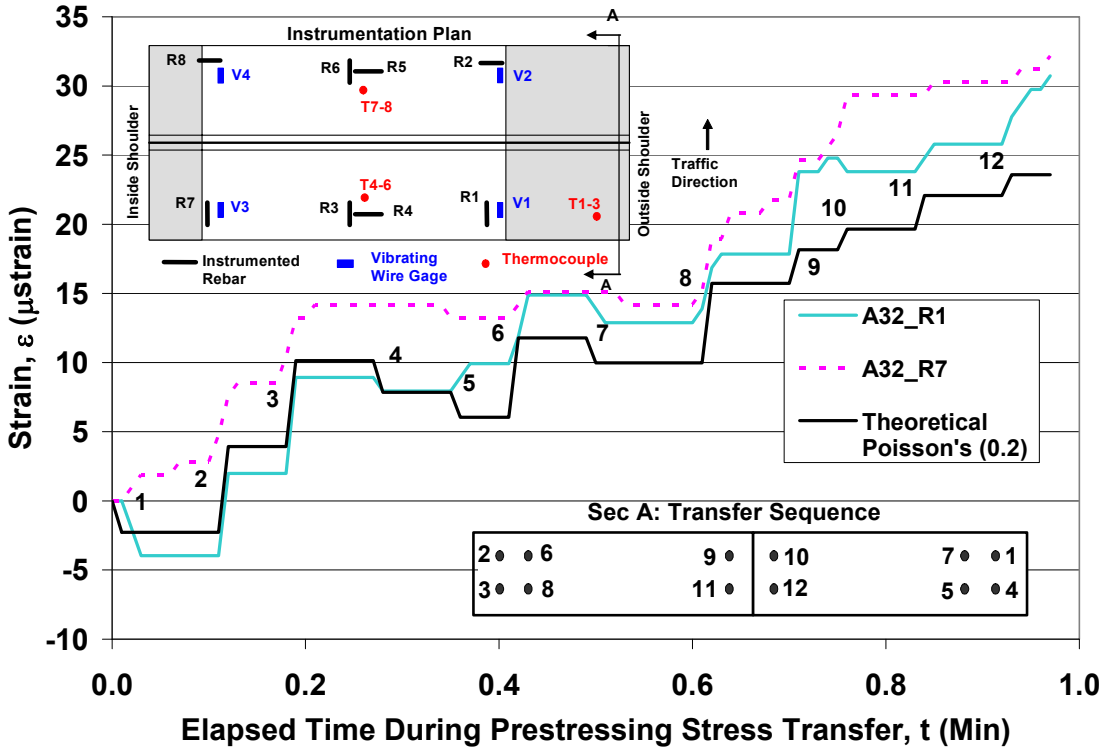

Figure 7.10 - Measured longitudinal strain on Panel A32 during pretension transfer

Theoretical values nearly match each point of stress transfer. Some discrepancies are present. When Strand 5 is cut, Rebar 6 behaves opposite of what is expected. Compression along that side of the panel should create a Poisson's effect such that Rebar 6 shows tensile strains. Out of plane eccentricities are most likely responsible for Rebar 6 showing compressive strains. Strand 5 is near the bottom of the bed. It, in conjunction with the transfer of adjacent Strand 4, could cause a temporary upward camber. When this happens, the top fiber shows tension while bending out of plane along the long dimension of the slab. At the top fiber perpendicular to the long dimension (parallel to Rebar 6) the tension half will contract laterally producing compressive strain.

8. POST-TENSIONING DURING CONSTRUCTION

8.1. INTRODUCTION

Post-tensioning the panel system is equally as important as pretensioning. It provides the confinement and crack control along the traffic direction. It locks the panels together globally, helping with load transfer and increasing the stiffness of the pavement sections between joints.

Section 3, the instrumented section, was stressed slightly different than Sections 1, 2, and 4. The strand at the crown was stressed first. This strand was instrumented with the four strandmeters. It was essential to stress it alone because the data acquisition, stress rate, and strandmeter position in the block-out needed to be closely monitored. It was also essential to record the effects of adjacent stressing with the strandmeters. Figure 8.2 shows the order in which the strands were stressed. They were stressed two at a time starting at the center of the panel. Unlike pretension transfer, there were little to no eccentricities developed during post-tensioning. The strands were stressed evenly on each side of the centroid from the inside out. This made the simplified theoretical calculations.

After the center strand was stressed. The research team switched the program to monitor all transverse gages. Each strand was stressed to the design stress at one end of the section (west end). The strands were then pulled again on the east end to ensure uniform stress distribution and alleviate frictional restraint within the ductwork

The following sections discuss the theoretical strain calculations and comparisons between measured strains. Strandmeter strain and frictional losses are also presented.

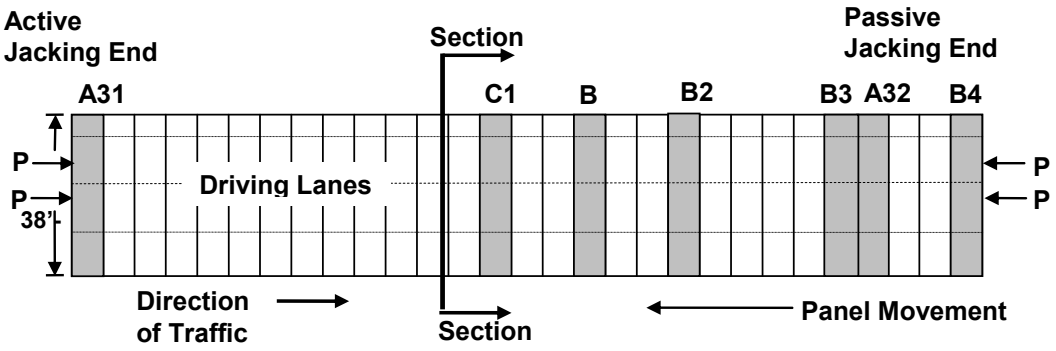

Figure 8.1 - Post-tensioning schematic of Section 3

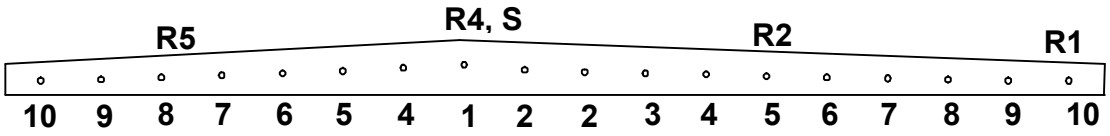

Figure 8.2 - Post-tensioning sequence and rebar locations at cross-section

Figure 8.3 - Post-tensioning a section of pavement

8.2. POST-TENSIONING DATA AND ANALYSIS

The following sections present theoretical calculations and measured strains in conjunction with theoretical curves. Idealized post-tensioning mechanical behavior is rather easy to model and validate. External forces that make the idealizations somewhat inaccurate include:

1. Friction between the panel and sub-grade
2. Friction between the strand and duct
3. Shims installed to re-align panels
4. Potential misalignment of post-tensioning ducts

8.2.1. THEORETICAL STRAIN CALCULATIONS

The two sections that follow outline the theoretical calculations for both the strain in the concrete and the strain in the strand. It should be noted that the external forces affecting each are independently exclusive. Although the stress in the strand provides the force that induces the strain in the concrete, the theoretical strain in the strand and strain in the concrete are not the same. Also, as discussed later, the strain in the strand is affected only by friction of the ductwork (Figure 8.4 and Figure 8.10). Strain is induced in the concrete after each panel slides together and makes full contact. Therefore, the strain in the concrete is affected by the resistant friction of the concrete and sub-grade (Figure 8.4 and Figure 8.10).

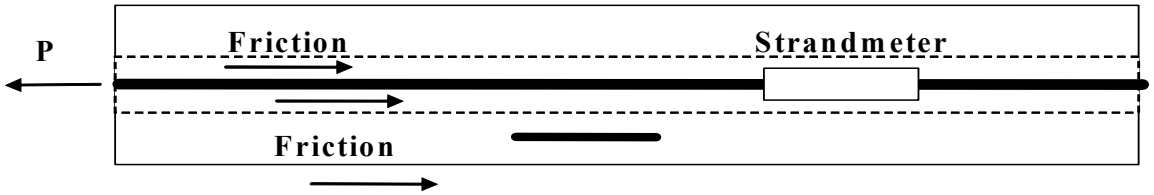

Figure 8.4 - Schematic of frictional forces on panel/strand during post-tensioning

8.2.1.1. THEORETICAL CONCRETE STRAINS

The fact that the strands are stressed two at a time on either side of the centroid, simplifies theoretical calculations. The strains are calculated similar to pretension transfer. However, the internal bending part of the stress equation is negligible. It simplifies to:

$$\sigma = \frac{P}{A} \qquad \textbf{8.1}$$

The prestressing force 'P' is different for post-tensioning. Bigger 0.6" (1.5 cm) diameter strands were used. The area of this strand is 0.217 in^2 (1.4 cm^2) The ultimate strength f_{pu} is the same (270 ksi or 1861 MPa) (PCI 1999). Also the design stress was $0.8f_{pu}$. The prestressing force becomes:

$$P = 0.217 \times 0.8 \times 270 \cong 46.9 kip; (209 kN) \qquad \textbf{8.2}$$

The area calculation requires idealization because the cross-section is designed with a 2% crown. The area changes for prestressing stress calculations depending on strand location. The post-tensioning cross-section for calculating strain is trapezoidal. Therefore, in order to calculate the strain at the different rebar it is necessary to calculate the stress at that location in the cross-section. The first step is to calculate the amount of applied force per linear inch along the length 'l' of the cross-section. This length is the width of the panel from shoulder to shoulder (38'-0" or 11.6 m). The total force applied 'F_{plf}' is the total number of strands 'n' that have been stressed times the force per strand 'P' (English units).

$$F_{plf} = \frac{(n \times P)}{(l \times 12)} = \frac{(n \times 46.9)}{(38 \times 12)} \times 1000 = 102.85n \qquad \textbf{8.3}$$

The 12 and 1,000 are conversion factors length (inch to feet) and force (lbs to kips). Once the force per inch is calculated, the depth of the panel at the rebar of interest must be calculated. This was done using the geometry of the cross-section including the slope of the crown and known depth at the ends and center. Similar triangles can then be used to find the depth 'd' of the cross-section at any rebar. The stress at that location is then calculated as follows (English units).

$$\sigma = \frac{F_{plf}}{d} = \frac{102.85n}{d} \qquad \textbf{8.4}$$

These values were tabulated for each individual rebar as a running sum based on the total number of strands stressed. Once stresses were calculated they were converted to strain with Hooke's Law:

$$\varepsilon = \frac{\sigma}{E} \qquad \textbf{8.5}$$

This time, the modulus of elasticity 'E' used for the panels was an average of the measured 28 day modulus recorded from field specimens brought to the lab. This average tested to be roughly 5.5 x 10^6 psi (3.8 x 10^4 MPa) (Davis 2006). The strain equation then simplifies to (English units):

$$\varepsilon = \frac{102.85n}{d \times E} = \frac{1.875 \times 10^{-6} n}{d} \qquad \textbf{8.6}$$

A running sum of strains at each rebar location was plotted against measured strains. Table 8.1 shows a summary of theoretical strain calculations.

Section 3
Material Properties

Steel		Concrete	
Yield Strength (ksi)	270	Inertia (in^4)	5.9E+06
Modulus (ksi)	28500	Area (in^2)	3894
Strand Diameter (in)	0.6	Poisson's Ratio	0.2
Strand Area (in^2)	0.217	28d Strength (psi)	7187
Percentage of Stress	80%	Modulus (psi)	5.5E+06
Stress in Strand (ksi)	216		
Force in Strand (lbs)	46872		

Transfer Step	Total No of Strands Stressed	Force per inch (lb/in)	Rebar 1				Rebar 2				Rebar 4				Rebar 5			
			Av. Dist from Crown X (in)	Depth @ Rebar (in)	Stress (psi)	Strain (µstr)	Av. Dist from Crown X (in)	Depth @ Rebar (in)	Stress (psi)	Strain (µstr)	Av. Dist from Crown X (in)	Depth @ Rebar (in)	Stress (psi)	Strain (µstr)	Av. Dist from Crown X (in)	Depth @ Rebar (in)	Stress (psi)	Strain (µstr)
1	1	103	235	6.2	-17	-3	125	8.4	-12	-2	4	10.8	-9	-2	-121	8.4	-12	-2
2	3	308	235	6.2	-50	-9	125	8.4	-37	-7	4	10.8	-28	-5	-121	8.4	-37	-7
3	4	411	235	6.2	-66	-12	125	8.4	-49	-9	4	10.8	-38	-7	-121	8.4	-49	-9
4	6	617	235	6.2	-99	-18	125	8.4	-73	-13	4	10.8	-57	-10	-121	8.4	-73	-13
5	8	822	235	6.2	-133	-24	125	8.4	-98	-18	4	10.8	-76	-14	-121	8.4	-98	-18
6	10	1028	235	6.2	-166	-30	125	8.4	-122	-22	4	10.8	-95	-17	-121	8.4	-122	-22
7	12	1233	235	6.2	-199	-36	125	8.4	-147	-27	4	10.8	-114	-21	-121	8.4	-146	-27
8	14	1439	235	6.2	-232	-42	125	8.4	-171	-31	4	10.8	-133	-24	-121	8.4	-171	-31
9	16	1645	235	6.2	-265	-48	125	8.4	-196	-36	4	10.8	-152	-28	-121	8.4	-195	-36
10	18	1850	235	6.2	-298	-54	125	8.4	-220	-40	4	10.8	-171	-31	-121	8.4	-220	-40

Table 8.1 - Theoretical strain calculations for rebar during post-tensioning

8.2.1.2. THEORETICAL STRAND STRAIN

The theoretical strain in the post-tensioning strand is easily calculated. The modulus 'E' of prestressing steel is roughly 28,500 ksi (193 MPa). The stress is calculated based on design information ($0.8f_{pu}$); therefore the strain equation becomes a constant.

$$\varepsilon = \frac{\sigma}{E} = \frac{(0.8 \times 270)}{28{,}500} = 7{,}580 \mu str \qquad \textbf{8.7}$$

This strain is compared to the maximum measured strain in the strandmeters. Conclusions about stress loss and frictional restraint become evident.

8.2.2. CONCRETE STRAINS DURING TRANSFER

Vibrating wire data was taken at the time of stress transfer. However, the process was too dynamic and readings contained large components of electrical noise. Only instrumented rebar strains in the longitudinal direction were monitored.

Comparisons throughout the section can be drawn because Rebar 1, 2, 4, and 5 are in the same cross-sectional locations for Panels C1, B1, B2, and B3. The output from each rebar location is graphed together with theoretical predictions for that spot in the cross-section. The predictions are shown with expected steps from each pair of strands that are stressed. These steps are visible in some of the measured data.

As stated in earlier chapters, panel alignment became a problem. To mitigate this, each panel was shimmed near the south edge (or closer to Rebar 1). This created an undesirable stress distribution along the cross-sections with concentrated stresses near the shims. Therefore Rebar 1 shows higher compressive strain values than expected (Figure 8.5). Panel C shows stress concentrations on the other end (Figure 8.8).

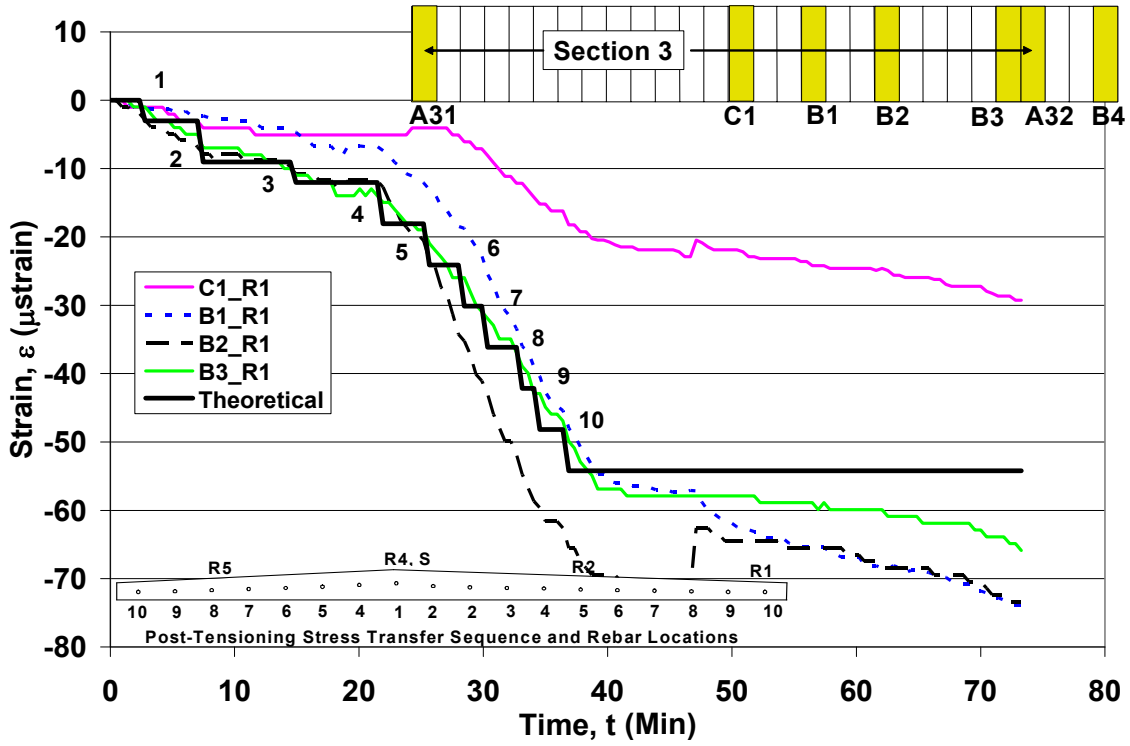

Figure 8.5 – Longitudinal strains at outside shoulder (R1) from post-tensioning

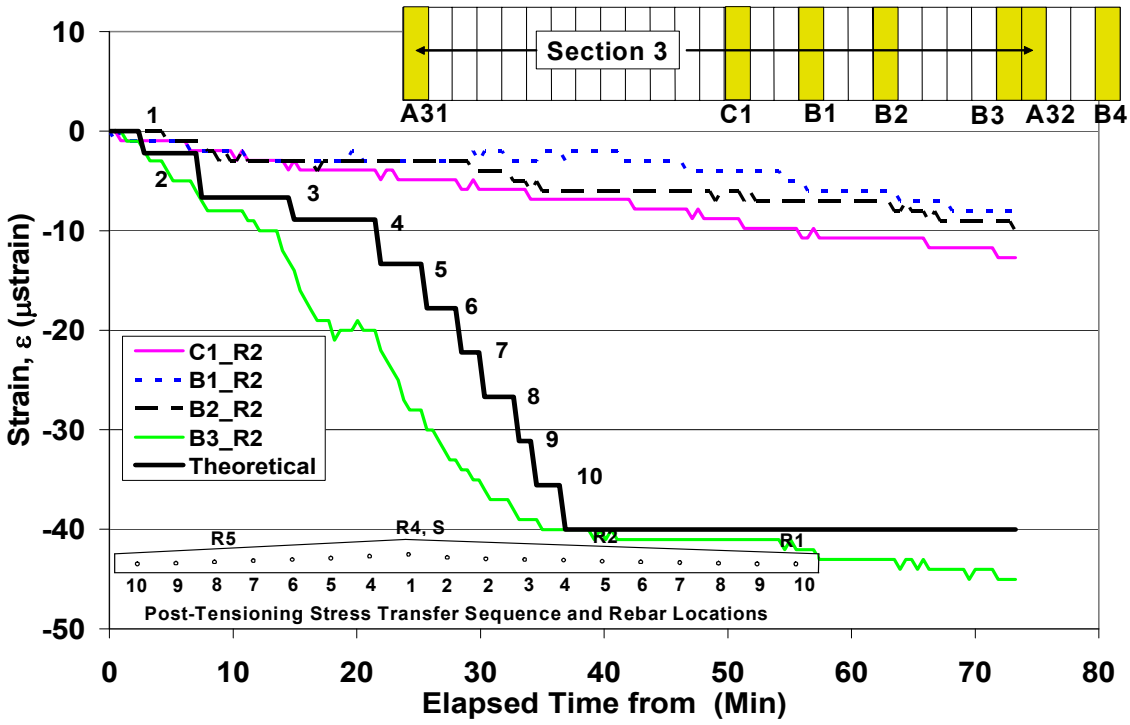

Figure 8.6 - Longitudinal strains at the outside lane (R2) from post-tensioning

The strain decreases across Panel C and Rebar 1 reports a lower strain reading (Figure 8.5). Rebar 1 readings are the most consistent.

The mating surfaces of the panels play a large role in reported strains within the concrete. This in conjunction with external forces such as friction and the added shims make further trends difficult to extract. Panels B1, B2, and B3 show higher strains near the right side. Generally, strains from Rebar 1, 2, and 4 are higher opposite the active jacking end (east side) and decrease as the panels get closer to the jack (Figure 8.5, Figure 8.6, and Figure 8.7 respectively). Strains in Panel B3 are generally the highest then progressively decrease at Panels B2 and B1 respectively (Rebar 1 strains are close).

As expected, this order is switched for Rebar 5. If a panel shows a higher than expected concentration of strain near the Rebar 1/Rebar 2 end, it is lower on the other (Rebar 5) end. Although the active stressing end is at the Panel A31 side of Section 3, higher strains were created at the opposite end first. This hypothesis is best represented by strain values for Rebar 2, Rebar 4, and Rebar 5. This is because the section was anchored at the active end. As the panels were stressed the gaps were filled from east to west (from Panel A32 to Panel A31). Sections 1 and 2 had already been stressed. None of the joint panels opened during stressing. Section 4, on the other side of Panel A32, was not attached. Therefore the point of least resistance was at Panel A32. Starting at Joint Panel A32 the slabs moved from right to left toward Panel A31. Because the strands slid through each panel, the main active force was from the bearing in Joint Panel A32, ultimately creating higher stresses at Panel B3. Frictional resistance then increased toward Panel A31 and the measured rebar strains became progressively lower from right to left as shown in Figure 8.10.

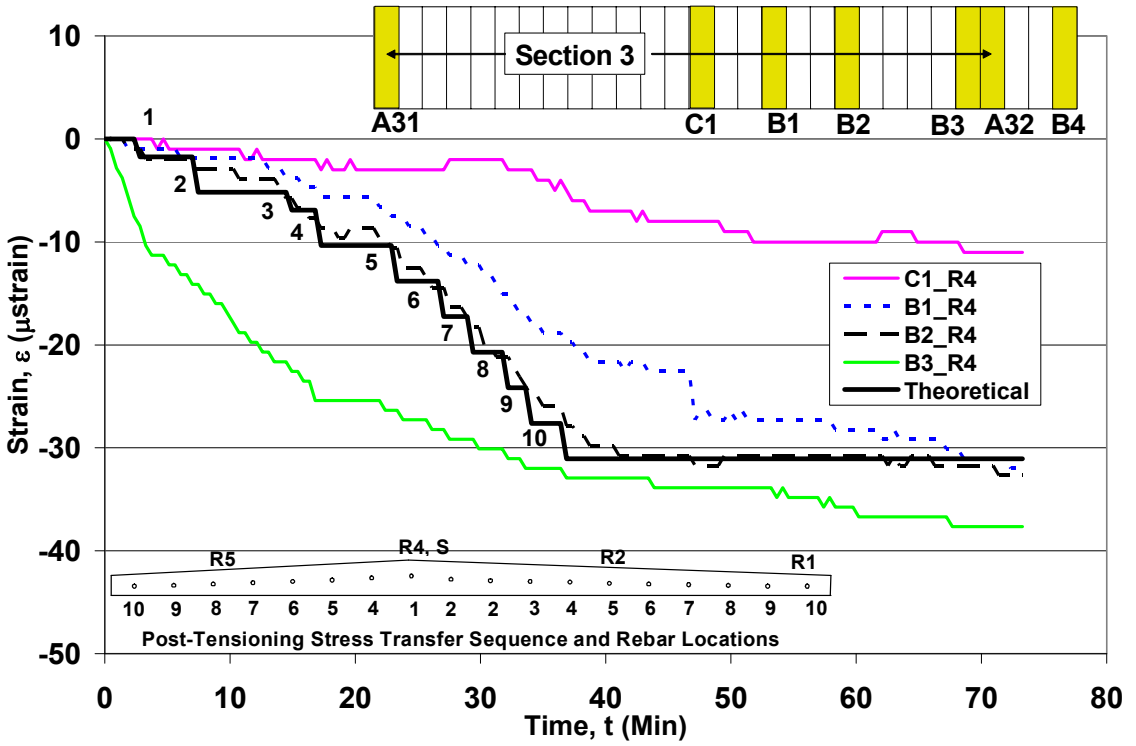

Figure 8.7 - Longitudinal strains at crown (R4) from post-tensioning

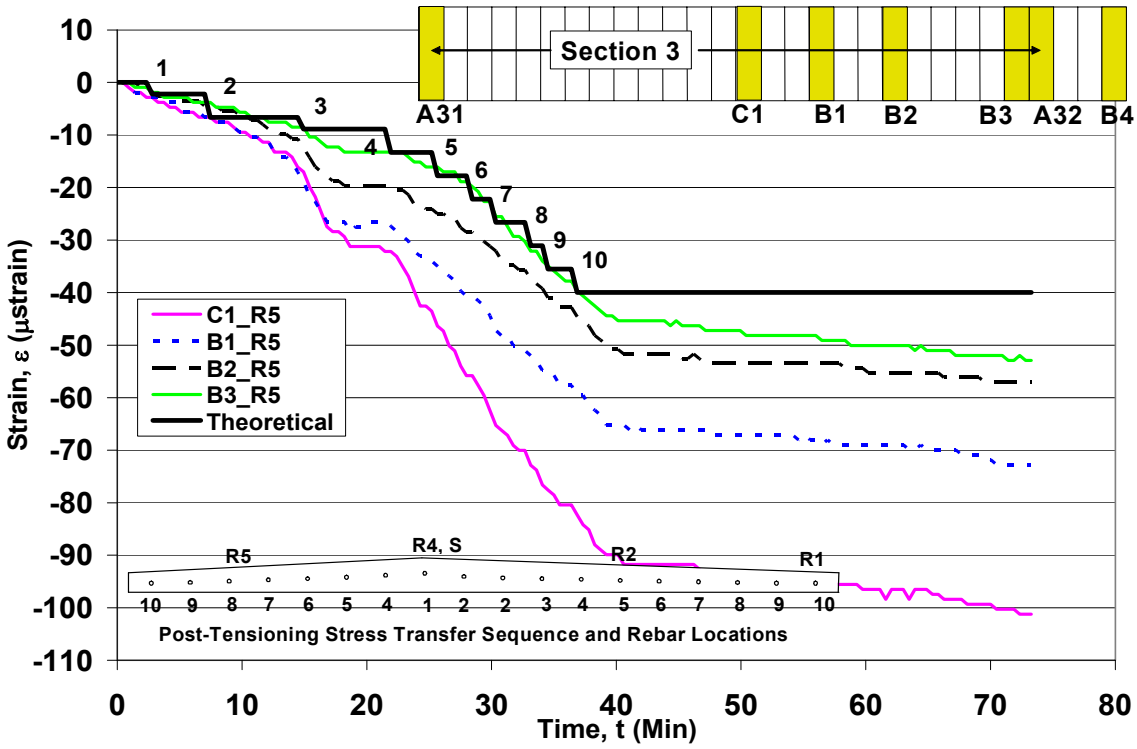

Figure 8.8 - Longitudinal strains at the inside lane (R5) from post-tensioning

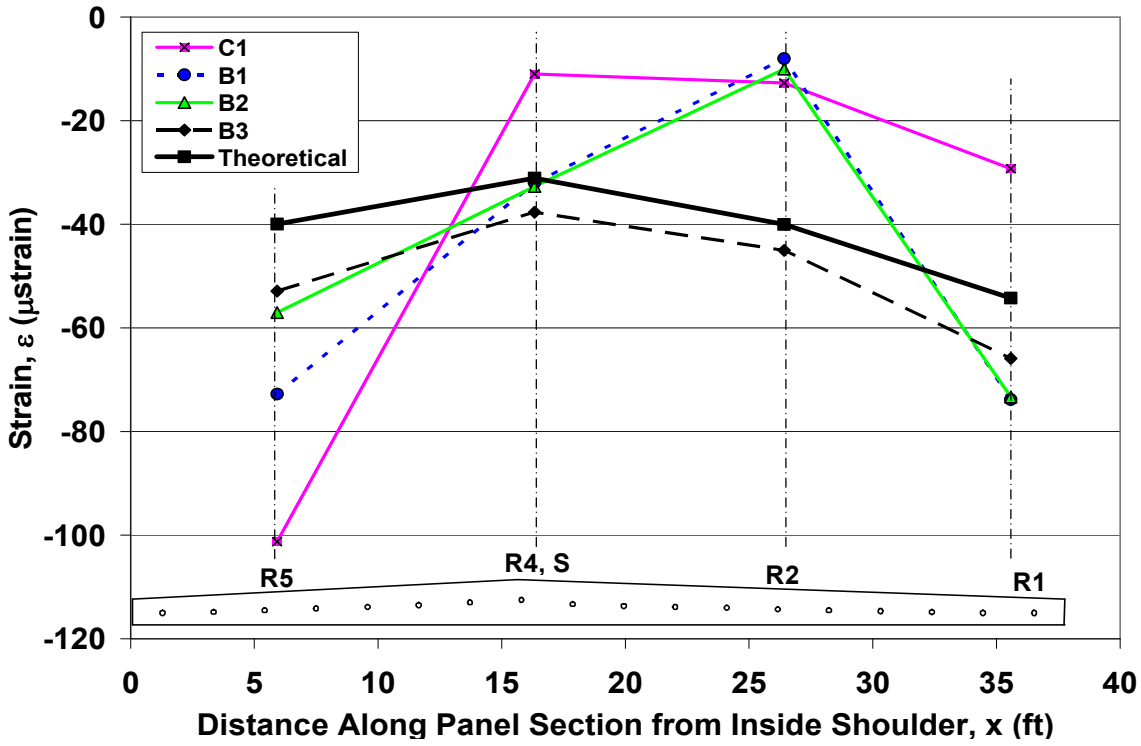

Figure 8.9 - Measured final post-tensioning strain through x-section of each panel

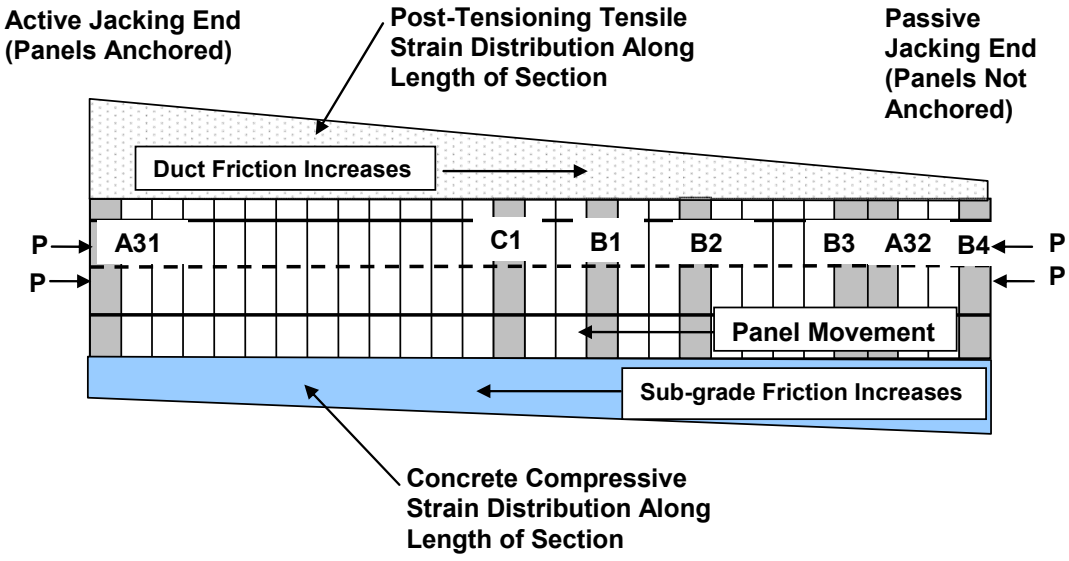

Figure 8.10 - Strain distribution in strand and concrete from post-tensioning

Theoretical values are closest to measured strains near the center of the cross-section (Rebar 4). Figure 8.9 shows a comparison of final strain distributions. Panel B3 strains are closest to theoretical in shape. Again anomalies are best explained by external factors such as irregularities in mating surfaces.

8.2.3. POST-TENSIONING STRAND STRAINS DURING AND AFTER TRANSFER

Four panels were instrumented with strandmeters: C1, B1, B2, and B3. Each gage was attached to the center strand. Strandmeter data is quite consistent for post-tensioning. Unlike the embedded vibrating wire gages, the strandmeters output an actual displacement. These readings are easily converted by dividing by the 8 inch gage length.

Data for Panels C1, B1 and B3 is presented. The strandmeter in Panel B2 had range problems before installation. It took data to nearly 5,500 μstr before going out of range. It is not shown for this reason.

During the early stages of design, the full ramifications of the strandmeter block-out size and application of stressing force were not adequately addressed. The block-outs were too short to accommodate stressing at only one end. When only one active jacking end is used the deformation accumulates per panel. For example if the strand will stretch 1 in. (2.5 cm) per 10'-0" (3 m) panel, then the total elongation of the strand (toward the jack) will be accumulated with 1" for every 10'-0". At 200'-0" (61 m) the strand would have moved 20 in. (51 cm). The block-outs were not long enough for the two panels closest to the jacking force (Panels C1 and B1). The strandmeters were watched and jacking was stopped to reposition the gages. Strandmeter B1 did hit the concrete before the team was able to stop stressing operations. As a result, small windows of data were lost (Figure 8.12).

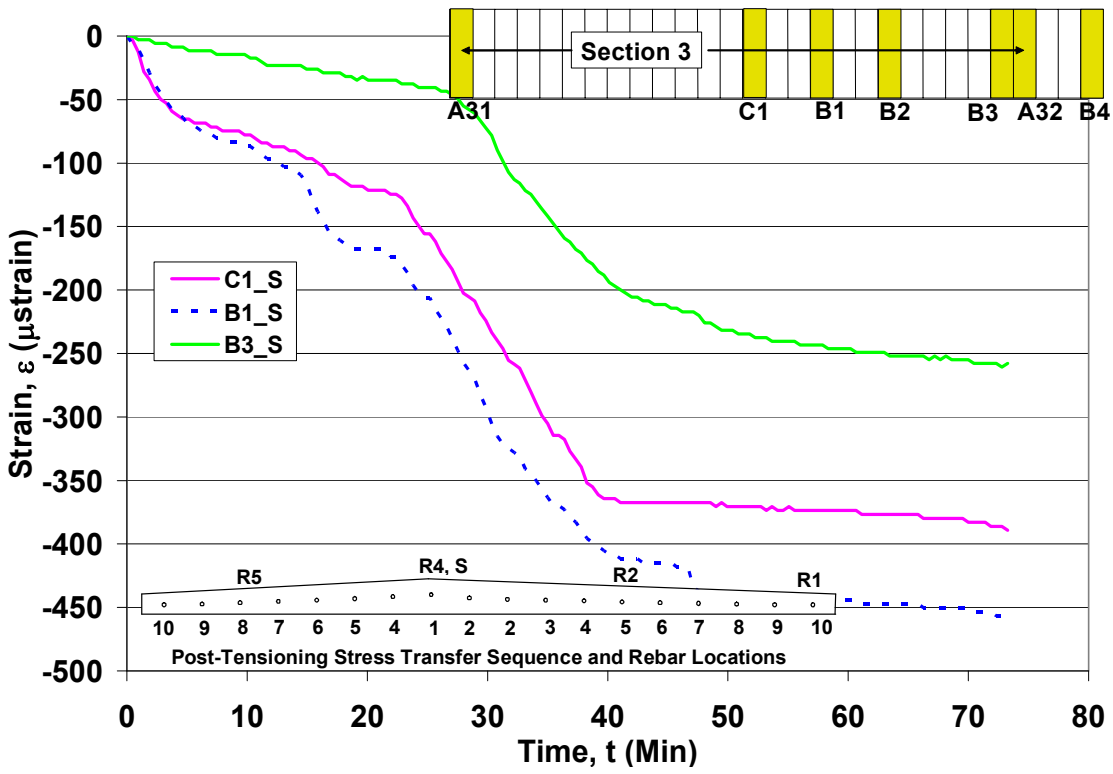

Figure 8.11 - Post-tensioning strain loss in center strand after jacking adjacent strands

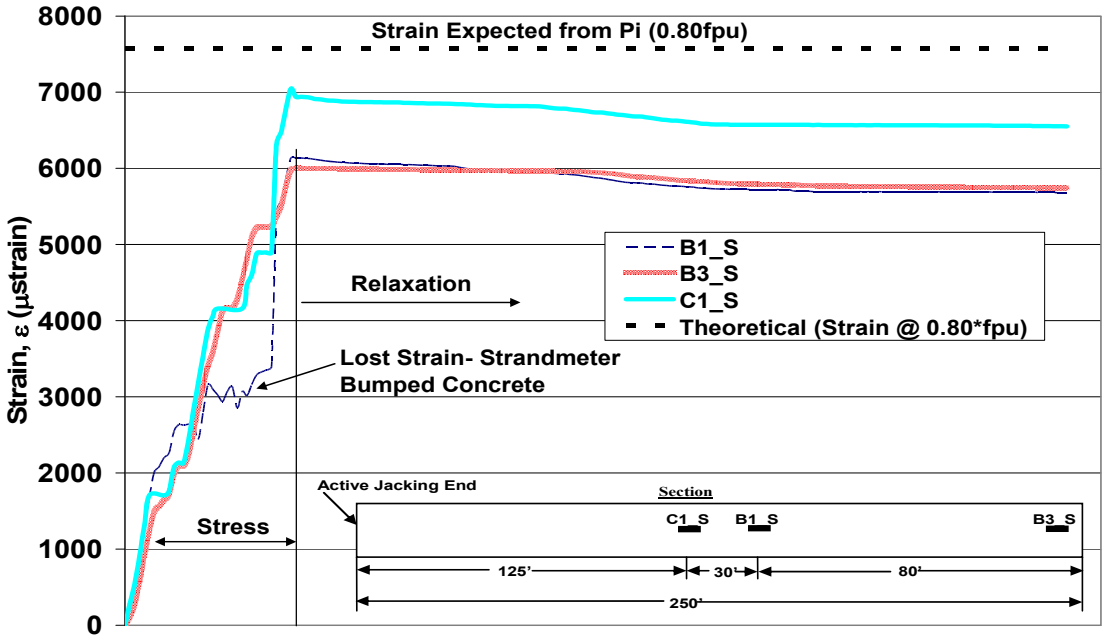

Figure 8.12 - Entire post-tensioning strain history of center strand

Figure 8.11 shows short-term relaxation of the middle strand during stressing of adjacent strands. That same data was added to Figure 8.12. Initial relaxation shows 250-450 μstr loss. This amounts to roughly 3.5-6.5% initial relaxation in stressing. It is less than the 10% recommended by PCI for design (PCI 1999). Only initial frictional resistance and relaxation is recorded on these graphs. The companion thesis by Brent Davis discusses long-term post-tensioning losses in detail with special consideration given to concrete creep (Davis 2006).

Unfortunately it is a complex problem to quantify frictional losses per linear foot from only two readings. However, strandmeters in both Panel C1 and Panel B3 are very consistent. The line at the top of Figure 8.12 shows the expected theoretical strain. The loss per linear foot in friction for the central instrumented strand can be easily calculated. From Panels C1 to B3 there is a 1,000 μstr loss. Note that, unlike the rebar in the concrete, these losses accumulate away from the active jacking end. This loss between Panels C1 and B3 translates to roughly 6,200 lbs (27580 N) of lost stressing force at the passive end (Panel B3). (Solve for stress and multiply by the area.)

$$P_{Loss} = E \times \varepsilon \times A_{Strand} = 6200 lbs; (27580 N) \qquad \textbf{8.8}$$

There are ten 10'-0" (3.05 m) panels between C1 and B3 therefore there is a 620lb (2758 N) loss per panel. This loss has to be in the post-tensioning ducts. Sliding friction at earth contact will not cause loss in post-tensioning per linear foot (Figure 8.4). Therefore, the PT ducts produced roughly 62 lbs/ft (84 N/m) resistance.

9. SERVICE PERFORMANCE

9.1. INTRODUCTION

The prestressed precast pavement was opened to traffic in mid January 2006. Figure 9.1 shows a picture of the finished roadway in service. The large number of instruments allowed different programs to run at various stages with data acquisition and monitoring tailored to specific locations. Not all instruments could be monitored at once during in-service. The research team selected key pieces that were proven useful in previous stages of instrumentation and monitoring. Redundant measurements were eliminated and a program was selected to acquire strain and thermal data as efficiently as possible.

Measurements were recorded almost continuously following post-tensioning. Data acquisition rates were adjusted from 5 min to 2 hrs. The 2 hr. sample rate proved to be the most efficient use of memory and power. The maximum sample rate was used for acquiring traffic data. The research team adjusted the sample rate, downloaded data, and uploaded new data acquisition programs from Columbia, MO using the network link interface. This made changes in the instrumentation and monitoring program very fast and easy.

The following sections discuss in-service data and monitoring of the precast pavement system. In-service performance is discussed including: temperature variations, thermal strains, and traffic effects. The last section outlines long-term observations such as: long-term strains from vibrating wire devices, global movement of the sections, and visual signs of degradation.

Figure 9.1 - Finished panel system in service

Figure 9.2 - Another view of the finished panel system in service

These sections only cover a small part of the year long monitoring program. Research by Grant Luckenbill, currently underway as a part of this project, will elaborate and summarize the seasonal performance and long-term viability of the system. Further studies and observations will be added.

9.2. DAY TO DAY SERVICE PERFORMANCE

The following sections present temperature and strain variations over three to fourteen day windows of time. In-service strains largely result from ambient thermal changes. Theoretical thermal strains are presented in conjunction with measured values. Traffic strain measurements were taken only to differentiate between traffic data and thermal data. Thermal strains are of higher magnitude and compose the focus of this year long study.

9.2.1. DAILY TEMPERATURE VARIATION

Thermal strains monitored show both daily and seasonal variations in pavement temperature. The best data, selected for presentation in this thesis, show large excursions between night and day temperatures as well as a seasonal change over several days. Early spring days produced the largest excursions in temperature between night and day. The sun would provide radiant heat during the day. Unlike winter temperatures, night temperatures would then fall well below daytime averages.

The figures on the following pages show day to night ambient temperature variations ranging from 10-15 °C (50-60°F). Corresponding panel temperatures were slightly under night-day extremities. This is because the concrete was able to store heat. The night-day thermal change was not sustained enough (in most cases) to achieve the

exact same ambient and panel temperatures. The base under the slab is insulated by the concrete and becomes a good source of heat, allowing the panels to stay above ambient temperatures—especially on the bottom (Figure 9.3).

Thermocouples toward the bottom of the panel stayed warmer. In Figure 9.3 Thermocouples 1, 4, and 7 are on the bottom of the panel (see as-builts in a previous chapter) and stay warmer than those in the same location but closer to the surface.

There is a 5°C (9°F) difference between Thermocouple T1 on the bottom and Thermocouple T3 on the top (Figure 9.3). Theoretically, if the CTE of the concrete is 6 μstr/°C, this produces a 30 μstr internal strain gradient from top to bottom. Although pretensioning and post-tensioning help mitigate this strain, larger internal gradients may lead to cracking (Emborg and Bernander 1994)

There are two types of thermal trends shown: day-to-day and seasonal. Data is presented in 3-14 day intervals during February, July, September, and October, 2006. Over several days two trends are clearly evident. There is a day to day fluctuation as well as a change in the daily average. This is noted as a seasonal trend because the days gradually grow colder. It has been marked on each thermal graph with a trend line. Thermal measurements were all very close. For this reason an average is plotted in order to view the overall trend. Figure 9.5 shows a sudden fall in temperature trend between day two and day three.

9.2.2. THEORETICAL STRAIN CALCULATIONS

The following sections discuss theoretical rebar strain during service. Theoretical calculations are based on thermal models (CTE) much like theoretical curing strains. Both are measured and theoretical strains are graphed concurrently.

9.2.2.1. THEORETICAL CONCRETE STRAIN

The following equation was used to calculate the expected thermal strain of hydrating concrete:

$$\Delta\varepsilon_{Thermal\ /\ Concrete} = CTE_{\ Concrete} \times (T_1 - T_0) \qquad \textbf{9.1}$$

The term 'T' represents temperature at two different points in time. This equation is different from the curing strain calculation in that the CTE is a constant. It has been estimated based on the known thermal data for Missouri limestone aggregate. The team assumed a CTE of 6 μstr/°C. Future work by Grant Luckenbill will further explore the thermal properties related to both the concrete and strain measuring devices.

9.2.2.2. THEORETICAL REBAR STRAIN

Theoretical measured in-service rebar strain is calculated similar to curing rebar strain except the CTE for concrete is constant because the concrete is a cured solid.

$$\Delta\varepsilon_{Thermal\ /\ Steel} = (CTE_{Concrete} - CTE_{Steel}) \times (T_1 - T_0) \qquad \textbf{9.2}$$

The CTE for steel is also constant. Note that if the concrete CTE is roughly 6 μstr/°C and steel is roughly 12 μstr/°C, the theoretical thermal steel strain is merely the negated theoretical thermal concrete strain. Both theoretical curves (concrete and rebar) are presented with measured strain data.

9.2.3. MEASURED DAILY IN-SERVICE STRAINS

Thermal changes induce strains in the pavement. Figure 9.3 to Figure 9.6 show measured and theoretical strains due to daily and seasonal thermal variations. The vibrating wire data are not corrected for temperature. The addition of the temperature correction made the magnitudes much higher than the theoretical concrete strain curves.

It is possible that the thermal effects on the vibrating wire gage are non-linear (similar to the strandmeters). The strandmeters only recommend thermal correction when there are excursions over 50°C (90°F). Hydration temperatures and excursions were much higher than in-service temperatures; therefore, the strain readings needed to be corrected for thermal effects in order to match theoretical predictions. Per manufacturer's recommendations, the strandmeters have not been corrected for temperature either. For the most part, strain readings are consistent with predictions.

Figure 9.3 shows strain and temperature reading for two days in February, 2006. Rebar 2, 4, and 5 are very close to theoretical rebar predictions. Rebar 3, the transverse bar, outputs a higher strain value. This is most likely due to the fact that it is located toward the extreme bottom fiber of the panel (2 in from bottom) (Table 4.5). When the top begins to heat, Rebar 3 measures a higher compressive strain within the cross-sectional strain gradient. The strandmeter appears to follow the same trend as the rebar only slightly out of phase (possible difference in thermal conductivity) (Figure 9.3).

Figure 9.4 shows measured rebar and vibrating wire strains in Joint Panel A32 during three days in September, 2006. The vibrating wire gages generally follow theoretical concrete strain. This was typical for nearly all panels. Vibrating Wire Gages V2 and V4 on the Section 4 side of Panel A32 output slightly different magnitudes than adjacent V.W. Gages V1 and V3. They appear to go into tension while V.W. Gages V1 and V3 compress (and visa versa). The joint in Panel A32 may not be allowing free expansion and contraction. Although it is somewhat speculative, Section 3 (the side with V.W. Gages V1 and V3) may be contracting as the temperature falls, pulling the adjacent half of Panel A32 into tension.

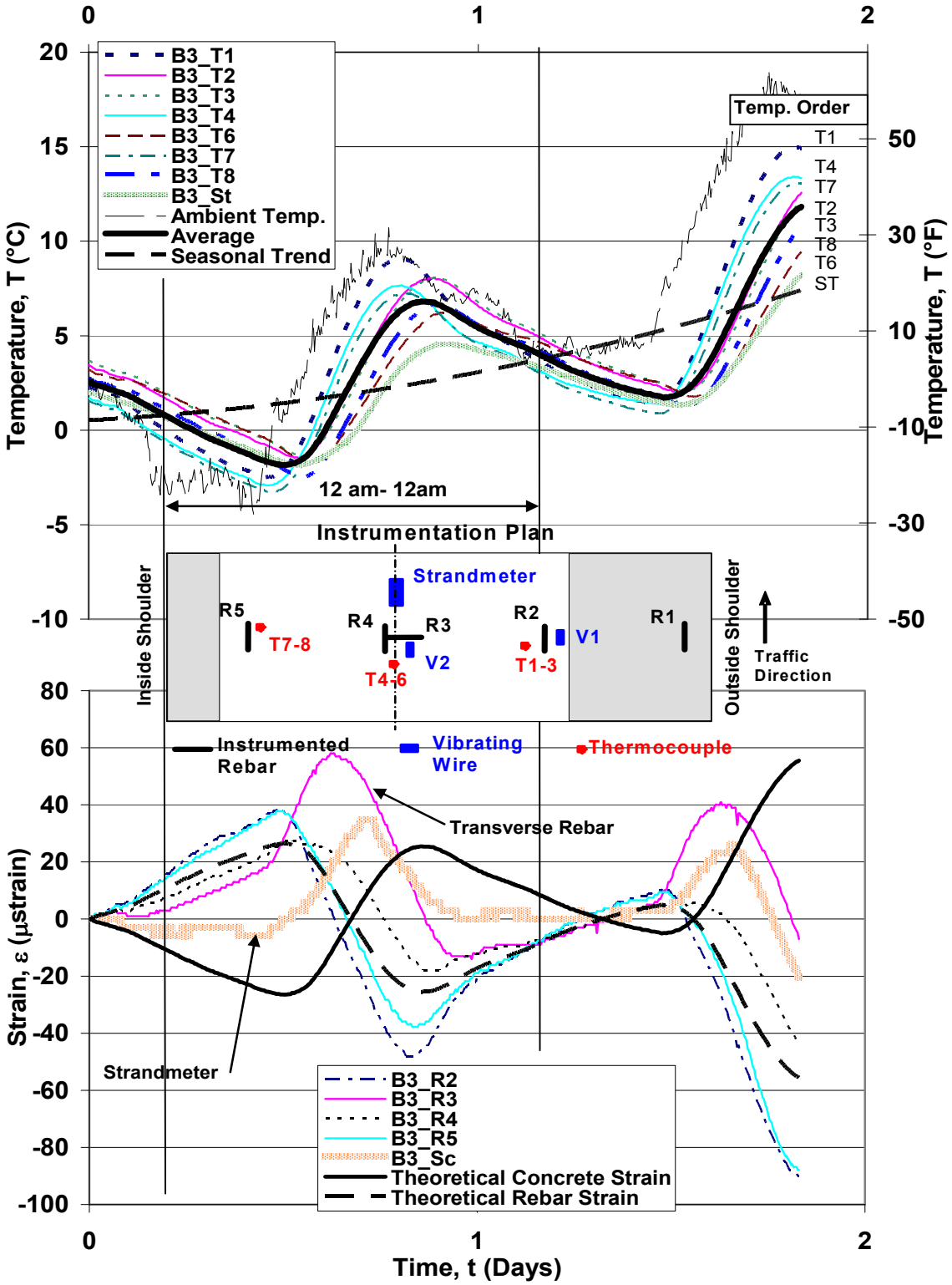

Figure 9.3 - Thermal response of B3 over two days in February (2/12-2/14/06)

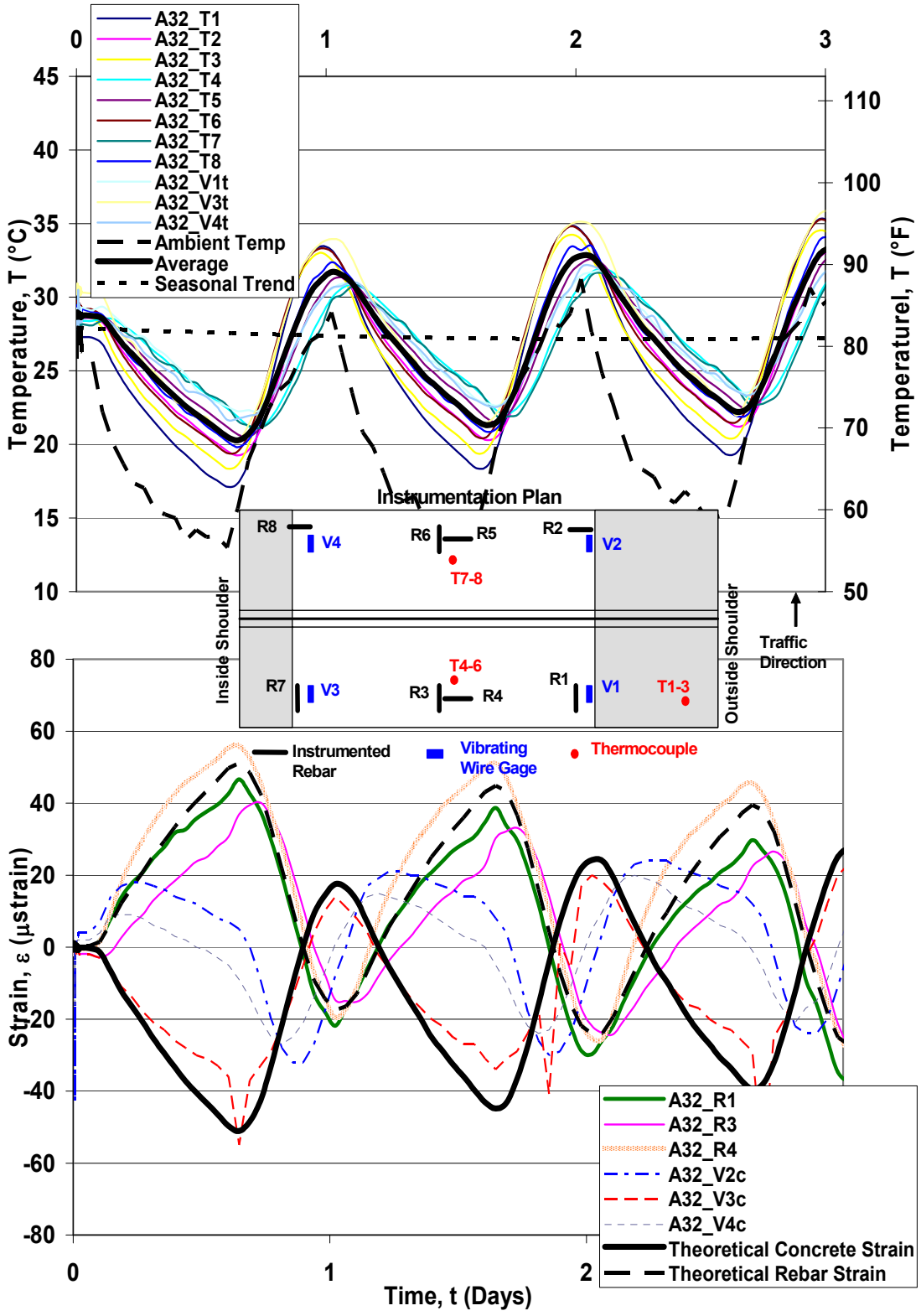

Figure 9.4 - Thermal response of A32 over three days in September (9/5-9/8/06)

Figure 9.5 shows measured rebar and strandmeter strain for Panel B2 over the first week in October, 2006. The strandmeters again follow rebar strain curves. This is expected because the device is measuring the strain in the steel strand.

The strand is totally de-bonded at the strandmeter but bonded to grout at the ends. As the panel cools, for example, the steel strand will want to shrink faster than the grout at the ends will allow. Therefore, it goes into tension just like the embedded rebar (Figure 9.5). All strandmeters have proved to be successful long-term devices with very little interference or noise. Rebar 5 shows higher strains early because it is closer to the top of the panel and in a thinner section than Rebar 3 (refer to as-builts).

Figure 9.6 presents a two week sample of rebar and vibrating wire data for Panel B5 during July, 2006. These two weeks were very hot. Temperatures approached 38°C (100°F). The highest in-service strains are reported during these hot days (125-200 μstr). Other samples (during cooler days) show strain excursions between 80-100 μstr. Excessive volumetric expansion can be detrimental. A 200 μstr expansion over a 250 ft (76 m) section would produce a 0.6 in (1.5 cm) elongation. It is unlikely the design gap (> 1 in or 2.5 cm) in each joint panel closed. Residual torsion and bending at the joints due to improper section alignment may have caused the smooth dowels to bind, preventing free expansion and contraction. This would produce added compression on the section. Therefore, longitudinal Rebar 2, 4 and 5 show much higher compressive strains than theoretical (in the heat of the day). Rebar 3 is transverse and is again unrestrained compared to the longitudinal bars. It matches the theoretical curve very closely. Vibrating wire gages again follow the theoretical concrete curve.

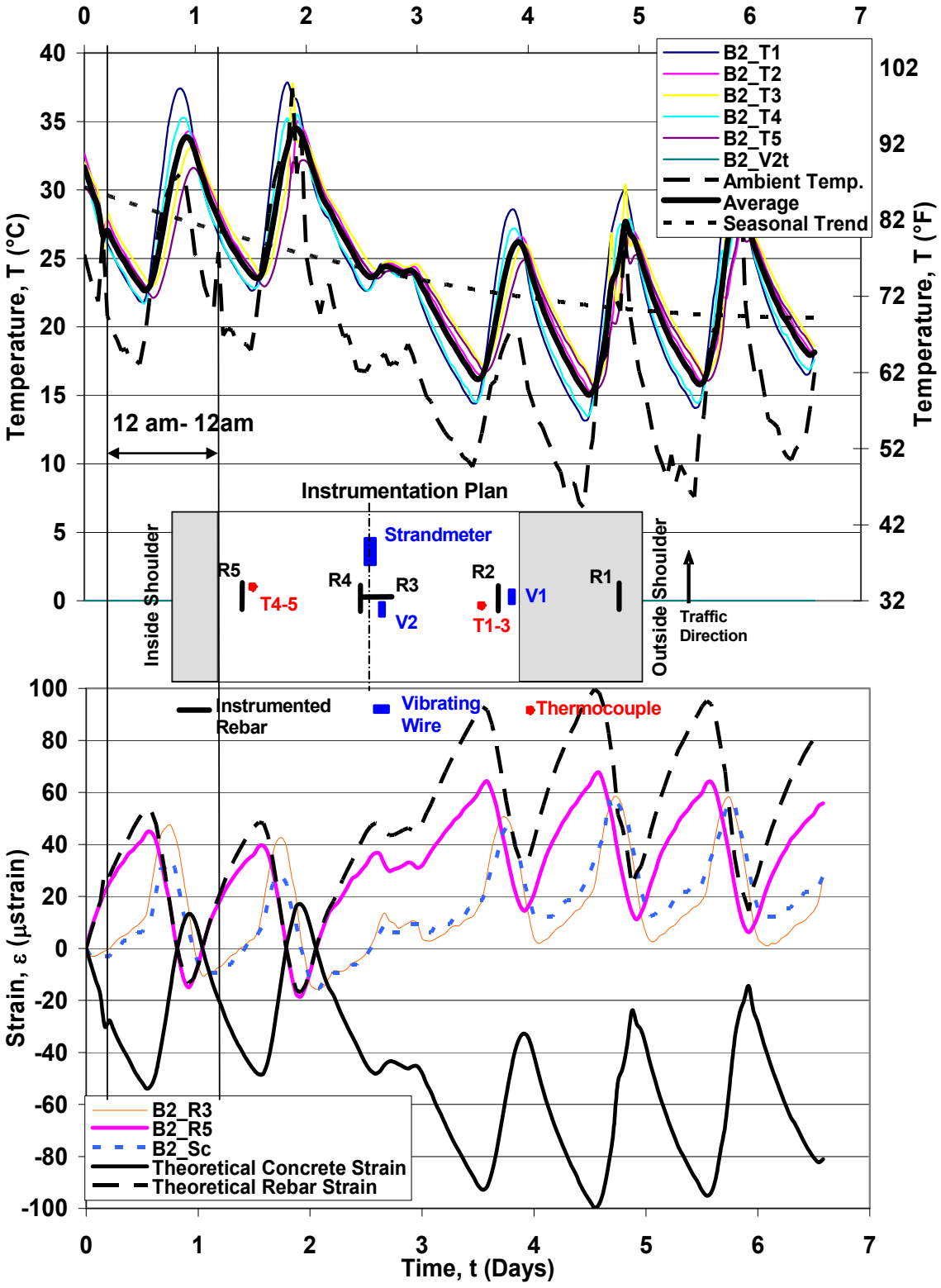

Figure 9.5 - Thermal response of B2 over seven days in October (10/2-10/9/06)

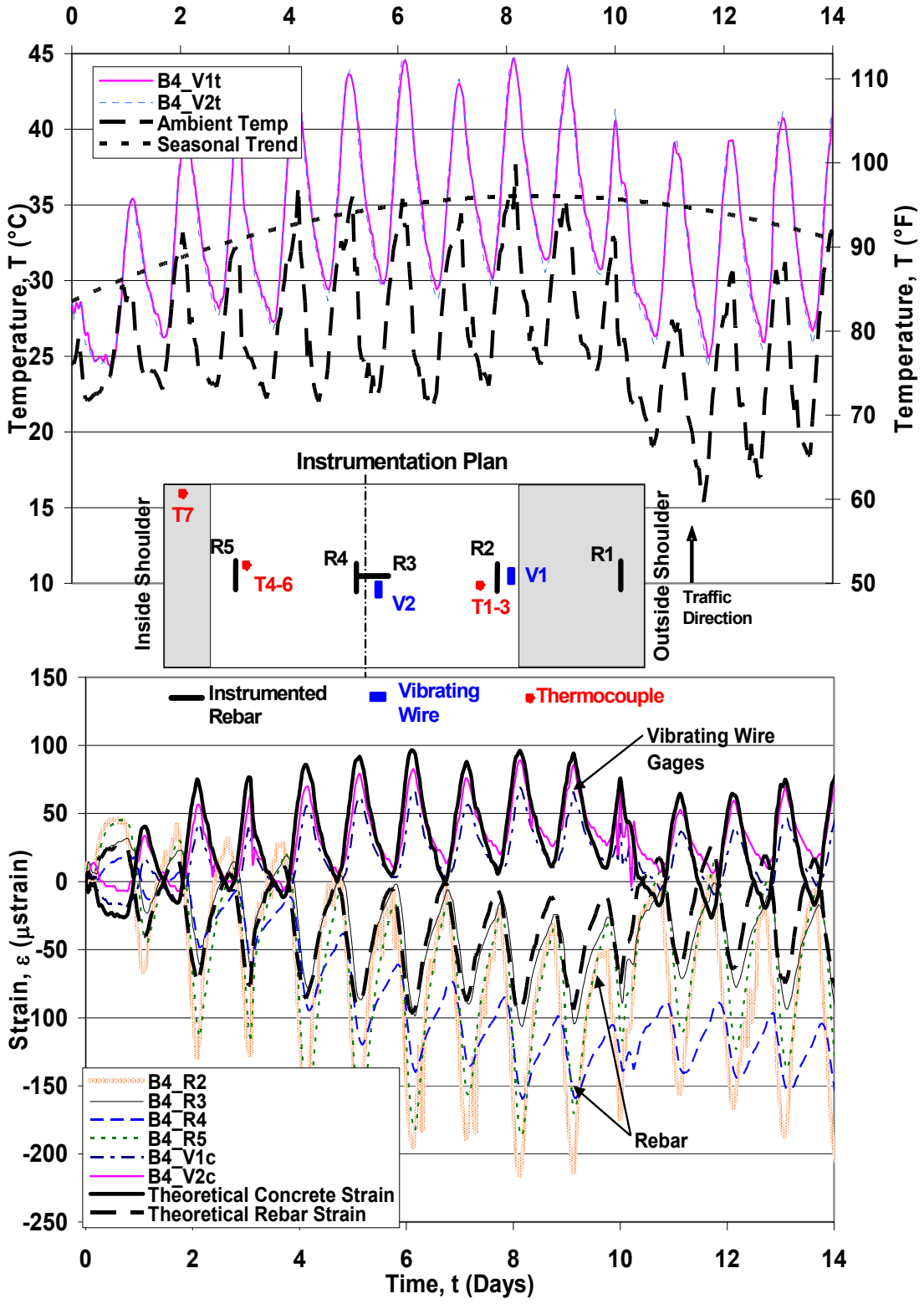

Figure 9.6 - Thermal response of B4 over fourteen days in July (7/11-7/25/06)

9.2.4. DAILY TRAFFIC VARIATION

Traffic data was taken in short selective increments. A small number of successful rebar were selected and the data acquisition program was changed to a maximum sample rate. The first two graphs presented (Figure 9.7and Figure 9.8) are results from remote data acquisition.

Figure 9.9 and Figure 9.10 were obtained by attaching rebar leads directly to the datalogger and physically counting trucks during maximum data acquisition (Luckenbill 2008-Anticipated)

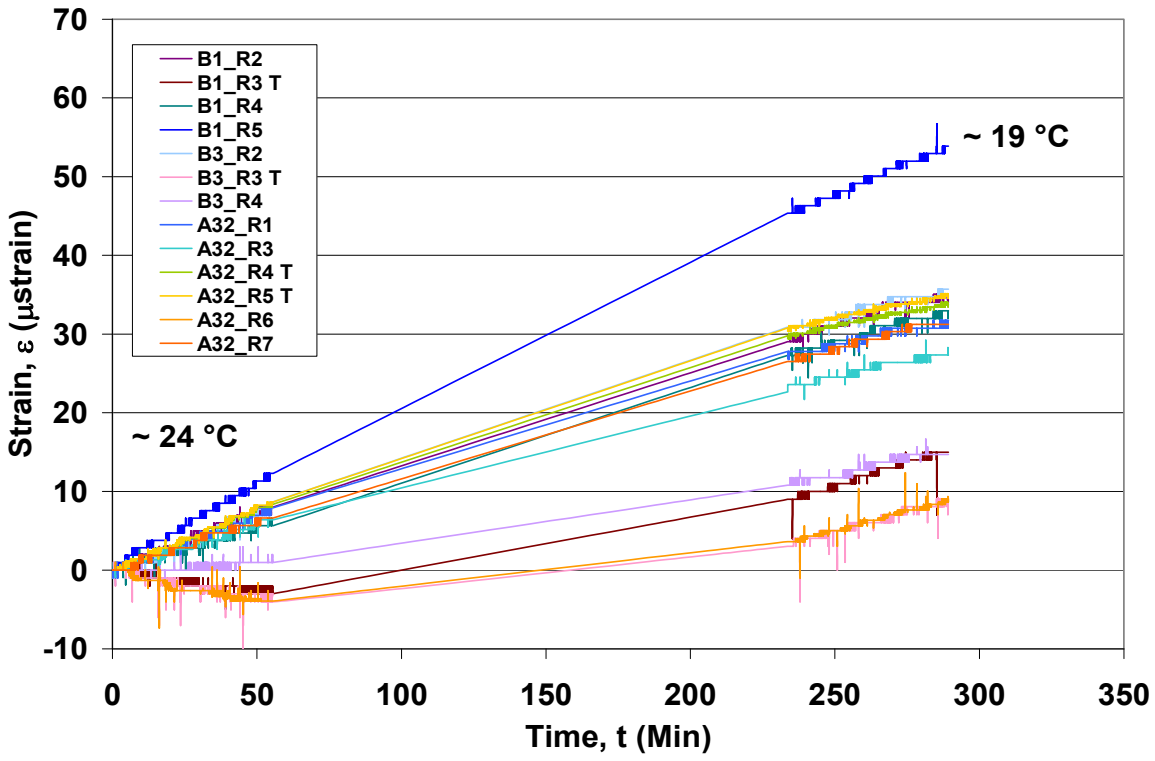

Figure 9.7 - Traffic strains in conjunction with slight thermal change

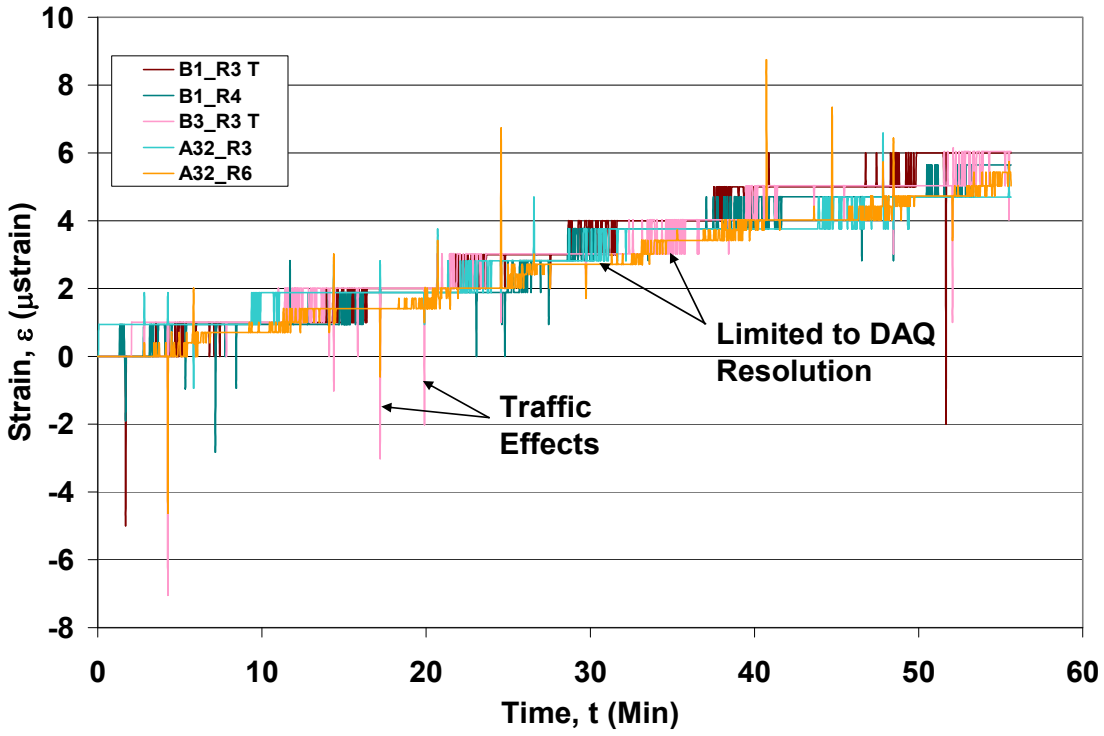

Figure 9.8 - Traffic strains shown at higher magnitudes than noise

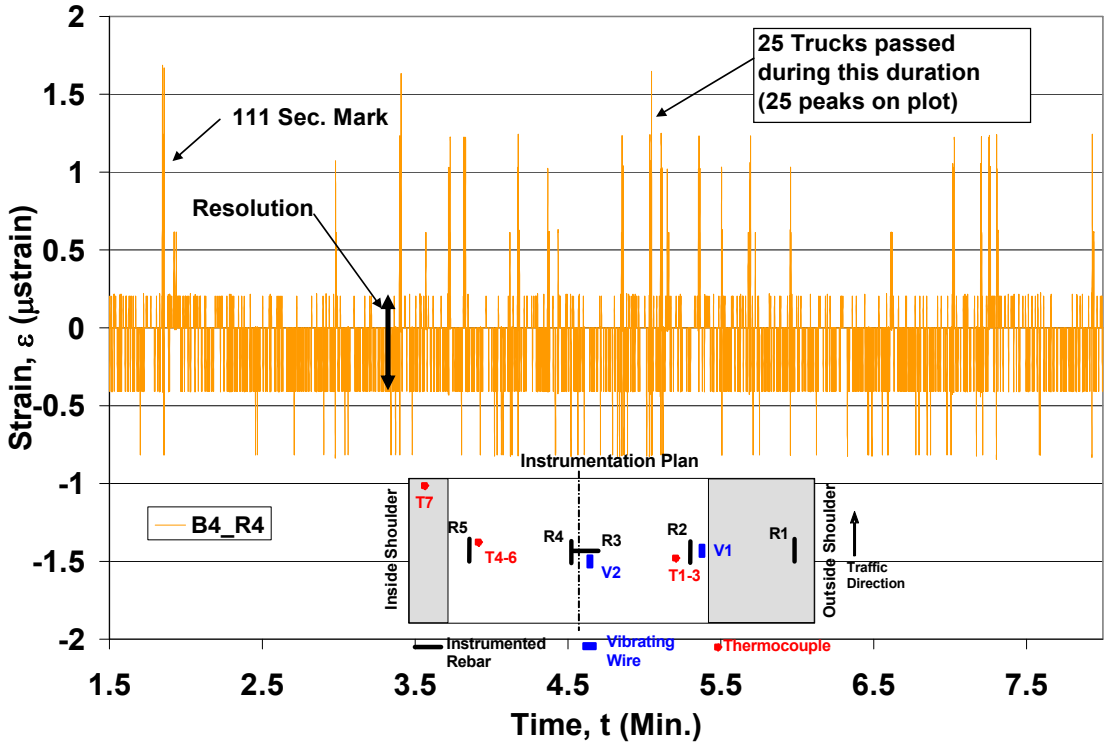

Figure 9.9 - Traffic data with manual count of passing trucks

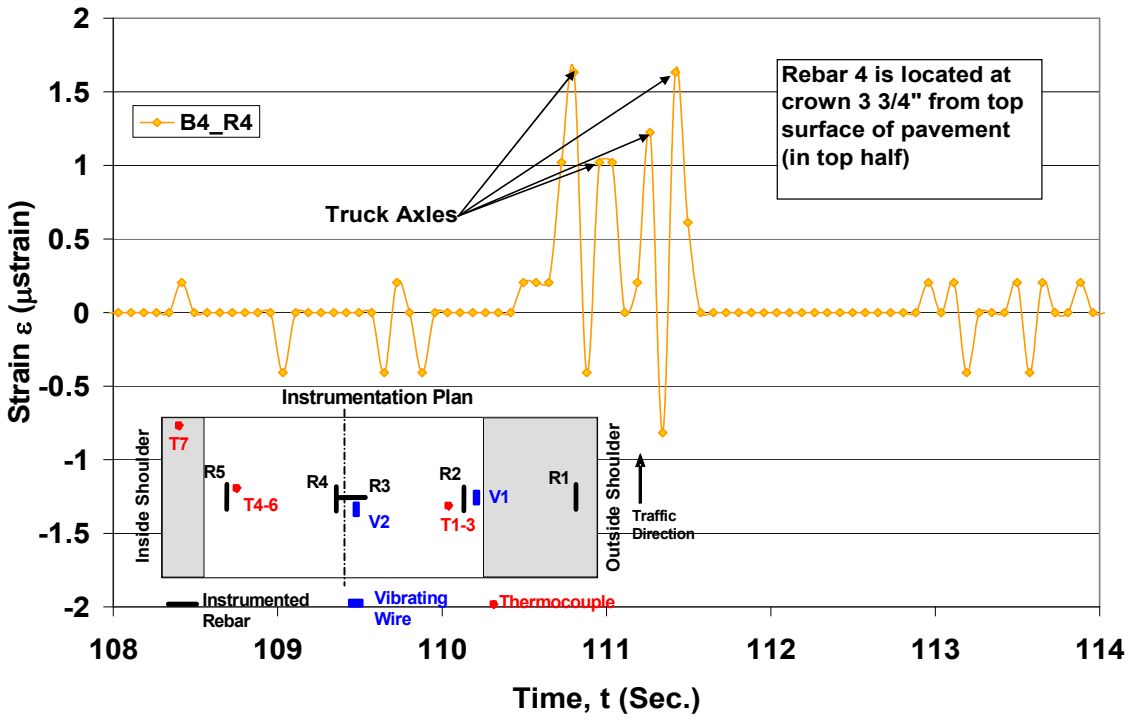

Figure 9.10 - Close-up of strain induced at R4 by a single truck load

As stated earlier, traffic strains are presented only to understand the effects of traffic on measured output. It is very clear that strains induced by traffic are miniscule compared to thermal strains. Figure 9.7 and Figure 9.8 show the effects of traffic in conjunction with thermal strain change. The stair steps shown are the oscillating resolution noise from the data acquisition system. The spikes in data are truck traffic. Figure 9.7 and Figure 9.8 show the strain increasing due to increasing temperature. Traffic data is superimposed on this daily trend.

Figure 9.9 and Figure 9.10 prove that the spikes are indeed truck traffic. The numbers of spikes match the number of counted trucks. Figure 9.10 shows a window of data where a truck is driving over a rebar. Several axle loads are visible. The maximum strain is about 1.5 μstr in compression. Rebar 4 is in the top of the slab therefore this would imply that positive moment bending occurred. There is some tensile response

between axles, however. Strain magnitudes from truck traffic are 1-2 % of the total strain induced by thermal loads.

9.3. LONG-TERM MEASUREMENTS

The following sections discuss long-term performance evaluations including: stress losses due to creep, global movement, and visual degradations. Most of the long term evaluation will be provided in the third thesis by Grant Luckenbill. Grant will tie both previous works together (this and Brent Davis's) with conclusions on long-term performance, overall feasibility, and economical considerations.

9.3.1. LONG-TERM STRAIN MEASUREMENT

Vibrating wire devices have been performing well. Because they are frequency based devices, long-term strain measurements are obtainable. The 'zero' or original datum for long-term strain measurements is at post-tensioning transfer. The companion thesis by Brent Davis discusses the evidence (to date) of creep loss in the post-tensioning tendons. Strandmeter data shows losses very close to theoretical predictions (Davis 2006).

9.3.2. LONG-TERM GLOBAL MOVEMENT

It is important to monitor internal stresses and strains during in-service conditions, but global movement is also a vital performance based criteria. To measure global movement, drop-in anchors were installed in each corner of the two instrumented joint panels (Panels A31, and A32). A tiny pilot hole was drilled on the head of each anchor to accommodate survey equipment. Figure 9.11 shows a survey being conducted.

The data points were compiled and converted into northing and easting coordinates by a MoDOT surveyor. The research team then compared the readings to the original zero datum and subtracted to calculate the total amount of change. Each change from a subsequent survey trip was done in the same manner in order to determine total movement from datum. Figure 9.12 shows a graphical representation (scaled by a factor of 10) of the accumulated movement at the corners of each section. The survey equipment is accurate only to a tenth of an inch. The maximum measured change from datum is 0.3". Therefore, global movement to date has not been large enough to be accurately measured with modern survey equipment.

Figure 9.11 - Surveying joint panel corners for movement with total station

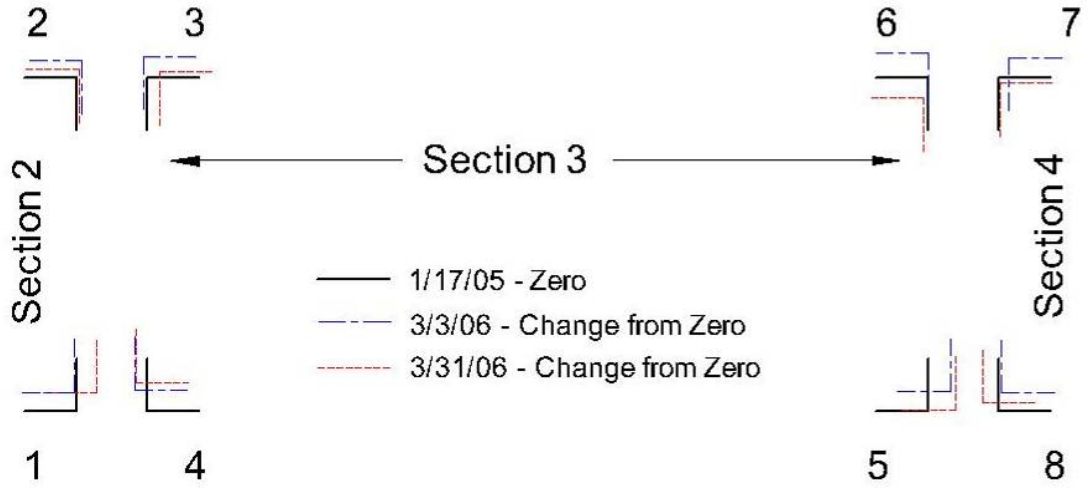

3/3/06 - Change from Zero				3/31/06 - Change from Zero			
Bolt No	North Change (y)	East Change (x)	Elevation	Bolt No	North Change (y)	East Change (x)	Elevation
1	0.2148	0.2197	0	1	0.2191	-0.0252	-0.12
2	0.0882	0.0228	0.12	2	0.1840	0.0612	0.12
3	0.0601	0.1458	0.12	3	0.2332	-0.0419	-0.12
4	0.3298	-0.1198	0	4	0.2496	-0.1384	0
5	0.0191	0.2897	0	5	0.2282	0.2449	0
6	-0.2356	-0.0578	-0.12	6	0.2785	-0.0004	0
7	-0.0672	0.0115	-0.24	7	0.2226	0.1153	0
8	0.1015	-0.1858	-0.24	8	0.2152	0.0335	-0.12

Figure 9.12 - Graphical representation of global movement (in) at section corners

9.3.3. VISUAL SURVEYS

Cracking and visual degradation surveys have recently been performed. Both longitudinal and transverse cracks have developed in the precast panels. Figure 9.13 and Figure 9.14 show the longitudinal crack that develops at a strandmeter block-out. This is most likely because the corners were cast too sharp allowing stresses to concentrate until a crack formed. Figure 9.13 shows a deteriorated joint panel with a transverse crack that runs from shoulder to shoulder. This panel split near the center during stressing operations. A patch mix was used to repair the loose concrete. It appears to be deteriorating. Additional surveys will monitor the propagation of new cracks.

Figure 9.13 - Longitudinal crack (left) deteriorating expansion joint (right)

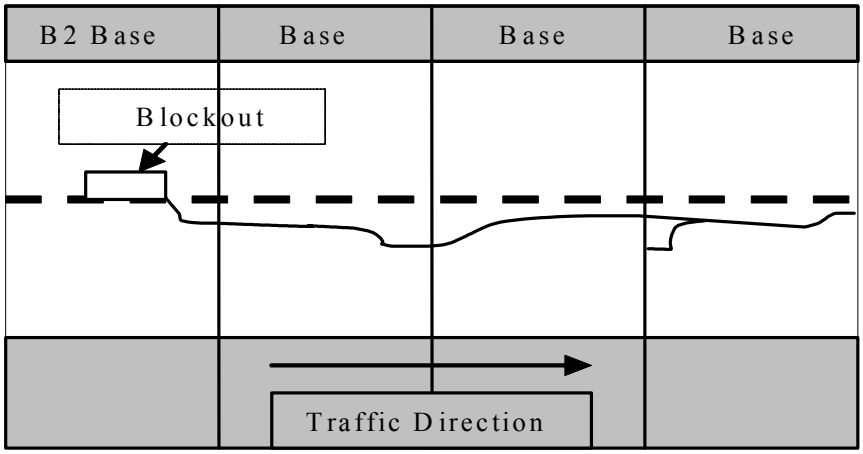

Figure 9.14 - Graphical plan of longitudinal crack (Luckenbill 2008-Anticipated)

10. CONCLUSIONS

10.1. SUMMARY OF THE RESULTS FROM THE INSTRUMENTATION

The instrumentation and monitoring of the precast prestressed pavement system on I-57 in southern Missouri was carried out successfully. Thirty-nine strain gaged bars, fourteen vibrating wire gages, four strandmeters, and thirty-eight thermocouples were installed in seven precast panels. Intense planning and coordination was required to ensure that the data acquisition system and implementation thereof was streamlined into the construction process as to not miss any critical moments in the various stages of development.

The following sections outline the conclusions from the experimental data. Each section outlines conclusive results observed at the critical stages in the life of the precast prestressed pavement system. They are presented in bulleted format for brevity.

10.1.1. HYDRATION AND EARLY AGE PERFORMANCE

- Curing strains were the highest measured strains at any stage. They ranged from 200-400 μstr.
- Actual measured rebar strains were about 200-300 μstr higher than theoretical. This is most likely due to added compression on the rebar from shrinkage.
- Measured temperatures were roughly 15-20°C (27-36°F) higher than the external ambient steam curing environment temperature. This can be attributed to the added heat from hydration.

- Successful vibrating wire gages responded early during curing because they are well suited for measuring strains in plastic concrete. Rebar require a higher force to induce equal strains. Subsequent bond strength must be developed on the rebar as well. Early strains are lost with rebar measurements.
- Successful vibrating wire gages do not show any signs of compression. This may prove that the magnitude of the strains from thermal expansion is greater than shrinkage strains.

10.1.2. PRETENSIONING TRANSFER

- Measured stress transfer strains were between 40-60 μstr.
- Both transverse and longitudinal measured strains were very close to theoretical predictions.
- Some out of plane eccentricities may be present due to inconsistencies in draping. Chairs were manually installed under the strands and their location relative to the ends of the panels dictates the height of the strand and thus the eccentricities developed.

10.1.3. POST-TENSIONING

- Post-tensioning strains ranged from 40-80 μstr.
- Inconsistencies in mating surfaces, friction of the panel and sub-grade, and the installation of shims for alignment make trends in measured rebar strain difficult to extract.

- The strain distribution along the length of the post-tensioned section is different for the post-tensioning strand and the rebar embedded in the concrete. In the post tensioning strand, higher strains are measured closer to the active jacking end. The rebar show an opposite trend. Strains in the concrete are higher at the passive end and gradually decrease toward the active jacking end. This is because the active end is fully anchored to a previously post-tensioned section. Panels then move toward the anchored end. The force is applied on each panel from the passive end toward the active end.
- There is a 3.5-6.5% initial relaxation in pretensioning force. This is less than the recommended 10% used for design (PCI 1999).
- There is a 10 μstr/ft or 62 lbs/ft loss in stressing force due to friction of the ductwork on the post-tensioning strand.

10.1.4. IN-SERVICE

- Cool or mild days show daily strains ranging from 50-100 μstr
- Hot summer days appear to produce the highest in-service strains ranging from 125-200 μstr. This is most likely due to extensive thermal expansion such that the expansion joints function improperly, transferring additional compressive stress into each section.
- Truck traffic produced 1.5 μstr in the panel. This is only 1-2% of the total strain produced from thermal loading
- The strain envelope for the panel system consists of three measurable strain trends.

- The first is very small traffic strains. These are superimposed onto daily and seasonal changes. They are hardly visible.
- The second is the day to night thermal changes. This can be described as an oscillating function with a 24 hr. frequency. The panel heats during the day and cools during the night. Strains are induced according to changes in local ambient temperature.
- The final trend is seasonal. This curve is comprised of the slow shift in average daily ambient temperatures.

10.2. RECOMMENDATIONS FOR FURTHER WORK

It is recommended that the difficulty with the vibrating wire strain gages be investigated. Both settling time with the data acquisition system and thermal corrections need to be examined. Additional testing in a laboratory environment may lead to more confidence in their performance on future projects.

It is suggested that a full economic study be performed. This may bring practical issues to the forefront of discussion. It would also provide practical information to designers who would then be able to examine and compare potential user costs. This would facilitate further installments of precast prestressed concrete pavement.

Long term performance with additional seasonal trends and summaries should be compiled. Laboratory studies and results should be examined in conjunction with data presented in this thesis as well as additional seasonal trends. The main focus should be on post-tensioning losses due to creep, measured and theoretical. Seasonal vibrating wire data should be gathered as well.

Additional surveys should be recorded that note degradation and cracking. Visual problems with joint and base panels should be discussed in order to provide a comprehensive performance evaluation.

These recommendations as well as other value added items will be included in a future thesis by Grant Luckenbill. His thesis will help summarize the overall performance of the system and related materials.

REFERENCES

AASHTO (1993). Design of Pavement Structures. Washington, DC.

ACPA (2004). Concrete Types, American Concrete Pavement Association. **2004**.

ASTM (2002). Standard Test Method for Flexural Strength of Concrete (Using Simple Beam with Third-Point Loading, ASTM**:** 3.

ASTM (2002). Standard Test Method for Fundamental Transverse, Longitudinal, and Torsional Resonant Frequencies of Concrete Specimens, ASTM**:** 7.

ASTM (2003). Standard Test Method for Resistance of Concrete to Rapid Freezing and Thawing, ASTM**:** 6.

ASTM (2005). Standard Test Method for Compressive Strength of Cylindrical Concrete Specimens, ASTM**:** 7.

ASTM (2005). Standard Test Method for Electrical Indication of Concrete's Ability to Resist Chloride Ion Penetration, ASTM**:** 6.

Authority, N. N. P. (1997). The Civil Engineering Research Foundation.

Boresi, A. P. and R. J. Schmidt (2003). Advanced Mechanics of Materials, John Wiley and Sons, Inc.

Brunner, R. J. (1975). Prestressed Pavement Demonstration Project, Transportation Research Board**:** 62-72.

Cable, N. D., F. B. McCullough, et al. (1986). New Concepts in Prestressed Concrete Pavement, Transportation Research Board**:** 1-11.

Chavez, C. I. M., F. B. McCullough, et al. (2003). Design of Post-Tensioned Prestressed Concrete Pavement, Construction Guidelines, and Monitoring Plan. Austin, TX, Center for Transportation Research - University of Texas at Austin.

Chen, Y. S., S. D. Murrell, et al. (2003). Precast Concrete Pavement Tests on Taxiway D-D at Laguardia Airport. Airfield Pavements Challenges and New Technologies, Las Vegas, Nevada.

Company, T. F. M. (2001). Super-Slab.

Davis, B. M. (2004). A Review of Rigid Pavement Design Including Recent Developments, University of Missouri -- Columbia; Dept. of Civil and Environ. Engineering.

Davis, B. M. (2006). Evaluation of Prestress Losses in an Innovative Prestressed Precast Pavement System. Civil and Environmental Engineering. Columbia, University of Columbia - Missouri.

Degussa (2006). Degussa Admixtures. **2006**.

Earney, T. P. (2007-Anticipated). Creep and Shrinkage Studies of High Performance Concrete. Civil and Environmental Engineering. Columbia, University of Columbia - Missouri; Doctoral Dissertation.

Earney, T. P., V. S. Gopalaratnam, et al. (2006). Early-Age Autogenous Shrinkage Measurements of High-Performance Concrete. The 6th International Symposium on Cement and Concrete, CANMET/ACI International Symposium on Concrete Technology for Sustainable Development, Xi'an, China.

Eatherton, M. (1999). Instrumentation and Monitoring of High Performance Concrete Prestressed Girders. Civil Engineering. Columbia, University of Missouri**:** 223.

Emborg, M. and S. Bernander (1994). "Assessment of Risk of Thermal Cracking in Hardening Concrete." Journal of Structural Engineering **120**(10): 2893-2912.

Farrington, R., W. C. Rovesti, et al. (2003). Overnight Concrete Pavement Replacement Using a Precast Panel and Expanding Polymer Positioning Technique - Washington Dulles International Airport Case Study. Airfield Pavements Specialty Conference, Las Vegas, NV.

FHWA (2003). "Long-Life Concrete Pavements Deliver Quality and Durability." Focus - U.S. Department of Transportation Federal Highway Administration.

Geokon (1996). Instruction Manual Model VCE - 4200, Geokon, Inc.

Gopalaratnam, D. V. S. (2004). MoDOT Research Proposal. MoDOT. Missouri.

Gopalaratnam, V. S., J. P. Donahue, et al. (2006). Precast Prestressed Panels for Rapid Full-Depth Pavement Repairs. ASCE Structures Congress, St. Louis, MO, American Society of Civil Engineers.

Kada H., M. L., N. Petrov, O. Bonneau, P.C. Aitcin (2002). "Determination of the Coefficient of Thermal Expansion of High Performance Concrete from Initial Setting." Materials and Structures **35**(1): 35-41.

Lane, B. and T. Kazmierowski (2006). "Precast Concrete Slab Repair Methods - Innovative Pavement Repair Trials in Canada." Concrete International **Vol. 28**(No. 11): 29-35.

Luckenbill, G. (2008-Anticipated). Pending Masters Thesis. Civil and Environmental Engineering. Columbia, MO, University of Missouri - Columbia.

Merritt, D., F. B. McCullough, et al. (2000). The Feasibility of Using Precast Concrete Panels to Expedite Highway Pavement Construction. Austin, TX.

Merritt, D. K. (2002). Development of a Precast Prestressed Concrete Pavement Near Georgetown, Texas. 2002 Transportation Research Board Annual Meeting.

Merritt, D. K., B. F. McCullough, et al. (2002). Construction and Preliminary Monitoring of the Georgetown, Texas Precast Prestressed Pavement, Center for Transportation Research; University of Texas at Austin**:** 140.

Merritt, D. K., F. B. McCullough, et al. (2001). Feasibility of Precast Prestressed Concrete Pavements. 7th International Conference on Concrete Pavements.

Merritt, D., F. B. McCullough, et al. (2000). The Feasibility of Using Precast Concrete Panels to Expedite Highway Pavement Construction. Austin, TX.

Mn/DOT (2005). Installation of Precast Concrete Pavement Panels on TH 62, Minnesota Department of Transportation.

Muench (2004). Pavement Facts. Asphalt Pavement Guide.

Naaman, A. E. (2004). Prestressed Concrete Analysis and Design - Fundamentals, Techno Press.

Nawy, E. G. (2003). Reinforced Concrete A Fundamental Approach. Upper Saddle River, New Jersey, Prentice Hall.

PCI (1999). PCI Design Handbook--Precast and Prestressed Concrete 5th Edition. Chicago, IL, Precast Prestressed Concrete Institute.

Powers, R. L. and J. P. Zaniewski (1987). Nine Year Performance Evaluation of Arizona's Prestressed Concrete Pavement, Transportation Research Board**:** 1-11.

Proctor, C. (2000). "Paving an Easier Way for Highways." Denver Business Journal.

Rice, J. L. (1981). Engineering Brief #24. Federal Aviation Administration.

Shackelford, J. F. and W. Alexander (2001). CRC Materials Science and Engineering Handbook. Boca Raton, FL, CRC Press LLC.

Stover, M. (2004). Prestressed Concrete Pavements - A Literature Review, University of Missouri -- Columbia; Dept. of Civil and Environ. Engineering.

Switzer, W. J., A. Fischer, et al. (2003). Overnight Pavement Replacement Using Precast Panels and Conventional Subgrade Material - Washington Dulles International Airport Case Study. Airfield Pavements Specialty Conference, Las Vegas, NV.

Tyson, S. S. and D. K. Merritt (2005). Pushing the Boundaries. Public Roads. **68**.

APPENDICES

A. DESIGN DOCUMENTS

The following pages contain design information from the precast prestressed panel system used on I-57 near Sikeston, MO. They were produced by The Transtec Group, Austin, TX. Their design work is presented only to provide further clarifications concerning the design and layout of the panel system.

PRECAST PAVEMENT PANEL LAYOUT
AND
TIE-IN DETAILS

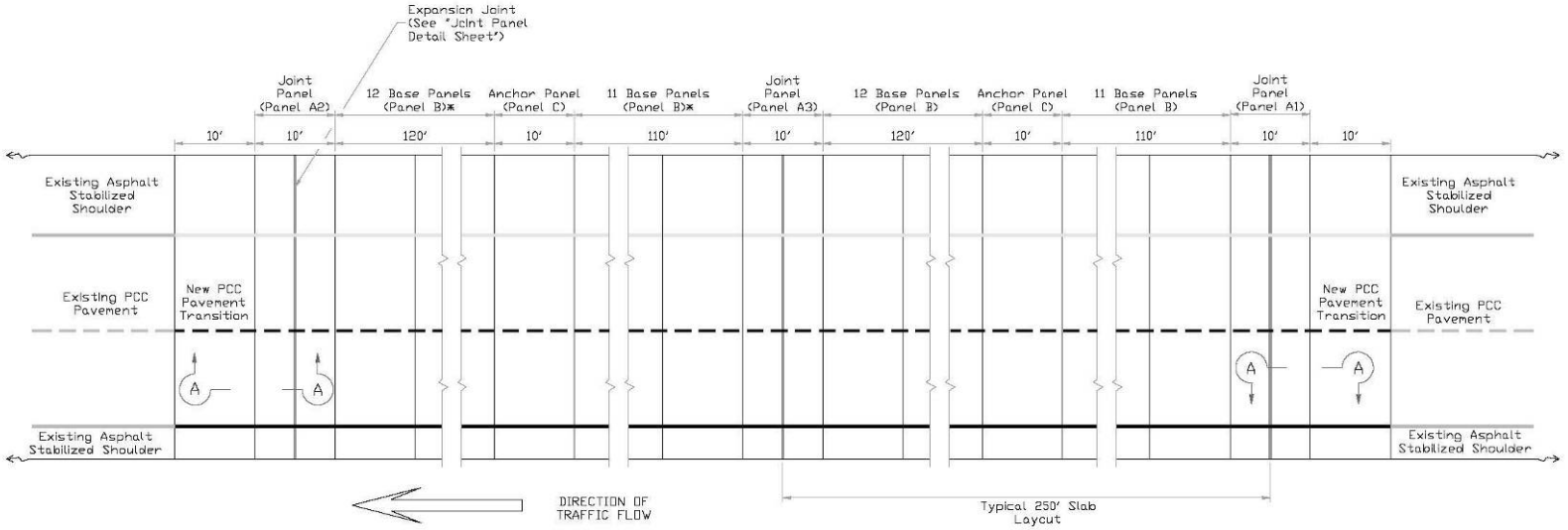

*Number of Base Panels may be reduced to stay within project limits. Base Panels should be evenly distributed on either side of the Anchor Panel (Type C). Total slab length (between expansion joints) should not be less than 100 ft.

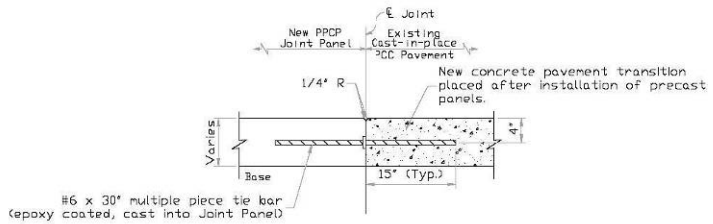

SECTION A-A: DETAIL FOR TIE-IN TO EXSITING PCC PAVEMENT

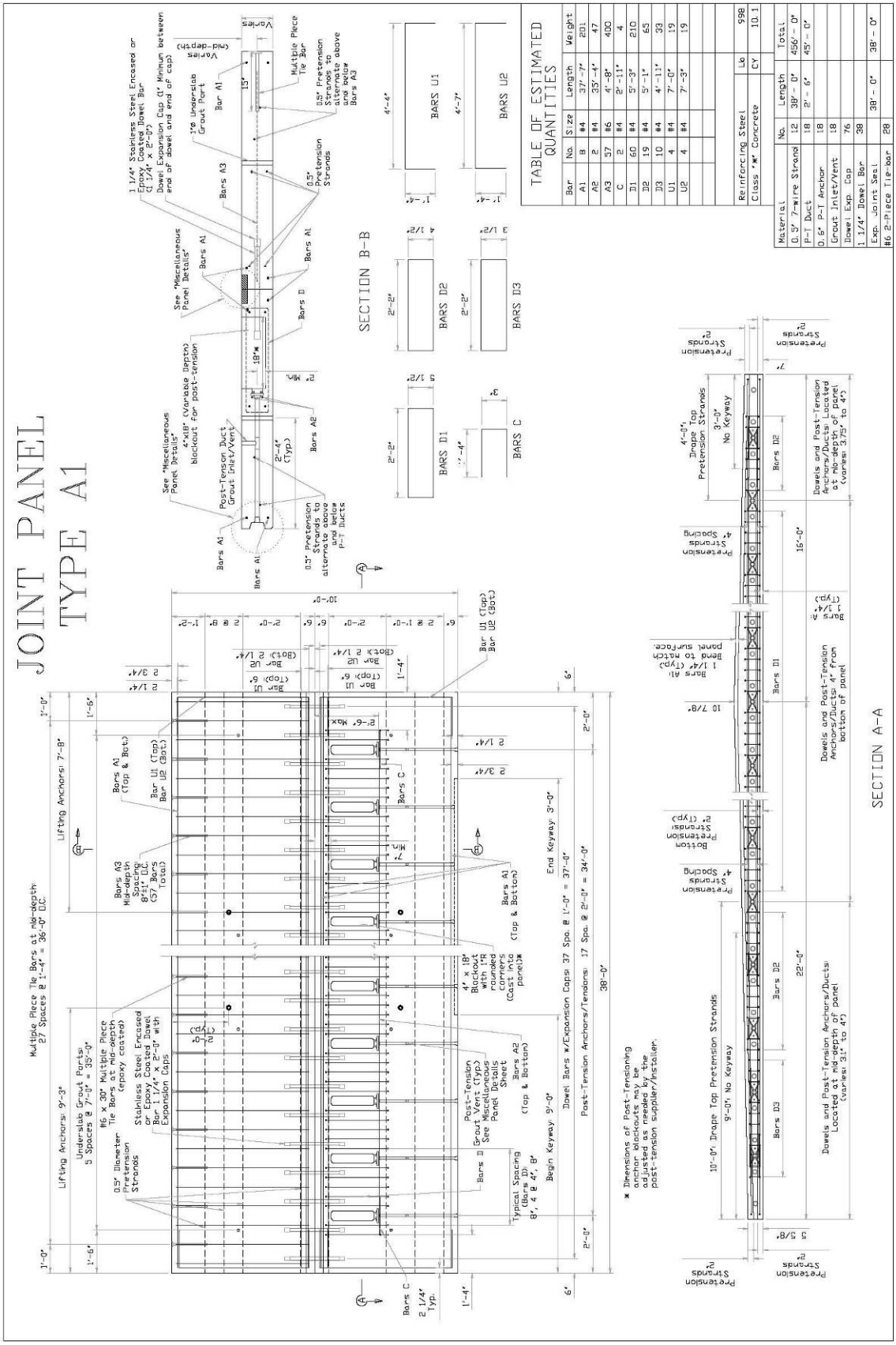
JOINT PANEL
TYPE A1
SECTION A-A
SECTION B-B
TABLE OF ESTIMATED QUANTITIES
Bar | No. | Size | Length | Weight
A1 | 8 | #4 | 37'-7" | 201
A2 | 2 | #4 | 35'-4" | 47
A3 | 57 | #6 | 4'-8" | 400
C | 2 | #4 | 2'-11" | 4
D1 | 60 | #4 | 5'-3" | 210
D2 | 19 | #4 | 5'-1" | 65
D3 | 10 | #4 | 4'-11" | 33
U1 | 4 | #4 | 7'-0" | 19
U2 | 4 | #4 | 7'-3" | 19
Reinforcing Steel | Lb | 998
Class "A" Concrete | CY | 10.1
Material | No. | Length | Total
0.5" 7-Wire Strand | 12 | 38'-0" | 456'-0"
P-T Duct | 18 | 21'-6" | 45'-0"
0.6" P-T Anchor | 18
Grout Inlet/Vent | 18
Dowel Exp. Cap | 76
1 1/4" Dowel Bar | 38
Exp. Joint Seal | 38'-0" | 38'-0"
#6 2-Piece Tie-bar | 28
Lifting Anchors: 9'-3"
Underslab Grout Ports: 5 Spaces @ 7'-0" = 35'-0"
#6 x 30" Multiple Piece Tie Bars at mid-depth (epoxy coated)
0.5" Diameter Pretension Strands
Stainless Steel Encased or Epoxy Coated Dowel Bar 1 1/4" x 2'-0" with Expansion Caps
Bars A3 Mid-depth Spacing 8"±1" D.C. (57 Bars Total)
Bars A1 (Top & Bot.)
Bar U1 (Top) Bar U2 (Bot.)
Bars C
Bars A1 (Top & Bottom)
Bars A2 (Top & Bottom)
Bars D3
Bars D2
Bars D1
Bars U1
Bar U1 (Top) Bar U2 (Bot.)
Bar U1 (Top) 6"
Bar U2 (Bot.) 2 1/4"
Lifting Anchors: 7'-8"
Multiple Piece Tie Bars at mid-depth 27 Spaces @ 1'-4" = 36'-0" D.C.
Begin Keyway 9'-0"
End Keyway 3'-0"
Dowel Bars w/Expansion Caps: 37 Spa. @ 1'-0" = 37'-0"
Post-Tension Anchors/Tendons: 17 Spa. @ 2'-0" = 34'-0"
38'-0"
Typical Spacing (Dia. D) 8", 6", 4", 8"
Post-Tension Grout Vent (Typ.) See Miscellaneous Panel Details Sheet
4" x 18" Blockout with 1"R rounded corners (Cast into panel)
2'-6" Max.
10'-0" Draped Top Pretension Strands
Dowels and Post-Tension Anchors/Ducts Located at mid-depth of panel (varies 31" to 41")
Dowels and Post-Tension Anchors/Ducts Located at mid-depth of panel (varies 31" to 41")
Pretension Strands 2" Bottom
Pretension Strands 4" Spacing
Pretension Strands 2" Top
4'-0" Drape Top Pretension Strands
3'-0" No Keyway
9'-0" No Keyway
15'-0"
22'-0"
Dowels and Post-Tension Anchors/Ducts Located at mid-depth of panel (varies 31.5" to 41")
Bars A1 1 1/4" (Typ.) Bend to match panel surface
10 7/8"
5 3/8"
Bars A1
Bars A3
Bars D
Bars D1
Bars D2
Bars D3
Bars U1
Bars U2
Bars C
Bars A2
0.5" Pretension Strands
0.5" Pretension Strands to alternate above and below P-T Ducts
Post-Tension Duct Grout Inlet/Vent
2'-4" (Typ.)
See "Miscellaneous Panel Details"
4"x18" (Variable Depth) blockout for post-tension
1 1/4" Stainless Steel Encased or Epoxy Coated Dowel Bar (1 1/4" x 2'-0") Dowel Expansion Cap (1" Minimum between end of dowel and end of cap)
1"ø Ungrouted Grout Port
Multiple Piece Tie Bar
Varies (Mid-depth)
Varies
BARS U1
BARS U2
BARS D1
BARS D2
BARS D3
BARS C
* Dimensions of Post-Tensioning anchor blockouts may be adjusted as needed by the post-tension supplier/installer.

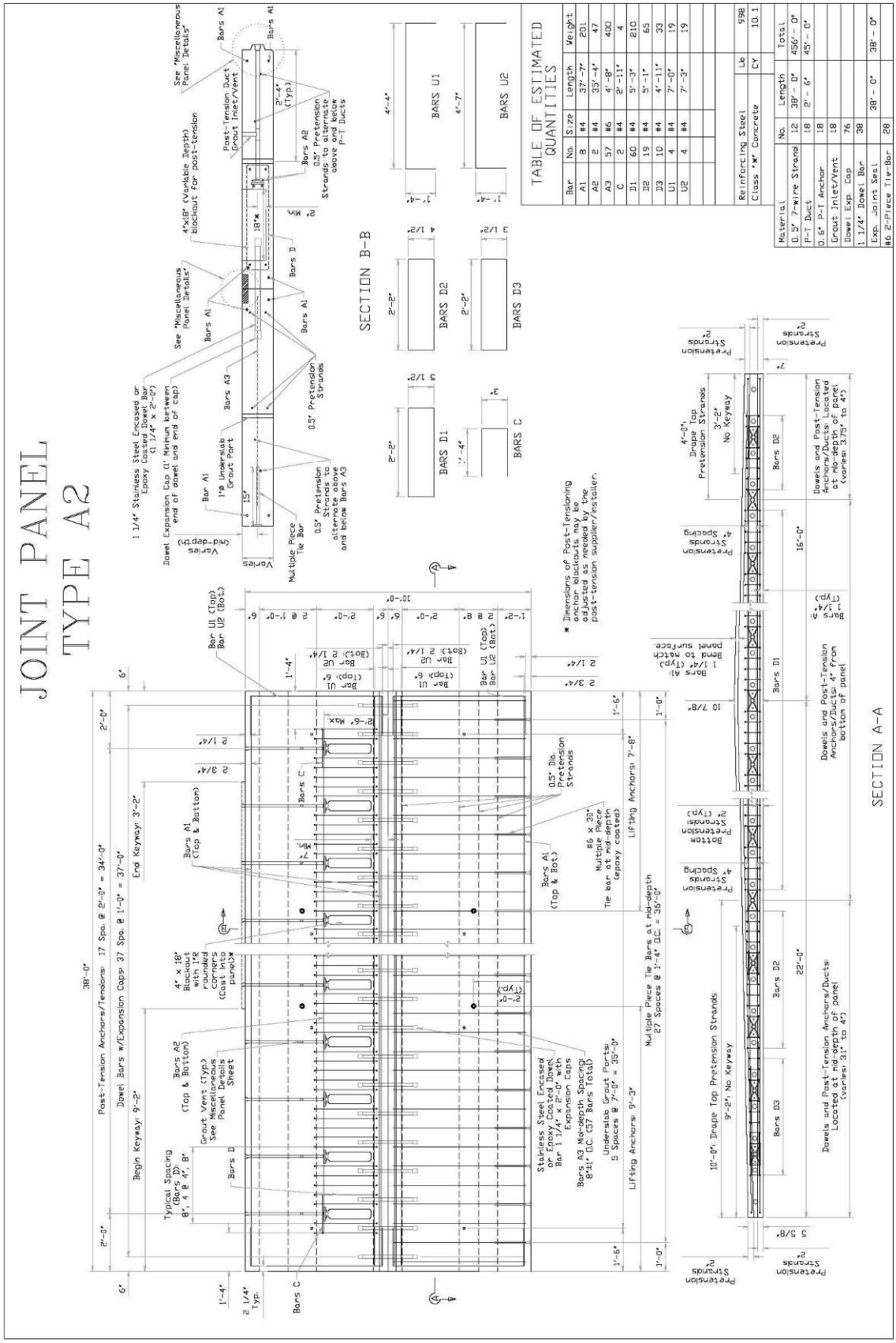
JOINT PANEL
TYPE A2
SECTION A-A
SECTION B-B
TABLE OF ESTIMATED QUANTITIES
Bar | No. | Size | Length | Weight
A1 | 8 | #4 | 37'-7" | 201
A2 | 2 | #4 | 35'-4" | 47
A3 | 57 | #6 | 4'-8" | 400
C | 2 | #4 | 2'-11" | 4
D1 | 60 | #4 | 5'-3" | 210
D2 | 19 | #4 | 5'-1" | 65
D3 | 10 | #4 | 4'-11" | 33
U1 | 4 | #4 | 7'-0" | 19
U2 | 4 | #4 | 7'-3" | 19
Reinforcing Steel | Lb | 998
Class "A" Concrete | CY | 10.1
Material | No. | Length | Total
0.5" 7-wire Strand | 12 | 38' - 0" | 456' - 0"
P-T Duct | 18 | 2' - 6" | 45' - 0"
0.6" P-T Anchor | 18
Grout Inlet/Vent | 18
Dowel Exp. Cap | 76
1 1/4" Dowel Bar | 38
Exp. Joint Seal | | 38' - 0" | 38' - 0"
#6 2-Piece Tie Bar | 28
Post-Tension Anchors/Tendons: 17 Spa. @ 2'-0" = 34'-0"
Dowel Bars w/Expansion Caps: 37 Spa. @ 1'-0" = 37'-0"
Begin Keyway: 9'-2"
End Keyway: 3'-2"
Typical Spacing (Bars D): 8", 4 @ 4", 8"
Bars A2 (Top & Bottom)
Grout Vent (Typ.) See Miscellaneous Panel Details Sheet
Bars D
4" x 18" Blackout with 1"R rounded corners (Cast into panel)
Bars A1 (Top & Bottom)
Bars C
Stainless Steel Encased or Epoxy Coated Dowel Bar 1 1/4" x 2'-0" with Expansion Caps
Bars A3 Mid-depth Spacing: 8'-1" (Dc. (57 Bars Total)
Underslab Grout Ports: 5 Spaces @ 7'-0" = 35'-0"
Lifting Anchors: 9'-3"
Multiple Piece Tie Bars at mid-depth 27 Spaces @ 1'-4" Dc. = 36'-0"
Lifting Anchors: 7'-8"
#6 x 38" Multiple Piece Tie bar at mid-depth (epoxy coated)
0.5" Dia. Pretension Strands
Bars A1 (Top & Bot)
Bar U1 (Top) Bar U2 (Bot)
Bar U1 (Top) Bar U2 (Bot)
Bars A1 1" Min. from Bottom of panel
Bottom Pretension Strands 4" Spacing
Pretension Strands 2" Typ.
Dowels and Post-Tension Anchors/Ducts Located at Mid-depth of panel (varies 3.5" to 4")
10'-0" Drape Top Pretension Strands 9'-2" No Keyway
Bars D3
Bars D2
22'-0"
Dowels and Post-Tension Anchors/Ducts: Located at mid-depth of panel (varies 3.5" to 4")
4'-0" Drape Top Pretension Strands 3'-2" No Keyway
Bars D2
16'-0"
Dowels and Post-Tension Anchors/Ducts Located at Mid-depth of panel (varies 3.75" to 4")
Pretension Strands 4" Spacing
Bars D1
Bars A1 1 1/4" (Typ.) from Bottom of panel
10 7/8"
5 3/8"
Pretension Strands 2"
Pretension Strands 2"
Pretension Strands 2"
Pretension Strands 2"
1 1/4" Stainless Steel Encased or Epoxy Coated Dowel Bar (1 1/4" x 2'-0")
Dowel Expansion Cap (1" Minimum between end of dowel and end of cap)
Varies (Mid-depth)
Bar A1
1"ø Underslab Grout Port
15"
Multiple Piece Tie Bar
0.5" Pretension Strands to alternate above and below Bars A3
Bars A1
Bars A3
Bars A1
See "Miscellaneous Panel Details"
4"x18" (Variable Depth) blockout for post-tension
Post-Tension Duct Grout Inlet/Vent
Bars A1
See "Miscellaneous Panel Details"
2'-4" (Typ.)
Bars A2
0.5" Pretension Strands to alternate above and below P-T Ducts
Bars D
18"
2" Min.
4'-4"
1'-4"
BARS U1
4'-7"
1'-4"
BARS U2
2'-2"
4 1/2"
BARS D2
2'-2"
3 1/2"
BARS D3
2'-2"
5 1/2"
BARS D1
3"
2'-4"
BARS C
* Dimensions of Post-Tensioning anchor blockouts may be adjusted as needed by the post-tension supplier/installer.

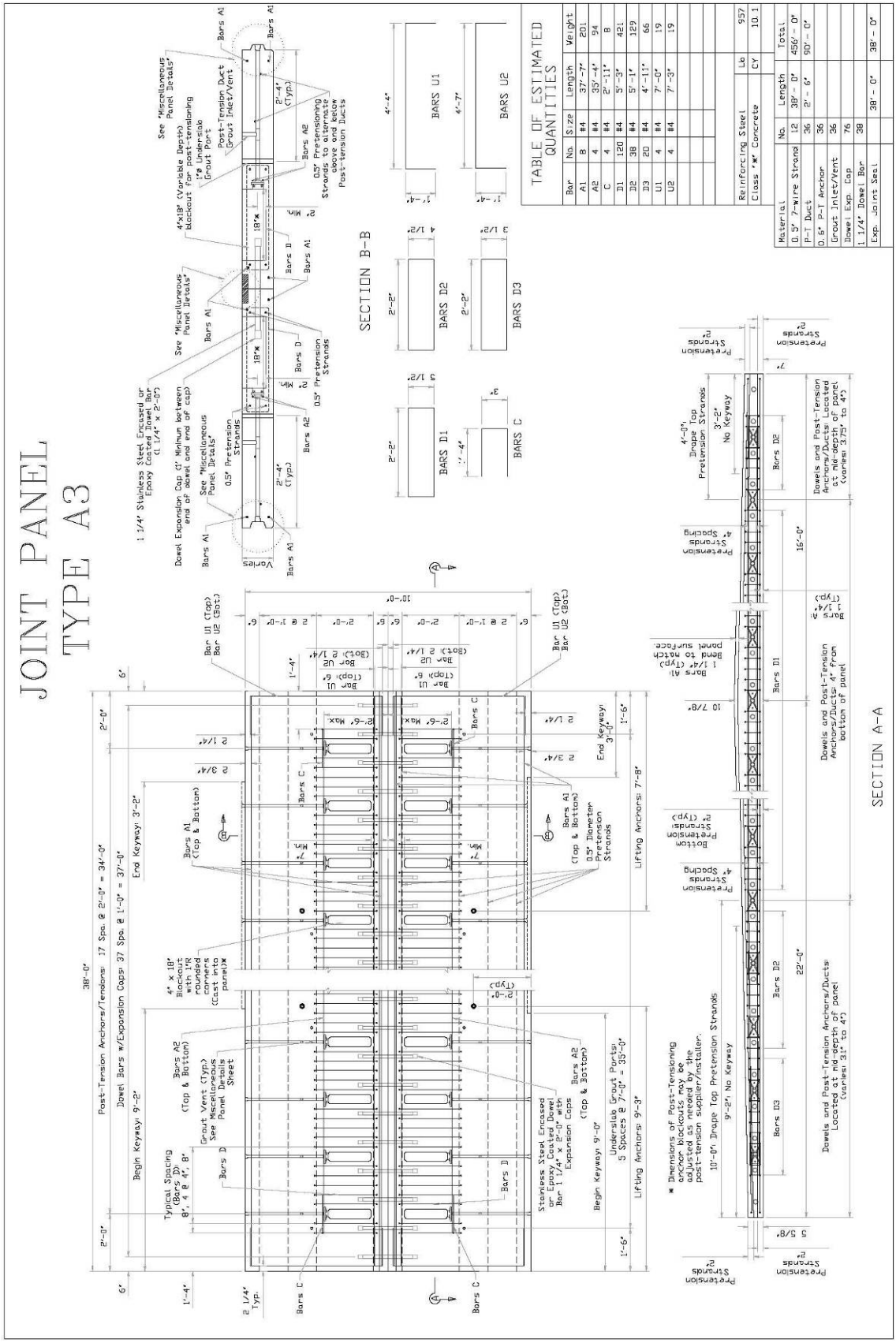
JOINT PANEL
TYPE A3
SECTION A-A
SECTION B-B
BARS U1
BARS U2
BARS D1
BARS D2
BARS D3
BARS C
TABLE OF ESTIMATED QUANTITIES
Bar* | No. | Size | Length | Weight
A1 | 8 | #4 | 37'-7" | 201
A2 | 4 | #4 | 35'-4" | 94
C | 4 | #4 | 2'-11" | 8
D1 | 120 | #4 | 5'-3" | 421
D2 | 38 | #4 | 5'-1" | 129
D3 | 20 | #4 | 4'-11" | 66
U1 | 4 | #4 | 7'-0" | 19
U2 | 4 | #4 | 7'-3" | 19
Reinforcing Steel | Lb | 937
Class "A" Concrete | Cy | 10.1
Material | No. | Length | Total
0.5" 7-wire Strand | 12 | 38'-0" | 456'-0"
P-T Duct | 36 | 2'-6" | 90'-0"
0.6" P-T Anchor | 36
Grout Inlet/Vent | 36
Dowel Exp. Cap | 76
1 1/4" Dowel Bar | 38
Exp. Joint Seal | 38'-0" | 38'-0"
Post-Tension Anchors/Tendons: 17 Spa. @ 2'-0" = 34'-0"
Dowel Bars w/Expansion Caps: 37 Spa. @ 1'-0" = 37'-0"
38'-0"
Begin Keyway: 9'-2"
End Keyway: 3'-2"
Typical Spacing (Bars D): 8", 4 @ 4", 8"
Grout Vent (Typ.) See Miscellaneous Panel Details Sheet
Stainless Steel Encased or Epoxy Coated Dowel Bar 1 1/4" x 2'-0" with Expansion Caps
Underslab Grout Ports: 5 Spaces @ 7'-0" = 35'-0"
Lifting Anchors: 9'-3"
Lifting Anchors: 7'-8"
0.5" Diameter Pretension Strands
4" x 18" Blockout with 1"R rounded corners (Cast-in panel)*
* Dimensions of Post-Tensioning anchor blockouts may be adjusted as needed by the post-tension supplier/installer.
10'-0" Drape Top Pretension Strands
9'-2" No Keyway
Dowels and Post-Tension Anchors/Ducts: Located at mid-depth of panel (varies: 31" to 4")
Dowels and Post-Tension Anchors/Ducts: Located at mid-depth of panel (varies: 3.75" to 4")
Dowels and Post-Tension Anchors/Ducts: 4" from bottom of panel
4'-0" Drape Top Pretension Strands
3'-2" No Keyway
Pretension Strands 4" Spacing
Bottom Pretension Strands 2" (Typ.)
Pretension Strands 2"
Bar U1 (Top) Bar U2 (Bot.)
Bar U1 (Top) Bar U2 (Bot.)
Bars A1 (Top & Bottom)
Bars A2 (Top & Bottom)
See "Miscellaneous Panel Details"
4"x18" (Variable Depth) blockout for post-tensioning
1"Ø Underslab Grout Port
Post-Tension Duct Grout Inlet/Vent
0.5" Pretensioning Strands to extend above and below Post-tension Ducts
0.5" Pretension Strands
1 1/4" Stainless Steel Encased or Epoxy Coated Dowel Bar (1 1/4" x 2'-0")
Dowel Expansion Cap (1" Minimum between end of dowel and end of cap)
Bars A1
Bars A2
Bars D
Bars C
Varies
2 1/4" Typ.

BASE PANEL
TYPE B

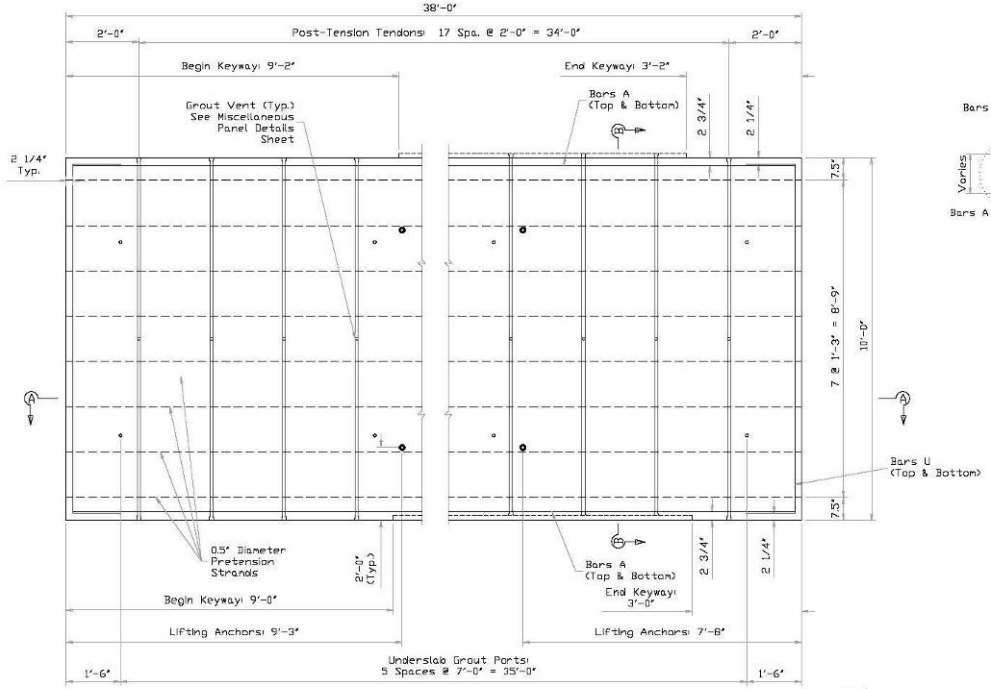

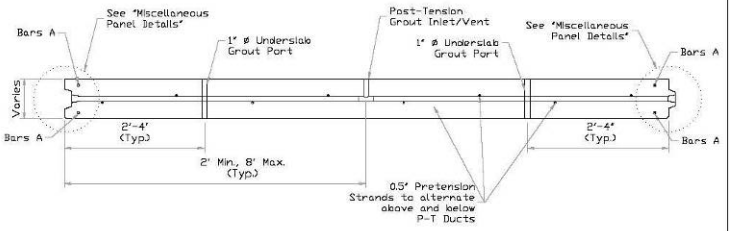

SECTION B-B

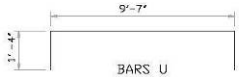

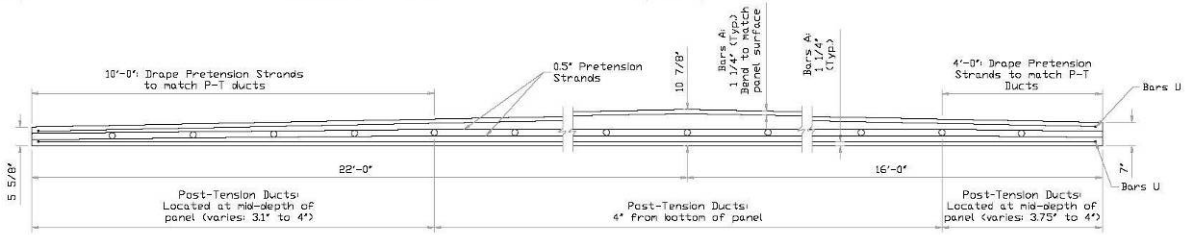

SECTION A-A

TABLE OF ESTIMATED QUANTITIES

Bar	No.	Size	Length	Weight
A	4	#4	37'-7"	100
U	4	#4	12'-3"	33
Reinforcing Steel			Lb	133
Class "X" Concrete			CY	10.1

Material	No.	Length	Total
0.5" 7-wire Strand	8	38' - 0"	304' - 0"
P-T Duct	18	10'-0"	180' - 0"
Grout Inlet/Vent	18		

BASE PANEL
TYPE C

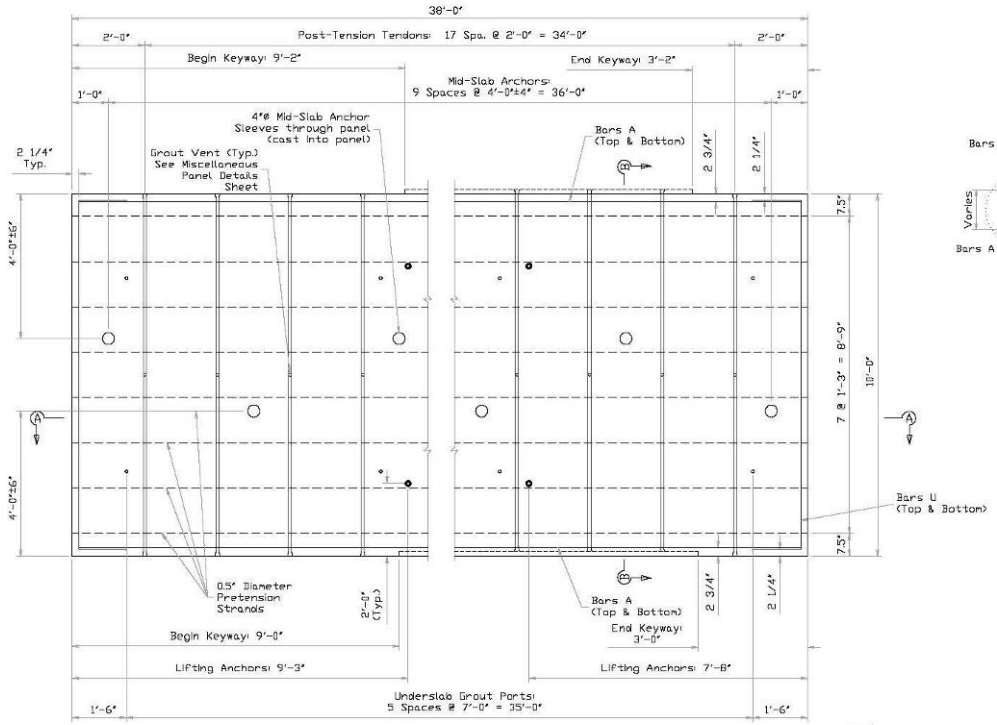

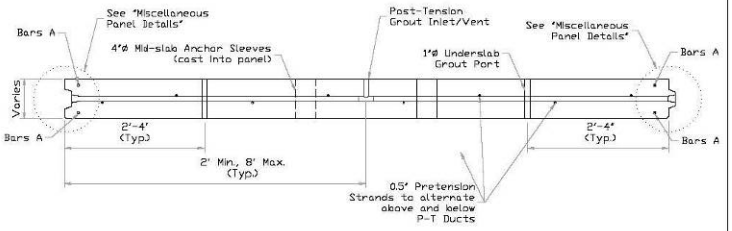

SECTION B-B

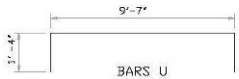

BARS U

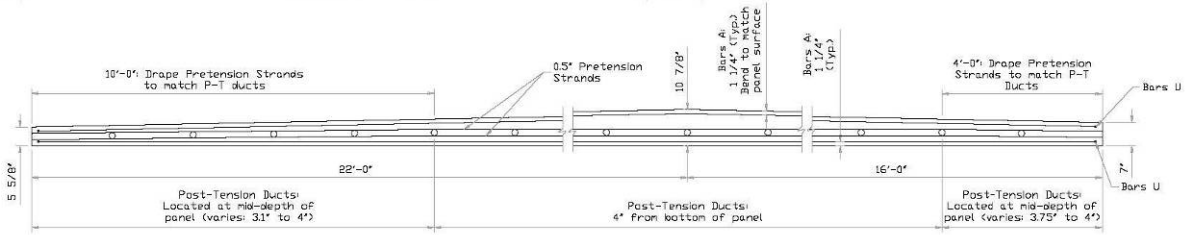

SECTION A-A

TABLE OF ESTIMATED QUANTITIES

Bar	No.	Size	Length	Weight
A	4	#4	37'-7"	100
U	4	#4	12'-3"	33
Reinforcing Steel			Lb	133
Class "X" Concrete			CY	10.1

Material	No.	Length	Total
0.5" 7-wire Strand	8	38'-0"	304'-0"
P-T Duct	18	10'-0"	180'-0"
Grout Inlet/Vent	18		

MISCELLANEOUS PANEL DETAILS

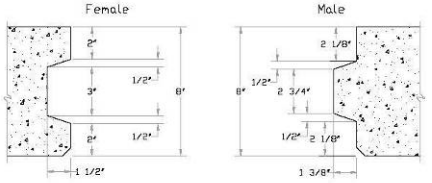

Lane Edge
(10' from oustide EOP, 4' from inside EOP)

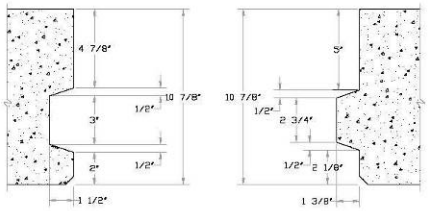

Lane Centerline
(22' from oustide EOP)

Inside Edge of Pavement
(Median)

Outside Edge of Pavement

KEYWAY DIMENSIONS

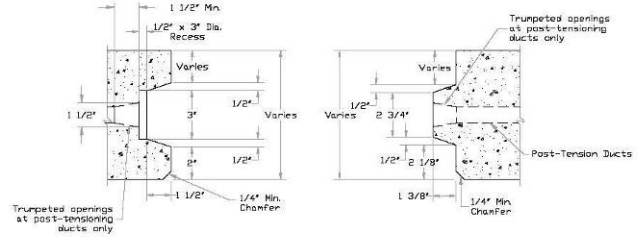

POST-TENSION DUCT OPENINGS AT KEYWAYS

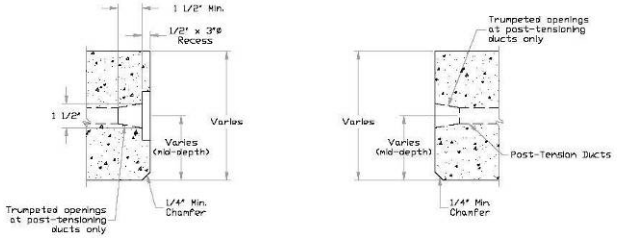

POST-TENSION DUCT OPENINGS AT NON-KEYWAYS

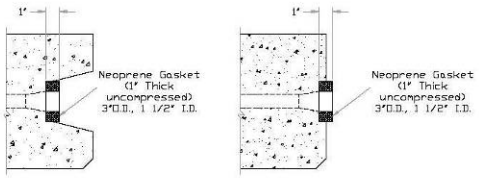

FEMALE KEYWAY

POST-TENSION DUCT SEAL DETAIL

NOT TO SCALE

TABLE OF ESTIMATED QUANTITIES (PER PANEL)

Material	No.
Foam/Neoprene Gasket	18

MISCELLANEOUS PANEL DETAILS

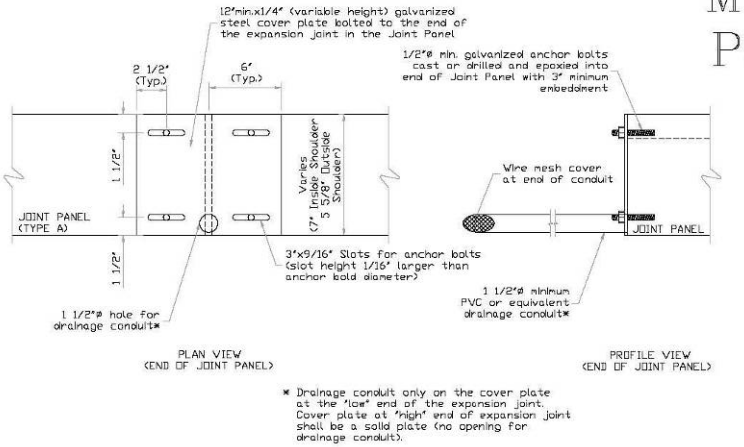

* Drainage conduit only on the cover plate at the "low" end of the expansion joint. Cover plate at "high" end of expansion joint shall be a solid plate (no opening for drainage conduit).

COVER PLATE AND EDGE DRAIN DETAIL (FOR JOINT PANELS)

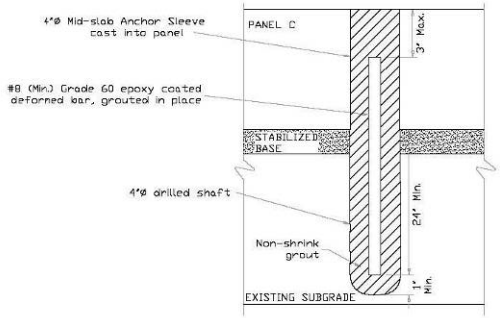

MID-SLAB ANCHOR DETAIL

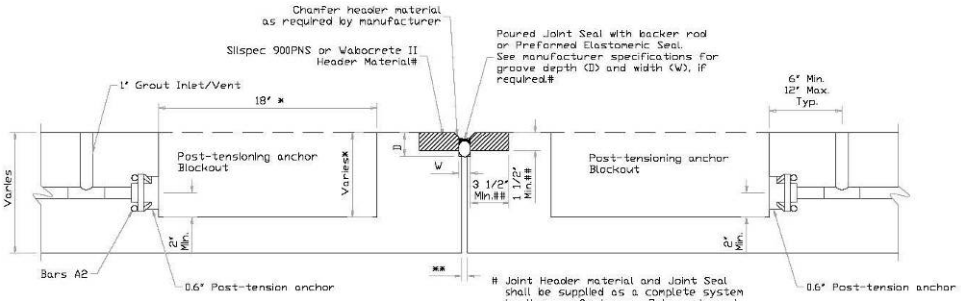

* Dimensions of anchor blockout may be adjusted as needed by the post-tensioning supplier/installer.

** Initial Joint Width (at depth of dowels) to be determined based upon ambient temperature after post-tensioning using table shown in the General Notes.

Joint Header material and Joint Seal shall be supplied as a complete system by the manufacturer. Only seals and header material that are compatible with each other shall be used.

Dimensions of recess shall be specified by the header material manufacturer. Recess shall be cast into the precast panels during fabrication. Surfaces of recess shall be prepared to ensure proper bonding between header material and concrete. Header material shall be installed according to manufacturer specifications.

EXPANSION JOINT/POST-TENSIONING ANCHOR DETAIL

TABLE OF ESTIMATED QUANTITIES (PER PANEL)

1/2" Dia. Anchor Bolts	8
1/4" Galvanized Steel Cover Plate	2
1 1/2"ø PVC or equivanent conduit	8
Anchor bars	10

B. PREPARATION OF INSTRUMENTED REBAR (EATHERTON 1999)

After attaching the strain-gages to the bar as shown in Figure B.1, the bars were then tested using a Vishay two channel conditioner to verify that the strain-gaged bar was working properly. Then the bars were protected and waterproofed so that they could withstand the forces of concrete placement and being submersed in a fresh concrete environment. Waterproofing involved five steps. First the instrumented bar was coated with polyurethane. This step is shown in Figure B.3.

After the polyurethane was applied, a layer of Teflon tape was used to reduce friction between the outer layers and the strain gages. This was done so that local strains on the protective layers would not be measured. The application of the Teflon tape layer is shown in Figure B.4.

The next layer used was rubber tape. This was a protective layer used to absorb shock caused by concrete falling on instrumented rebar from several feet of height. The application of the rubber tape is shown in Figure B.5.

After the rubber tape, measures were taken to seal the gages so that moisture would not affect the measurement. A layer of silicon was smeared over the rubber tape. Around the ends of the rubber tape a bead of silicon surrounded the bar. This layer of silicon was allowed to dry before further sealing.

After the first coat of silicon dried another layer of silicon was applied to the gaged area. This layer was not allowed to dry before a 6" section of ¾" heat shrink was used to seal the entire instrumented section (Eatherton 1999).

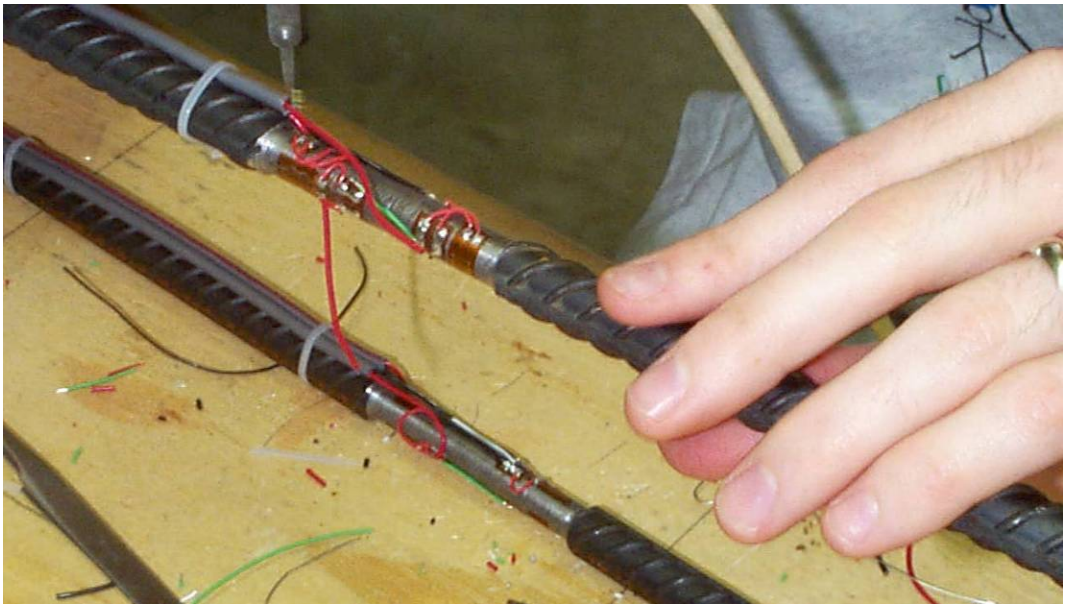

Figure B.1 - Soldering connections on an instrumented rebar

Figure B.2 - Applying a coat of polyurethane to instrumented rebar

Figure B.3 - Teflon tape covers the gages and reduces friction with outer protective layers

Figure B.4 - Application of rubber tape to protect the gages from falling concrete

Figure B.5 - The instrumented rebar after silicon has been applied to the gaged area

Figure B.6 - The finished instrumented rebar next to an un-waterproofed bar

C. CALIBRATION OF GAGES

The following pages show example calibration graphs from rebar, vibrating wire gages, and strandmeters. Tables showing their respective calibration constants are also included. Early thermal studies of a vibrating wire gage and rebar in an oven are presented. Further thermal investigations of similar nature continue.

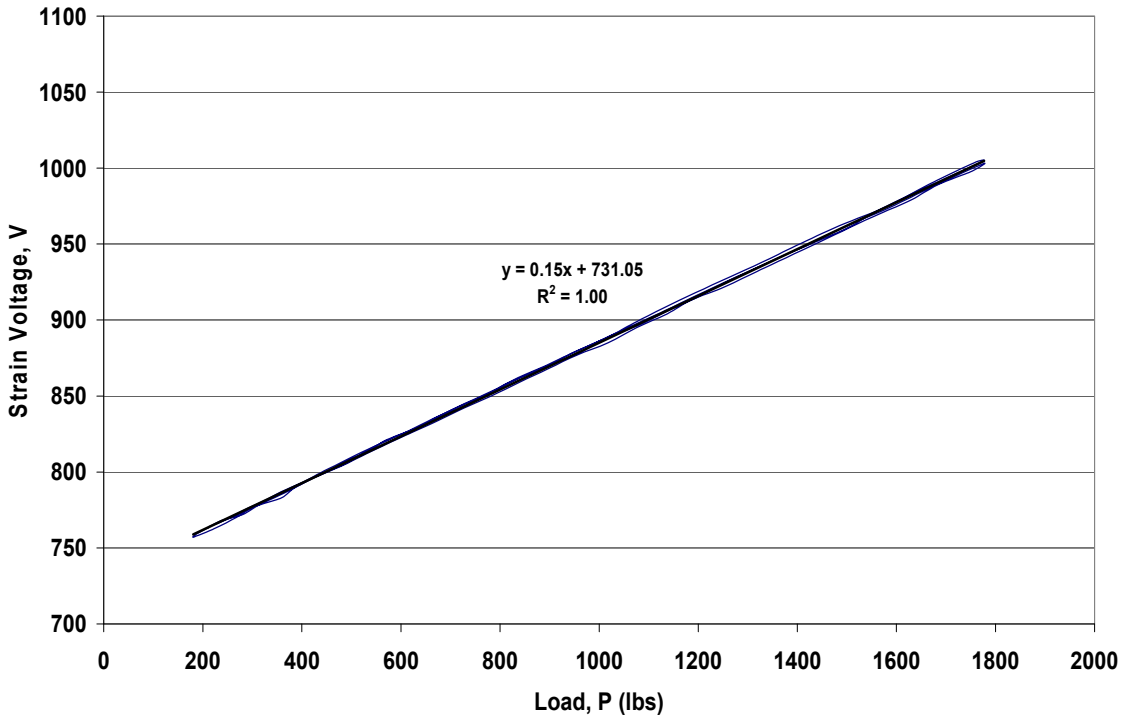

Figure C.1 – Example graph from calibration of rebar

Table C.1 - Calibration constants for instrumented rebar

Gage ID	Calibration Constant (lbs/mV)	Excitation for Calibration (mV)	Gage ID	Calibration Constant (lbs/mV)	Excitation for Calibration (mV)
A31-R1	665	4070	B3-R1	675	4040
A31-R2	651	4090	B3-R2	656	4040
A31-R3	653	4080	B3-R3	684	4040
A31-R4	681	4080	B3-R4	666	4040
A31-R5	667	4080	B3-R5	671	4080
A31-R6	645	4060	A32-R1	674	4040
C1-R1	681	4000	A32-R2	646	4090
C1-R2	661	4020	A32-R3	670	4040
C1-R3	651	4070	A32-R4	701	4090
C1-R4	684	4060	A32-R5	655	4040
C1-R5	645	4050	A32-R6	677	4000
B1-R1	675	4020	A32-R7	650	4080
B1-R2	687	4080	A32-R8	667	4080
B1-R3	680	4040	B4-R1	659	4080
B1-R4	640	4040	B4-R2	645	4040
B1-R5	639	4020	B4-R3	637	4040
B2-R1	663	4030	B4-R4	690	4020
B2-R2	680	4020	B4-R5	672	4060
B2-R3	665	4090	Thermo	691	4050
B2-R4	647	4000	New 17	660	4000
B2-R5	600	4000	New 19	677	4000

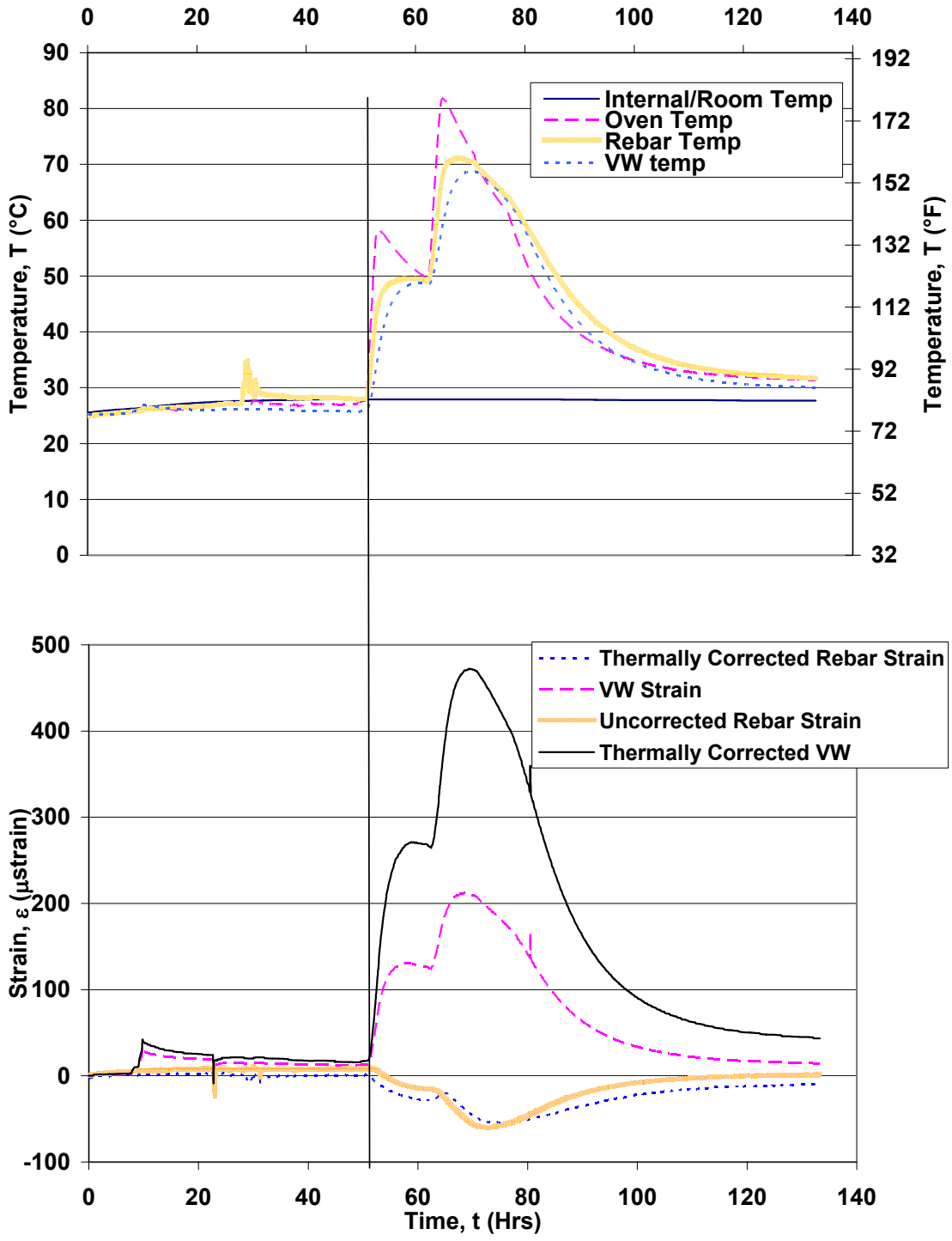

Figure C.2 – Early thermal study of rebar and vibrating wire gage in oven

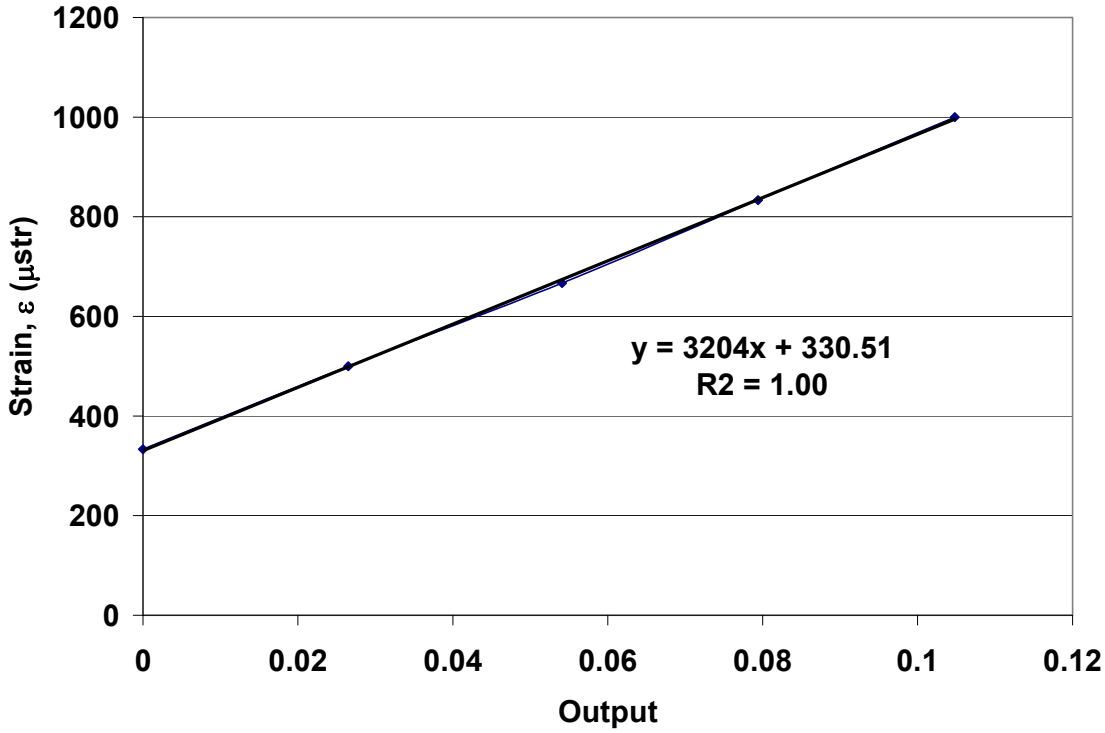

Figure C.3 – Graph of vibrating wire gage calibration

Table C.2 - Calibration constants for vibrating wire gages

Gage ID	Calibration Constant (ustr/output)
C1-V1	3551.2
C1-V2	2974.1
B1-V1	3504.2
B1-V2	3508.6
B2-V1	3146.8
B2-V2	3150
B3-V1	3204.4
B3-V2	3357
A32-V1	3173.7
A32-V2	3367.6
A32-V3	3044
A32-V4	3741
B4-V1	3167.1
B4-V2	3173.8

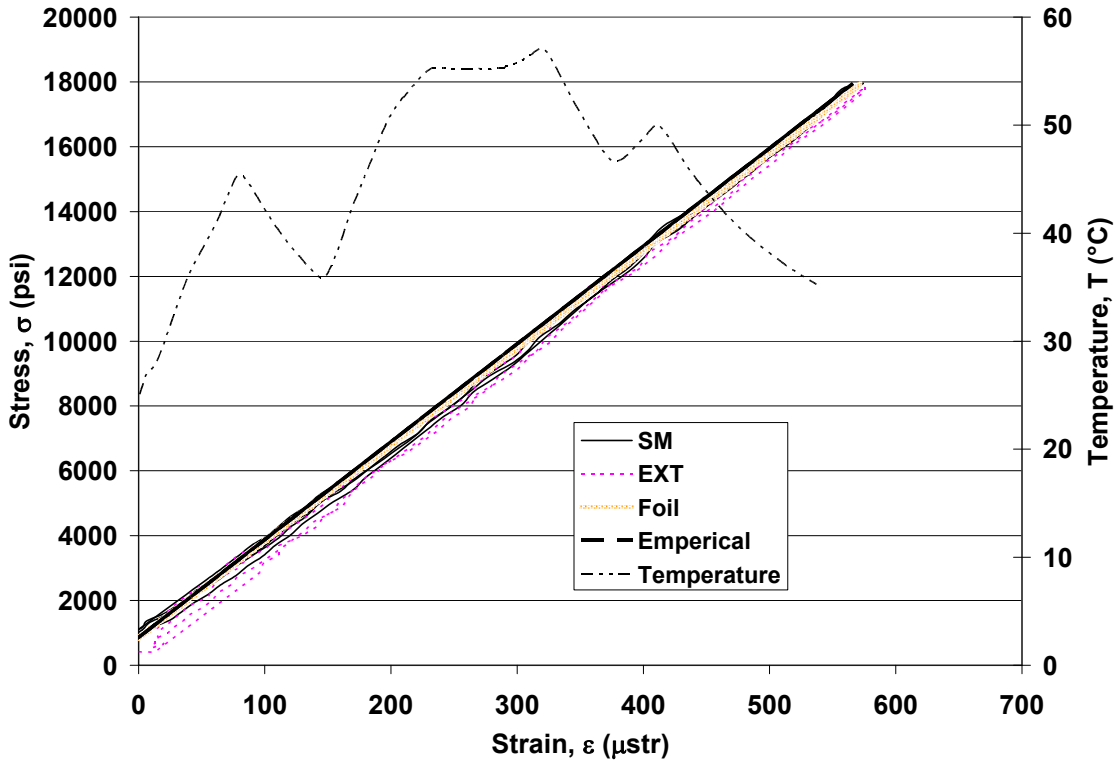

Figure C.4 – Example graph from strandmeter calibration (with thermal changes)

Table C.3 - Calibration constants for strandmeters

	Gage Factor (inches/digit)			
Strandmeter I.D.	**Lower Range**	**Upper Range**	**Average**	**Factory**
B1 (Serial # 14260)	2.545E-05	2.601E-05	2.573E-05	2.501E-05
B2 (Serial # 14259)	2.504E-05	2.448E-05	2.476E-05	2.508E-05
B3 (Serail # 14255)	2.265E-05	2.368E-05	2.316E-05	2.495E-05
C1 (Serial # 14257)	2.489E-05	2.493E-05	2.491E-05	2.468E-05

D. ADDITIONAL STRESS TRANSFER CALCULATIONS

Table D.1 - Pretensioning stress transfer calculations for Base Panels B1-4

B1,B2, B3, and B4

Material Properties

Steel		Concrete	
Yield Strength (ksi)	270	Inertia (in^4)	1540800
Modulus (ksi)	28500	Poisson's Ratio	0.2
Strand Diameter (in)	0.5	28d Strength (psi)	7100
Strand Area (in^2)	0.153	Time @ Stress (day)	0.5
Percentage of Stress	0.75	f'c (psi)	3500
Stress in Strand (ksi)	202.63	Modulus (psi)	3372165.48
Force in Strand (lbs)	31002.74		

Rebar 3	Depth 'd' (in)	10.7	Area (in^2)	1284	
Panel Strand	**Stress P/A**	**Moment Arm 'e' of Force (in)**	**Rebar from N.A. 'y' (in)**	**Stress My/I (psi)**	**Strain (μstr)**
1.00	-24.15	-52.5	5	-5.28	-8.73
2.00	-48.29	52.5	5	0.00	-14.32
3.00	-72.44	37.5	5	3.77	-20.36
4.00	-96.58	-37.5	5	0.00	-28.64
5.00	-120.73	-22.5	5	-2.26	-36.47
6.00	-144.87	22.5	5	0.00	-42.96
7.00	-169.02	7.5	5	0.75	-49.90
8.00	-193.16	-7.5	5	0.00	-57.28

Table D.2 - Pretensioning stress transfer calculations for Anchor Panel C1

C1

Material Properties

Steel		Concrete	
Yield Strength (ksi)	270	Inertia (in^4)	1584000
Modulus (ksi)	28500	Poisson's Ratio	0.2
Strand Diameter (in)	0.5	28d Strength (psi)	7100
Strand Area (in^2)	0.153	Time @ Stress (day)	0.5
Percentage of Stress	0.75	f'c (psi)	3500
Stress in Strand (ksi)	202.63	Modulus (psi)	3372165.48
Force in Strand (lbs)	31002.74		

C1 - Rebar 3	Depth 'd' (in)	11	Area (in^2)	1320	
Panel Strand	**Stress P/A**	**Moment Arm 'e' of Force (in)**	**Rebar from N.A. 'y' (in)**	**Stress My/I (psi)**	**Strain (μstr)**
1.00	-23.49	-52.5	2	-2.06	-7.57
2.00	-46.97	52.5	2	0.00	-13.93
3.00	-70.46	37.5	2	1.47	-20.46
4.00	-93.95	-37.5	2	0.00	-27.86
5.00	-117.43	-22.5	2	-0.88	-35.09
6.00	-140.92	22.5	2	0.00	-41.79
7.00	-164.41	7.5	2	0.29	-48.67
8.00	-187.90	-7.5	2	0.00	-55.72

Table D.3 - Pretensioning stress transfer calculations for Joint Panel A32

A32

Material Properties

Steel		Concrete	
Yield Strength (ksi)	270	Inertia (in^4)	1540800
Modulus (ksi)	28500	Poisson's Ratio	0.2
Strand Diameter (in)	0.5	28d Strength (psi)	7100
Strand Area (in^2)	0.153	Time @ Stress (day)	0.5
Percentage of Stress	0.75	f'c (psi)	3500
Stress in Strand (ksi)	202.63	Modulus (psi)	3372165.48
Force in Strand (lbs)	31002.74		

Rebar 4	**Depth 'd' (in)**	10.7	**Area (in^2)**	1284		**Rebar 1 and 7 Strain**	**Rebar 3**
Joint Panel Strand	**Stress P/A**	**Moment Arm 'e' of Force (in)**	**Rebar from N.A. 'y' (in)**	**Stress My/I (psi)**	**Strain (μstr)**		
1.00	-24.15	54	48	52.15	8.31	-2.27879	-1.6611704
2.00	-48.29	-54	48	0.00	-14.32	3.92894	2.86408692
3.00	-72.44	-54	48	-52.15	-36.95	10.1367	7.38934426
4.00	-96.58	54	48	0.00	-28.64	7.85788	5.72817385
5.00	-120.73	48	48	46.36	-22.05	6.05057	4.41069386
6.00	-144.87	-48	48	0.00	-42.96	11.7868	8.59226077
7.00	-169.02	48	48	46.36	-36.37	9.97951	7.27478079
8.00	-193.16	-48	48	0.00	-57.28	15.7158	11.4563477
9.00	-217.31	-6	48	-5.79	-66.16	18.1517	13.2320816
10.00	-241.45	6	48	0.00	-71.60	19.6447	14.3204346
11.00	-265.60	-6	48	-5.79	-80.48	22.0806	16.0961685
12.00	-289.75	6	48	0.00	-85.92	23.5736	17.1845215

Rebar 1,7	**Depth 'd' (in)**	7.80	**Area (in^2)**	936

Based on Poisson's effect

Rebar 2,8	**Depth 'd' (in)**	7.8	**Area (in^2)**	936	
Joint Panel Strand	**Stress P/A**	**Moment Arm 'e' of Force (in)**	**Rebar from N.A. 'y' (in)**	**Stress My/I (psi)**	**Strain (μstr)**
1.00	-33.12	54	-48	-52.15	-25.29
2.00	-66.25	-54	-48	0.00	-19.64
3.00	-99.37	-54	-48	52.15	-14.00
4.00	-132.49	54	-48	0.00	-39.29
5.00	-165.61	48	-48	-46.36	-62.86
6.00	-198.74	-48	-48	0.00	-58.93
7.00	-231.86	48	-48	-46.36	-82.50
8.00	-264.98	-48	-48	0.00	-78.58
9.00	-298.10	-6	-48	5.79	-86.68
10.00	-331.23	6	-48	0.00	-98.22
11.00	-364.35	-6	-48	5.79	-106.33
12.00	-397.47	6	-48	0.00	-117.87

Rebar 5	**Depth 'd' (in)**	10.5	**Area (in^2)**	1260		**Rebar 3 and 6 Strain**
Joint Panel Strand	**Stress P/A**	**Moment Arm 'e' of Force (in)**	**Rebar from N.A. 'y' (in)**	**Stress My/I (psi)**	**Strain (μstr)**	
1.00	-24.61	54	-48	-52.15	-22.76	4.50959
2.00	-49.21	-54	-48	0.00	-14.59	2.89111
3.00	-73.82	-54	-48	52.15	-6.42	1.27263
4.00	-98.42	54	-48	0.00	-29.19	5.78221
5.00	-123.03	48	-48	-46.36	-50.23	9.95135
6.00	-147.63	-48	-48	0.00	-43.78	8.67332
7.00	-172.24	48	-48	-46.36	-64.82	12.8425
8.00	-196.84	-48	-48	0.00	-58.37	11.5644
9.00	-221.45	-6	-48	5.79	-63.95	12.6695
10.00	-246.05	6	-48	0.00	-72.97	14.4555
11.00	-270.66	-6	-48	5.79	-78.54	15.5606
12.00	-295.26	6	-48	0.00	-87.56	17.3466

Rebar 3,6	**Depth 'd' (in)**	10.60	**Area (in^2)**	1272

Based on Poisson's effect

E. ADDITIONAL RESULTS AND GRAPHS

The following appendices present additional results graphs. These reinforce theories and trends addressed in the body of the thesis.

E.1. HYDRATION AND EARLY AGE RESPONSE

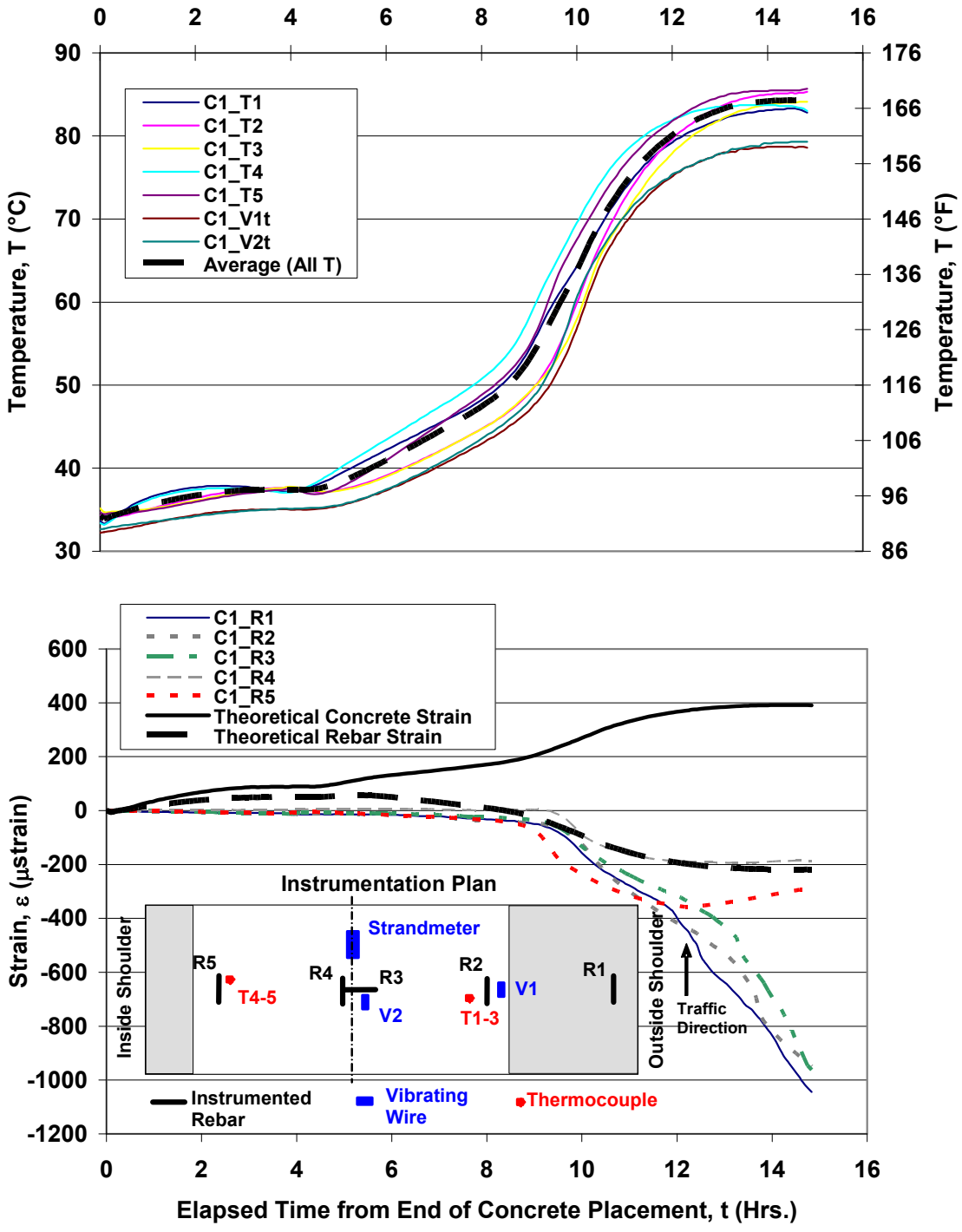

Figure E.1 – Curing and hydration of Panel C1

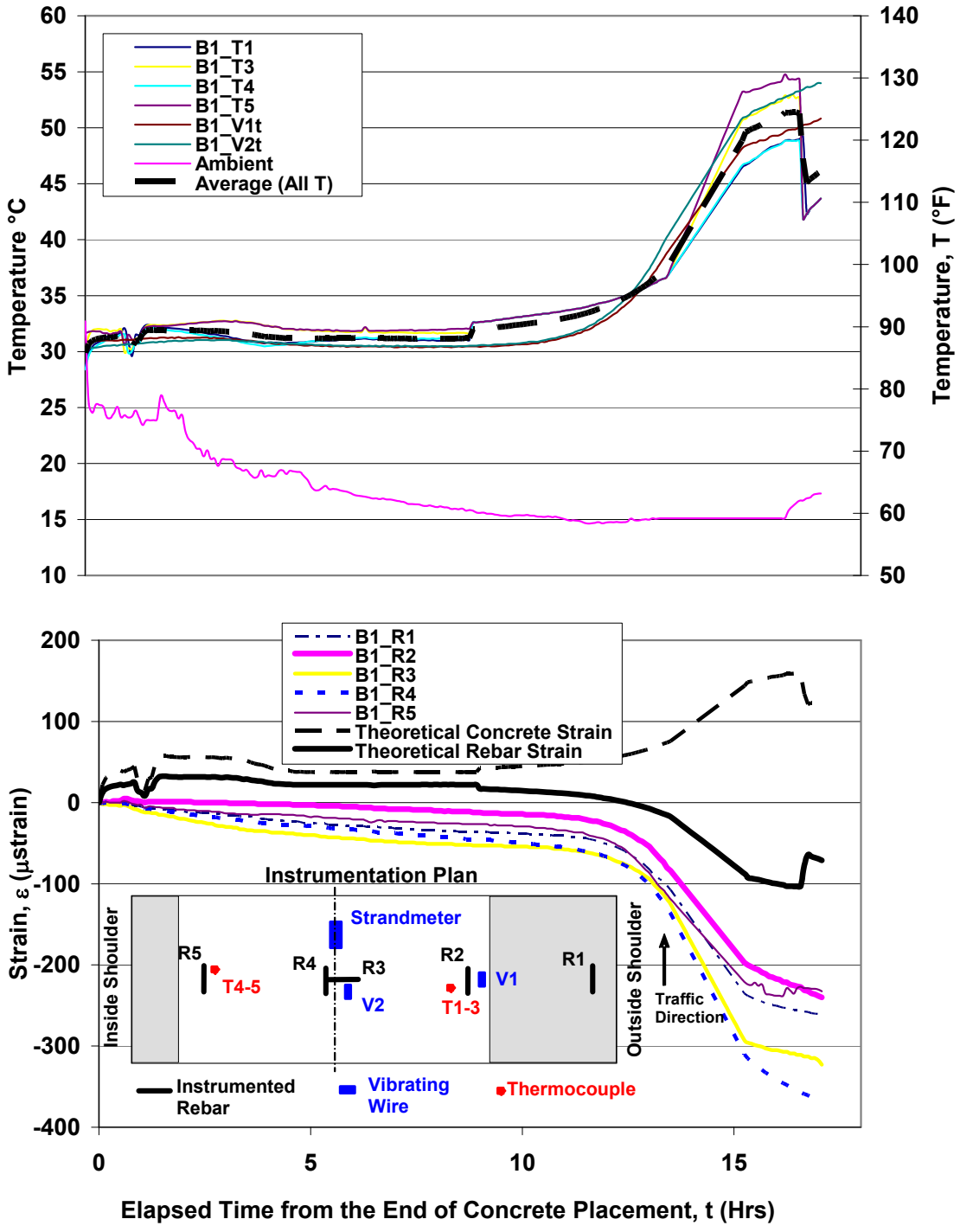

Figure E.2 – Curing and hydration of Panel B1

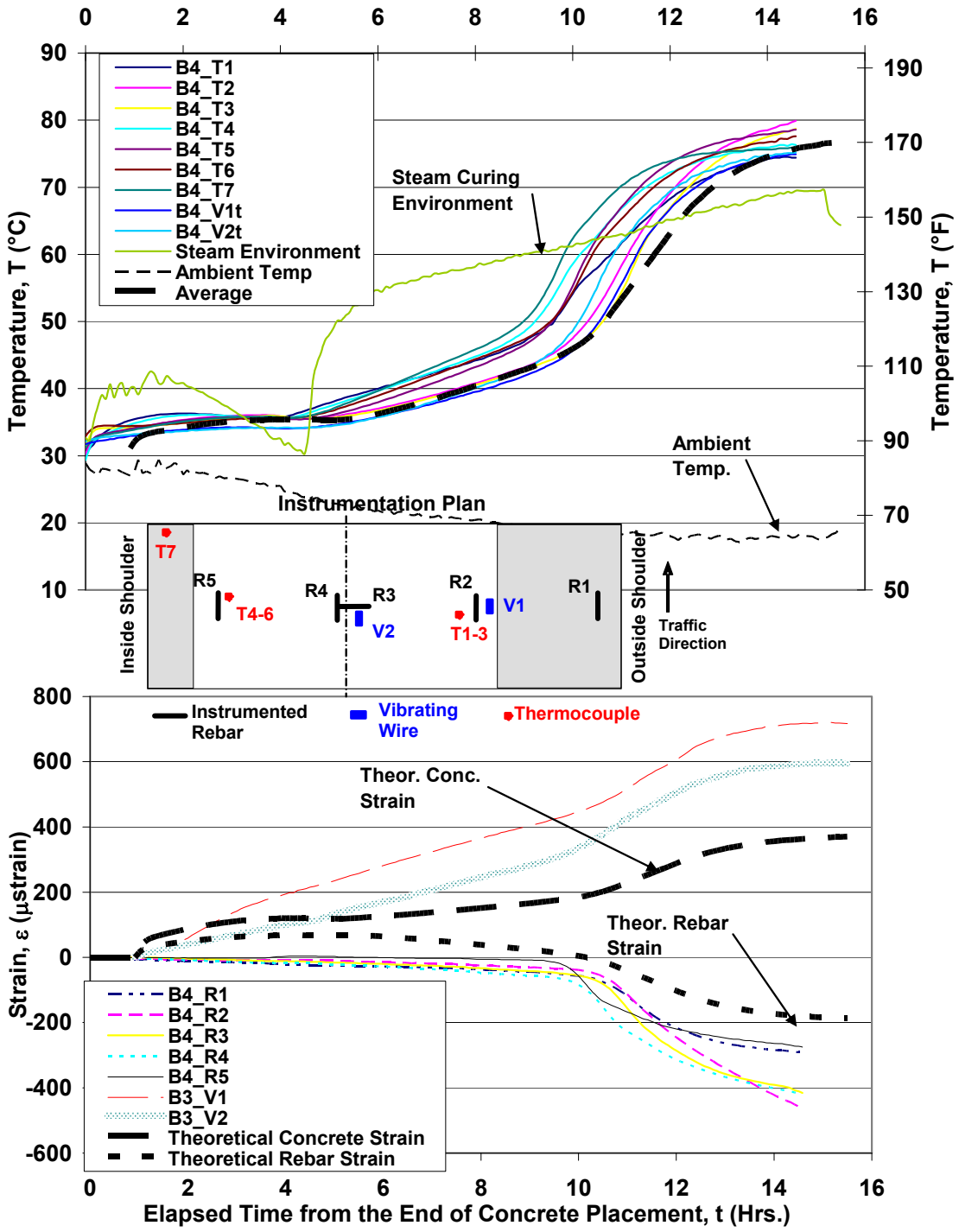

Figure E.3 – Curing and hydration of Panel B4

E.2. PRETENSIONING STRESS TRANSFER

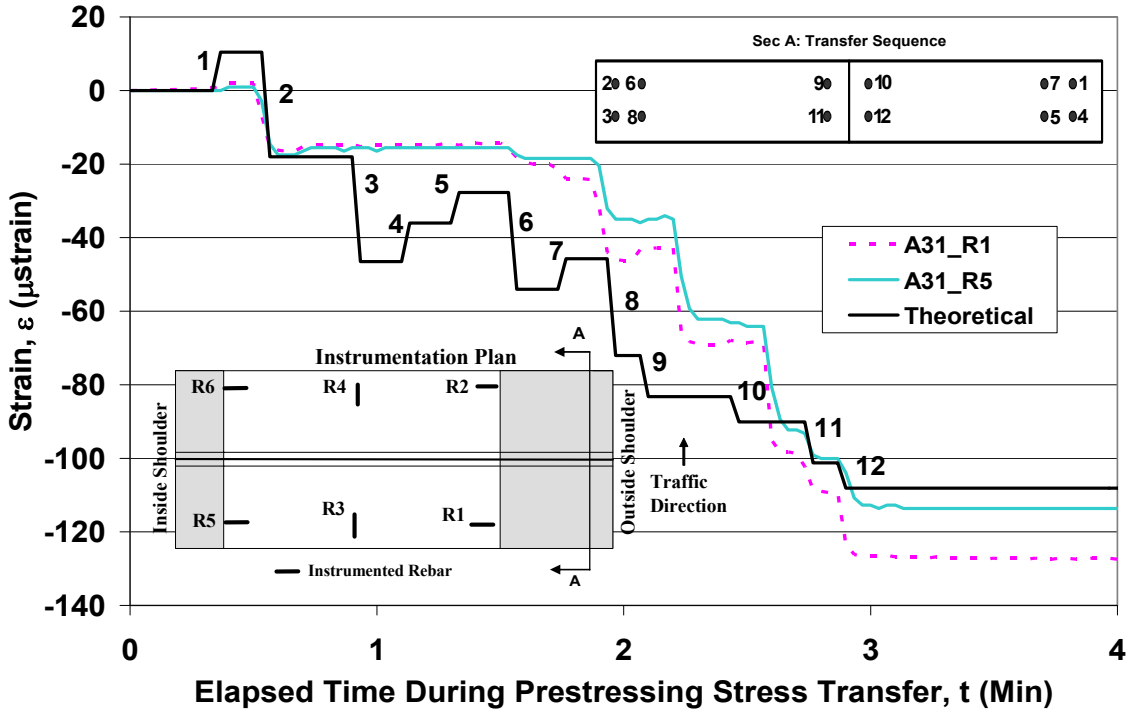

Figure E.4 – Strains from stress transfer of Panel A31 rebar

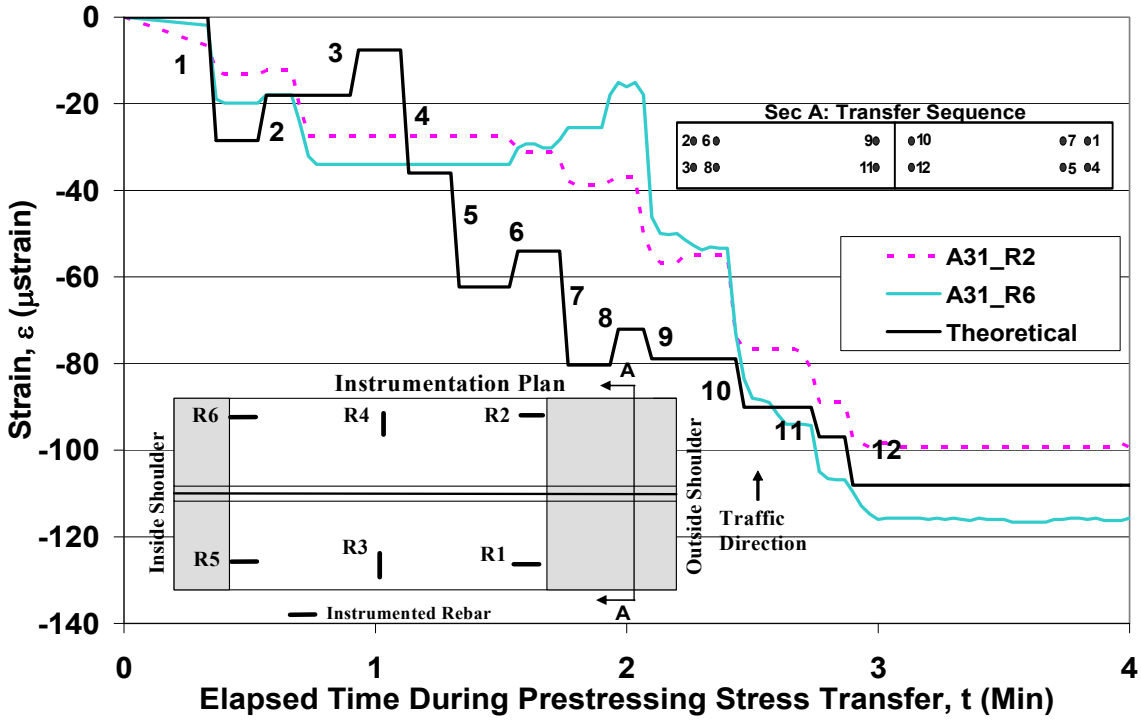

Figure E.5 – Strains from stress transfer of Panel A31 rebar

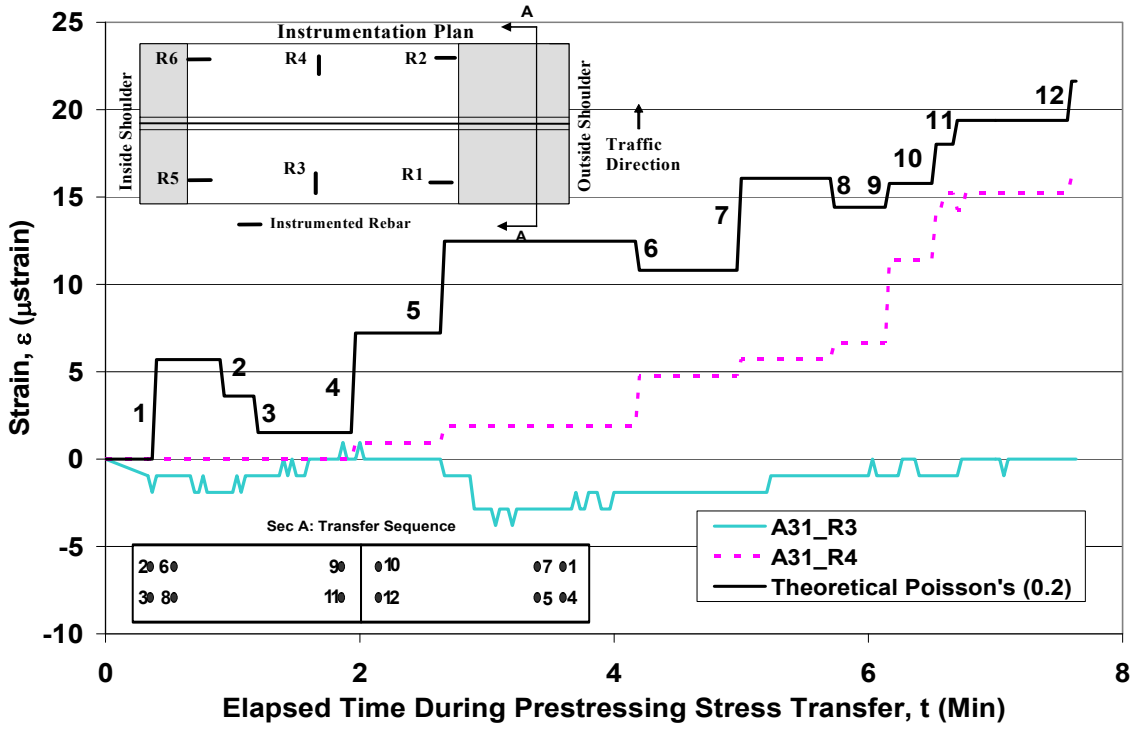

Figure E.6 – Strains from stress transfer of Panel A31 longitudinal rebar

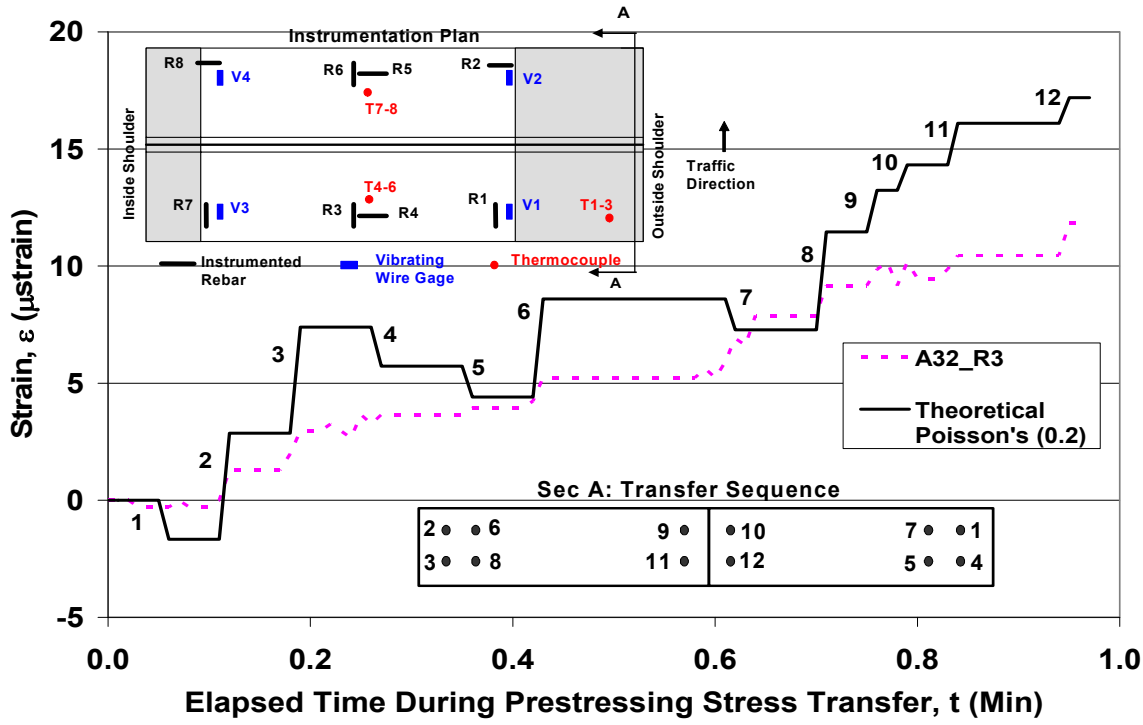

Figure E.7 – Strains from stress transfer of Panel A32 longitudinal rebar

E.3. POST-TENSIONING DURING CONSTRUCTION

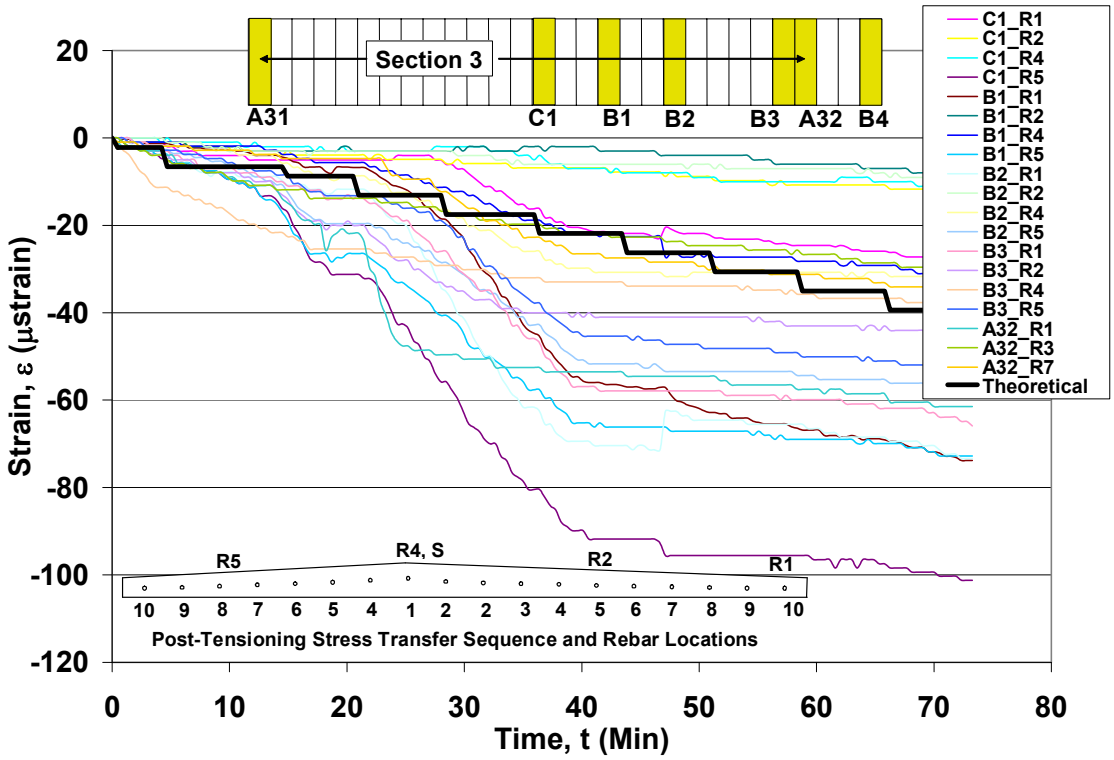

Figure E.8 – Summary of post-tensioning strains in Section 3

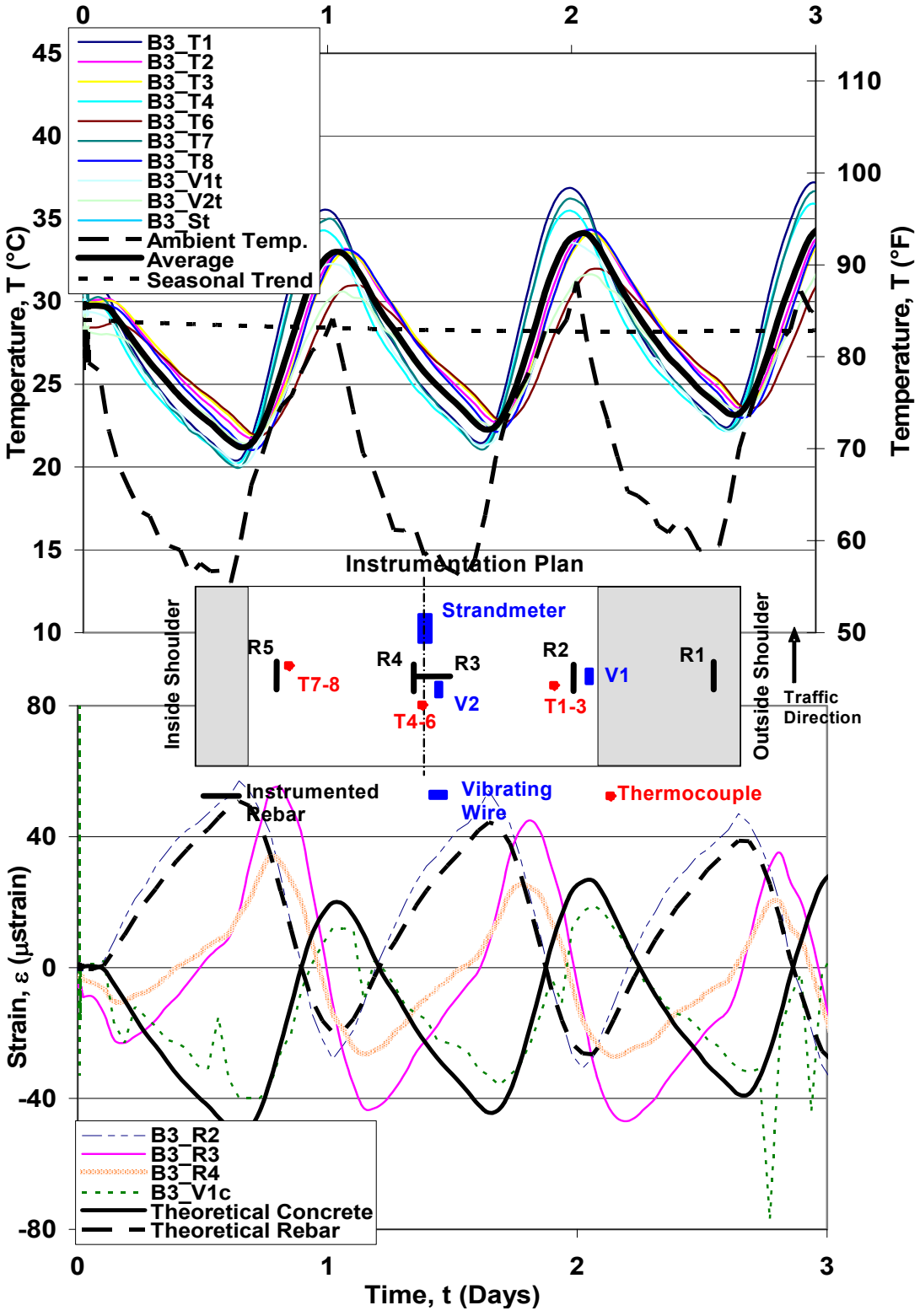

Figure E.9 – In-service data for Panel B3 over three days in September 2006

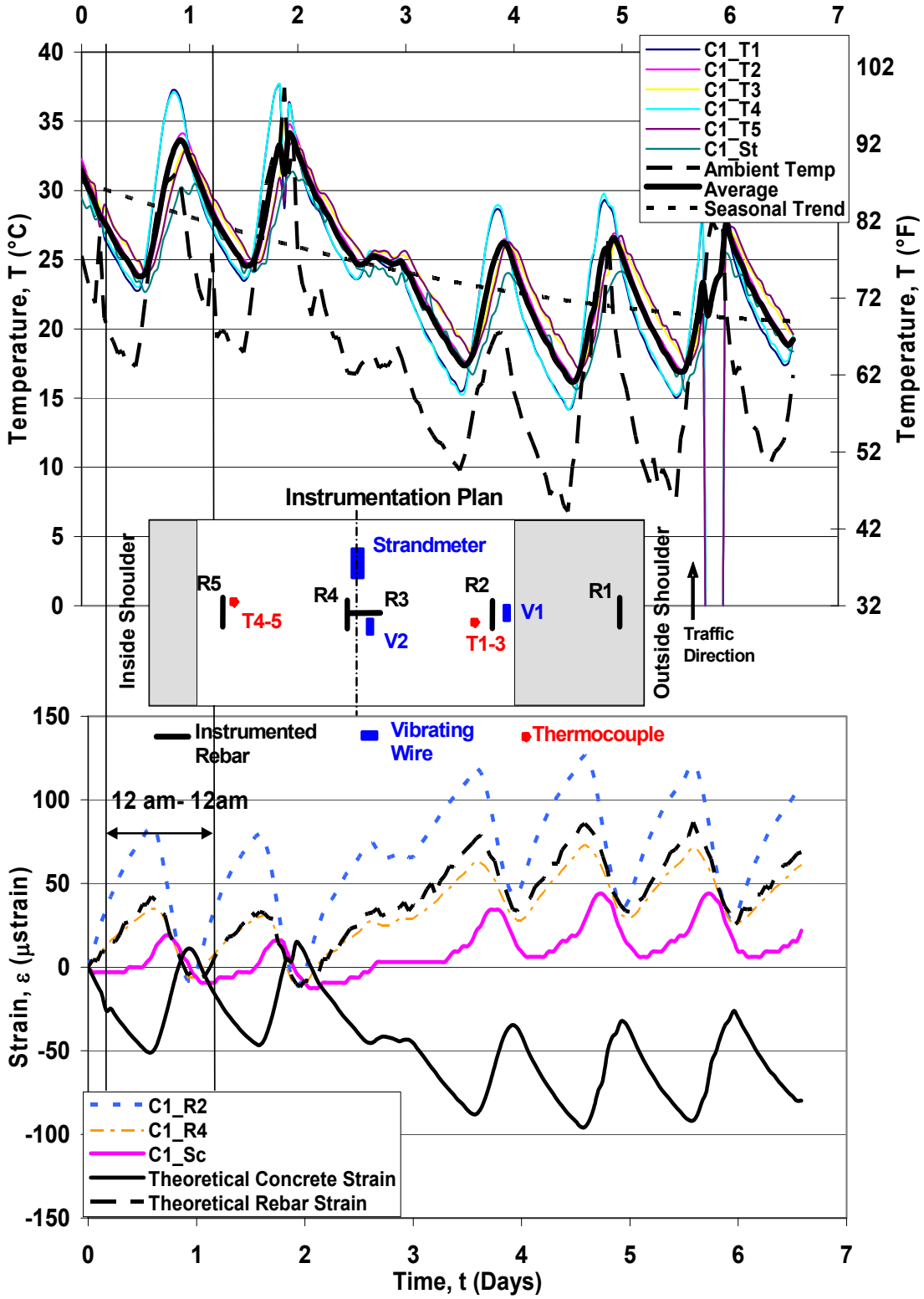

Figure E.10 – In-service data for Panel C1 over seven days in October 2006

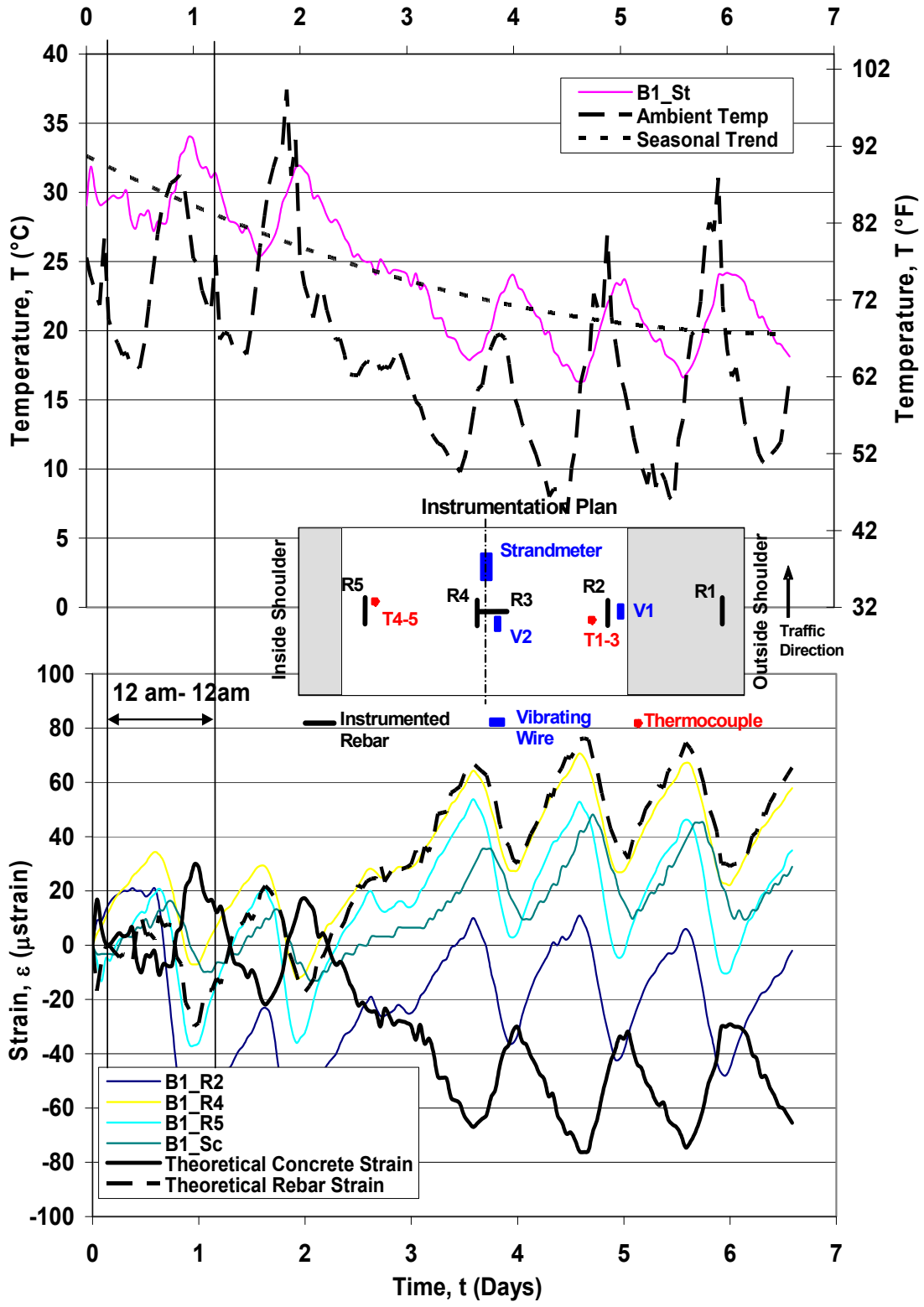

Figure E.11 – In-service data for Panel B1 over seven days in October 2006

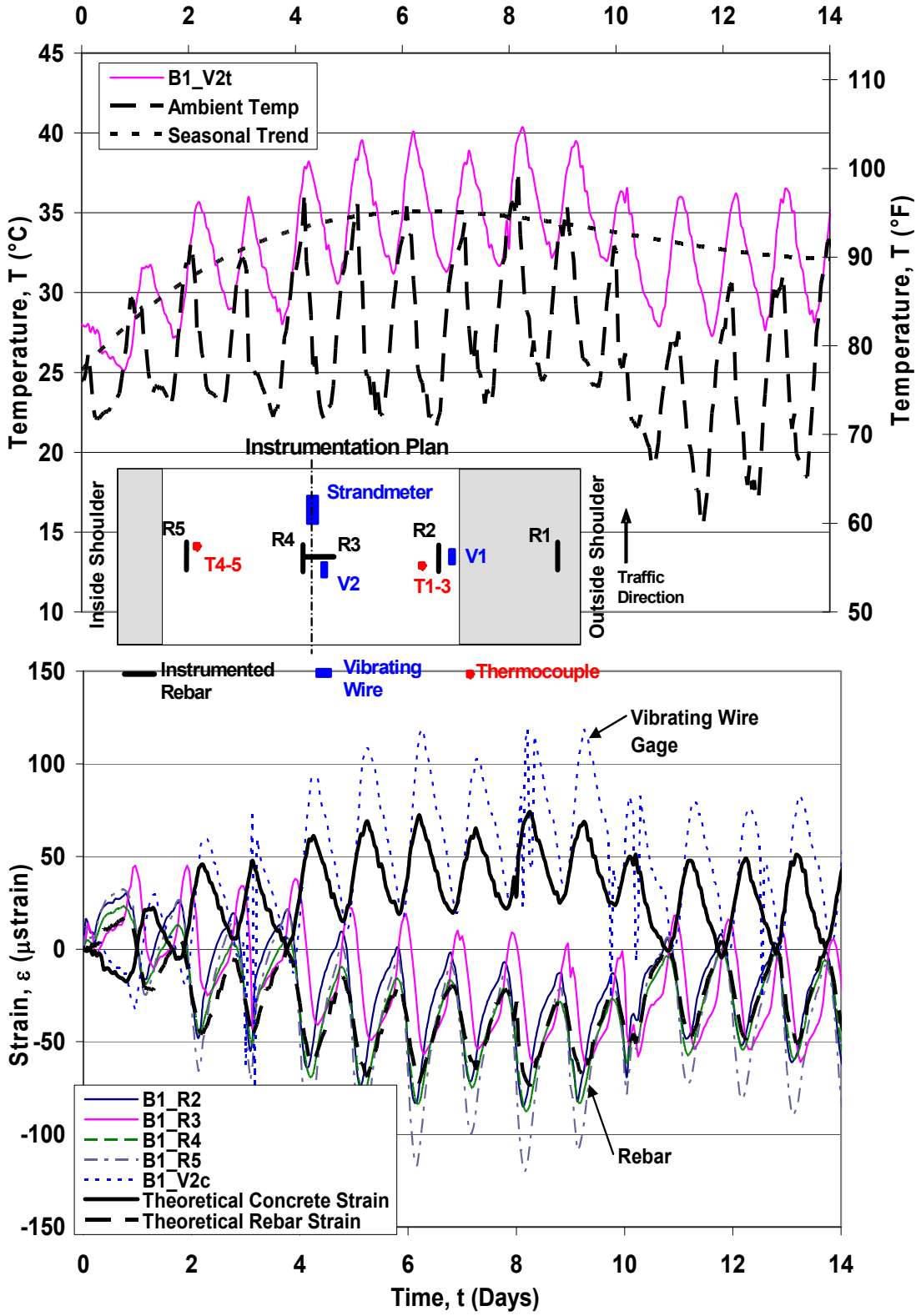

Figure E.12 – In-service data for Panel B1 over fourteen days in July 2006

F. TIMELINE FOR THE PROJECT

Late 2003	Missouri secures recommendation for the pilot project
2004-2005	Scheduled meetings between all parties to discuss design, planning, and coordination.
10/1/05	CPI began casting panels
10/11-10/14/05	Cast and instrumented Panels B1-B4, and C1. Stress transferred at that time.
12/7-12/13/05	Cast and instrumented joint Panels A31 and A32. Stress transferred.
12/12-12/21/05	Installation of panels on-site
12/22-12/23/05	Threading and post-tensioning operations
1/16/06	Open to traffic